OFFICE OF CIVILIAN RADIOACTIVE WASTE MANAGEMENT
ANALYSIS/MODEL COVER SHEET
Complete Only Applicable Items
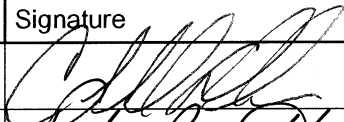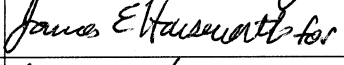
1. QA: __QA__

Page: 1 of: 211

2. ☑ Analysis Check all that apply

Type of Analysis	☐ Engineering
	☐ Performance Assessment
	☑ Scientific

Intended Use of Analysis	☐ Input to Calculation
	☐ Input to another Analysis or Model
	☑ Input to Technical Document
	☑ Input to other Technical Products

Describe use:
See Block 12

3. ☑ Model Check all that apply

Type of Model	☑ Conceptual Model	☐ Abstraction Model
	☐ Mathematical Model	☐ System Model
	☑ Process Model	

Intended Use of Model	☐ Input to Calculation
	☐ Input to another Model or Analysis
	☑ Input to Technical Document
	☑ Input to other Technical Products

Describe use:
See Block 12

4. Title:
Unsaturated Zone Flow Patterns and Analysis

5. Document Identifier (including Rev. No. and Change No., if applicable):
MDL-NBS-HS-000012 REV 00

6. Total Attachments:
0

7. Attachment Numbers - No. of Pages in Each:
N/A

	Printed Name	Signature	Date
8. Originator	C.F. Ahlers	*[signature]*	10/17/01
9. Checker	P. Persoff	*[signature]*	10/17/01
10. Lead/Supervisor	G.S. Bodvarsson	*James E Houseworth for*	10/17/01
11. Responsible Manager	G.S. Bodvarsson	*James E Houseworth for*	10/17/01

12. Remarks:

Q. Hu contributed Section 6.2
L. Pan contributed Section 6.3.1
H.H. Liu contributed Sections 6.3.2 and 6.5.1
G. Li contributed Section ~~6.4.2, 6.5.3, and 6.5.4~~ 6.4.1.1
J. Liu contributed Sections 6.4.3 and 6.5.2
Y-S. Wu contributed Sections 6.4.2, 6.5.3, and 6.5.4

CAa 10/17/01

Description of Use for Blocks 2 and 3

This AMR provides documentation of seepage estimates and effect of flow patterns on seepage as presented in "Supplemental Science and Performance Analyses, Volume 1: Scientific Bases and Analyses" (BSC 2001 [155950]) and documents activities used for TSPA sensitivity studies as documented in "Supplemental Science and Performance Analyses, Volume 2: Performance Analyses" (BSC 2001 [154659]).

2. Analysis or Model Title:
Unsaturated Zone Flow Patterns and Analysis

3. Document Identifier (including Rev. No. and Change No., if applicable):
MDL-NBS-HS-000012 REV 00

4. Revision/Change No.	5. Description of Revision/Change
REV 00	Initial Issue

CONTENTS

CONTENTS (CONTINUED)

CONTENTS (CONTINUED)

CONTENTS (CONTINUED)

FIGURES

Page

FIGURES (CONTINUED)

FIGURES (CONTINUED)

FIGURES (CONTINUED)

FIGURES (CONTINUED)

Page

INTENTIONALLY LEFT BLANK

TABLES

Page

INTENTIONALLY LEFT BLANK

ACRONYMS

1-D	One-dimensional, one dimension
2-D	Two-dimensional, two dimensions
3-D	Three-dimensional, three dimensions
ACC	Accession Number
AMR	Analysis/Model Report
AP	Administrative Procedure
BSC	Bechtel SAIC Company
CPM	Calibrated Properties Model
CRWMS	Civilian Radioactive Waste Management System
DIRS	Document Input Reference System
DKM	Dual-Permeability Model
DTN	Data Tracking Number
EBS	Engineered Barrier System
ECM	Effective Continuum Model
ECRB	Enhanced Characterization of Repository Block
ESF	Exploratory Studies Facility
FTM	Flow and Transport Model
FY	Fiscal Year
GFM	Geologic Framework Model
LBNL	Lawrence Berkeley National Laboratory
M&O	Management and Operating Contractor
MINC	Multiple Interacting Continua
OCRWM	Office of Civilian Radioactive Waste Management
PA	Performance Assessment
PMR	Process Model Report
Q	Qualified
QAP	Quality Administrative Procedure
QARD	Quality Assurance Requirements and Description
QIP	Quality Implementing Procedure

ACRONYMS (CONTINUED)

RSS   Repository Safety Strategy
RTTF   Residence Time/Transfer Function
RWPM   Random Walk Particle Method

SD   Site Description
SCM   Software Confirguration Management
SMPA   Seepage Model for Performance Assessment
SN   Scientific Notebook
SR   Site Recommendation
STN   Software Tracking Number
SZ   Saturated Zone

TBV   To Be Verified
TDMS   Technical Data Management System
TOUGH   Transport Of Unsaturated Groundwater and Heat
TSPA   Total System Performance Assessment
TU   Tritium Units

U.S. DOE   United States Department of Energy
U.S. NRC   United States Nuclear Regulatory Commission
UZ   Unsaturated Zone

YMP   Yucca Mountain Site Characterization Project

MAJOR HYDROGEOLOGIC UNITS

(Also see Table 6.5-1 for the following and other geologic units and model layers.)

CFu   Crater Flat undifferentiated hydrogeologic unit
CHn   Calico Hills nonwelded hydrogeologic unit
PTn   Paintbrush Tuff nonwelded hydrogeologic unit
TCw   Tiva Canyon welded hydrogeologic unit
TSw   Topopah Spring welded hydrogeologic unit

1. PURPOSE

This Analysis/Model Report (AMR) documents the development of an expected-case model for unsaturated zone (UZ) flow and transport that will be described in terms of the representativeness of models of the natural system. The expected-case model will provide an evaluation of the effectiveness of the natural barriers, assess the impact of conservatism in the Total System Performance Assessment (TSPA), and support the development of further models and analyses for public confidence building. The present models used in *Total System Performance Assessment for the Site Recommendation* (Civilian Radioactive Waste Management System Management and Operating Contractor (CRWMS M&O) 2000 [153246]) underestimate the natural-barrier performance because of conservative assumptions and parameters and do not adequately address uncertainty and alternative models. The development of an expected case model for the UZ natural barrier addresses issues regarding flow-pattern analysis and modeling that had previously been treated conservatively. This is in line with the Repository Safety Strategy (RSS) philosophy of treating conservatively those aspects of the UZ flow and transport system that are not important for achieving regulatory dose (CRWMS M&O 2000 [153246], Section 1.1.1). The development of an expected case model for the UZ also provides defense-in-depth in areas requiring further analysis of uncertainty and alternative models. In general, the value of the conservative case is to provide a more easily defensible TSPA for behavior of UZ flow and transport processes at Yucca Mountain. This AMR has been prepared in accordance with the *Technical Work Plan for Unsaturated Zone (UZ) Flow and Transport Process Model Report* (Bechtel SAIC Company (BSC) 2001 [155051], Section 1.3 – Work Package 4301213UMG). The work scope is to examine the data and current models of flow and transport in the Yucca Mountain UZ to identify models and analyses where conservatism may be reduced and uncertainty may be better characterized either through new analyses or development of new, alternative, models. This AMR supports Site Recommendation (SR) activities by documenting analyses and models reported in *FY01 Supplemental Science and Performance Analyses, Volume 1: Scientific Bases and Analyses* (BSC 2001 [155950]). However, except for the model results reported in Section 6.4.2, this AMR does not support TSPA as documented in either *FY01 Supplemental Science and Performance Analyses, Volume 2: Performance Analyses* (BSC 2001 [154659]) or *Total System Performance Assessment for the Site Recommendation* (CRWMS M&O 2000 [153246]). Furthermore, this AMR represents scoping studies to aid in determining whether work beyond the scope of the models and analyses used to support TSPA-SR (CRWMS M&O 2000 [153246]) is warranted. If the decision is made to use any of these models and analyses for TSPA for License Application, further verification and validation will be required. The model results reported in Section 6.4.2 are used for TSPA sensitivity studies as documented in *FY01 Supplemental Science and Performance Analyses, Volume 2: Performance Analyses* (BSC 2001 [154659], Section 3.2.2.3).

The following topics are addressed for development of an expected case:

(1) Synthesis of geochemical information (Section 6.2)

(2) Comparison of different transport codes (Section 6.3.1)

(3) Effects of matrix block discretization on flow and transport (Section 6.3.2)

(4) Effects of drift degradation, including rock fall and rock bolts, on drift seepage (Section 6.4.1)

(5) Effects of flow focusing on drift seepage (Section 6.4.2)

(6) Percolation redistribution in the Paintbrush nonwelded (PTn) unit (Section 6.4.3)

(7) Effects of episodic flow on drift seepage (Section 6.4.4)

(8) Flow in the vitric portion of the Calico Hills Formation (Section 6.5.1)

(9) Fault properties in the Calico Hills (Section 6.5.2)

(10) Perched water models and lateral diversion (Section 6.5.3)

(11) Effects of radionuclide release into the rock matrix (Section 6.5.4)

In order to address topics 4, 5, 7, and 8, new models are developed and validated in this AMR.

Caveats and Limitations

The analyses and models documented here are limited in scope as documented in individual subsections of Section 6. Extension of the results of these analyses and models beyond the scope within which they are performed may lead to erroneous conclusions. For example, many of the models documented here are numerical in nature such that the results must be interpreted and used only after careful consideration of the conceptual model and model parameters (e.g., time step size, mesh discretization, and equivalent hydrologic properties).

2. QUALITY ASSURANCE

The activities documented in this AMR were evaluated under Administrative Procedure (AP)-2.21Q, *Quality Determinations and Planning for Scientific, Engineering, and Regulatory Compliance Activities,* and were determined to be subject to the requirements of the United States Department of Energy (U.S. DOE) Office of Civilian Radioactive Waste Management (OCRWM) *Quality Assurance Requirements and Description* (QARD) (DOE 2000 [149540]). This evaluation is documented in *Technical Work Plan for Unsaturated Zone (UZ) Flow and Transport Process Model Report* (BSC 2001 [155051], Attachment 1, Work Package 4301213UMG). Electronic management of information was evaluated in accordance with AP-SV.1Q, *Control of the Electronic Management of Information*, and controlled under YMP-LBNL-QIP-SV.0, *Management of YMP-LBNL Electronic Data*. This evaluation is documented in the Technical Work Plan (TWP) (BSC 2001 [155051], Attachment 2, Work Package 4301213UMG).

This AMR reports on natural barriers (the Tiva Canyon Welded, Paintbrush Nonwelded, Topopah Springs Welded, and Calico Hills Nonwelded Hydrogeologic Units) that have been included in the Q-List (YMP 2000 [149733]) as items important to waste isolation. The AMR contributes to the analyses and modeling data used to support performance assessment. The conclusions of this AMR do not affect the repository design or permanent items as discussed in QAP-2-3, *Classification of Permanent Items.*

The modeling activities documented in this AMR were conducted in accordance with the quality assurance program of the Yucca Mountain Site Characterization Project (YMP) using OCRWM APs and YMP Quality Implementing Procedures (QIPs) for the Lawrence Berkeley National Laboratory (LBNL) as identified in the TWP (BSC 2001 [155051], Table 6-1).

INTENTIONALLY LEFT BLANK

3.   COMPUTER SOFTWARE AND MODEL USAGE

The software used in this study is listed in Table 3-1. All qualified software was obtained from Software Configuration Management (SCM), in accordance with AP-3.10Q, *Analyses and Models*, Attachment 1, Section 3, and is appropriate for its intended use, and was used only within the range of validation in accordance with AP-SI.1Q, *Software Management*.

Table 3-1.   Computer Software and Routines

Software Name and Version	Software Tracking Number (STN)	DIRS Ref. Number	Platform and Operating System (See Notes)
DCPT V1.0	10078-1.0-00	132448	3
DCPT V2.0	10078-2.0-00 (unqualified)	154342	3
EARTHVISION V5.1	10174-5.1-00	152614	4
GSLIB V1.0MSISIMV1.203	10001-1.0MSISIMV1.203-00	134136	1
GSLIB V2.0MSISIMV2.0	10098-2.0MSISIMV2.0-00	154340	1
infil2grid V1.6	10077-1.6-01	134754	1
iTOUGH2 V4.0	10003-4.0-00	139918	1 and 2
ITOUGH2 V3.2	10054-3.2-00	154337	1
ITOUGH2 V3.2_drift	10055-3.2_DRIFT-00	112757	1
T2R3D V1.4	10006-1.4-00	113942	1 and 2
TOUGH2 V1.4	10007-1.4-01	146496	1 and 2
TOUGH2 V1.5	10007-1.5-00 (unqualified)	154322	1 and 2
Wingridder V1.1	10024-1.1-00	154341	3
WINGRIDDER V2.0	10024-2.0-00 (unqualified)	154785	3
AddBound V1.0	10357-1.0-00	152823	1
AssignRock V1.0	10465-1.0-00	154321	1
bot_sum.f V1.0	10349-1.0-00	153471	2
CalBT.for V1.0	10504-1.0-00	154788	3
CutNiche V1.3	10402-1.3-00	152828	1
mddf.f V2.0	10456-2.0-00	154347	1
meshbd.f V1.0	10467-1.0-00	152871	1
MINCgridv1.f V1.0	10469-1.0-00	154343	2
mininipresf.f 1.0	10470-1.0-00	152872	1
minrefine3df.f V1.0	10472-1.0-00	152880	1
mk_generGL.f V1.0	10476-1.0-00	154349	1
MoveMesh V1.0	10358-1.0-00	152824	1
parallelf.java V1.0	10457-1.0-00	154346	3
Perm2Mesh V1.0	10359-1.0-00	152826	1
RoutineRick1 V1.1	10474-1.1-00	156137	1
vf_con.for V1.0	10466-1.0-00	154345	3

Notes: Platform with Operating System
1.   SUN UltraSparc with Unix OS
2.   DEC-Alpha with Unix OS
3.   PC with MS Windows
4.   SGI with Unix OS

The use of all codes identified in Table 3-1 is documented in Section 6 and in the supporting scientific notebooks identified in Section 6. The unqualified software codes, DCPT V2.0 (LBNL 2001 [154342]), TOUGH2 V1.5 (LBNL 2001 [154322]) and WINGRIDDER V2.0 (LBNL 2001 [154785]), were obtained from SCM in accordance with AP-3.10Q, Attachment 1, Section 3. These codes have been submitted to SCM to meet the Interim Use of Unqualified Software to support Site Recommendation (SR) products in accordance with Section 5.10, AP-SI1.1Q,

Software Management.. For each of these three codes, a Software Activity Plan for use of unqualified software, a Software User Request, and a copy of the code have been submitted to SCM to meet the Interim Use of Unqualified Software requirements of AP-SI.1Q.

Tecplot V7.0 and Microsoft Excel 2000 SR-1 were used to plot data generated by simulations documented within this AMR and the references specified. Several computations were performed using commercial off-the-shelf software and are exempt from AP-SI.1Q. All information needed to reproduce the work is included in this AMR and the references specified.

Results generated using FEHM V2.0 (CRWMS M&O 2000 [141418]) are cited in Sections 6.3.1 and 7.3.1 and are documented in CRWMS M&O (2000 [134732]). As such, FEHM V2.0 is not included in the list of software used.

The following studies, documented in this AMR, use previously developed and validated models:

1. The analysis of the impact of rock fall on seepage (Section 6.4.1.1) uses models documented in *Seepage Model for PA Including Drift Collapse* (CRWMS M&O 2000 [153314]; DTN: LB0011SMDCREV1.002 [153570]) and *Drift Degradation Analysis* (CRWMS M&O 2000 [151635]; DTN: MO0109RDDAAMRR.003 [156306])

2. The analysis of percolation redistribution in the PTn (Section 6.4.3) uses models documented in *UZ Flow Models and Submodels* (CRWMS M&O 2000 [122797]; DTNs: LB991131233129.003 [147119], LB990701233129.002 [125604], LB990801233129.022 [156331]) and *Calibrated Properties Model* (CRWMS M&O 2000 [144426]; DTN: LB997141233129.001 [104055]).

3. The model of transient percolation used to evaluate the impact on seepage (Section 6.4.4) is based, in part, on previously developed and validated models documented in *UZ Flow Models and Submodels* (CRWMS M&O 2000 [122797]) and DTN: MO9901MWDGFM31.000 [103769]. (Note that the TDMS now shows DTN: MO9901MWDGFM31.000 [103769] to be superseded by DTN: MO0012MWDGFM02.002 [153777], however, the new DTN does not include the data used for development of this analysis. The comment section on the Technical Data Information Form for the more recent DTN also contains the statement, "GFM2000 does not invalidate GFM3.1. Changes to rock layer elevations in the repository area are very small in magnitude; rarely as large as 25 feet." Because a variance of 25 feet is less than the uncertainty in the depths for stratigraphic layers as reported in *Geologic Framework Model Analysis Model Report* (BSC 2001 [154622], Section 7), this AMR maintains the use of the original DTN.)

4. The model of an unfractured vitric Calico Hills used to evaluate the impact on flow and transport (Section 6.5.1) is based, in part, on previously developed and validated models documented in *Calibrated Properties Model* (CRWMS M&O 2000 [144426]) and *UZ Flow Models and Submodels* (CRWMS M&O 2000 [122797]).

5. The analysis of uncertainty regarding perched water representations (Section 6.5.2) uses the model documented in *UZ Flow Models and Submodels* (CRWMS M&O 2000

[122797]; DTNs: LB990801233129.003 [122757], LB990701233129.001 [106785], LB991121233129.001 [147328], LB991121233129.002 [147334]) and the model documented in Section 6.5.1 (DTN: LB0103CHVUPROP.001).

6. The analysis of uncertainty regarding fault properties below the Topopah Spring welded hydrogeological unit (Section 6.5.3) uses the model documented in *UZ Flow Models and Submodels* (CRWMS M&O 2000 [122797]; DTNs: LB990701233129.001 [106785], LB990801233129.003 [122757]).

7. The analysis of the impact of radionuclide release to the rock matrix (Section 6.5.4) uses the model documented in *UZ Flow Models and Submodels* (CRWMS M&O 2000 [122797]) which is subsequently modified as documented in Section 6.5.3 (DTN: LB0104AMRU0185.009).

Data developed with these models and analyses and input and output files for the models and analyses are submitted and listed under the DTNs listed in Section 8.4.

INTENTIONALLY LEFT BLANK

4. INPUTS

This section provides documentation for data used as input to this AMR. The Q-status of all inputs and a description of the data are shown in the Document Input Reference System (DIRS) database. The inputs to the models were obtained from the Technical Data Management System (TDMS). Acquired and developed data used to characterize the seepage conditions in the models are discussed below.

4.1 DATA AND PARAMETERS

Table 4-1. Input Data Used

Inputs	Section Used In	Description of Data Used
LB0110MESHPROP.001 [156336]	6.3.1	These UZ model grid and flow simulation data are the most appropriate for use as input to the analysis presented in Section 6.3.1.
LB990701233129.001 [106785]		
LB990801233129.003 [122757]		
GS000399991221.002 [147022]	6.3.2	These fracture geometry, calibrated properties, and infiltration data are the most appropriate for use as input to the analysis presented in Section 6.3.2.
LB990501233129.001 [106787]		
LB997141233129.001 [104055]		
LB0010SCMREV01.002 [153393]	6.4.1.1	These seepage mode, calibrated properties, and drift degradation data are the most appropriate for use as input to the analysis presented in Section 6.4.1.1.
LB0011SMDCREV1.001 [153574]		
LB0011SMDCREV1.002 [153570]		
LB997141233129.001 [104055]		
MO0109RDDAAMRR.003 [156306]		
BSC 2001 [155187], Section 6.5.1.2.2	6.4.1.2	These rock bolt and model parameter data are the most appropriate for use as input to the model presented in Section 6.4.1.2.
BSC 2001 [155187], Table 4-10		
CRWMS M&O 2000 [153314], Section 6.3		
LB0010SCMREV01.002 [153393]		
LB00090012213U.001 [153141]	6.4.2	These model parameter and air permeability data are the most appropriate for use as input to the model presented in Section 6.4.2.
LB0012AIRKTEST.001 [154586]		
LB002181233124.001 [146878]		
LB990901233124.004 [123273]		
LB991121233129.001 [147328]		
GS000399991221.002 [147022]	6.4.3	These UZ model and chloride data are the most appropriate for use as input to the analysis presented in Section 6.4.3.
GS950608312272.001 [145617] *		
GS990208312272.001 [146134]		
LA0002JF12213U.002 [156281]		

Inputs	Section Used In	Description of Data Used
LA9909JF831222.004 [145598]		
LB990701233129.002 [125604]		
LB990801233129.022 [156331]		
LB991131233129.003 [147119]		
LB997141233129.001 [104055]		
CRWMS M&O 2000 [114277], Table III-1	6.4.4	These model parameter and geologic model data are the most appropriate for use as input to the model presented in Section 6.4.4.
LB991091233129.004 [126111]		
LB997141233129.001 [104055]		
MO9901MWDGFM31.000 [103769]		
GS990308312242.007 [107185]	6.5.1	These uncalibrated properties, Calibrated Properties Model, and Busted Butte data are the most appropriate for use as input to the model presented in Section 6.5.1.
GS990708312242.008 [109822]		
LB990501233129.001 [106787]		
LB991091233129.001 [125868]		
LB990701233129.001 [106785]	6.5.2	These three-dimensional, UZ-flow-model data are the most appropriate for use as input to the analysis presented in Section 6.5.2.
LB990801233129.003 [122757]		
GS950608312272.001 [145617] *	6.5.3	These UZ model, perched water, saturation and water potential, chloride, and diffusion data are the most appropriate for use as input to the analysis presented in Section 6.5.3.
GS960308312312.005 [107230]		
GS970208312312.003 [119786]		
GS980508312313.001 [109746]		
GS980708312242.010 [106752]		
GS980808312242.014 [106748]		
GS990208312272.001 [146134]		
LA9909JF831222.004 [145598]		
LB990701233129.001 [106785]		
LB990801233129.003 [122757]		
LB990801233129.004 [117129]		
LB990801233129.019 [144659]		
LB9908T1233129.001 [147115]		
LB991121233129.001 [147328]		
LB991121233129.002 [147334]		
MO0109HYMXPROP.001 [155989]		

* Chloride abundance data from UE-25 UZ#16 were used from the DTN: GS950608312272.001 [145617]. This DTN has been superceded by DTN: GS010708312272.002 [156375]. The chloride abundance data from UE-25 UZ#16 have remained unchanged.

4.2 CRITERIA

This AMR complies with the DOE interim guidance (Dyer 1999 [105655]). Subparts of the interim guidance that apply to this analysis or modeling activity are those pertaining to the characterization of the Yucca Mountain Site (Subpart B, Section 15). The compilation of information regarding geology of the site is in support of the License Application (Subpart B, Section 21(c)(1)(ii), and the definition of geologic parameters and the conceptual model used in the performance assessment (Subpart E, Section 114(a)). The compilation of information regarding hydrology of the site is in support of the License Application (Subpart B, Section 21(c)(1)(ii)), and the definition of hydrologic parameters and conceptual models used in performance assessment (Subpart E, Section 114(a)). The compilation of information regarding geochemistry and mineral stability of the site is in support of the License Application (Subpart B, Section 21(c)(1)(ii)); and the definition of geochemical parameters and conceptual models used in performance assessment (Subpart E, Section 114(a)).

The Nuclear Regulatory Commission (NRC) *Issue Resolution Status Report Key Technical Issue: Unsaturated and Saturated Flow under Isothermal Conditions* (NRC 1999 [140371], subissues 4 and 6) establishes the technical acceptance review criteria that the NRC staff will use in their review of DOE's submittals describing deep percolation (Subissue 4) and matrix diffusion (Subissue 6). Additionally, the NRC Issue Resolution Status Report Key Technical Issue: Radionuclide Transport (NRC 2000 [153313], Subissues 1 and 2) establishes technical-acceptance review criteria that the NRC staff will use in their review of DOE's submittals describing radionuclide transport through porous rock (Subissue 1) and fractured rock (Subissue 2) in the UZ of the Yucca Mountain.

4.3 CODES AND STANDARDS

No specific formally established standards have been identified as applying to this analysis and modeling activity.

INTENTIONALLY LEFT BLANK

5. ASSUMPTIONS

5.1 ASSUMPTIONS FROM PREVIOUS WORK

The models and analyses presented in this AMR are generally based on previous work and represent refinements to the previous work, or sensitivity studies to assess the impact of alternative models and/or parameters. As such, most of the assumptions used in this AMR are cited or quoted from other AMRs that document the previous work. Quoted assumptions are shown indented and italicized. In addition, new assumptions necessary for this AMR are documented below in plain text).

5.2 ASSUMPTIONS SPECIFIC TO THE SYNTHESIS OF GEOCHEMICAL DATA

Section 6.2 is a review and synthesis of geochemical data. Much of Section 6.2 is based upon *Analysis of Geochemical Data for the Unsaturated Zone* (BSC 2001 [154874]) which invokes several assumptions, generally that water-quality data in the TDMS are sufficiently precise, accurate, and representative to support conclusions based on analysis of the data. No assumptions specific to this AMR are necessary, as no additional analyses of the data are documented in this AMR.

5.3 ASSUMPTIONS SPECIFIC TO COMPUTATIONAL METHODS FOR TRANSPORT

The assumption documented in Section 5.2, quoted below, of *Analysis Comparing Advective-Dispersive Transport Solution to Particle Tracking* (CRWMS M&O 2000 [141389]) is applicable to the comparison of transport computational methods documented in Section 6.3. These assumptions do not require verification.

> *The transport processes included in this analysis are… advection, diffusion and dispersion, and equilibrium sorption of solutes. Radioactive decay has been ignored to facilitate comparisons between the simulation outputs. It is assumed that inclusion of radioactive decay would not significantly affect the comparison among the methods. This assumption is justified because radioactive decay is mathematically simple and is handled identically by all the simulators.*

5.3.1 Assumptions Specific to Comparison of Transport Codes

The assumption documented in Section 5.3 of *Analysis Comparing Advective-Dispersive Transport Solution to Particle Tracking* (CRWMS M&O 2000 [141389]) is specifically applicable to the analyses documented in Section 6.3.1. It does not require verification.

Section 5.3 of *Analysis Comparing Advective-Dispersive Transport Solution to Particle Tracking* (CRWMS M&O 2000 [141389]) states:

> *All standard numerical flow and transport simulators, including those used here, rely upon spatial and temporal discretization, and therefore provide spatially and temporal approximations of the natural system… Also, the methods tested here*

use dual-permeability grids… It is assumed that the spatial and temporal discretizations, and the appropriate use of dual-permeability grids, do not cause significant errors and do not distort the comparisons among the methods. This assumption is justified by the process of grid development, in which various degrees of grid refinement are tested until further refinement yields little improvement.

5.3.2 Assumptions Specific to Matrix Block Discretization and Its Effects on Unsaturated Zone Flow and Transport Simulations

The UZ flow and transport models use dual permeability grids (Doughty 1999 [135997], pp. 74–79) with each gridblock not further discretized as in a MINC scheme (Pruess and Narasimhan 1985 [101707], pp. 14–26). The question considered in Section 6.3.2 is whether a MINC scheme (which greatly increases the computational effort) would be justified. To decide the question, both schemes are compared in a two-dimensional model. The assumption that a two-dimensional model is adequate for investigation of the mountain-scale effect of different matrix block discretization schemes is specifically applicable to the model documented in Section 6.3.2. *Rationale*: The use of a two-dimensional model does not bias the results as long as all model parameters, except the matrix block discretization scheme, remain unchanged between the two simulations. No further justification or confirmation is required.

5.4 ASSUMPTIONS SPECIFIC TO PROCESSES AFFECTING SEEPAGE

There are no general assumptions that cover all of the investigated seepage-affecting processes. Assumptions specific to each process are given below.

5.4.1 Assumptions Specific to Seepage Enhancement Due to Drift Degradation

The following assumptions quoted from Section 5 of *Seepage Model for PA Including Drift Collapse* (CRWMS M&O 2000 [153314]) are specifically applicable to the models documented in Section 6.4.1. These assumptions require no further justification. (The quote below is italicized and indented; notes for clarification are inserted as plain text.)

5.1   Continuum Approach

Assumption: It is assumed that the continuum approach is a valid concept to calculate percolation flux and drift seepage at Yucca Mountain.

Rationale: The continuum approach can be considered appropriate for seepage studies if it is capable of predicting seepage threshold and seepage percentages for a drift in a fractured formation. The appropriateness of using the continuum approach to simulate flow through fractured rock was studied by Jackson et al. (2000 [141523], pp. 189–202) using synthetic and actual field data. They concluded that heterogeneous continuum representations of fractured media are self-consistent, i.e., appropriately estimated effective continuum parameters are able to represent the underlying fracture-network characteristics. Furthermore, Finsterle (2000 [151875], pp. 2055–2066) demonstrated that simulating seepage into underground openings excavated from a highly fractured formation could be

performed using a model based on the continuum assumption, provided that the model is calibrated against seepage-relevant data (such as data from liquid-release tests). Synthetically generated data from a model that exhibits discrete flow and seepage behavior were used to calibrate a simplified fracture continuum model. Seepage predictions for low percolation fluxes made with the calibrated fracture continuum model were consistent with the synthetically generated data from the discrete feature model.

The continuum approach is considered applicable for seepage studies if applied within the framework described in this AMR. Inverse modeling should be used for the estimation of process-specific, model-related, and scale-dependent parameters, and the same or similar conceptual model should be used for the subsequent seepage predictions (i.e., the Seepage Model for PA). Under these conditions, this assumption does not require confirmation.

5.2   *Unsaturated flow*

Assumption: Adopting the continuum approach, water flow under unsaturated conditions is assumed to be governed by Richards' equation (Richards 1931 [104252], pp. 318–333).

Rationale: Richard's equation states that isothermal flow of water in a porous medium occurs under the combined effect of gravitational and capillary forces, that flow resistance is a function of saturation, and that, for the purposes of this representation, movement of the nonwetting air phase can be neglected. This general concept is believed reasonable for unsaturated water flow through both porous matrix and fractures and does not require confirmation.

(Note: The general assumption that the Richards/Darcy approach to modeling flow in porous media and fractures is valid is well documented in the scientific literature, e.g., de Marsily (1986 [100439]), Freeze and Cherry (1979 [101173]), and Domenico and Schwarz (1990 [100569]).)

5.3   *Air Permeabilities*

Assumption: Permeabilities determined from air-injection tests are assumed representative of the hydraulic conductivity of the excavation-disturbed zone around the opening.

Rationale: A detailed discussion of this assumption is given in CRWMS M&O (2000 [141400], Sections 5.1 and 5.2.1). The assumption holds for the purposes of the current application, where postexcavation air-injection tests were conducted in a dry fracture network. Air-permeability estimates are used to condition the generation of a spatially correlated, random permeability field. Potential inaccuracies in this assumption are compensated for by the estimation of the van Genuchten $1/\alpha$ parameter (Luckner et al. 1989 [100590], pp. 2191–2192). Air-injection tests are a standard method to obtain drift-scale permeability

values (CRWMS M&O 2000 [141400], Section 6.1). The use of these values during calibration and prediction of seepage ensures consistency.

Excavation effects increase the permeabilities around the niches and the Cross Drift (Wang and Elsworth 1999 [104366], pp. 751–757; CRWMC [sic] M&O 2000 [141400], Section 6.1.2.2). Since seepage is determined by the formation properties within the boundary layer in the immediate vicinity of the opening, it is reasonable to use postexcavation air-permeability data for seepage calculations.

(Note: The assumption is that air-injection tests can be used to determine an intrinsic permeability of the flow system that is relevant for the subsequent liquid-release tests and their analysis. Whether the relevant flow system is the fracture system only or is some combination of the fractures and matrix is immaterial to the assumption. The rationale for the assumption is that the permeability of the relevant flow system is associated mainly with the fractures in the excavation disturbed zone. The matrix permeability is many orders of magnitude less than that of the fractures (CRWMS M&O 2000 [145771], Sections 6.1.1 and 6.2.1). The relevant geologic layers, the Tptpmn and Tptpll (see Table 6.5-1) do not have high clay mineral content that could swell with the introduction of more water into the system and create a difference between the dry intrinsic permeability (air-injection tests) and the wet intrinsic permeability (liquid-release tests).)

This assumption does not require confirmation.

5.4   Characteristic curves

Assumption: Relative permeability and capillary pressure are assumed to be described as continuous functions of effective liquid saturation, following the expressions given by the van Genuchten-Mualem model (Luckner et al. 1989 [100590], pp. 2191–2192) as implemented in the iTOUGH2 code (Finsterle 1997 [104043], p. 224). Capillary strength (represented by the $1/\alpha$ parameter) and permeability are not correlated.

Rationale: The van Genuchten-Mualem model is the standard model used in the suite of UZ flow and transport models; it was chosen here for consistency. Furthermore, the applicability of relative permeability and capillary pressure functions is consistent with the continuum assumption (see Section 5.1) and is appropriate to represent fractures that are rough and/or partially filled with porous material. The functional relationship describing the potential correlation between permeability and capillary strength is unknown. An increase in permeability may be attributed to larger fracture apertures (which would reduce capillary strength) or to an increase in fracture density (which would not affect capillary strength). The capillary strength parameter $1/\alpha$ is taken to be constant and will be subjected to estimation by inverse modeling. The calibration process and the consistent conceptualization in the downstream models (specifically the Seepage Model for PA) make this assumption a valid approach.

This assumption does not require confirmation.

5.5   Matrix Imbibition

Assumption: The transient effects from matrix imbibition in a fracture-matrix system are assumed to be small and do not need to be modeled explicitly in the SCM [sic – seepage calibration model] *(CRWMS M&O 2000* [sic] *[153045]). Further, the imbibition and flow into the matrix continuum is not considered in the SMPA.*

(Note: CRWMS M&O 2001 [153045] is the correct reference cited above.)

(Note: SMPA refers to the Seepage Model for Performance Assessment.)

Rationale: Matrix permeability is low, and the potential for matrix imbibition is limited because of relatively low porosity and relatively high liquid saturation. In a fracture-matrix system, the transient effects from matrix imbibition are restricted to intermediate times, i.e., they are insignificant (1) for a short-term liquid-release test with insufficient time for matrix imbibition, and (2) for a long-term seepage experiment, when near-steady late-time data are no longer affected by matrix imbibition. To match intermediate times during a long-term test, an effective porosity is estimated by inverse modeling to account for the storage capacity of both the fracture system and the matrix. Porosity estimates are irrelevant in the subsequent simulations of seepage under natural flow conditions, which are near steady state.

For SMPA, the imbibition and flow into the matrix continuum is not considered. The rationale is that in the current AMR, except for the episodic percolation flux case (Sections 6.5 and 6.6.6), we are calculating steady-state flow conditions over long time frames. At steady-state, the flow exchange between fracture and matrix continua will settle to a small amount with the matrix close to full saturation. The flow partitions between the fracture and matrix continua according to their effective permeabilities and porosities, and it follows that the matrix with its five to six orders-of-magnitude lower permeability would not have significant effects on seepage into drift, which would be controlled by the flow in the fracture continuum. For the episodic percolation flux case (Sections 6.5 and 6.6.6), the matrix continuum provides a damping effect on seepage in the fracture continuum, and neglecting it represents a conservative case.

(Note: Matrix and fracture permeabilities are presented in CRWMS M&O (2000 [144426], Section 6.1.4).)

5.6   Evaporation

Assumption: The effect of evaporation on the observed seepage rates is insignificant, i.e., water removal from the formation, at the drift surface, and from the capture system by evaporation and vapor diffusion is assumed to be small.

Rationale: Under isothermal conditions, potential evaporation at the drift wall or in the capture system is small compared to the amount of water being released.

Seepage experiments in the middle nonlithophysal zone of the Topopah Spring welded unit were conducted in niches that were closed off by a bulkhead, which leads to comparatively high relative humidity and low air circulation. Moreover, a humidifier was used in some of the experiments to ensure high relative humidity. For these conditions, Ho (1997 [141521], pp. 2665–2671) and Or and Ghezzehei (2000 [144773], pp. 381–393) provide a detailed description of evaporation mechanisms on the scale of individual water droplets within fractures or emerging from fractured formations. The evapo-infiltration thresholds calculated by Ho (1997 [141521], p. 2670) are significantly lower than the applied injection rates, suggesting a very minor influence of evaporation on measured seepage rates in experiments conducted in the niches.

Evaporation from a large surface of free or nearly free water, however, may be significant. As injected water reaches the opening, it spreads along the surface on account of capillarity within the rough surface. As a result, water potentially seeping into the opening may not only form droplets with a small surface area, but may be spread over a large area, providing a large surface for evaporation. Depending on the evaporation potential of the air in the opening, the water film covering the wall of the opening may evaporate at a rate comparable to the injection or seepage rates.

Moreover, evaporation may be significant during periods of active ventilation with high airflows in the drift in combination with low injection rates. Under these specific conditions, the evaporation rate may exceed the potential seepage rate, preventing the development of liquid droplets that drip into the opening. Ventilation effects are evident from the seepage data collected in the Cross Drift (see Section 6.3.3.3). To reduce the impact from ventilation effects, calibration of the SCM [sic – seepage calibration model] was restricted to seepage rate data collected during nighttime and weekends, when ventilation was turned off.

Currently, no quantitative estimates of evaporation potential under the conditions of the seepage experiments are available. The simplified assumption that evaporation rates are small compared to the injection rates is non-conservative if used for inverse modeling and is therefore an assumption that needs to be verified (TBV-4951 [153049]).

It is important to realize that a non-conservative assumption made in an inverse model is a conservative assumption when used for seepage predictions in a forward model. Specifically, neglecting evaporation effects by prescribing a 100% relative-humidity boundary condition in a forward seepage prediction model (such as the SMPA) is a conservative assumption. While such a model underestimates vapor flow, it yields the maximum liquid-phase influx, which is defined here as drift seepage. The underestimation of vapor flow is irrelevant, since the assumption of 100% relative humidity already implies that the moisture content in the drift environment is as high as possible, maximizing the amount of moisture that can condense within the waste-emplacement drift. In a ventilated drift, the development of a dry-out zone increases the capillary pressure and local

storage volume and thus reduces the risk of reaching seepage conditions; the assumption of 100% relative humidity in the drift is again conservative. The assumption is also reasonable for the time when ventilation is stopped and the waste-emplacement drift is closed. A repository design that includes ventilation yields reduced seepage.

5.7   *Percolation flux range used in this AMR*

Assumption: It is assumed that the range of values for percolation flux used in simulations in this AMR is appropriate.

Rationale: For SMPA calculations, five values for Q_p are used, ranging from 5 to 500 mm/yr; more specifically $Q_p = 5$, 14.6, 73.2, 213 and 500 mm/yr. The justification for the choice of this range is so that the range covers various estimates of percolation fluxes. Wu et al. [sic-Wu and Bodvarsson] *(1999 [117161], p. 210) calculated the percolation flux expected at the repository level, based on a 3D UZ model of Yucca Mountain. They obtained an average fracture flow of 4 to 5 mm/yr at the repository level under present climate conditions. Ritcey and Wu (1999 [139174], p. 262) found that under a climate scenario simulating the most recent glacial period, the percolation flux ranges from 0 to 120 mm/yr, with the peak of the probability distribution to be around 20 mm/yr. The upper limit of 500 mm/yr is chosen to accommodate potential flow focusing in the geologic layers above the drift and to safely bracket an uncertainty range more than four times the high flux value of 120 mm/yr. In cases where seepage is very low or zero, even larger Q_p values are also used to find when seepage might occur.*

This assumption does not require confirmation.

5.4.1.1   Assumptions Specific to Seepage Enhancement Due to Rockfall

There are no additional assumptions specific to the model documented in Section 6.4.1.1.

5.4.1.2   Assumptions Specific to Seepage Enhancement Due to Rock Bolts

The assumption that grout material permeability and capillarity may be loosely correlated is specifically applicable to the model documented in Section 6.4.1.2. *Rationale*: Studies of porous media suggest that permeability and capillarity are correlated in porous media (Wang 1992 [110043]; Leverett 1941 [100588]). Extension of this correlation observed in porous media, to fractured rock is considered appropriate if the correlation is defined loosely (Finsterle 2000 [151875]). Perfect correlation between fracture permeability and capillarity is achieved only if the number of fractures remains constant. If the number of fractures increases without the average fracture aperture increasing then permeability may increase without capillarity increasing. Thus, a loose correlation that allows for some off-correlation behavior to capture this uncertainty is assumed here. No further confirmation is required.

The assumption that disconnecting mesh elements near the drift wall adequately represents discrete fracture effect for investigation of seepage enhancement due to rock bolts is specifically applicable to the model documented in Section 6.4.1.2. *Rationale*: The major effect of a discrete fracture conceptual model for the effect of rock bolts on seepage will be to isolate the last portion of the flow path toward the drift wall. Flow in the rock bolt hole that is not diverted into this last fracture must enter the drift. Flow in the rock bolt hole prior to the last fracture will, at Yucca Mountain, encounter enough fractures that a continuum model will adequately reproduce inflow and outflow from the rock bolt hole. It is sufficient to restrict the connections between the rock bolt hole and the formation adjacent to the drift wall so that flow in the rock bolt hole that bypasses the "last fracture" is forced into the drift. No further confirmation is required.

5.4.2 Assumptions Specific to Seepage Enhancement Due to Flow Focusing

The assumption that a two-dimensional model is adequate for reproduction of flow focusing or weeps formation is specifically applicable to the model documented in Section 6.4.2. *Rationale*: In a two-dimensional, heterogeneous-permeability field, such as the ones used for the model documented in Section 6.4.2, areas of low permeability (or relative permeability) create barriers that divert flow laterally. Flow incident on a barrier will be diverted to one side or the other or be split and flow both ways around the barrier. In a three-dimensional model, however, the flow incident on a barrier may flow any direction around the barrier. The two-dimensional model, because of the more limited flow diversion pathways should predict more flow focusing, i.e., flow incident on a barrier in a two-dimensional model will be focused into fewer flow channels than that in a three-dimensional model. This assumption creates a conservatism in the model. This conservatism may be partially or wholly offset by nonconservatisms due to other assumptions. No further confirmation is required.

The assumption that consideration of only one scale of heterogeneity is adequate for reproduction of flow focusing or weeps formation is specifically applicable to the model documented in Section 6.4.2. *Rationale*: The heterogeneous permeability fields used for the model of flow focusing are essentially random, using 1 and 3 m correlation lengths. Heterogeneity introduced by larger-scale features such as very large fractures or small faults is not considered. Note that heterogeneity introduced by larger faults is beyond the scale of this model. These large-scale heterogeneities may introduce more flow focusing than the small-scale heterogeneity alone. This assumption creates a nonconservatism in the model. This nonconservatism may be partially or wholly offset by conservatism due to other assumptions or conservatism in the reported result of the model. No further confirmation is required.

The assumption that use of a single continuum model is adequate for reproduction of flow focusing or weeps formation is specifically applicable to the model documented in Section 6.4.2. *Rationale*: Flow in the TSw, particularly the Tptpmn (see Table 6.5-1 for geologic definitions), which has very low matrix permeability, is predicted by the UZ Flow model to be dominantly, 80% or more, in the fracture system (CRWMS M&O 2000 [122797], Table 6-11). Further, under steady-state flow, interaction between flow in the matrix and the fractures is limited to areas adjacent to layer interfaces. However, for the purposes of modeling of flow focusing, the results of Section 6.4.2 show that the focusing distribution is virtually independent of percolation rate, and thus the assumption assigning 100% of the flow to the fractures not affect the prediction of a flow-focusing distribution. No further confirmation is required.

The assumption that use of mountain-scale flow parameters (other than permeability) is adequate for reproduction of flow focusing or weeps formation is specifically applicable to the model documented in Section 6.4.2. *Rationale*: Where the average hydraulic conductivity of the flow system is orders-of-magnitude more than the percolation rate, the parameter of importance becomes the structural parameters of the heterogeneous hydraulic conductivity (permeability) field rather than any other model parameter. So, while the use of Yucca Mountain specific parameters is of some importance, scale-specific parameters are not. No further confirmation is required.

5.4.3 Assumptions Specific to Percolation Redistribution and Lateral Flow in the PTn

The following assumptions, 1 and 5–9, are quoted from *UZ Flow Models and Submodels* (CRWMS M&O 2000 [122797], pp. 31–32) and are specifically applicable to the models documented in Section 6.4.3. No further confirmation of the assumptions is required. (The quote below is italicized and indented; notes for clarification are inserted as plain text.)

> 1. *The water table is used as the bottom model boundary which is subject to constant water pressure (equal to the atmospherical pressure). Rationale: The water table is a surface where the water pressure is a fixed single value. Within the numerical models, only one single set of model primary variables for solving Richards' equations is specified for the bottom boundary and this is equivalent to specifying a constant saturation.*

> 5. *The lateral boundaries of the model domain are subject to no-flow boundary conditions. Rationale: The boundaries of the northern and southern model domain are located so far away from the potential repository area that lateral flow effects along these boundaries on flow at the potential repository should be small. The eastern boundary is for most parts along the Bow Ridge fault, and no lateral flow crossing the fault is reasoned. The western boundary is separated from the potential repository by the Solitario Canyon fault, therefore this boundary condition effects are expected to be insignificant.*

(Note: Because faults are modeled as high permeability vertical structures, they act much like lateral boundaries for flow, so a lateral boundary separated from an area of interest, e.g., the potential repository, by a fault will have little influence on the area of interest. Furthermore, a lateral boundary that is coincident with a fault will have little influence away from the boundary because lateral bounaries like permeable or impermeable faults create barriers to lateral flow forcing flow to become vertical, parallel with the fault.)

> 6. *Perched water occurrence results from permeability barrier effects. Rationale: Consistent with the conceptual model that ambient conditions reflect long-term, steady-state or transient flow through the unsaturated zone, perched water under steady-state flow conditions may only be due to a permeability barrier.*

(Note: Perched-water occurrence under long-term, transient flow, or near-steady flow, conditions requires a permeability barrier. Under shorter-term transient flow conditions, perched-water

occurrence may be attributable to capillary-barrier effects. This assumption, while a natural consequence of assumption 8, quoted below, is given here for completeness.)

      7. Under steady-state flow conditions, moisture flow and tracer transport processes can be decoupled. Rationale: Steady-state flow conditions result in an unchanging flow field, and as long as the concentrations of tracers and/or radionuclides are such that they do not significantly change the properties of the fluid, which is the case for simulations documented in this AMR, then the flow field does not have to be coupled to transport.

      8. Water flow through the UZ is assumed to occur under steady-state conditions. Transient, "fast-pathway" flow, such has conveyed ^{36}Cl to the ESF horizon, is assumed not to contribute significantly to the total flow through the UZ.

(Note: The rationale for this assumption is provided in CRWMS M&O (2000 [141187], Section 6.1.2 and 6.1.6).)

      9. The dual-permeability formulation is assumed to be appropriate for simulating flow and transport through fractured tuffs.

(Note: The rationale for this assumption is provided in CRWMS M&O (2000 [141187], Section 6.4).)

5.4.4   Assumptions Specific to the Effect of Episodic Percolation on Seepage

Assumptions 1 and 5–9, documented in *UZ Flow Models and Submodels* (CRWMS M&O 2000 [122797], pp. 31–32), are quoted above in Section 5.4.3 and are specifically applicable to the model documented in Section 6.4.4. No further confirmation is required.

The assumption that the infiltration data received under Input Transmittal Number (ITN) 00316.T are correct is specifically applicable to the model documented in Section 6.4.4. *Rationale*: The upper-bound, glacial-average, infiltration scenario is used to conservatively define the highest possible infiltration in order to test whether episodic infiltration incident upon the outcrop of the TSw west of Yucca Crest will result in episodic percolation at the repository horizon. The negative results of the model using these data justify this assumption. Furthermore, comparison of the data received under ITN: 00316.T with other infiltration scenarios shows that the upper-bound, glacial-average, infiltration scenario has the highest infiltration and has a similar spatial distribution, as expected. No further confirmation is required.

5.5   ASSUMPTIONS SPECIFIC TO UNSATURATED ZONE FLOW AND TRANSPORT BELOW THE REPOSITORY

Assumptions 1 and 5–9, documented in *UZ Flow Models and Submodels* (CRWMS M&O 2000 [122797], pp. 31–32), are quoted in Section 5.4.3 and are specifically applicable to the models documented in Section 6.5. No further confirmation is required.

5.5.1 Assumptions Specific to Fracture Flow in the Vitric Calico Hills Formation

Assumptions documented in Section 5 of *Analysis of Hydrologic Properties Data* (CRWMS M&O 2000 [145771]) and assumptions 1, 7, and 8 documented in *Calibrated Properties Model* (CRWMS M&O 2000 [144426], Section 5) are specifically applicable to the models documented in Section 6.5.1. No further confirmation is required.

Section 5 of *Analysis of Hydrologic Properties Data* (CRWMS M&O 2000 [145771]) states (the quote below is italicized and indented; notes for clarification are inserted in unindented, plain text):

> 1. *The subsurface heterogeneity of the unsaturated zone of Yucca Mountain is adequately represented by a number of model layers, each of which is assumed to have uniform hydrologic properties. This is based on the following considerations. First, the overall behavior of flow and transport processes in the unsaturated zone of Yucca Mountain is mainly determined by relatively large-scale heterogeneities introduced by stratification of the tuffs. Second, the complexity of a heterogeneity model needs to be consistent with the data availability. More complicated models generally introduce larger degrees of uncertainty in rock property estimations when data are limited. This is because more complicated models correspond to larger numbers of variables. Third, this layered approach is supported by field observations, such as matrix water saturation distributions. For a given geologic unit, measured matrix saturation distributions are very similar from different boreholes (Flint 1998, pp. 24-30, Figures 5-9), indicating that matrix flow behavior and effective hydraulic properties should be similar within the unit. A further discussion on this assumption is provided in an AMR describing conceptual and numerical models for UZ flow and transport. Based on the above reasoning, no confirmation is needed for this assumption.*

(Note: CRWMS M&O (2000 [141187] describes the conceptual and numerical model for UZ flow and transport.)

(Note: Flint 1998 [100033])

> 2. *Another major assumption is that van Genuchten (1980, pp. 892-898) relationships, originally developed for porous media, can be used as constitutive relations for the active fracture continuum. Not all connected fractures are active in conducting liquid water in the unsaturated zone of Yucca Mountain (Liu et al. 1998, pp. 2638-2641). The active fracture continuum consists of fractures that actively conduct liquid water. The use of van Genuchten relations is based on a conceptual model that flow in fractures can be described using porous medium equivalence. A further discussion on this conceptual model is provided in an AMR describing conceptual and numerical models for UZ flow and transport. No confirmation is needed for this assumption.*

(Note: CRWMS M&O (2000 [141187]) describes the conceptual and numerical model for UZ flow and transport.)

(Note: van Genuchten 1980 [100610])

(Note: Liu et al. 1998 [105729])

> 3. *Since a systematic approach for upscaling properties directly from small-scale measurements is still lacking for unsaturated fractured rocks, simple averaging schemes are assumed to be appropriate in most cases for the upscaling purpose in the analyses to be reported in this study. The relation of Paleologos et al. (1996, p. 1336), originally developed for porous media, is assumed to be appropriate for upscaling matrix permeability when an upper limit of 1.5 orders of magnitude is used for the amount of upscaling. Hydrologic property data have been determined on scales that are generally much smaller than the scales characterizing the subsurface heterogeneity (e.g., characteristic sizes for model layers). While considerable progress has been made in developing upscaling schemes for porous media, the scale-dependent behavior of a hydrologic property for fractured rocks can be very different from that for porous media. For example, the existence of fractures in a fractured rock, which may act as a capillary barrier, can increase tortuosity of liquid water in the matrix, and therefore reduce large-scale matrix permeability compared with the case without fractures. It is necessary to make this assumption to determine the rock properties using small-scale measurements. Note that the rock properties to be reported in this report are mainly used as initial estimates for use in the inversion process documented in an AMR describing calibrated properties model. The upscaling issue is further considered in the inversion process which results in the large-scale properties by matching the large-scale simulation results with grid block-scale observations averaged from small-scale data. Based on the above reasoning, no confirmation is needed for this assumption.*

(Note: Paleologos et al. 1996 [105736])

> 4. *It is assumed that a van Genuchten fracture* m *value, estimated from the middle nonlithophysal zone of the Topopah Spring welded unit (UZ Model layer tsw34), can be used as a representative estimate for all of UZ Model layers. This is based on the following considerations. First, for other model layers, there are limited data for determining the* m *values. Second, the* m *value determined in this report is only used as an initial guess for use in the inversion process documented in an AMR describing calibrated properties model. The inversion process results in more accurate* m *values for the model layers because it adjusts rock properties to make model simulation results match the relevant observations. Based on these considerations, no confirmation is needed for this assumption.*

(Note: CRWMS M&O (2000 [144426]) describes the calibrated properties model.)

Assumptions 1, 7, and 8 documented in *Calibrated Properties Model* (CRWMS M&O 2000 [144426], Section 5) states (the quote below is italicized and indented; notes for clarification are inserted in unindented, plain text):

> 1. *It is assumed that one-dimensional (1-D) vertical flow adequately describes the flow patterns around the boreholes used for rock mass (nonfault) property calibration…*
>
> *Inverse modeling involves many forward simulations, and therefore is computationally intensive. 1-D, columnar models are used because the time that is required for each forward simulation is short (a minute or less). Therefore many simulations, thousands in this case, can be accomplished in a reasonable (i.e., less than a day) time period. The effect of using 1-D columnar models is that all flow is forced to be vertical; there is no lateral flow. From the surface to the repository, lateral flow is not expected to be significant because perched water has not been found here. Below the repository, in the Calico Hills nonwelded unit (CHn…) and the Crater Flat undifferentiated unit (CFu), areas of perched water exist where lateral flow may be significant. Properties needed to produce perched water and varying degrees of lateral flow are not addressed in this AMR but will be addressed in a future AMR supporting the Unsaturated Zone Flow and Transport PMR. This future AMR will also address the suitability of other CHn and CFu properties with respect to flow changes as a result of perched water and lateral flow.*

(Note: CRWMS M&O (2000 [122797]) addresses perched water and lateral flow.)

> 7. *It is assumed that reported saturation values greater than 1.0 are equal to 1.0…*
>
> *Measurement error causes calculated saturation values (based on measurements of initial, saturated, and dry weight) to be greater than 1.0, but this is not physical, if possible saturation is physically constrained to a maximum of 1.0.*
>
> 8. *Because of data limitations and the way data were interpreted, estimates of uncertainty cannot be directly calculated for some of the data. In these cases, an appropriate uncertainty is selected (assumed) based on the uncertainties of similar data.*

(Note: The assumption is that appropriate uncertainties for one type of data may be estimated based solely on the uncertainty of similar data. The uncertainty assumed and the rationale for each particular assumption are presented in CRWMS M&O (2000 [144426], Section 6.1.2).)

The assumption that all flow in the vitric portion of the Calico Hills Formation (CHn(v)) is in the matrix such that it may be modeled using a single continuum is specifically applicable to the model documented in Section 6.5.1. *Rationale*: This assumption is supported by unsaturated zone flow tests conducted in nonwelded tuffs at Busted Butte and in Exploratory Studies Facility (ESF) Alcove 4. The tests at Busted Butte conducted in the upper CHn(v) show flow taking place completely in the matrix even though fractures are present, as reported in *Unsaturated*

Zone and Saturated Zone Transport Properties (U0100) (CRWMS M&O 2001 [154024], Section 6.8.9). Tests in ESF Alcove 4 that are conducted in the Paintbrush Tuff nonwelded hydrogeologic unit (PTn), which is comprised of nonwelded, vitric tuffs similar to those of the CHn(v), also show that flow around a large, through-going fracture is matrix dominated as reported in *In Situ Field Testing of Processes* (CRWMS M&O 2000 [141400], Section 6.7). Only when the matrix around the fracture becomes satiated does the fracture begin to flow. Thus, a single-continuum, matrix-only model for the CHn(v) is appropriate for all but saturated flow, which is neither expected nor predicted in the CHn(v) (CRWMS M&O 2000 [122797], Section 6.2). No further confirmation is required.

5.5.2   Assumptions Specific to Fault Characteristics in the CHn and CFu

The assumption that the limited data specific to the CHn fracture system and analog data, documented in *Analysis of Hydrologic Properties Data* (CRWMS M&O 2000 [145771], Sections 6.1 and 6.4.2) sufficiently describe the expected values and distributions for fracture permeability and capillarity of the CHn and Crater Flat undifferentiated tuffs (CFu) is specifically applicable to the model documented in Section 6.5.2. *Rationale*: The limited data characterizing the CHn fracture system, i.e. one measurement of permeability and 39 fractures observed in boreholes (CRWMS M&O 2000 [145771], Tables 5 and 6, respectively), make the estimates of fracture permeability and capillarity highly uncertain. This uncertainty is increased by the application of these data, which are all from the upper layers of the CHn, to the entirety of the CHn and Crater Flat undifferentiated tuffs (CFu). The uncertainty of permeability is treated by sensitivity studies with variation of permeability over two orders of magnitude. This is about four times the average observed standard deviation of fracture permeability for any one layer (CRWMS M&O 2000 [145771], Table 5). The uncertainty of capillarity is treated by variation over one order of magnitude. Capillarity, or the van Genuchten α parameter, is proportional to the cube root of fracture permeability over fracture frequency (CRWMS M&O 2000 [145771], equations 7 and 9), and the uncertainty of fracture frequency is about a factor of two (CRWMS M&O 2000 [145771], Table 6). This, combined with the uncertainty of permeability, gives a rough estimate of the uncertainty of van Genuchten α parameter as about a quarter an order of magnitude, again four times less than the variation used in the sensitivity study. In addition to the large ranges around the expected values, an alternative model of an impermeable fault is modeled. These ranges as well as the alternative model should sufficiently characterize the uncertainty of fault parameters. No further confirmation is required.

5.5.3   Assumptions Specific to Perched Water Models

There are no additional assumptions specific to the model documented in Section 5.5.3.

5.5.4   Assumptions Specific to Radionuclide Release into Matrix Rock

The assumption that radionuclides released from the emplacement drifts would have to diffuse or advect through rock matrix prior to entering the fracture system is specifically applicable to the model documented in Section 6.5.4. *Rationale*: In the absence of substantial and/or long term percolation out of the emplacement drift into the fracture system, the most likely immediate pathway for radionuclides out of the engineered barrier system (EBS) will be through the matrix. This is because, first, the rock matrix forms approximately 99% of the boundary of the

emplacement drift (the other approximately 1% being fractures that are open to the drift) (CRWMS M&O 2000 [145771], Sections 6.1 and 6.2); and second, the rock below the drift invert will be drier because of a shadow effect (Houseworth et al. 2001 [155876]), will have lower (more negative) capillary pressure, and will imbibe water escaping the drift. Radionuclides will be forced to diffuse or advect through the rock matrix until encountering a flowing fracture. No further confirmation is required.

INTENTIONALLY LEFT BLANK

6.   ANALYSIS/MODEL

6.1   INTRODUCTION

When analyses and models are used to represent the real world, a certain amount of uncertainty is inherent in those analyses and models. This uncertainty is generally due to data limitations. That is, because the data are only a sampling of a process or property, or represent a process or property at a single, or multiple but discrete, scale(s), there is inherent uncertainty about the representation of that process or property by the data. In the analyses and models used for unsaturated zone (UZ) flow and transport, uncertainty has been treated in several ways: (1) by characterizing the uncertainty in the analysis or model by defining a most likely scenario and then by varying key parameters to define a probability distribution about the most likely scenario of other, less likely, scenarios, (2) by specifying a process, e.g. seepage enhancement due to rock bolts, as low consequence and then treating that process conservatively, and (3) where no data exist for a process or property, and thus the uncertainty of that process or property can not be characterized, by using data about an analogous process or property to define the scenario.

In addition to how they treat uncertainty, analyses and models used to represent the real world are required to simplify the processes and properties of the real world. Because the real world is extremely complex, i.e. processes and properties can be extremely variable in space and time and may have different effective characteristics when considered on different scales, analyses and models must use simplified descriptions of the processes and properties to efficiently predict flow and transport in the UZ.

In general, uncertainty and simplification have been treated in a conservative manner. Conservatism allows performance to be judged with confidence that conditions are not likely to be worse. However, it is difficult to predict how treatment of uncertainty and simplification in upstream models will eventually affect the results of more complex downstream models. Low consequence processes that are conservatively treated in upstream models may cause higher consequence impacts to downstream model results.

In an effort to better understand the consequences of the previous treatment of uncertainty and simplification, supplemental studies have been performed, and are presented here for several areas of interest. Section 6.2 is a review of the geochemical data available for conceptual model development and numerical model calibration and validation. This is a data type that is frequently difficult to interpret and is also difficult to use for model calibration and/or validation, as it requires a fully developed flow and transport model. Section 6.3 is a review of computation methods currently used for transport calculations and an investigation of alternative methods specifically to capture transient matrix diffusion behavior, a process that has previously been treated in a simplified manner. Section 6.4 is an investigation of several processes affecting seepage using more detailed models and/or alternative approaches to those previously used. Section 6.5 is an investigation of several processes affecting flow and transport below the repository using alternative approaches to those previously used.

Most of the studies documented in this AMR represent analyses that use previously developed models to better characterize uncertainty and to ascertain the importance of further investigation on a property or process. As such, they do not require validation, specifically:

- Section 6.2 documents a summary of geochemical data that does not rely on developed models and, thus, does not require validation.

- Section 6.3.1 documents a comparison of different codes. A validation-type exercise for the newly developed DCPT V2.0 (LBNL 2001 [154342]) is included for informational purposes to demonstrate the fitness of this code, however information about the validation of a code is found in the software documentation.

- Section 6.4.1.1 documents the development of new data through an analysis that uses a previously developed and validated model.

- Sections 6.3.2, 6.4.3, 6.5.2, 6.5.3, 6.5.4, document supplemental uncertainty analyses evaluating the effect of alternative parameter combinations using previously developed and validated models.

The development and validation of new models is documented in Sections 6.4.1.2, 6.4.2, 6.4.4, and 6.5.1.

The Scientific Notebooks (SNs) listed in Table 6.1-1 document the input and output files presented in DTNs listed in Section 8.4 and provide all details needed to reproduce the modeling activities performed in support of the discussions and conclusions in this AMR.

Table 6.1-1.   Scientific Notebooks

LBNL Scientific Notebook ID	YMP M&O Scientific Notebook ID	Page numbers	Citation
YMP-LBNL-CFT-GL-1	SN-LBNL-SCI-033-V1	128–129, 145–149	Li 2000 [153480]
YMP-LBNL-CFT-GL-2	SN-LBNL-SCI-189-V1	22–67	Bodvarsson 2001 [156334]
YMP-LBNL-DSM-CFA-1	SN-LBNL-SCI-180-V1	62, 63, 68–70	Bodvarsson 2001 [156334]
YMP-LBNL-GSB-1.1.2	SN-LBNL-SCI-003-V1	81–83	Ahlers 2000 [155853]
YMP-LBNL-GSB-1.6.4	SN-LBNL-SCI-085-V2	24–25	Bodvarsson 2001 [156334]
YMP-LBNL-GSB-LHH-2	SN-LBNL-SCI-098-V1	90–94, 129–141	Liu 1999 [155675]
YMP-LBNL-GSB-LP-3	SN-LBNL-SCI-155-V1	142–145	Pan 2001 [155954]
YMP-LBNL-UZ-CFA-1	SN-LBNL-SCI-003-V2	19, 29–35	Bodvarsson 2001 [156334]
YMP-LBNL-UZ-JL-2.0	SN-LBNL-SCI-206-V1	72–88	Bodvarsson 2001 [156334]
YMP-LBNL-YSW-2	SN-LBNL-SCI-120-V1	216–254	Wu 2001 [155676]
YMP-LBNL-YSW-4	SN-LBNL-SCI-200-V1	7–32	Bodvarsson 2001 [156334]
YMP-LBNL-YSW-JH-2	SN-LBNL-SCI-143-V1	122–123, 152	Hinds 2001 [155955]
YMP-LBNL-YSW-KEZ-1	SN-LBNL-SCI-197-V1	9–13, 39–48, 85	Zellmer 2001 [155956]
YMP-LBNL-YSW-KZ-1	SN-LBNL-SCI-202-V1	7–23	Bodvarsson 2001 [156334]

The importance of the models and analyses documented in this AMR is documented in Table 6.1-2. The following Sections do not document models or analyses: Section 6.2, Synthesis of Geochemical Information, documents available geochemical information; Section 6.3.1, Comparison of Transport Codes, documents codes used or available for use to simulate transport through the unsaturated zone at Yucca Mountain; Section 6.3.2, Matrix Block Discretization and its Effects on Unsaturated Zone Flow and Transport Simulations, documents advantages and disadvantages of using alternate matrix block discretization schemes.

Table 6.1-2   Importance of Model or Analysis

Model or Analysis (Section)	Importance
Seepage Enhancement due to Rockfall (6.4.1.1)	Level 3 – Used to confirm conservatism of abstraction approach
The Effect of Rock Bolts on Seepage (6.4.1.2)	Level 3 – Used to confirm conservatism of abstraction approach
Focusing and Discrete Flow Paths in the TSw (6.4.2)	Level 2 – Climate, Net Infiltration into the Mountain, and Unsaturated Flow
Percolation Redistribution and Lateral Flow in the PTn (6.4.3)	Level 3 – Alternative model for public confidence building
The Effect of Episodic Percolation on Seepage (6.4.4)	Level 3 – Used to confirm conservatism of abstraction approach
Fracture Flow in the Vitric Calico Hills Formation (6.5.1)	Level 3 – Alternative model for public confidence building
Fault Characteristics (6.5.2)	Level 3 – Uncertainty analysis for public confidence building
Perched Water Models (6.5.3)	Level 3 – Alternative model for public confidence building
Radionuclide Release into Matrix Rock (6.5.4)	Level 3 – Alternative model for public confidence building

6.2 SYNTHESIS OF GEOCHEMICAL INFORMATION

Geochemical information offers unique insights over large scales, both spatially and temporally, into the flow and transport processes in the UZ of Yucca Mountain. Different types of fluid samples analyzed in Yucca Mountain studies include precipitation, surface waters, pore waters, gases from the unsaturated zone, and perched water. Fluid geochemical parameters of importance to site characterization and repository evaluations include major, minor, and trace species, ages of fracture minerals, stable isotopes (hydrogen, carbon, oxygen), cosmogenic and atmospheric radionuclides (tritium, carbon-14, chlorine-36), radiogenic isotopes (isotopes of strontium, uranium, and uranium decay products), oxidation/reduction potentials, pH, redox-sensitive elements, and others (BSC 2001 [154874], Section 6.2). Data on stable isotopes, cosmogenic and atmospheric radionuclides, and radiogenic isotopes are used primarily for site-characterization purposes to develop and calibrate models for the hydrologic flow system. The major constituent and trace-element concentration data are used in both site characterization and radionuclide transport issues.

Geochemical and isotopic data have been used to constrain, calibrate, and validate the UZ Flow and Transport Model (FTM). For example, geochemical modeling of pore-water concentrations of chloride, sulfate, and chlorine-36 (CRWMS M&O 2000 [122797], Section 6.4) and calcite deposition in fractures and cavities (CRWMS M&O 2000 [122797], Section 6.5) has been used to constrain hydrological parameters such as infiltration/percolation flux.

This subsection presents a synthesis of available geochemical information at Yucca Mountain to support the continuous development of conceptual models for the FTM. Uncertainty issues regarding geochemical data and the limitations of the modeling approach are discussed in appropriate subsections. The synthesis is intended to present the data clearly and concisely in order to facilitate its further use in the development of conceptual and numerical models for flow distribution, perched water, and transport mechanisms in the UZ of Yucca Mountain and to reduce uncertainty in those areas. A discussion about matrix diffusion is also presented, based on the various lines of geochemical evidence.

6.2.1 Synthesis of Available Geochemical Data

Figure 6.2-1 illustrates a summary of the available geochemical and isotopic information related to UZ flow and transport, with brief discussions on each item presented below in this section.

6.2.1.1 Summary of Findings: Geochemical Composition of Pore Waters in the Different Hydrogeologic Units and in Perched Water

This subsection is based largely on the discussion in *Analysis of Geochemical Data for the Unsaturated Zone* (BSC 2001 [154874], Section 6.5.3). Pore-water samples were extracted by tri-axial compression or by centrifugation from unsaturated core samples recovered from dry-drilled boreholes. Pore waters extracted from the PTn are calcium-chloride or calcium-sulfate-type waters. Data for TSw pore waters are sparse because of the difficulty of extracting sufficient sample for analysis from densely welded core. In general, the TSw pore waters have equal quantities of Na and Ca. The dominant anion is bicarbonate, with a much smaller proportion of

sulfate than typical PTn waters. In terms of relative proportions of anions, the chemical composition of TSw waters is intermediate between those of the PTn and CHn.
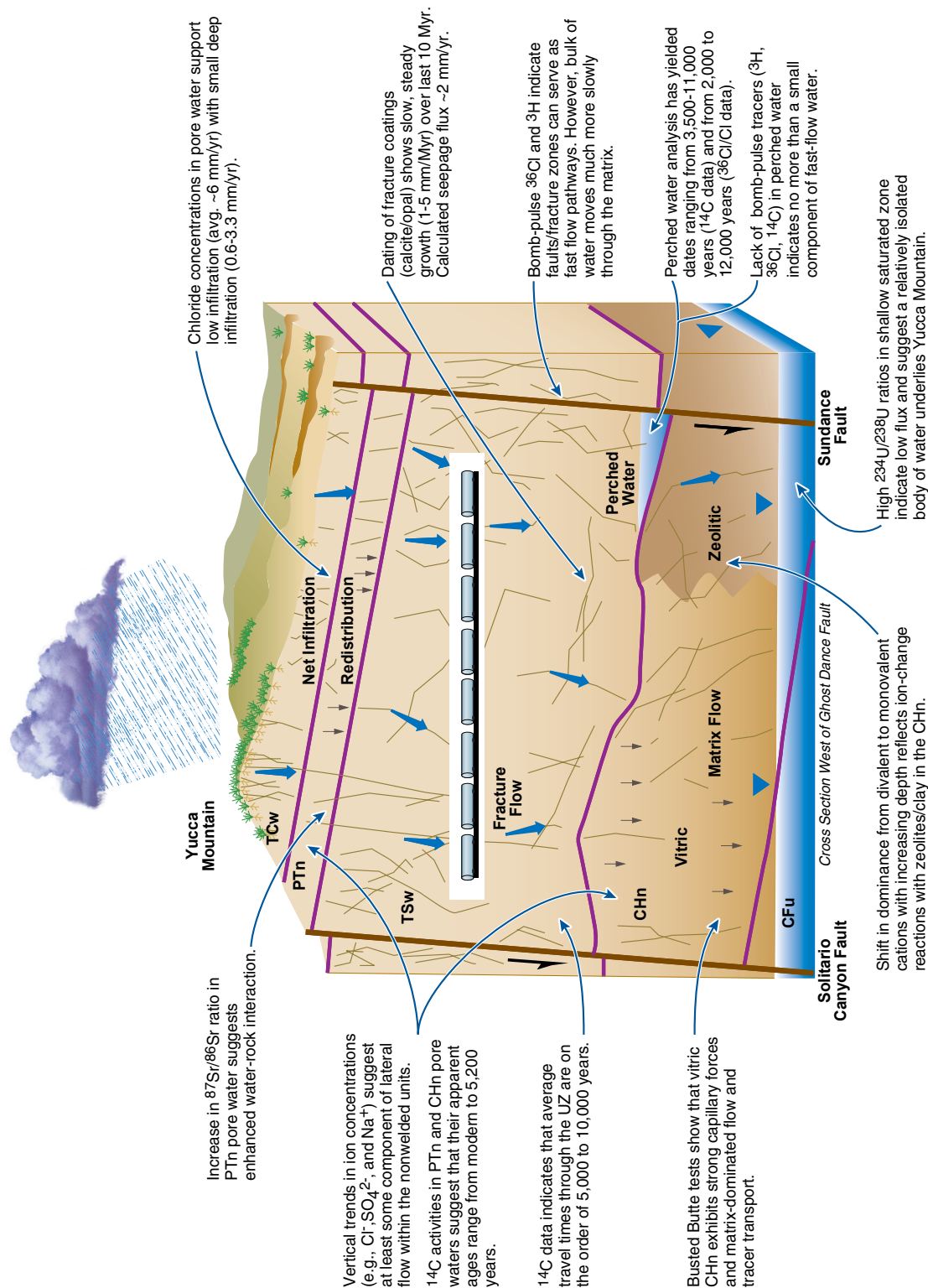
Figure 6.2-1.   Geochemical and Isotopic Information Related to UZ Flow and Transport

Pore waters extracted from the CHn unit are sodium carbonate-bicarbonate-type waters. Sodium concentration increases with increasing depth within the CHn. This shift in dominance from divalent to monovalent cations primarily reflects ion-exchange reactions with zeolites in the CHn unit (Figure 6.2-1). The zeolites preferentially take up calcium and magnesium while releasing sodium to the water (BSC 2001 [154874], Figures 14–16). Such ion-exchange processes (that lead to sorption and retardation) are also expected to operate on any cationic radionuclides (e.g., cesium and strontium) released from the potential repository into aqueous solutions that migrate into the zeolitic CHn. Deviations from vertical trends in ion concentrations (chloride, sulfate, sodium) suggest at least some component of lateral flow within the nonwelded units (BSC 2001 [154874]).

The pore-water strontium (Sr) data obtained from borehole USW SD-7 show that the ratio of $^{87}Sr/^{86}Sr$ increases with depth from ground surface to the repository horizon. This increase is steeper within the nonwelded units of the PTn and is flatter in the underlying TSw (BSC 2001 [154874], Figure 38). The increase in pore-water $^{87}Sr/^{86}Sr$ indicates that water infiltrating into or percolating through nonwelded PTn tuff reacts readily and acquires a strontium isotope signature that reflects interaction with this unit (Figure 6.2-1). Water infiltrating into welded tuff (TCw or TSw) tends to retain the strontium isotope composition of the overlying soil or PTn.

The existence of perched water bodies beneath Yucca Mountain is of interest because of potential implications for flow and transport in the UZ. Perched-water compositions are generally distinct from the compositions of unsaturated pore waters, although they are very similar to saturated-zone water compositions, suggesting that these waters are subject to similar water-rock interactions (e.g., mineral/rock dissolution and ion exchange) (BSC 2001 [154874], Section 6.5.3.2).

Chloride concentration data for pore waters from the TCw, PTn, TSw, and CHn hydrogeologic units were compared against data for precipitation, surface waters, perched waters, and saturated zone (SZ) waters to elucidate general trends (BSC 2001 [154874], Section 6.5.3.1). The smaller concentration of chloride, which behaves as a conservative groundwater tracer, in perched water implies that pore waters and perched waters have distinctly different histories of geochemical evolution, undergoing different degrees of evaporation and/or water-rock interaction. There are differing interpretations to explain the difference between chloride concentrations in perched and pore waters (CRWMS M&O 2000 [151940], Section 3.8.2). One explanation is that the perched water was derived from fracture water that is more dilute than that traveling through the matrix. Another explanation is that the perched water was derived from areas of higher infiltration (and lower chloride) that are found generally to the north of the potential repository area. A third explanation is that the perched water only forms during relatively short periods (thousands of years) of high infiltration associated with wetter glacial cycles. These hypotheses for the origin of perched water are not mutually exclusive.

The data available on pore-water and perched-water chemistry are limited in several ways (BSC 2001 [154874], Section 6.5.4). First, complete pore-water analyses are available mainly for those horizons in Yucca Mountain that contain nonwelded tuffs with relatively high porosities. Very few complete pore-water analyses are available for well-indurated, low-porosity rocks (for example, welded tuffs in the repository horizon). Second, pore-water and perched-water analyses are only available for samples from a limited number of boreholes. Third, the procedure for

extraction of water from the pores may have an impact on the water chemistry. Despite these restrictions, the major ion chemistry of the pore waters is sufficiently consistent and the controls on this chemistry are sufficiently well understood that bounds can be placed on the likely range of variations to be expected. An important parameter in estimation of these bounds is the net infiltration rate over the regulatory period.

Apparent infiltration rates were estimated by the chloride mass balance method, using chloride concentrations for pore-water samples (BSC 2001 [154874], Section 7.4). The infiltration rates in the PTn were generally higher than the rates estimated for alluvium (which is less than 0.5 mm/yr), presumably caused by lateral flow and mixing within the PTn unit. PTn samples beneath deep alluvium had infiltration rates between 0.6 and 3.3 mm/yr. The overall average infiltration rate for pore-water samples collected along the Main Drift and Cross Drift (30 samples) is about 6 mm/yr (Figure 6.2-1).

6.2.1.2   Summary of Findings: Ages of Pore Waters in the Different Hydrogeologic Units and in Perched Water

The best-developed isotopic method for dating groundwater is that using ^{14}C (BSC 2001 [154874], Section 6.6.4.1). In general, ^{14}C activities in pore waters from both the PTn and CHn yield apparent ages ranging from modern to 5,200 years (Figure 6.2-1). Apparent ages are based on the assumption (see Section 5.2, assumption "a") that the initial ^{14}C activity is 100 pmc (Percent Modern Carbon) and that the carbon isotopic composition of the sample has not been significantly altered by any geochemical processes so that changes relative to the initial atmospheric ^{14}C activity are solely the result of radioactive decay. The data do not show any trend with stratigraphic depth in the UZ. In fact, larger ^{14}C activities are interspersed among smaller ^{14}C activities in a vertical profile. These profile inversions are consistent with a conceptual model in which fracture flow and perhaps lateral flow occur in some of the units. Radiocarbon ages for PTn pore-water samples span a narrower range than for CHn pore waters, as expected if the CHn unit were fed by fracture flow mixing to variable extents with slower matrix flow (BSC 2001 [154874], Section 7.2).

Questions regarding corrections to the radiocarbon ages remain to be resolved. The extent of contamination of pore-water samples with drilling air has not been quantified; such contamination would shift the isotopic signature to apparently younger ages. Pore-water and perched-water ^{14}C activities can also be diluted by the dissolution of older carbon in the carbonate minerals, which would result in anomalously old apparent ages. Reaction with or incorporation of gas-phase CO_2 from deep in the unsaturated zone can also result in an anomalous apparent age (BSC 2001 [154874], Section 7.2).

The ^{14}C values for perched water indicate an apparent age of 3,500 to 11,000 years (BSC 2001 [154874], Section 6.9.3). The ^{36}Cl analyses of perched water indicate its ages ranging from 2,000 to 12,000 years for the different perched-water bodies sampled, which is in general agreement with ^{14}C-based ages (BSC 2001 [154874], Section 6.6.3.6).

The fact that perched water samples appear to be up to 11,000 years old, based on ^{14}C and ^{36}Cl ages, supports the explanation that the perched water was derived from an earlier period(s) of increased infiltration rates (Section 6.2.1.1). Major ion concentrations and uranium isotope data

suggest that these water bodies were formed by water flowing through fractures in the UZ rather than through the matrix. These waters do not appear to have equilibrated with water in the matrix of units in which the perched-water bodies are found. This supports a distinct origin (e.g., fracture flow) for these waters and a very slow exchange between fracture and matrix reservoirs (BSC 2001 [154874], Section 7.5).

6.2.1.3   Summary of Findings: Chlorine-36 and Tritium

Chlorine-36 analyses exist for several hundred rock samples from surface-based boreholes and the ESF (BSC 2001 [154874], Section 7.2). Bomb-pulse concentrations are present in the PTn at several locations and in the vicinity of some fault zones in the ESF, which indicates that water has flowed to at least the depth of the ESF in less than 50 years. This water presumably flowed along pathways that included fractures and/or faults (Figure 6.2-1). To account for the data, there must also be flow pathways such as fractures and/or faults through the PTn. It is difficult to quantify how much of the total percolation flux results from fracture flow. The available hydrochemical data, *in toto,* suggest the proportion is small, which implies that most of the water in the UZ moves through the matrix (BSC 2001 [154874], Section 7.3).

The analytical uncertainty for tritium analysis is 4 tritium unit (TU) based on counting statistics. All values above 25 TU are considered to lie outside the range of the population of background samples (BSC 2001 [154874], Sections 6.2.6 and 6.6.2.2). The limitation of this approach is that "background" in this case includes postbomb waters that have decayed to prebomb tritium levels. Detectable levels of tritium (> 25 tritium units) have been observed in the Bow Ridge Fault Zone in ESF Alcove 2 and in about 6% of the pore waters extracted from core samples from 11 surface-based boreholes. These detections occur within the TCw, PTn and TSw, and also in some samples from the CHn, as deep as the Prow Pass member of the CFu (BSC 2001 [154874], Section 6.6.2.3). No bomb-pulse tritium was detected in TSw samples from the drillhole transecting the Ghost Dance fault in the Northern Ghost Dance Fault Access Drift (Alcove 6), despite the fact that elevated levels of ^{36}Cl were detected in Alcove 6. Tritium data for some of the UZ boreholes show several inversions in which samples with larger tritium concentrations occur below samples with background values in a vertical profile. Such inversion is strong evidence for the occurrence of fracture and lateral flow at Yucca Mountain (BSC 2001 [154874], Section 7.2). No postbomb water is detectable in the perched water by any of the three bomb-pulse isotope signals (^{3}H, ^{14}C and ^{36}Cl) (BSC 2001 [154874], Section 7.2).

To provide additional confirmation about the fast-flow water, work is currently underway to evaluate more thoroughly the distribution of ^{36}Cl/Cl across two structural zones within the ESF (Drill Hole Wash Fault and Sundance Fault) that exhibited bomb-pulse signatures in previous studies. The work uses a suite of bomb-pulse indicators including ^{36}Cl/Cl, ^{3}H, ^{99}Tc, and ^{129}I (BSC 2001 [154874], Section 6.10.3.10).

6.2.1.4   Summary of Findings: Uranium Isotopes

Uranium isotopic ratios have been used to address the prevalence and frequency of fracture flow through the UZ at Yucca Mountain and the issue of local recharge to the water table. Substantial differences in ^{234}U/^{238}U activity ratios between pore water and fracture water (from ^{234}U/^{238}U in

fracture minerals as well as perched water) imply that there may be minimal liquid exchange between these two types of flow pathways (BSC 2001 [154874], Section 6.6.7).

Groundwater from the SZ beneath Yucca Mountain has elevated $^{234}U/^{238}U$ activity ratios (between 6 and 8.5) compared to water from wells in adjacent areas to the south (between 1.5 and 4 (BSC 2001 [154874], Figure 42)). Groundwater obtained from Paleozoic carbonate rocks at depth beneath Yucca Mountain (UE-25 p#1) has a much smaller $^{234}U/^{238}U$ ratio of 2.32, which is typical of the regional carbonate aquifer and is indicative of the stratification of shallow and deep aquifers at the site (Figure 6.2-1). The anomalous uranium isotopic compositions of shallow SZ water beneath Yucca Mountain are similar to the $^{234}U/^{238}U$ compositions measured for deep UZ minerals and perched-water bodies within the welded TSw. This similarity supports the concept of recharge through the thick UZ at Yucca Mountain, and that much of the local recharge derives from flow through fracture pathways in the deep UZ rather than from percolation through the matrix column (BSC 2001 [154874], Section 6.6.7).

6.2.1.5 Summary of Findings: Fracture-Lining Minerals

Deposits of calcite and opal lining fractures and cavities in the ESF contain spatial and temporal information on past migration of water through the UZ at Yucca Mountain. These mineral coatings provide a record of past water percolation through the connected fracture network in areas where solutions exceed chemical saturation with respect to various mineral phases. Observations of (1) mineral textures, (2) the fact that less than 10% of all fractures and open spaces contain coatings of calcite and opal, and (3) the restriction of minerals to fracture footwalls and cavity floors are all consistent with deposition from thin films of descending fracture water at locations where solutions lose carbon dioxide and water vapor (BSC 2001 [154874], Sections 6.10.3 and 7.6).

Calcite is abundant in the calcic soils at Yucca Mountain, leading to rapid saturation of infiltrating water with respect to calcite. The volcanic rocks are calcium-poor, so infiltrating water is essentially the only source of Ca available to form the calcite in the UZ. Therefore, the calcite that has formed in a cavity can be related directly to an amount of water required to transport that amount of Ca into the cavity. The calculated amount of water would be a minimum estimate of the amount of water that actually seeped into the cavity, unless the water evaporated completely within the cavity. The total seepage flux for the whole UZ, based on measurements of total calcite abundance in the ESF, indicates a flux of about 2 mm/yr, which is within an order of magnitude of the estimated long-term infiltration flux at the surface (BSC 2001 [154874], Section 6.10.3.5).

Geochronological data indicate that calcite and opal grow at extremely slow and relatively uniform rates for millions of years. Radiocarbon, uranium-thorium, and uranium-lead ages for outer (youngest) mineral surfaces range from less than 10,000 to about 1.5 million years. Uranium-lead ages for interior (older) layers of opal and chalcedony range from 0.5 to 10 million years and result in calculated long-term average deposition rates of about 1 to 5 mm/million years. These rates are consistent with estimates based on uranium-thorium ages for subsamples deposited over the last half-million years (BSC 2001 [154874], Section 7.6).

Stable isotope compositions ($\delta^{13}C$ and $\delta^{18}O$) of calcite deposited over the last several million years span a wide range of values, indicating deposition from water originating from both pluvial and interpluvial precipitation. This is consistent with climate fluctuations documented throughout the region. However, uniform mineral growth rates imply that fracture flow in the deep UZ at Yucca Mountain did not vary substantially despite these climate variations. In addition, $^{230}Th/U$ ages do not show clustering that can be correlated with cycles of pluvial-interpluvial climate over the last 200,000 years. Initial $^{234}U/^{238}U$ ratios calculated for opal and calcite deposited within the potential repository horizon also imply that deep UZ fracture flow at Yucca Mountain was low in volume or infrequent.

A combination of hydrogeologic factors has resulted in the long-term hydrologic stability of the fracture-flow system at the level of the potential repository horizon (BSC 2001 [154874], Section 7.6). These factors include (1) increased runoff and surface drainage in response to additional precipitation, (2) downslope diversion along the colluvium-bedrock interface, (3) increased vegetation during wetter climates (leading to greater rates of evapotranspiration), and (4) the presence of nonwelded tuffs with large matrix permeabilities in the PTn overlying the fractured, densely welded tuffs.

6.2.1.6   Summary of Findings: Busted Butte Studies

The Busted Butte test facility is located 8 km southeast of the potential Yucca Mountain repository area and was chosen as a test location, based on its readily accessible exposure of the TSw and vitric CHn (CRWMS M&O 2001 [154024], Sections 6.8.1.1 and 6.8.1.2).

Tracer tests in the Busted Butte indicate that strong capillary forces in the rock matrix of the vitric CHn are likely to modulate fracture flow from overlying units, thereby damping pulses of infiltrating water. The vitric CHn behaves as a porous medium, which will provide a large degree of contact between potential radionuclides and the rock matrix, and hence prolong their travel time through this unit (Figure 6.2-1).

The Phase-1B experiment of the Busted Butte tests showed that, even when injection occurs immediately adjacent to a fracture, water appears to be imbibed quickly into the surrounding matrix. Under the injection rate of 10 mL/hr, the transport times for the nonsorbing tracers were observed to be on the order of 30 days over a distance of about 28 cm, whereas pure fracture flow would have resulted in travel times of minutes to hours at this flow rate. For a sorbing tracer like lithium, the low and late breakthrough indicates that sorption significantly delayed its migration (CRWMS M&O 2001 [154024], Section 6.8.9).

6.2.2   Summary of Findings: Matrix Diffusion

6.2.2.1   Geochemical Evidence Related to Matrix Diffusion

It is well accepted that matrix diffusion can be a very important mechanism for the removal of solute/radionuclides from advective transport in the fractures in the saturated system (Freeze and Cherry 1979 [101173], pp. 408–413; Neretnieks 1993 [123099]). This mechanism is especially important for the sorbing radionuclides because matrix diffusion increases the chances for the radionuclide to contact with the matrix sorbent, which consequently leads to their sorption.

Matrix diffusion will occur wherever there is a solute concentration gradient between fracture and matrix water; this is also true for back-diffusion, in which solute is transferred from matrix to fracture in response to concentration gradient. The importance of matrix diffusion in the UZ, however, has not been fully determined. Relevant lines of geochemical evidence presented in BSC 2001 [154874] have been reviewed with respect to their implications for matrix diffusion and solute transport. It appears that the evidence does not directly support the significant contribution of matrix diffusion in the UZ. On the other hand, the geochemical evidence does not refute the occurrence of matrix diffusion. Basically, this is related to the constraints of geochemical studies, as discussed below:

- The sampling and analysis protocol for geochemical studies might be one of the major reasons for the lack of direct evidence of matrix diffusion. As the pore water is extracted from the rock samples, it homogenizes the diffusion concentration profiles, while the measurable chemical/isotopic tracer concentration might be only in the centimeter range from the fracture-matrix interface (see the discussion of Section 6.5.2.1).

- Very few pore-water analyses have been performed on the densely welded samples, because the low porosity (and hence low storage of water) does not yield sufficient sample size for analysis. It happens that, in the densely welded tuff, fractures exist in large numbers and significantly affect flow and transport because of the large permeability contrast between fractures and matrix.

- Fracture water percolating through the UZ has not been sampled at Yucca Mountain (BSC 2001 [154874], Section 6.10.3.3), and this makes it difficult to obtain the direct and convincing evidence required to interpret matrix diffusion from the geochemical studies. Specific measurements of the concentration profile in the matrix from the flowing fractures are required to investigate matrix diffusion in the unsaturated fractured rocks.

- The chemical/isotopic tracer source term is very difficult to constrain in the geochemical studies that use natural tracers. Well-defined tracer tests are necessary (Section 6.2.3).

- Mass transfer between the fractures and rock matrix can occur by imbibition, because of the capillary pressure gradient (from fractures to the matrix) as well as matrix diffusion in response to the concentration gradient (in both directions between the fractures and matrix). Matrix imbibition, if it occurs, will mask and overwhelm the contribution of matrix diffusion.

There are no available reports about the direct geochemical measurements of matrix pore water and adjacent fracture water at Yucca Mountain. The only related data were presented by Thordarson (1965 [106585], pp. 75–80), who reported a marked difference in the salinity (i.e., dissolved solids) of the matrix pore and fracture water in zeolitized bedded tuff in Rainier Mesa and its vicinity at the Nevada Test Site. The specific conductance of the matrix pore water is 25 to 35 times (with the corresponding salinity roughly 18 to 30 times) greater than that of water perched in fractures. Note that these are average values, instead of discrete comparisons between

matrix water and that in the adjacent flowing fracture. The difference, which indicates limited interaction between fracture and matrix water, was explained to be related to differences in the residence time of the matrix pore water and fracture water, or to relatively saline matrix pore water at the time of its introduction into the tuff (Thordarson 1965 [106585], pp. 75–80).

Nevertheless, the current approach to matrix diffusion (CRWMS M&O 2000 [141389]) is supported by the analyses of flow and transport tests in Alcove 1 (CRWMS M&O 2000 [122797], Section 6.8.1). Alcove 1 is located near the North Portal of the ESF in the upper lithophysal zone of the TCw. The tests involved water application at the ground surface and seepage observation in Alcove 1 approximately 30 m below. At a second stage of the tests, a conservative tracer, bromide, was introduced into the infiltrating water. Hydrological properties calibrated to earlier seepage data were used in the tracer simulation. The simulated breakthrough curve closely matches the tracer concentration data and suggests the importance of matrix diffusion in delaying tracer transport.

6.2.2.2   Approach to Representing Tortuosity Factor in Matrix Diffusion Evaluation

The effective diffusion coefficient (D_e), which is the product of D_0, tortuosity factor (τ, $\tau < 1$) and water content (i.e., porosity ϕ and water saturation S_w), is used to account for rock geometry and saturation effects on matrix diffusion. The τ value describes the tortuous nature of pore networks, including dead-end pores and steric hindrance (in extremely narrow pores). In most cases, only the porosity of geological media can be easily determined while the τ values are unknown. This is also true for the YMP, because there are very limited experimental data on the τ distribution in the various Yucca Mountain geologic units. Only the diffusion in a few saturated devitrified tuffs has been experimentally conducted.

Since aqueous diffusion is analogous to electrical conductivity in porous media, a relationship similar to Archie's law (Archie 1942 [154430]) (i.e., an empirical correlation describing electrical conductivity in porous rocks) should be able to predict τ based solely on ϕ, as shown below (Grathwohl 2000 [141512], pp. 28–35, Eq. 2-33). (Note that Grathwohl's symbol ε for porosity is replaced by ϕ and τ as defined is $1/\tau_f$ as used by Grathwohl):

$$\tau = \phi^{m-1} \qquad\qquad (Eq. 1)$$

where m denotes the empirical Archie's law exponent. The concentration gradient that gives rise to the diffusive flux in this case is analogous to the electrical field. Grathwohl (2000 [141512], pp. 28–35) has compiled the observed m values in the literature. The m value varies between 1.8 and 2.0 in consolidated materials, and is 1.3 in unconsolidated sand. For a typical ϕ value of 0.4 for sandy materials, τ will be 0.76 for the m value of 1.3, which is consistent with reported τ values in sandy materials (e.g., Hu and Brusseau 1994 [122837]). In diffusion experiments with sedimentary rocks, values of m are observed to be close to 2 (i.e., $\tau = \phi$). Generally, in materials of low porosity (e.g., < 0.2), larger values of m (≥ 2) are found (Grathwohl 2000 [141512], pp. 28–35).

The approach of using the porosity value to approximate tortuosity was confirmed experimentally with the tested Yucca Mountain tuff samples under saturated conditions. From

[3]H_2O diffusion experiments in six devitrified tuff samples, a τ estimate of 0.0806 ± 0.035 was obtained for the tuff with the measured average porosity being 0.0767 ± 0.019 (Hu and Brusseau 1995 [122846]; CRWMS M&O 2000 [144331], Section 6.1.2.4); with the m value close to 2. This approach is expected to be applicable for the saturated system or where water saturation is high (e.g., tuff matrix in the welded units).

Less information exists on the effect of water content on effective diffusion coefficient in the tuff. Conca and Wright (1990 [101582]) determined D_e values for K^+ ions for a variety of water contents and grain sizes on angular gravels. For volumetric water contents ranging from 0.5% to 6%, the D_e ranged from 10^{-14} m^2/s to 10^{-11} m^2/s (i.e., the dependence was much stronger than what could be expected from a linear relationship between D_e and water content). At low moisture contents, many of the pores can be separated by thin films of liquid on the surfaces of the particles that surround empty pores, through which diffusion is evidently very slow. Rowell et al. (1967 [154646]) found that very little movement of chloride in a sandy loam soil occurred at moisture contents lower than 0.075. The tortuosity factor was 1×10^{-6}, 1.8×10^{-4}, and 9.9×10^{-3} at moisture contents of 0.013, 0.034, and 0.067, respectively. At higher moisture contents, the impedance factor increased in an almost linear relationship to the moisture content. The effects of water content, as well as the contribution of surface and internal waters to diffusion in porous tuff, deserve more attention. Diffusion models, which relate the effective diffusion coefficient to water content, porosity, and other parameters (such as suggested by Millington and Quirk (1961 [139143]) and Olesen et al. (1996 [155700])) can be employed in modeling diffusion in unsaturated media.

6.2.2.3 Testing to Reduce Uncertainty in Matrix Diffusion

The following tests should help to further evaluate matrix diffusion related to the conceptual models for the UZ Flow and Transport Model.

1. Field testing of matrix diffusion and transport: tests planned in YMP 2001 [155724] are specifically designed to validate a matrix diffusion conceptual model, wherein liquid tracers will be introduced into the enhanced characterization of repository block (ECRB) Alcove 8 and monitored 20 m below in Niche 3 in the ESF. The tests are to demonstrate the importance of matrix diffusion by using multiple nonsorbing tracers with different diffusivities. If matrix diffusion is important, it will be critical to accurately determine the fracture-matrix interface area that largely determines the degree of matrix diffusion. This area has been roughly estimated from fracture mapping data and has never been confirmed from the flow and transport data. Tracer-test results from Alcove 8/Niche 3 tests will estimate the fracture-matrix interface area under both saturated and unsaturated conditions.

2. Laboratory testing of matrix diffusion and transport: tracer tests are to be performed in a tuff block of 0.1–1.0 cubic meter in size to complement the larger-scale Alcove 8/Niche 3 field tests. The fracture network in the block will be characterized by mapping and flow testing (both gas and liquid). An appropriate background water (e.g., J-13 water) with and without a series of nonreactive tracers, each with different diffusivities, will be introduced to the top of the block to investigate matrix diffusion during seepage in the unsaturated, fractured system. Rates of water addition and

collection, tracer concentration, and other parameters will be monitored. Rock samples perpendicular to fractures will be collected, and tracer penetration into the matrix from fractures will be examined to provide a direct measure of matrix diffusion. Using models to analyze the data, the fracture-matrix interface area will also be evaluated.

3. Fracture water percolating through the UZ has not been sampled at Yucca Mountain. Fracture water is likely to have compositions similar to or even more chemically evolved than runoff samples, considering the interactions that take place during infiltration through calcite- and opal-rich soils and possible silicate/water interaction that occurs within the nonwelded tuffs of the PTn. To fully evaluate and interpret geochemical and isotopic information in the context of UZ flow and transport (e.g., matrix diffusion), fracture water needs to be collected and its chemical composition analyzed. Protocols need to be developed to collect reliable fracture water samples.

6.2.3 Conclusions and Recommendations

This subsection presents a synthesis of available geochemical information at Yucca Mountain to support the conceptual models used by the UZ Flow and Transport Model. The following conclusions can be drawn from this section:

1. Vertical trends of ion concentrations (chloride, sulfate, sodium) in the different hydrogeologic units suggest at least some component of lateral flow within the nonwelded units. The increase in pore-water $^{87}Sr/^{86}Sr$ in the PTn tuff suggests enhanced water-rock interaction. The shift in dominance from divalent to monovalent cations reflects the ion-exchange reactions with zeolites in the CHn unit. Busted Butte tests show that vitric CHn exhibits strong capillary forces and matrix-dominated flow and tracer transport. Chloride concentrations in pore water suggest low infiltration (avg. ~6 mm/yr) with even lower percolation at depth (0.6–3.3 mm/yr).

2. Carbon-14 activities in PTn and CHn pore waters suggest that their apparent ages range from modern to 5,200 years. The general trends of ^{14}C data indicate that average travel times through the UZ are on the order of 5,000 to 10,000 years. Perched water analysis has yielded dates ranging from 3,500 to 11,000 years (from ^{14}C data) and from 2,000 to 12,000 years (from $^{36}Cl/Cl$ data).

3. Bomb-pulse ^{36}Cl and ^3H indicate that faults/fracture zones can serve as fast flow pathways. However, most of the water moves much more slowly through the matrix. Lack of bomb-pulse tracers in perched water suggests no more than a small component of fast-flow water.

4. Because of the constraints of the geochemical studies, available geochemical evidence does not directly support or disprove the significance of matrix diffusion in the UZ. Tests are suggested to evaluate matrix diffusion conceptual models for the UZ Flow and Transport Model.

6.3 COMPARISON OF TRANSPORT-COMPUTATION METHODS

Modeling transport processes, especially in dual-permeability media, can be very complex. Conservative simplification of the transport processes is used in order to increase computational efficiency. For the UZ at Yucca Mountain this has generally meant neglecting the complex interaction of early time matrix diffusion and flow between fractures and matrix, or completely neglecting early time matrix diffusion altogether. In Section 6.3.1, codes previously used for transport modeling and a newly developed code are evaluated with respect to predicting transport at Yucca Mountain. In Section 6.3.2, flow and transport predicted by two matrix discretization schemes are evaluated with particular attention paid to early time diffusion.

6.3.1 Comparison of Transport Codes

Modeling 3-D chemical transport in unsaturated, heterogeneous, fractured porous media such as the UZ of Yucca Mountain is a challenging task in terms of both scientific basis and computing resources. The current models used in transport calculations are developed using the software codes T2R3D V1.4 (LBNL 1999 [113942]), FEHM Particle Tracker V2.0 (used in TSPA-SR, CRWMS M&O 2000 [153246]), and DCPT V1.0 (LBNL 1999 [132448]) (used in *Analysis Comparing Advective-Dispersive Transport Solution to Particle Tracking*, CRWMS M&O 2000 [141389]). T2R3D V1.4 (LBNL 1999 [113942]) is based on the integral finite-difference method of solving advection-dispersion equations (LBNL 1999 [113942]). FEHM Particle Tracker V2.0 uses the node-based particle-tracking method (CRWMS M&O 2000 [141418]) while DCPT V1.0 (LBNL 1999 [132448]) uses the random-walk-particle-tracking method (LBNL 1999 [132448]). The models developed using these three codes are based on the same dual-permeability grid with the steady-state flow field calculated using TOUGH2 V1.4 (LBNL 2000 [146496]).

The dual-permeability grid consists of two overlapped meshes that represent the fracture and the matrix continua, respectively, in a dual-continuum approach. The dual-continuum approach conceptualizes the flow and transport in fractured porous media as two spatially overlapping and interactive subprocesses (Figure 6.3-1). Global flow and transport can take place in both the fracture and the matrix continua, while mass transfer between the fractures and the matrix occurs locally in every grid cell. The major advantage of the dual-continuum model is its ability to capture the macro features of the flow and transport in the fractured porous rock with minimum computational resources. In the following subsections, each of these three codes and modeling approaches are described; inherent characteristics of each are presented.
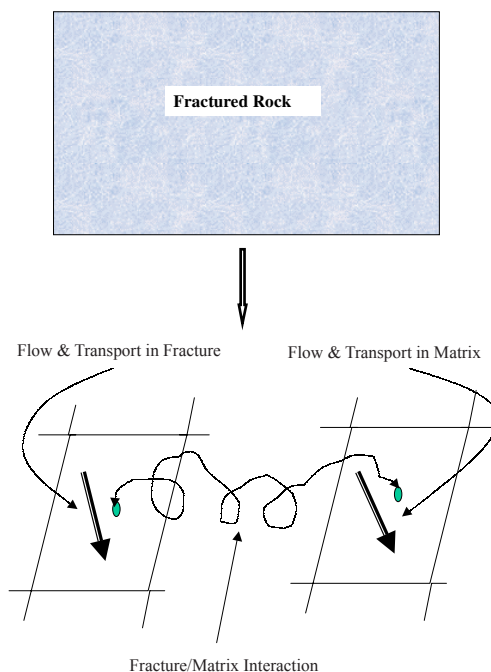
Figure 6.3-1.   Schematic of the Dual-Continuum Model

6.3.1.1   Current Modeling Codes

6.3.1.1.1   T2R3D V1.4

T2R3D V1.4 (LBNL 1999 [113942]) uses an integral finite-difference method to solve the advection-dispersion equations based on the dual-continuum grid. It treats the fracture-matrix interaction as an additional connection between the fracture grid node and the matrix grid node. The local mass transport between the fractures and the matrix is calculated using a finite-difference approximation, whereas both the interface area and the nodal distance are calculated based on the geometrical features of the fracture system (LBNL 1999 [113942]). It is capable of incorporating the anisotropy of the dispersion tensor. The primary dependent variable is the mass fraction, expressed on grid nodes. After tracers, representing radionuclides, released into the fracture continuum, the concentration gradient at the fracture-matrix interface is sharper near the front boundary of the tracer plume than further away from the front. But the finite-difference approximation of the concentration gradient at the fracture-matrix interface [used in T2R3D V1.4 (LBNL 1999 [113942])] does not make this distinction and uses instead a fixed node distance, and the average concentration in the matrix block, to calculate the diffusive flux at the fracture-matrix interface. Such average values account for the average behavior of the fracture-matrix mass exchange, but the small-scale features of the concentration gradient are missed. This discretization error could lead T2R3D V1.4 (LBNL 1999 [113942]) to significantly underestimate diffusive flux at early time, which results in overestimation of breakthrough at the water table for cases with small molecular diffusion coefficients and large fracture spacing. T2R3D V1.4 (LBNL 1999 [113942]) avoids this problem by making use of a Multiple Interactive Continua (MINC) or similar grid, which further splits the matrix gridblock into multiple nested sub-blocks. Using a more detailed grid would result in decreased efficiency of the simulations, and may not be acceptable for large-scale and multiple-realization transport

calculations used in the PA calculations of the Yucca Mountain UZ. In addition, the question of how to connect submatrix blocks of the MINC grid in the global matrix water flow field remains a difficult problem. Another disadvantage of T2R3D V1.4 (LBNL 1999 [113942]) is that it may suffer numerical dispersion and mixing, especially for cases with a coarser grid such as those likely to be used in the TSPA calculation.

6.3.1.1.2   FEHM V2.0

FEHM V2.0 uses the residence time/transfer function (RTTF) approach for tracking particles that calculates the probability of the residence time for a particle in a cell, as well as the probability of which adjacent cell the particle will enter if it leaves the current cell (CRWMS M&O 2000 [141418]). This approach is based upon analogies between the cumulative probability distribution function of the residence time and relative concentration as a function of time for a cell with a given flow path length (to account for diffusion/dispersion). In FEHM V2.0, particles can move between nodes only via advection. The residence time of a particle in a cell is calculated in two stages. It is first calculated as the ratio of the fluid mass in the cell to the sum of the outlet mass flow rates from the cell. Then it is used as a scaling factor to calculate a new residence time from a dimensionless residence time, to account for the diffusion/dispersion processes between nodes in the same continuum. The dimensionless residence time is determined randomly based on the cumulative probability distribution function of the residence time equivalent to a 1-D analytical solution of the advection-dispersion equation for the cell (with a step input function). A similar approach is used to determine the modified residence time that accounts for the effects of the fracture-matrix diffusion process for the particles in the fracture continuum.

The cumulative probability distribution function is based on an analytical solution for a dual-porosity system (i.e., where there is no water flow through the matrix or the fracture-matrix interface). The reason for this two-stage approach in FEHM V2.0 is to provide a more rapid calculation method that also avoids the discretization errors associated with large matrix grid cells. Note that the residence time from the first modification stage (accounting for the diffusion/dispersion in the same continuum) is a random value, but will be used to characterize the fracture-matrix transport system (i.e., the ratio of travel length along a fracture over the pore-water velocity in the fracture) in the second modification stage (accounting for diffusion between fracture and matrix). This implies that different fracture-matrix transport systems can exist for particles entering the same cell.

How the introduction of randomness into the fracture-matrix transport system affects the overall simulation of the transport is not theoretically clear. However, numerical experiments show that this effect may lead FEHM V2.0 to underestimate the increase in residence time due to diffusion into the matrix of particles traveling in the fractures (CRWMS M&O 2000 [134732], Section 6.2.5). For the particles in the matrix continuum, the fracture-matrix diffusion process is neglected in FEHM V2.0. In principle, the fracture-matrix diffusion process should increase the residence time for the particles traveling in the fracture continuum and decrease the residence time for the particles traveling in the matrix continuum, when the pore-water velocity in the fracture continuum is higher than that in the matrix continuum. (Velocities in the fractures are typically larger than those in the matrix by several orders of magnitude.) As a result, FEHM V2.0 can either underestimate or overestimate the breakthrough of nuclides to the water table,

depending on particular scenarios. Numerical experiments confirm this observation as shown in *Particle Tracking Model and Abstraction of Transport Processes* (CRWMS M&O 2000, [141418], Section 7) and *FY01 Supplemental Science and Performance Analysis, Volume 1: Scientific Basis and Analysis* (BSC 2001 [155950]). Furthermore, although FEHM V2.0 avoids the 1-D numerical dispersion by incorporating a 1-D analytical solution, it is not free from numerical mixing caused by multiple dimensional discretization and particle residence times.

6.3.1.1.3 DCPT V1.0

DCPT V1.0 (LBNL 1999 [132448]) simulates the transport of a plume by tracking the random walk of particles in a continuous 3-D space. However, the velocity field and other parameters are expressed on the grid nodes (grid cell-wise constant). A full dispersion tensor is incorporated. Particles travel either in the fractures or in the matrix. In DCPT V1.0 (LBNL 1999 [132448]), the mass exchange between the fractures and the matrix is simulated as a random-switch process between two continua controlled by the particle-transfer probabilities. This model is based upon analogies between the particle-transfer probabilities (either from fracture to matrix or vice versa) and the mass flux through the fracture-matrix interface with respect to the mass amount in each continuum. The approach is similar to the residence time/transfer function (RTTF) method used in the particle-tracking algorithm of FEHM V2.0. The difference is that DCPT V1.0 (LBNL 1999 [132448]) calculates the probability of a particle leaving the current continuum after a given duration, while FEHM V2.0 calculates the probability of how much time a particle will spend in a given cell. Although the continuum-switching of each particle is statistically independent of other particles, the calculation of the particle-transfer probabilities needs parameters describing the fracture-matrix system based on an approximation of the concentration gradient at the fracture-matrix interface.

In this regard, the concentration gradient at the interface will decrease as the particles diffuse farther into the matrix with time. DCPT V1.0 (LBNL 1999 [132448]) does not consider this dynamic feature, and uses the same approximation of the concentration gradient at the interface as that in T2R3D V1.4 (LBNL 1999 [113942]) to derive the solution of the particle-transfer probability. Thus, it has the same problem with dual-permeability grids as T2R3D V1.4 (LBNL 1999 [113942]). The transport calculation results found for these codes agree with each other (CRWMS M&O 2000 [141389]). However, DCPT V1.0 (LBNL 1999 [132448]) is free of numerical dispersion and mixing because the particles move in a continuing space. On the other hand, the pore water velocity is not available at every point except for some simple cases where an analytical solution of velocity is available. For the UZ of the Yucca Mountain, the velocity fields are calculated using TOUGH2 V1.4 (LBNL 2000 [146496]) on a discretized space (numerical grid). The exact velocity is unknown and has to be estimated from the flux on the interfaces between gridblocks. In multidimensional, heterogeneous, fractured porous media, accurate estimation of the velocity field from the fluxes on the interfaces remains a difficult problem for random-walk particle-tracking methods such as DCPT V1.0 (LBNL 1999 [132448]).

6.3.1.1.4 Methodological Uncertainties

Despite progress in understanding and modeling transport in fractured porous media, and the advances in computer resources in the past few decades, simulating transport of a tracer in heterogeneous fractured porous media is still a challenge. One of main difficulties is how to

simulate the mass transfer between fractures and matrix, two subdomains often having very different velocities. A discrete-fracture-network model, which describes the detailed spatial structure of a fracture-matrix transport system, is not feasible for the real-world problems such as those in the UZ of Yucca Mountain, because of the high requirements in both computer resources and field-measured data (parameters). Therefore, a dual-continuum approach is used in current models to numerically simulate the UZ transport system. However, discretization errors may be a significant problem when mass transfer between fractures and the matrix is mainly controlled by a slow diffusion process into a large matrix block (i.e., large fracture spacing, small fracture-matrix interface, and small diffusion coefficient), especially at early times (for example as shown in Figure 6.3-5).

The net effect is underestimation of the mass transfer flux into the matrix at early times, which usually makes the model (i.e., T2R3D V1.4 (LBNL 1999 [113942]), DCPT V1.0 (LBNL 1999 [132448])) a conservative predictor in the repository performance evaluation. FEHM V2.0 tends to avoid this discretization problem by using an analytical solution for a dual-porosity transport system. However, its implementation biases the calculation of the residence time because it excludes the diffusion process for the particles that entered the matrix via advection and ignores the differences in concentration gradients between early and later times. It may also introduce other uncertainties related to extending the 1-D analytical solutions for a dual-permeability system in which global water flow exists in both continua. The analytical solution on which it is based applies to a dual-porosity system where there is no flow through the matrix or the fracture-matrix interface. As a result, it can be either a conservative or an optimistic predictor in the repository performance evaluation, depending on particular scenarios.

The challenge is how to model the mass transfer between the fractures and the matrix within the framework of the dual-continuum approach, without missing the small-scale features of the diffusion front between the fractures and the matrix.

6.3.1.2   Improved Modeling Approach: DCPT V2.0

As discussed above, the dual-continuum model is a practical approach for simulation of the UZ transport, but it may be over-conservative. The reason is because the finite-difference approximation used to calculate mass transfer between fractures and the matrix may be subject to significant discretization errors for the cases with a larger matrix block. Recently, Pan and Bodvarsson (2001 [155875]) proposed a more accurate model for the fracture-matrix mass transfer within the framework of the dual-continuum random walk particle method (RWPM) by introducing the concept of *active range* to calculate particle transfer probability. Active range is defined as a function of particle age (the time since the particle first entered the domain) to capture the slower process of propagation (diffusion) of a disturbance in the fracture in the matrix without adding any additional sub-blocks for the matrix (as the MINC approach does). The following section describes the details of the model and its underlying theory.

6.3.1.2.1   Description of DCPT V2.0

The fracture-matrix mass transfer is simulated by tracking the particles transferred in either direction between the fractures and the matrix. This transfer is governed by the particle transfer probability. Equivalent to the finite-difference approximation for calculation of the mass transfer

rate between the fractures and the matrix, the particle transfer probability from Continuum 1 to Continuum 2 can be determined as (Pan and Bodvarsson 2001 [155875], Equation 5a or 5b and A7—after substitution of equivalent symbols):

$$P_{12} = \frac{F_{12}}{F_{out} + F_{12}}[1 - \exp(-\Delta t / T_c)] \qquad \text{(Eq. 1)}$$

where F_{12} is a parameter that describes the combined strengths of the water flow and the diffusion process through the interface between two continua. It is defined as follows ($Q_{12} = q_{fm}A_{12}$) (Pan and Bodvarsson 2001 [155875], Equation 6a or 6b):

$$F_{12} = \max(Q_{12}, 0) + \frac{D_{12} A_{12}}{S_{12}} \qquad \text{(Eq. 2)}$$

where the effective dispersion coefficient at the fracture-matrix interface is $D_{12} = D_{fm}\theta_m$, the fracture-matrix interface area is A_{12}, the characteristic distance of the fracture-matrix system is S_{12}, and θ_m is volumetric water content in the matrix. F_{out} is a parameter that is the sum of the total water outflow from the cell to adjacent cells and the strength of the dispersion process through their interfaces through Continuum 1 (Pan and Bodvarsson 2001 [155875], Equation 6b or 6e). The strength of the dispersion process can be calculated like the second term of Equation 2, but for each interface with the adjacent cells in the same continuum instead of the fracture-matrix interface. T_c is the characteristic time of Continuum 1 and is defined as a function of the water body volume in the cell (V_0), the retardation factor. (R) based on κ_d and defined in Equation 2 of Pan and Bodvarsson (2001 [155875]), F_{12}, and F_{out} (of Continuum 1) (Pan and Bodvarsson 2001 [155875], Equation 6c or 6f):

$$T_c = \frac{V_0 R}{F_{12} + F_{out}} \qquad \text{(Eq. 3)}$$

Equation 1 shows that the particle transfer probability is a function of the time step Δt, but not t itself. In other words, the particle transfer process is assumed to be a stationary random process (i.e., the probability density function is independent of time). This is because the concentration gradient at the fracture-matrix interface can be represented as the difference of the average concentrations in the fractures and the matrix divided by the node spacing (a fixed characteristic distance). In terms of particle walking, this is equivalent to assuming that the particles in a given pulse will have the same range to walk within the matrix over time. However, this is not a proper assumption at early times, when a plume has just entered the domain. Physically, a pulse in the fracture only has limited influence in the matrix at early times; significant time will be needed for the pulse to have its full range of influence, especially for cases with larger fracture spacing. As depicted in Figure 6.3-2 (lower part), the probability density function of the particle becomes wider and flatter with increasing time ($t_3 > t_2$ and $t_2 > t_1$). To catch this dynamic feature, the particle transfer probability defined in Equation 1 with Equation 2 and Equation 3 has to be modified by introducing a new concept: the active range. The active range is defined for each pulse such that the probability of finding a particle of the pulse outside of the range is practically zero; that is, all particles are confined to this spatial range over a time step. This leads to the replacement of the characteristic distance S_{12} and the water body volume V_0 in Equations 2 and 3

with the effective distance $S_{12}(t)$ and the effective volume $V_0(t)$, both of which are related to the active range. For parallel fracture systems, they can be defined as:

$$S_{12}(t) = S_{12} \frac{B^*(t)}{B} \qquad \text{(Eq. 4)}$$

and

$$V_0(t) = V_0 \frac{B^*(t)}{B} \qquad \text{(Eq. 5)}$$

where $B^*(t)$ is the active range within the matrix at time t. B is defined such that $2B$ is the fracture spacing. The effective volume for the fractures is assumed to be constant because the fracture aperture is usually so small that the active range can quickly reach its full capacity.
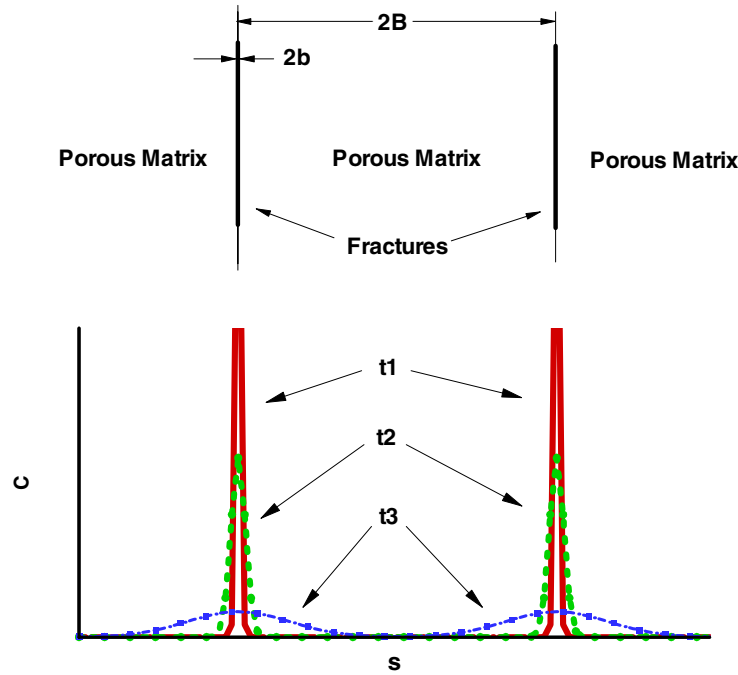
Figure 6.3-2.   Schematic of the Propagation of a Pulse in Fracture-Matrix System with Time

To get a scheme for estimating the active range $B^*(t)$, consider the transport in a system of parallel-plate fractures separated by porous rock (Figure 6.3-2). By the superposition principle, only the one-dimensional governing equation (in fracture-matrix dimension) is needed to derive the active range (temporarily ignoring advection):

$$\frac{\partial}{\partial t}[RC] = \frac{\partial}{\partial s}\left(D_{12}\frac{\partial C}{\partial s}\right) \qquad \text{(Eq. 6)}$$

where s is the distance into the matrix. With sources (and ignoring the fracture aperture $2b$ because b is much smaller than B) (Pan and Bodvarsson 2001 [155875], Equation 7):

$$C(s,0) = M_s \; \delta(s - 2iB) \qquad \text{(Eq. 7)}$$

where $\delta(s - 2iB)$ is a Dirac delta function whose value is zero everywhere except for an infinite value at point zero, which makes initial concentrations nonzero at the fractures only. The term M_s is a scaling factor that makes the concentration, C, in the final solution become a dimensionless variable within a range between 0 and 1. The i is the index of the fracture (from 0 to infinite). The solution to Equation 6, subject to Equation 7 follows the example of Bear (1988 [101379], Equation 10.6.10) for a single source (Pan and Bodvarsson 2001 [155875], Equation 8). For $s \geq 0$ and using symmetry:

$$C(s,t) = \frac{2 M_s}{(4 \pi D_{12} \, t/R)^{1/2}} \sum_{i=0}^{\infty} \exp(-\frac{(s - 2iB)^2}{4 D_{12} \, t/R}) \qquad \text{(Eq. 8)}$$

For very small time, only the first term in the series need be considered (Pan and Bodvarsson 2001 [155875], Equation 9):

$$C(s,t) \approx \frac{2 M_s}{(4 \pi D_{12} \, t/R)^{1/2}} \exp(-\frac{s^2}{4 D_{12} \, t/R}) \qquad \text{(Eq. 9)}$$

The concentration in Equation 9 can be interpreted as the probability of finding a particle (initially at $s = 0$) at location s and time t. Therefore, the probability a particle will be located in the active range $[0, B^*]$ is found by integrating Equation 9 with respect to s from 0 to B^* (Pan and Bodvarsson 2001 [155875], Equation 10):

$$P(0 \leq s \leq B^*) = \operatorname{erf}\left(\frac{B^*}{\sqrt{4 D_{12} \, t / R}}\right) \qquad \text{(Eq. 10)}$$

Equation 10 implies that B^* should be proportional to the square root of t. By definition, a B^* should be selected such that $P(0 \leq s \leq B^*)$ is close to 1. An adequate active range for short time can be expressed as (Pan and Bodvarsson 2001 [155875], Equation 11):

$$B^*(t) = \min\left(4 \; \sqrt{4 D_{12} \, t/R}, \; B\right) \qquad \text{(Eq. 11)}$$

The corresponding $P(0 \leq s \leq B^*)$ is close to 1 and B is half of the fracture spacing, which is the maximum active range by definition.

For a longer time, B^* approaches B, and the other terms in Equation 8 cannot be ignored. There is no simple solution like Equation 9 for that case. However, because the purpose is to get a proper $B^*(t)$, can be taken as the relative effects of the other terms in Equation 8 on the active range are equal to their relative contributions to concentration. In other words, the active range can be modified as follows (Pan and Bodvarsson 2001 [155875], Equation 12):

$$B^*(t) = \min\left(4 \; \sqrt{4 D_{12} \, t/R} \, W(t), \; B\right) \qquad \text{(Eq. 12)}$$

The weighting function $W(t)$ is obtained as the ratio of the two-term solution over the one-term solution as defined in Equation 8 at a given B^*, and can be approximated as (Pan and Bodvarsson 2001 [155875], Equation 13):

$$W(t) \approx 1 + \frac{1}{1 + \dfrac{B(B - B^*)}{D_{12}\, t/R}}$$ (Eq. 13)

The reason for taking only two terms in calculating the weighting function is because further terms are insignificant for typical values of B.

A similar approach can be used to incorporate the effects of fracture-matrix water flow on the active range. In a dual continuum model, the total water flow rate through the interface is known at $s = 0$) and at $s = B$ (where Q is zero). One can take a linear interpolation and get the final scheme for the active range as (Pan and Bodvarsson 2001 [155875], Equation 14):

$$B^*(t) = \min\left(4\sqrt{4 D_{12}\, t/R}\, W(t) + \frac{Q_{12}\, t}{A_{12}}\left(1 - \frac{B^*}{B}\right) B \right)$$ (Eq. 14)

Note that the time, t, used in the above equations is for a single pulse. Multiple initial values of time (i.e., $t = 0$) have to be defined for cases with multiple pulses. In other words, for the same pair of fracture and matrix cells at the same simulation time, the particle transfer probability may be different for different individual particles depending upon which pulse they originated in. The implementation in DCPT V2.0 (LBNL 2001 [154342]) tracks the age of each particle, which is defined as the time elapsed since the particle was released into the domain. Thus, the particle transfer probability is a function of the age of the particle.

The above derivation of the active range is valid only for particles initially released in the fractures. The active ranges for particles released into the matrix would be different, and depend on how far from the interface they are initially located, which is not known in practice. It is assumed that all particles initially released into the matrix are uniformly distributed within the matrix, and thus the active range will always be B. A parameter called "initial status" is assigned to each particle to distinguished which continuum it is released into initially (at $t_p=0$) where t_p is the age of the particle.

6.3.1.2.2   Verification with Analytical Solutions (Parallel Fractures)

An analytical solution for solute transport in fractured porous media with parallel fractures (Figure 6.3-3) was derived by Sudicky and Frind (1982 [105043]) with solute transport between fractures and matrix occurring through matrix diffusion in the horizontal direction only, and ignoring the matrix advection and diffusion in the vertical direction. In this dual-porosity model, water enters and leaves only via the fracture. Table 6.3-1 shows the relevant parameters for the test cases 1 and 2 with fracture spacing 1 m and 10 m, respectively. The values used, Table 6.3-1, are representative of typical values used for Yucca Mountain Modeling (see assumptions listed in Section 5.3). The analytical solution is obtained using parallelf.java V1.0 (LBNL 2001 [154346]).

This work is further documented in Pan (2001 [155954], pp.142–145). The grid used for the DCPT simulations is generated using WINGRIDDER V2.0 (LBNL 2001 [154785]).

Table 6.3-1.   Transport Parameters for a Parallel Fracture System

Parameter	Value
Molecular diffusion coefficient	2.5×10^{-11} m^2 /s
Fracture spacing	1.0 m (Case 1) or 10.0 m (Case 2)
Retardation factor	30
Velocity in fracture	1.1574×10^{-5} m/s (1.0 m/d)
Grid spacing	0.5 m
Matrix volume per cell	0.25 m^3 (Case 1) or 25.0 m^3 (Case 2)
Fracture volume per cell	0.5×10^{-5} m^3
Fracture-matrix interface area	0.5 m^2
Domain length (vertical)	36.75 m

DTN: LB0104AMRU0185.014

In Figures 6.3-4 through 6.3-6, results are shown in the form of breakthrough curves at the bottom of the model. These calculations are for a step increase in concentration at the top of the model, and the breakthrough curves are normalized concentration C/C_o. Figure 6.3-4 shows that for Case 1 (1 m fracture spacing) both DCPT V1.0 (LBNL 1999 [132448]) and DCPT V2.0 (LBNL 2001 [154342]) give breakthrough curves that agree well with the analytical solution (Note: CalBT.for V1.0 (LBNL 2001 [154788]) is a required preprocessor for DCPT V1.0 (LBNL 1999 [132448])). However for fracture spacing =10 m (Case 2, Figure 6.3-5), DCPT V1.0 (LBNL 1999 [132448]) overestimates the breakthrough at early times. The breakthrough curve reaches approximately 60% as early as 0.1 year (the earliest arrival, not shown in the figure). At much later times, however, DCPT V1.0 (LBNL 1999 [132448]) agrees well with the analytical solution. This phenomenon clearly indicates that the finite-difference approximation is accurate only for later times; the degree of the problem depends on the fracture spacing. DCPT V2.0 (LBNL 2001 [154342]) agrees nearly perfectly with the analytical solution in both cases because it catches the dynamic feature of the fracture-matrix mass transfer process. Additionally, the fracture spacing should have little effect at early times for this case, according to Equations 13 and 14. Figure 6.3-6 depicts the analytical solutions for Case 1 and Case 2 and shows that the early time breakthrough curve (until 5,000 years) is independent of the fracture spacing.
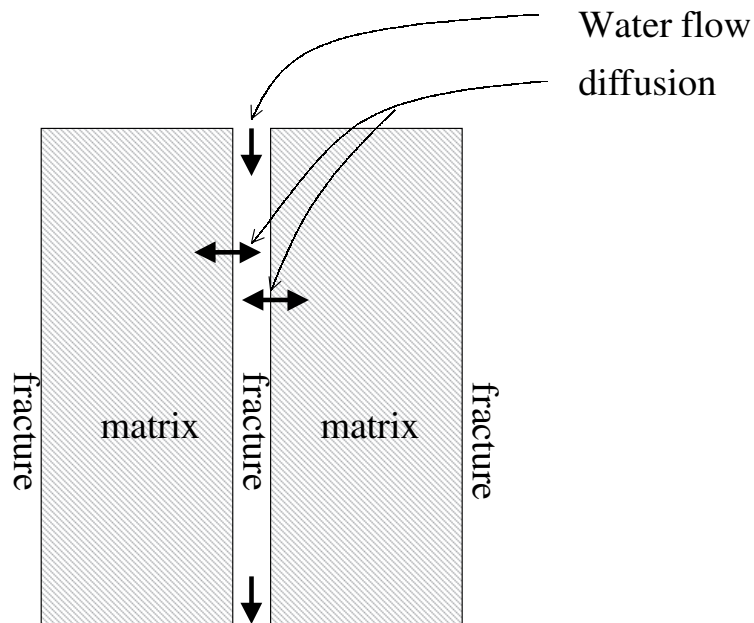
Figure 6.3-3.   Schematic of a Parallel Fracture System without Water Flow between the Fractures and the Matrix
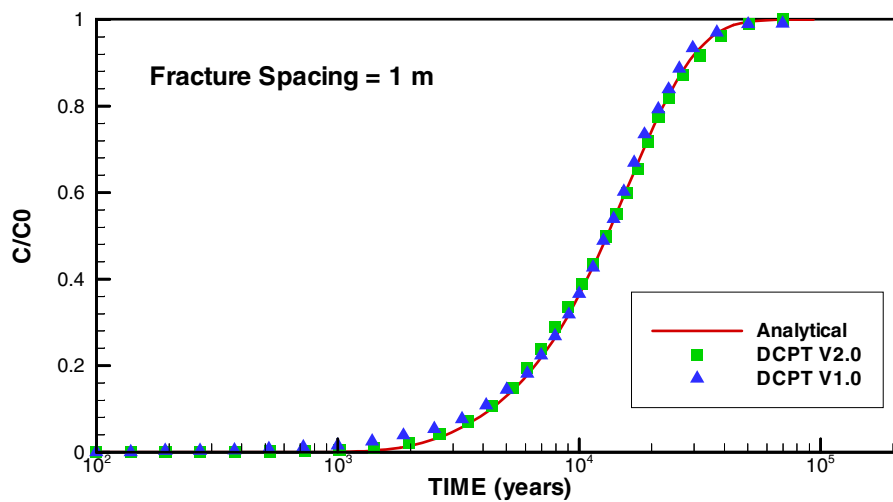
DTN: LB0104AMRU0185.001

Figure 6.3-4.   The Predicted Breakthrough by DCPT V1.0 (LBNL 1999 [132448]) and DCPT V2.0 (LBNL 2001 [154342]) and the Analytical Solution for the Case with 1 m Fracture Spacing
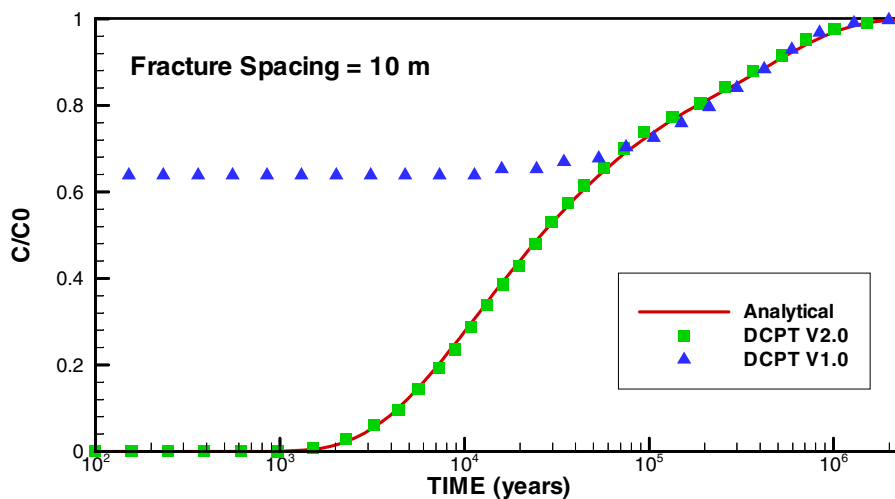
DTN: LB0104AMRU0185.001

Figure 6.3-5.   The Predicted Breakthrough by DCPT V1.0 (LBNL 1999 [132448]) and DCPT V2.0 (LBNL 2001 [154342]) and the Analytical Solution for the Case with 10 m Fracture Spacing
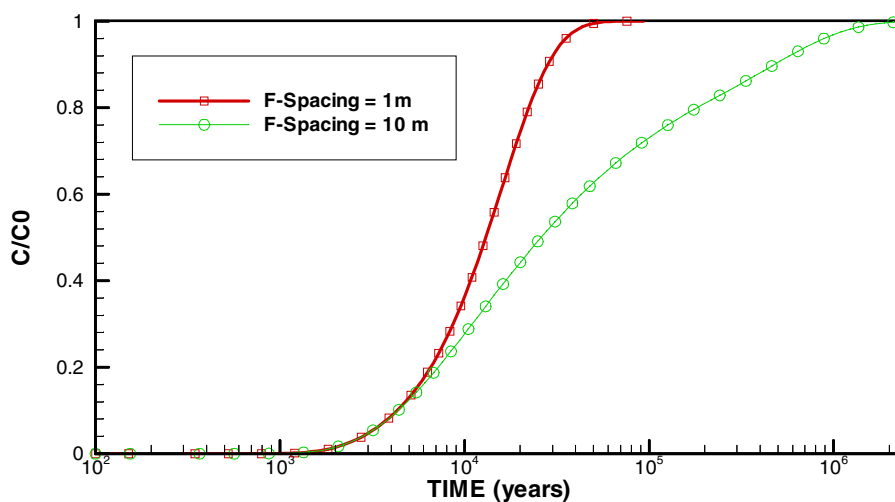
DTN: LB0104AMRU0185.001

Figure 6.3-6.   The Effect of Fracture Spacing on the Breakthrough as Function of Time (analytical solution)

6.3.1.2.3 Results: UZ transport

The case of TSPA UZ transport with the present-day mean infiltration map and Perched Water Table Model #1 is used to assess the impact of the different models of the fracture-matrix mass transfer. The grid for the transport simulations is created using DTN: LB0110MESHPROP.001 [156336] and Wingridder V1.1 (LBNL 2001 [154341]). Input files for DCPT are created using DNTs: LB990801233129.003 [122757]; LB9907012333129.001 [106785] and TOUGH2 V1.4 (LBNL 2000 [146496]). Figure 6.3-7 shows the cumulative breakthrough curves of two radionuclides at the water table predicted by the current model (DCPT V1.0 (LBNL 1999 [132448])) and the more-refined model (DCPT V2.0 (LBNL 2001 [154342])), respectively. The current model predicts faster early breakthrough compared to the more refined model for both radionuclides, especially for the conservative radionuclide.
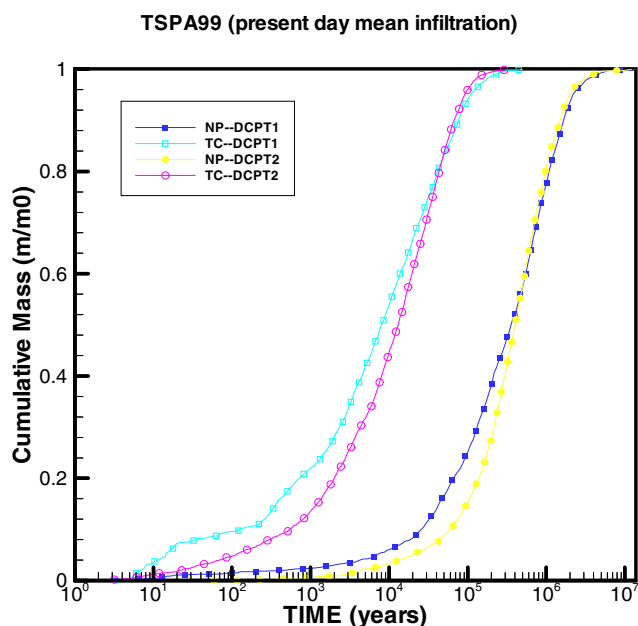
DTN: LB0104AMRU0185.001

Figure 6.3-7.   The Predicted Cumulative Breakthrough Curves for Base Case of the UZ Transport System by DCPT V1.0 (LBNL 1999 [132448]) and DCPT V2.0 (LBNL 2001 [154342]), for Sorbing (Np) and Non-sorbing (Tc) Tracers

6.3.1.3 Conclusions

Well-controlled experiments related to transport in unsaturated, fractured porous rock will be necessary to verify the numerical model and to deepen our understanding of the fracture-matrix mass transfer process. No analytical solution has ever been developed in the literature for transport in unsaturated fractured porous media with global water flow occurring in both continua, no such experiments have been performed either. An example of a well-controlled experiment could be a lab experiment of tracer with a large-enough block (1 m^3) of fractured rock. This experiment is important for building an accurate numerical model because many aspects of the fracture-matrix interaction process are still unknown. Many numerical experiments

show that the fracture-matrix mass transfer is a critical process that controls how fast radionuclides migrate to the water table.

Development of numerical models for flow and transport with higher spatial resolution is another necessary task in reducing the prediction uncertainty. The current numerical models use rather coarse grids (vertically up to 60 m and laterally up to 200 m) because of limitations on computational resources. T2R3D and FEHM may suffer multidimensional numerical mixing caused by the coarser grids, while DCPT may suffer inaccurate interpolation of the pore velocity field. Furthermore, a coarse grid is expected to allow TOUGH2 to underestimate the capillary effects in the case where the critical layers are thin, which will lead to very different flow fields and transport pathways for nuclides. In such a complex and heterogeneous media as the UZ, the effects on radionuclide travel time could be very large. Calculation of detailed flow fields within the UZ needs parallelization of TOUGH2. Considerable effort is also required to develop particle trackers that can simulate transport with large grids very efficiently.

6.3.2 Matrix Block Discretization and its Effects on Unsaturated Zone Flow and Transport Simulations

Because fractures and the matrix have very different hydraulic properties, flow and transport between them significantly affect the overall flow and transport behavior in the UZ. Consequently, the accuracy for calculating flow and transport between them, largely determined by the matrix block discretization schemes, is a critical issue for simulating overall flow and transport processes and for assessing the performance of the potential repository. As discussed in the AMR *Conceptual and Numerical Models for UZ Flow and Transport* (CRWMS M&O 2000 [141187], Section 6.4), a dual-permeability model (DKM) has been used in the UZ Flow and Transport Model as the baseline approach for the matrix block discretization. This was based on considerations regarding flow and transport behavior in the UZ, scale of the problem, data availability, and computational feasibility (CRWMS M&O 2000 [141187], Section 6.4.2).

In the DKM, the matrix is treated as a single continuum (as will be discussed in this section). Therefore, capillary pressure and concentration gradients between fractures and the matrix are presented using a single-matrix-node approximation that cannot accurately describe the steep fronts near fracture-matrix interfaces. This issue is especially important for modeling matrix diffusion and radionuclide transport in the UZ. The objectives of this study are as follows:

- Evaluate the DKM for modeling UZ flow and transport by comparing simulation results obtained with the DKM with a more accurate matrix block discretization scheme.

- Make recommendations of possible actions for improving the currently used matrix discretization schemes, based on the simulation results.

6.3.2.1 Matrix Block Discretization

In the continuum approach, each gridblock within a given model domain generally includes a fracture block and a matrix block. Depending on the matrix block discretization scheme used for a numerical simulation, the matrix block can either be treated as a single matrix gridblock or

further subdivide into a number of matrix gridblocks. Several matrix-block discretization schemes within the context of the continuum approach are available in the literature for modeling flow and transport in unsaturated fractured rock (Doughty 1999 [135997], pp. 74–79). Typical schemes include the effective-continuum model (ECM) (Pruess et al. 1990 [100819]), the dual-porosity model (Warren and Root 1963 [100611]), the DKM, and the multiple interacting continua (MINC) model (Pruess and Narasimhan 1985 [101707]). These schemes are illustrated in Figure 6.3-8 for a one-dimensional column of gridblocks.

In the ECM (Figure 6.3-8(a)), liquid saturation is partitioned into the matrix and fracture in accordance with the principle of thermodynamic equilibrium, which requires that capillary pressure in the matrix and fracture components of a gridblock be equal. This is equivalent to assuming that flow and transport between fractures and the matrix occurs instantaneously. In other words, both fractures and the matrix are combined as a single continuum in a numerical simulation.

In the dual-porosity model (Figure 6.3-8 (b)), each gridblock includes a fracture gridblock and a matrix gridblock. Unlike the ECM, the fracture and matrix gridblocks need not be in thermodynamic equilibrium. Therefore, in this approach, flow and transport occurs between fractures and the matrix, but is ignored between matrix gridblocks. The DKM is the same as the dual-porosity model, except that global flow and transport between matrix blocks is allowed (Figure 6.3-8 (c)).

The schemes mentioned above can give rise to poor solutions for transient flow and transport in unsaturated fractured rocks because of the thermodynamic equilibrium assumption (in the ECM) and the use of one matrix gridblock (in the other two schemes) (Doughty 1999 [135997], pp.74–79). These schemes cannot accurately consider the highly transient flow and transport between fractures and the matrix. To overcome this problem, Pruess and Narasimham (1985 [101707]) proposed the multiple interacting continua (MINC) model (Figure 6.3-8 (d)), which is similar to the DKM except that the matrix is further subdivided into several continua, depending on the distances to the fracture-matrix interface. Specifically, all fractures will be lumped into a fracture continuum (as in the dual-porosity model and the DKM), all matrix material within a certain distance from the fractures will be lumped into matrix continuum #1, matrix material at larger distance becomes matrix continuum #2, and so on. In other words, the matrix block is subdivided into a number of matrix gridblocks. The MINC can more accurately resolve sharp gradients near the fracture-matrix interface and is therefore more suitable for modeling transient flow and transport.
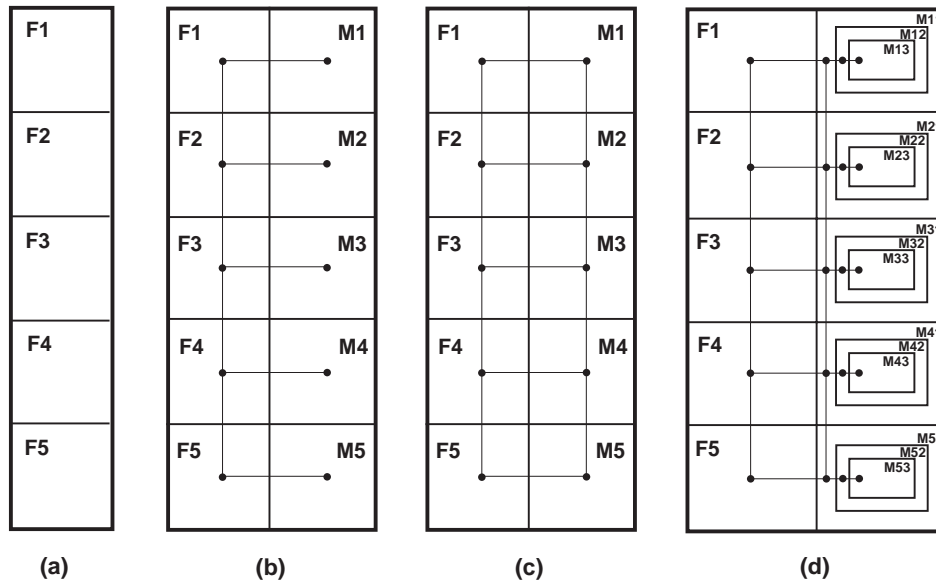
Figure 6.3-8.   Schematic Diagram of a One-dimensional Column of Gridblock, Modeled as (a) ECM, (b) Dual-porosity, (c) Dual-permeability, and (d) MINC with Three Matrix Continua (Gridblocks)

Although the MINC is more accurate than the other schemes, it needs much more computational effort because more matrix gridblocks are involved for a given fracture block. Therefore, the DKM has been used as the baseline approach in the UZ flow and transport models. To evaluate the accuracy of the DKM in modeling flow and transport in UZ, simulation results obtained from the DKM are compared with those obtained from a MINC model (Figure 6.3-9). In this MINC model, a fracture network is conceptualized as two perpendicular sets of vertical fractures, and the matrix is divided into five matrix continua (gridblocks), as shown in Figure 6.3-9. Ratios of the distances (from interfaces between the matrix continua to the fracture-matrix interface) to the corresponding fracture spacing are 0.004, 0.032, 0.108 and 0.256, respectively. Very fine discretization is used near the fracture-matrix interface. All the matrix continua are globally connected in the vertical direction. In the horizontal directions, only the first matrix continuum is globally connected while the connection parameters (e.g., node distance and interface area) are the same as those in the DKM for the same fracture configuration.
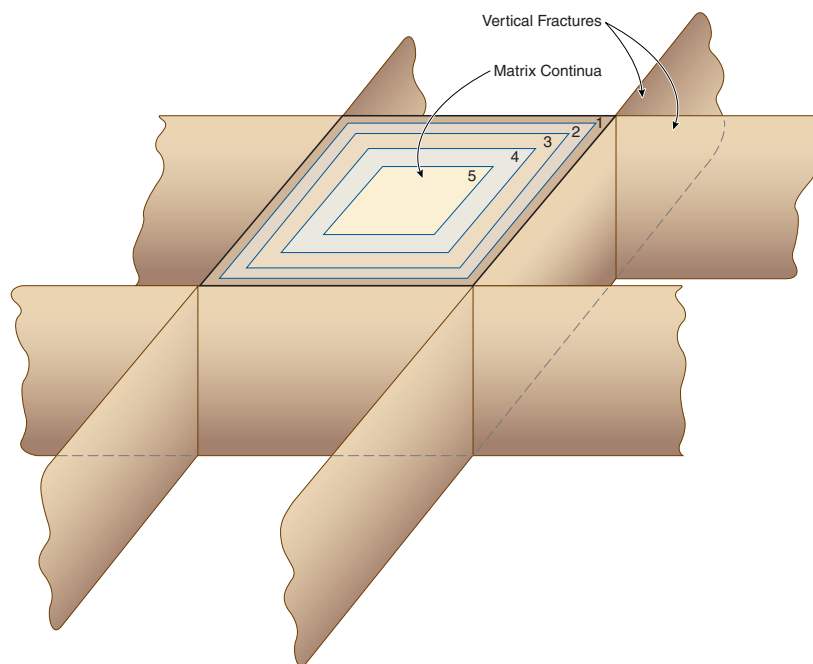
NOTE: Not to scale

Figure 6.3-9.   Matrix Discretization for the MINC Scheme Used in this Study

6.3.2.2   Numerical Simulations

Because a simulation with the MINC approach is computationally intensive, a site-scale, two-dimensional (2-D) cross section was employed for all the simulations in this study (Figures 6.3-10 and 6.3-11). The cross section was selected because the vitric Calico Hills Formation is not present in this location, such that matrix diffusion was expected to be a significant mechanism for radionuclide transport between fractures and the matrix below the potential repository. In the vitric Calico Hills formation (characterized by porous medium flow), diffusion from fractures to matrix is no expected to be significant. Simulation results are compared for the two matrix block discretization schemes (the DKM and the MINC). The initial and boundary conditions for flow and transport, together with rock properties, remain the same in all the simulations. The DKM and MINC grids were generated using a subroutine MINCgridv1.f V1.0 (LBNL 2001 [154343]) from an ECM grid (DTN: LB0110AMRU0185.015) generated with WINGRIDDER V2.0 (LBNL 2001 [154785]). The analysis is documented in the related scientific notebook (Liu 1999 [155675], pp. 129–141).
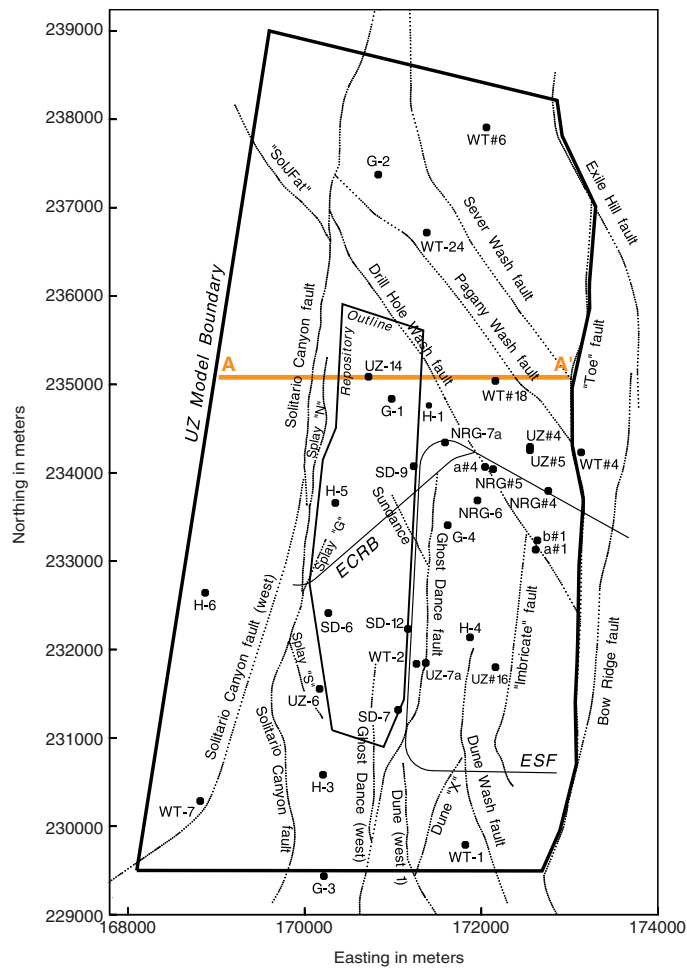
Figure 6.3-10. Plan View of the UZ Model Domain Showing the Location of East-West Cross Section A-A' Used in Numerical Simulations
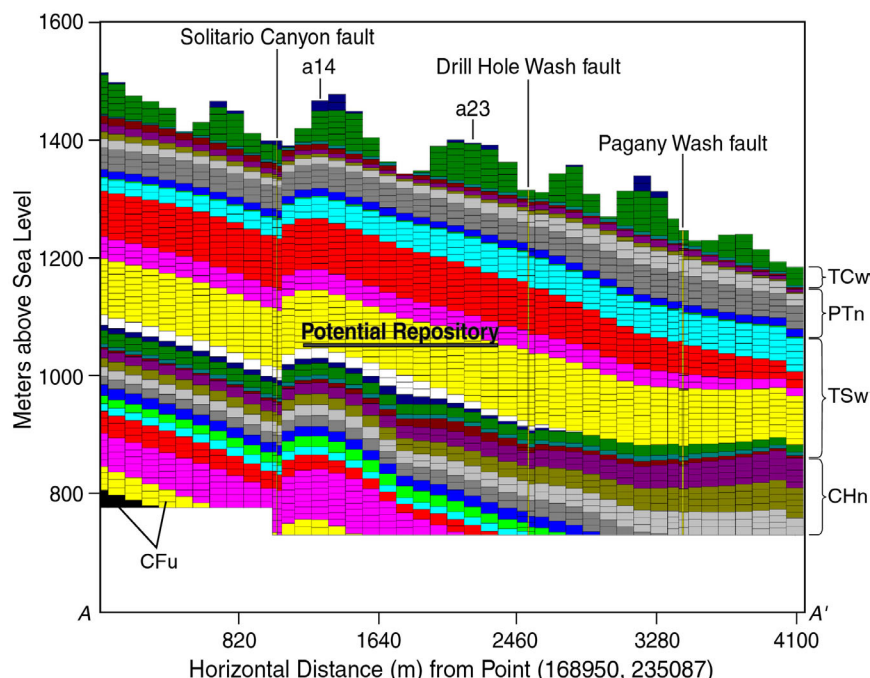
Figure 6.3-11.   Two-dimensional Numerical Grids for the East West Cross Section A-A'

The top model boundary for the 2-D vertical cross-sectional model domain coincides with the bedrock surface of the mountain. Surface net infiltration is applied to the top boundary using a source term for flow and transport simulations. The present-day infiltration map (DTN: GS000399991221.002 [147022]), the fracture geometry (DTN: LB990501233129.001 [106787]), and the calibrated, base-case, UZ property set (DTN: LB997141233129.001 [104055]) were used in this study. The infiltration map is interpolated onto the top boundary using Infil2grid V1.6 (LBNL 1999 [134754]). The bottom boundary is located at the water table. Zero flow flux in the horizontal direction is applied at the left and right boundaries. The steady state flow fields were simulated with the EOS9 module of TOUGH2 V1.4 (LBNL 2000 [146496]), which solves Richards' equation. Transport runs were carried out by the T2R3D code V1.4 (LBNL 1999 [113942]).

In the tracer transport simulations, a conservative (nonadsorbing) component is transported from the potential repository to the water table under steady-state flow conditions. As initial condition, all tracer mass is in water in the fracture continuum in the potential repository. The simulation results for tracer transport are represented by the cumulative mass of tracer arriving at the water table over time, normalized by the total initial mass introduced at the potential repository. For the cross section under consideration, the potential repository is located between Nevada east coordinates 170152.36 m and 171304.17 m. The elevation of the potential repository ranges from 1050.6 m to 1055.8 m. Hydrodynamic dispersion does not have a significant effect on solute transport through the unsaturated fracture-matrix system, as discussed in an AMR *UZ Flow Models and Submodels* (CRWMS M&O 2000 [122797], Section 6.8.1) and is therefore ignored herein. Two molecular diffusion coefficients, 0 and 3.2×10^{-11} m^2/s, were used in the simulations for all model layers. The latter is consistent with the matrix molecular diffusion coefficients for Tc reported in the AMR *Unsaturated Zone and Saturated Zone Transport Properties (U0100)* (CRWMS M&O 2001 [154024], Table 16).

6.3.2.3   Results and Discussions

Figures 6.3-12 and 6.3-13 show comparisons between simulated results obtained with the DKM (solid line) and the MINC (circles), respectively, for the two vertical columns (a14 and a23) from the 2-D cross section. These two columns intercept the potential repository horizon.   The simulated matrix saturations are in good agreement for the two schemes of matrix block discretization, indicating that, under steady-state flow conditions, the whole matrix block can be treated as a single continuum, as used in the DKM. This is further supported by the observation that with the MINC, all five matrix continua have almost the identical water saturations and potentials (Figure 6.3-14). In other words, all five matrix continua are hydraulically in equilibrium, consistent with the assumption used in the DKM. This is not surprising considering that the matrix has small van Genuchten alpha (or very strong capillarity) and flow between different matrix continua is purely determined by the capillary forces. Note that the gravity term is not involved in a horizontal connection between matrix continua (Figure 6.3-9).
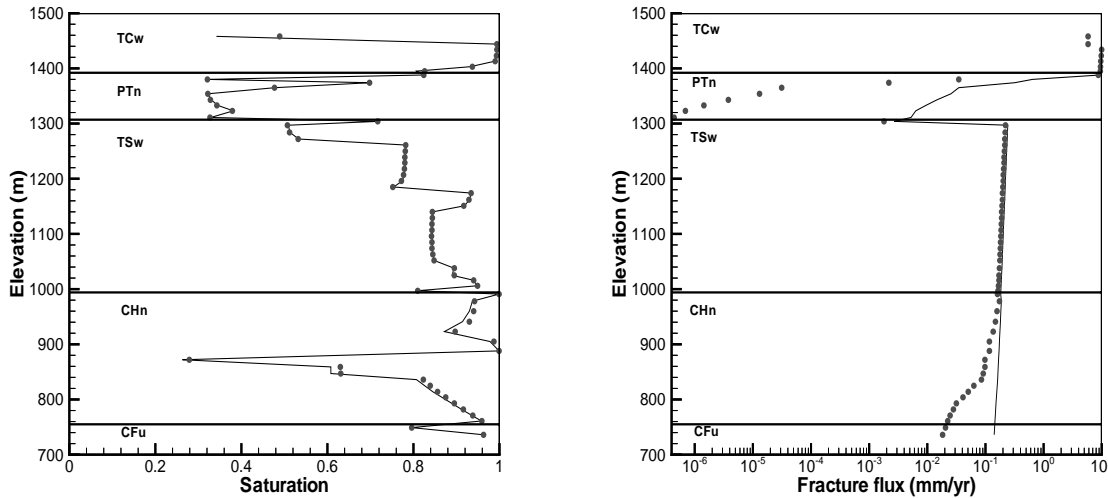
DTN: LB0104AMRU0185.002

NOTE: The column is located at point (170250 m, 235087 m) in Cross section A-A'.

Figure 6.3-12.   Comparisons Between Simulation Results Obtained Using the DKM (solid line) and the MINC (circles) for a Vertical Column a14
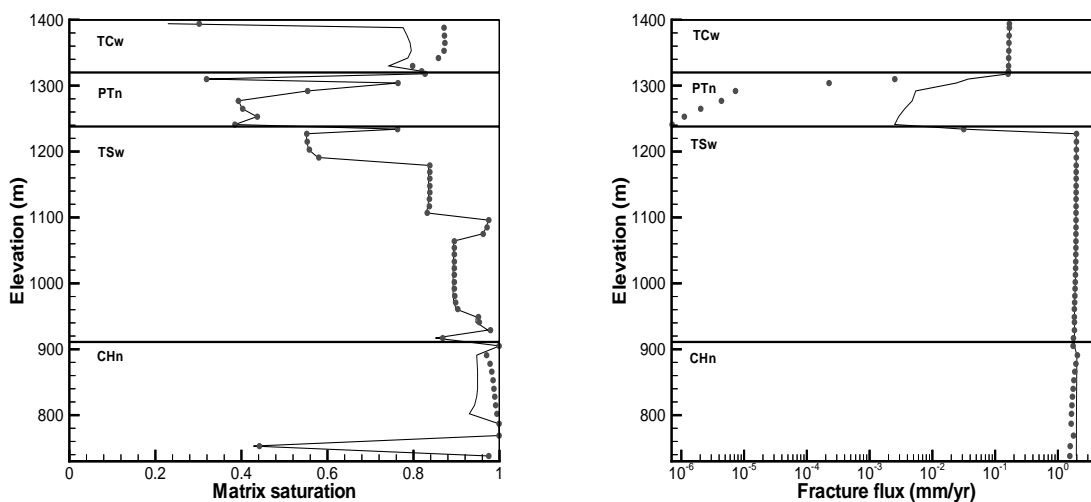
DTN: LB0104AMRU0185.002

NOTE: The column is located at point (171150 m, 235087 m) in Cross section A-A'.

Figure 6.3-13. Comparisons Between Simulation Results Obtained Using the DKM (Solid Line) and the MINC (circles) for a Vertical Column a23
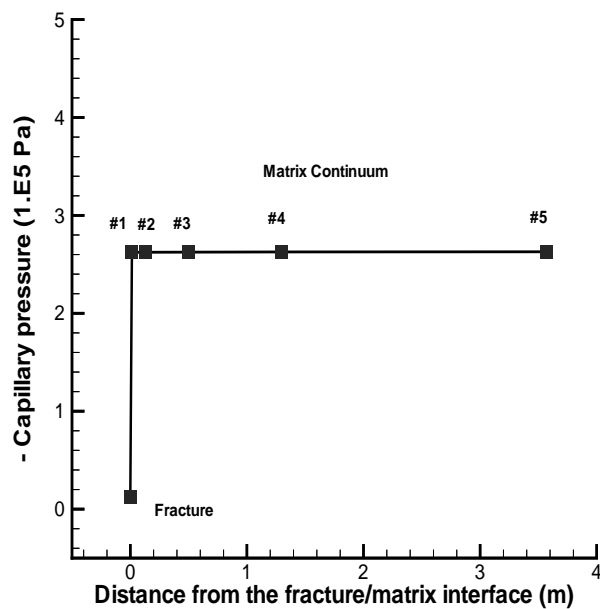
DTN: LB0104AMRU0185.002

Figure 6.3-14. Capillary Pressure Distribution within a Matrix Block at Elevation of 923 m for Column s14

Figures 6.3-12 and 6.3-13 also show comparisons between simulated distributions of water flux in fractures for the two vertical columns. While a fairly good agreement is achieved between the DKM and the MINC, fracture flux (liquid flux in the fractures) in the PTn is estimated by the DKM to be higher. This is likely to be because a steep capillary-pressure gradient exists near the fracture-matrix interface, although capillary-pressure is nearly uniform within a matrix block (e.g., Figure 6.3-14). In a conventional DKM, the connection distance between nodes corresponding to the fracture and matrix gridblocks is determined based on the method of Warren and Root (1963 [100611]). For a fracture network given in Figure 6.3-9, this connection distance is calculated as the fracture spacing divided by a factor of 8 (Warren and Root 1963 [100611]; Pruess 1983 [100605], Table 1). This is considerably larger than the connection distance between the fracture gridblock and the matrix gridblock corresponding to matrix continuum #1 in the MINC scheme (Figures 6.3-9 and 6.3-14). Because calculated flux decreases as the connection distance increases, the DKM may underestimate the flux from fractures to the matrix and therefore overestimate the fracture flux.

The above discussion is also consistent with the finding presented in the *Unsaturated Zone Flow and Transport Model Process Model Report* (CRWMS M&O 2000 [151940], Figure 3.6-9). The current site-scale UZ model based on the DKM might overestimate fracture flow in the vitric part of the CHn. (In the cross section shown in Figure 6.3-11, there is no vitric part in the CHn.) The PTn and the vitric part of the CHn have similar rock hydraulic properties. The current UZ model predicts about 20% of liquid water occurring in fractures within this vitric part (CRWMS M&O 2000 [151940], Figure 3.6-9). However, tracer tests from the Busted Butte site clearly indicated that unsaturated flow occurs only in the matrix in the vitric part of the CHn (see Section 6.5.1).

While very similar fracture flux distributions in the TSw are obtained using the two schemes for matrix block discretization, fracture fluxes are higher in the CHn and CFu for the DKM estimates (Figures 6.3-12 and 6.3-13). Compared with the TSw, these units have relatively small fracture permeabilities and large effective fracture-matrix interface areas indicated by the small values of active fracture parameter γ (DTN: LB997141233129.001 [104055]). A combination of these factors and the fine discretization of the matrix block results in a larger flux from fractures to the matrix and consequently smaller fracture fluxes for the MINC scheme than those for the DKM. The differences in fracture flux are not a result of lateral flow in the relevant units, because very close total water fluxes (including contributions from both the matrix and fractures) are obtained at the water table (for each of the two columns) for both the DKM and the MINC.
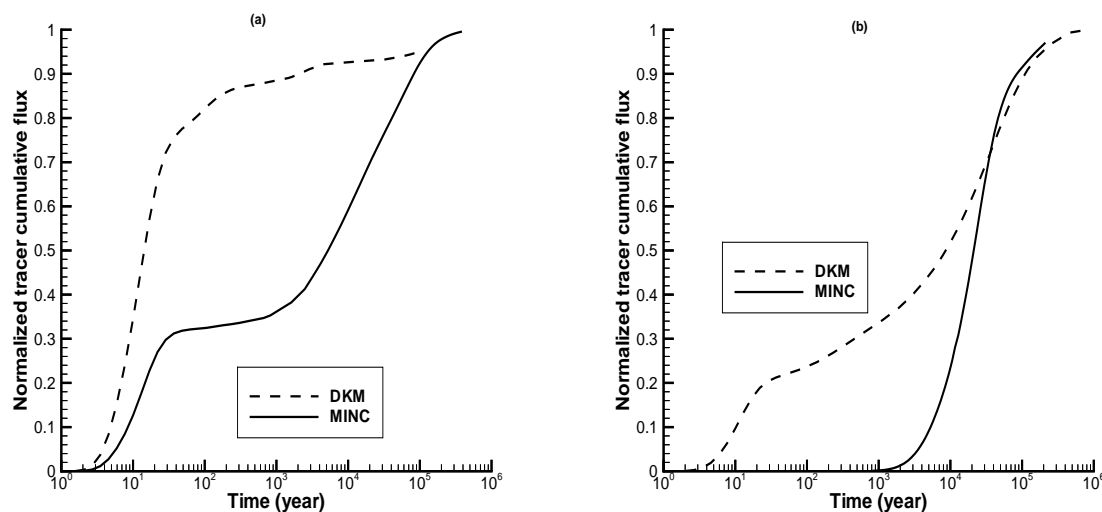
DTN: LB0104AMRU0185.002

Figure 6.3-15. Normalized Tracer Cumulative Flux at Water Table as a Function of Time for Molecular Diffusion Coefficient (a) $D_m = 0$ and (b) $D_m = 3.2 \times 10^{-11}$ m^2/s

Figure 6.3-15 shows simulated tracer transport results with and without diffusion (molecular diffusion coefficients $D_m = 0$ and 3.2×10^{-11} m^2/s). The use of $D_m = 0$ allows for investigation of effects of pure advection. In this case (Figure 6.3-15a), both schemes correspond to very similar breakthrough times (less than 10 years), but different values for the tracer cumulative flux. This results from the differences in fracture fluxes in the CHn and CFu units, as discussed above. For the DKM, the majority of tracer mass is transported through fractures by advection from the potential repository (within TSw) to the water table, as implied by the relative uniform fracture flux distributions within the TSw unit and the below (Figures 6.3-12 and 6.3-13). On the other hand, only a relatively small portion of the tracer mass is transported through the fractures to the water table for the MINC scheme.

Comparisons between simulated transport results for the two molecular diffusion coefficients further confirms the importance of the matrix diffusion indicated by the Alcove 1 test and modeling study that is discussed in the AMR *UZ Flow Models and Submodels* (CRWMS M&O 2000 [122797], Section 6.8.1). For each scheme of the matrix-block discretization, significantly different breakthrough curves are simulated for the two different molecular diffusion coefficients. The comparisons also suggest the necessity to accurately consider the solute concentration gradient near the fracture-matrix interface. For example, similar breakthrough times are simulated for both matrix-block discretization schemes for $D_m = 0$, but significantly different breakthrough times are observed for $D_m = 3.2 \times 10^{-11}$ m^2/s. This is mainly a result of using different discretization schemes. (Matrix diffusion is estimated by the DKM to be smaller at early time than it is with the MINC.) Because the MINC is expected to provide more accurate results, it is likely that the DKM may underestimate the breakthrough time for radionuclide transport from the potential repository to the water table.

6.3.2.4   Conclusions and Recommendations

The MINC simulation results show that under steady-state flow conditions, all the matrix continua within a given gridblock have almost the identical water saturations and potentials, indicating that the matrix can be treated as a single continuum. In other words, the dual-permeability concept is valid for modeling steady-state flow processes in the unsaturated zone of Yucca Mountain.

Comparisons between simulation results indicate that the current dual-permeability approach may overestimate fracture fluxes in some units, resulting from a too-large connection distance used between the fracture and matrix gridblocks. This is consistent with the noted discrepancy between the previously simulated fracture fluxes in the vitric Calico Hill formation and those implied from the tracer test results at the Busted Butte site. It is recommended to use a reduced connection distance in generating DKM grids for future flow simulations. The determination of this reduced distance needs further investigation.

Simulation results demonstrate the significance of matrix diffusion and accurate representation of concentration gradient near fracture-matrix interfaces on the overall radionuclide transport processes in the unsaturated zone of Yucca Mountain. Because the DKM underestimates matrix diffusion at the early time, it is very likely that this model provides conservative estimates of the breakthrough time for radionuclide transport from the potential repository to the water table. This issue can be resolved in future site-scale flow and transport simulation using one of the following three approaches:

1. Directly use MINC for both flow and transport in the site-scale UZ model. This is the most reliable approach, but it is computationally intensive.

2. Take advantage of the finding that the DKM is valid for modeling steady-state flow processes as long as the reduced connection distance is used. In this case, flow fields are simulated with the DKM and then mapped into a MINC grid. The transport is simulated for the MINC grid using computationally efficient T2R3D V1.4 (LBNL 1999 [113942]) which only solves the solute transport equation.

3. Improve the current particle trackers such that they could handle the sharp concentration gradient for a DKM grid and the corresponding flow fields. A detailed discussion of the current particle trackers and their capabilities is given in Section 6.3.1.

6.4   PROCESSES AFFECTING SEEPAGE

Many factors influence the amount of water that may seep into emplacement drifts. Beyond the primary factors of the average incident percolation flux, the hydrologic characteristics of the rock, and the size and general shape of the drifts, several other factors may also affect the amount of seepage. Seepage enhancement due to some of these other factors has been treated quite conservatively, while for others, no seepage enhancement has been applied. In Section 6.4.1, seepage enhancement due to small-scale changes in drift geometry from rock fall (i.e., drift degradation) and rock bolts is considered, and new seepage enhancement distributions are proposed based on more detailed analyses as well as new properties. Sections 6.4.2, 6.4.3, and 6.4.4 consider the effect of the detailed nature of percolation at the repository horizon. In Section

6.4.2, characterization of flow focusing on a scale intermediate between those of the mountain and drift-scale models previously used is documented, and new seepage enhancement distributions due to flow focusing are proposed. In Section 6.4.3, a comparison of the calibration of alternate model parameters against geochemical data and the resultant predictions of percolation distribution at repository horizon are documented. In Section 6.4.4, investigation of the extent of episodic percolation at the repository horizon due to infiltration directly on TSw outcrop west of Yucca Crest is documented, and the previously used seepage enhancement factor is confirmed. Except for the model used to investigate flow focusing (Section 6.4.2), the models and analyses presented in Section 6.4 are scoping investigations using more detailed or alternative approaches and are not intended for direct use in TSPA. They do, however, provide confirmation of the approach and conservatism used in TSPA-SR (CRWMS M&O 2000 [153246]).

6.4.1   Seepage Enhancement due to Drift Degradation

Drift degradation may enhance seepage because of small-scale changes to the drift wall geometry. Investigations of seepage enhancement because of drift degradation at Yucca Mountain, which incorporate the latest calibrated properties and are more detailed than previous investigations, are presented here. Two issues with respect to drift degradation are addressed: 1) in Section 6.4.1.1, the effect of changes to drift wall shape due to rockfall in the Tptpmn and Tptpll are addressed, 2) in Section 6.4.1.2, the effect of changes to the drift wall shape and properties due to degradation of rock bolts used as ground support in Tptpmn is addressed.

6.4.1.1   Seepage Enhancement due to Rockfall

The objectives of this section are to calculate seepage values for different values of percolation flux down to the drift, to discuss the effect on seepage due to excavation-induced rockfall from drift ceiling in the Topopah Spring middle nonlithophysal (Tptpmn) unit and the Topopah Spring lower lithophysal (Tptpll) unit.

The model used in this section follows that presented in *Seepage Model for PA Including Drift Collapse* (CRWMS M&O 2000 [153314], Sections 5 and 6) and the methodology is also described in Birkholzer et al. (1999 [105170], pp. 358–362). The physical framework and mathematical construct of this model is identical to that of seepage calibration model (CRWMS M&O 2001 [153045], Sections 5 and 6), with the only difference being the manipulation of the output data to obtain seepage results.

6.4.1.1.1   Seepage Model

The conceptual model is a heterogeneous permeability field (DTN: LB0011SMDCREV1.001 [153574]) for the fracture continuum generated with parameters discussed below, using the SISIM module of the GSLIB package (Specifically, GSLIB V2.0MSISIMV2.0 (LBNL 1999 [154340])). The model follows that of the seepage calibration model (CRWMS M&O 2001 [153045], Section 6) and is also described in Birkholzer et al. (1999 [105170], pp. 358–362), which provides the scientific and technical background for this section. The 3D field is 19.22 m vertical, 15.25 m wide normal to drift axis, and 10.065 m along the drift axis. With the drift of 5.5 m diameter, an overlying thickness of 8.845 m, an underlying thickness of 4.875 m, and the

distance to either side boundary of 4.875 m, the vertical cross-sectional dimensions were chosen to be wide enough to capture the main flow feature [i.e. flow diversion around the drift (Philip et al. 1989 [105743], p. 21, Figure 1)]. The distance along the drift axis is 10.065 m. The side boundary conditions are no-flow, the lower boundary condition is gravity drainage, and the upper boundary surface is simulated by an extra grid cell with constant percolation flux connected to all the grid cells in the first row. Flow is thus free to move into these cells according to local property parameters of these cells. Regarding the no-flow boundary condition on the two planes at the end of the waste package normal to the drift axis: for a homogeneous, constant-property medium, these planes are symmetry planes between successive waste packages, and a no-flow boundary condition is justified. For a heterogeneous system, the issue is the length of the flow domain versus the spatial correlation length λ. In the simulations below, $\lambda = 0.305$ m so that the length of the domain is about 33 correlation lengths and the effect of the no-flow boundary should not have a significant effect on the flow results. The fracture continuum permeability k_{FC} and the standard deviation of ln k_{FC} will be given in the Section 6.4.1.1.2.

The mesh consists of over 100,000 grid cells. The grid cell dimension of 0.305 m × 0.305 m × 0.305 m is chosen to be the same as in degraded emplacement drift profiles (CRWMS M&O (2000 [151635]; DTN: MO0109RDDAAMRR.003 [156306]).

The spatial correlation length λ is chosen to be equal to the grid size of 0.305 m. This choice implies an uncorrelated spatial distribution of permeability values. This is consistent with CRWMS M&O (2001 [153045], Section 6.3.2.1) where λ is 0.2 m, which is smaller than our grid size for the case of the lower lithophysal zone. The AMR, *Seepage Calibration Model and Seepage Testing Data* (CRWMS M&O 2001 [153045], Section 6.4.2.1, Figure 9), presents semi-variograms indicating an uncorrelated permeability structure for the middle nonlithophysal zone.

At the drift wall, the nodal distance between the drift surface and the grid cell representing the drift is set to be very small, so that the boundary condition can be applied directly at the drift wall. The length of the last vertical connection between the drift wall and the neighboring gridblocks representing the formation is set equal to 0.05 m. This is done to make our model consistent with the seepage calibration model (CRWMS M&O 2001 [153045], Sections 6.3.2.2 and 6.4.2.2), whose parameter values are used in the current calculations. The choice of this 0.05 m vertical connection to the drift wall implies a direct gravity-controlled vertical flow, with no horizontal diversion within this 0.05 m distance. (This is sometimes called a "needle" or "discrete surface fracture" effect.) Because of this 0.05 m vertical gravity flow at the drift wall, a capillary pressure higher (i.e., less negative) than -490 Pa at the grid cells in the formation next to the drift wall will allow seepage into the drift: the -490 Pa is insufficient to balance the hydrostatic pressure that develops along the 0.05 m vertical connection. For $1/\alpha$ values of 870 Pa, seepage occurs when saturation in the grid cell next to the drift wall exceeds 90%.

Flow calculation was performed using ITOUGH2 V3.2_drift (LBNL 1999 [112757]). A number of routines were also used for preprocessing of inputs for ITOUGH2 V3.2_drift (LBNL 1999 [112757]). Specifically, iTOUGH2 V3.2_drift (LBNL 1999 [112757]) input files are generated and reformatted using the routines mddf.f V2.0 (LBNL 2001 [154347]), meshbd.f V1.0 (LBNL 2001 [152871]), mininipresf.f 1.0 (LBNL 2001 [152872]), minrefine3df.f V1.0 (LBNL 2000

[152880]), and mk_generGL.f V1.0 (LBNL 2001 [154349]). Their use is described and documented in Li (2000 [153480], pp. 128–129, 145–149).

6.4.1.1.2   Input Data

The first parameter set, Set A, is the set of calibrated mean parameters for the middle nonlithophysal zone documented in *Seepage Model for PA Including Drift Collapse* (CRWMS M&O 2000 [153314]):

$k_{FC} = 1.38 \times 10^{-12} m^2$	DTN: LB0010SCMREV01.002 [153393]
$1/\alpha = 589$ Pa	DTN: LB0010SCMREV01.002 [153393]
$n = 2.55$	DTN: LB997141233129.001 [104055]
$\sigma = 1.93$	DTN: LB0010SCMREV01.002 [153393]

Here σ=1.93 is used for both sets as a more conservative value (i.e., the greatest value for 3 niches).

The second parameter set, Set B, is chosen to be the set of mean calibrated parameters for the lower lithophysal unit documented in *Seepage Model for PA Including Drift Collapse* (CRWMS M&O 2000 [153314]):

$k_{FC} = 1.86 \times 10^{-11} m^2$	DTN: LB0010SCMREV01.002 [153393]
$1/\alpha = 871$ Pa	DTN: LB0010SCMREV01.002 [153393]
$n = 2.57$	DTN: LB997141233129.001 [104055]
$\sigma = 1.93$	DTN: LB0010SCMREV01.002 [153393]

An additional parameter Set B′ is defined:

$k_{FC} = 1.86 \times 10^{-11} m^2$	DTN: LB0010SCMREV01.002 [153393]
$1/\alpha = 537$ Pa	DTN: LB0010SCMREV01.002 [153393]
$n = 2.57$	DTN: LB997141233129.001 [104055]
$\sigma = 1.93$	DTN: LB0010SCMREV01.002 [153393]

This parameter set B′ is same as Set B, except the $1/\alpha$ is reduced to account for the effects of the lithophysal cavities on seepage. As discussed in *Seepage Calibration Model and Seepage Testing Data* (CRWMS M&O 2001 [153045], Section 6.3.3.3), since SMPA does not include lithophysal cavities explicitly, it is necessary to represent this effect by a reduced $1/\alpha$ value. One calibration case was run with and without lithophysal cavities in the model. The reduction of the $\log(1/\alpha)$ value caused by the presence of lithophysal cavities is found to be 0.21 (CRWMS M&O 2001 [153045], Section 6.3.3.3), suggesting a value of $\log(1/\alpha)$ of 2.73, which translates to the $1/\alpha$ value of 537 Pa.

Based on the information presented in *Drift Degradation Analysis* (CRWMS M&O 2000 [151635]), alternative drift rockfall modes are evaluated, and four scenarios are identified for seepage model studies.

All the cases are computed for 3-D heterogeneous unsaturated systems. Because some cases involve more than one run, altogether more than 40 runs were made.

Detailed discussions of fracture continuum permeability k_{FC}, standard deviation of ln k_{FC}, spatial correlation length, λ, of k_{FC}, and percolation flux are given in CRWMS M&O (2000 [141400], Sections 5.1 and 5.2.1).

For our calculations, four values for Q_p are used, ranging from 14.6 to 500 mm/yr; more specifically $Q_p = 14.6$, 73.2, 213 and 500 mm/yr. For the seepage model in Tptpll, where seepage is zero for $Q_p = 500$ mm/yr, even larger Q_p values (1000, 1500, 2000, and 2500 mm/yr) are used to find when seepage might occur.

6.4.1.1.3   Impact of Rockfall on Seepage

Drift degradation may occur in three ways: loosening of rock blocks and hence wider fracture aperture (fracture dilation), rock-fall from the ceiling of the drift and extended rock failure in the drift roof.

In *Seepage Model for PA Including Drift Collapse* (CRWMS M&O 2000 [153314]), four drift degradation submodels were designed to evaluate the impact of drift degradation on seepage: fracture dilation, 1.0 m^3 rockfall from the drift crown, 1.0 m^3 rockfall from the spring line, and extended rock failure reaching 3 m depth. Table 6.4-1 presents the calculated seepage percentages for parameter Set A for three realizations (R1, R2 and R3) with drift degradation modes and compares them with the no-degradation case. Only the $Q_p = 500$ mm/yr cases are shown. The results show that the effect of a single rockfall is not significant for seepage because of the increased likelihood of the creation of topographic lows. A deeper rock failure in the drift roof increases seepage. Calculations were also made with parameter Set B with the results of zero seepage for all cases, with or without drift degradation.

Table 6.4-1.   Seepage Percentage (%) for Alternative Drift Degradation Scenarios, for $Q_p = 500$ mm/yr and Parameter Set A

Condition	Seepage Percentage		
	R1	R2	R3
No-degradation case	7.1	7.1	13
1 m rock fall from crown of drift	7.2	7.3	12
1 m rock fall from springline of drift	7.1	7.1	13
3 m rock failure in drift roof	9.0	11	15

DTN: LB0011SMDCREV1.002 [153570]

Previous studies show that extended rock failure causes the largest impact on seepage. To make a more quantitative evaluation, instead of the schematic rock failure profile used earlier, detailed degraded-drift profiles calculated using a discrete-region key-block analysis (CRWMS M&O 2000 [151635]; DTN: MO0109RDDAAMRR.003 [156306]) were used. The key-block analysis provides the following detailed 3-D profiles, using 0.305 m (1 foot) grid size.

For Topopah Spring middle nonlithophysal unit (Tptpmn):

(1) Worst degradation (largest rockfall volume) drift profile

(2) Profile at 75th percentile

(3) No degradation (91.9% of stochastically-generated cases).

For Topopah Springs lower lithophysal unit (Tptpll):

(1) Worst degradation (largest rockfall volume) drift profile

(2) Profile at 75th percentile

(3) No degradation (99.6% of stochastically-generated cases)

For the Tptpmn, 91.9 percent of the drift length exhibits no drift degradation. Of the 8.1 percent that does exhibit degradation, the 75th percentile means that 75 percent of the 8.1 percent has a rockfall volume less than that shown in the 75th percentile drift profile. Similarly for Tptpll, 0.4 percent (100 percent to 99.6 percent) of the drift length exhibits drift degradation, with the 75th percentile profile indicating that 75 percent of 0.4 percent of the drift length has a rockfall volume that is less than that shown.

A typical example of the detailed degraded drift profile is shown in Figure 6.4-1 for the "worst" degradation case in the Tptpmn unit.

Degraded emplacement drift profiles are generated for four cases: Tptpmn worst-case profile, Tptpmn 75 percentile profile, Tptpll worst-case profile, and Tptpll 75 percentile profile (CRWMS M&O 2000 [151635]; DTN: MO0109RDDAAMRR.003 [156306]).

(a) Isometric View

24.4 m

(b) Side View

(c) Cross Section View
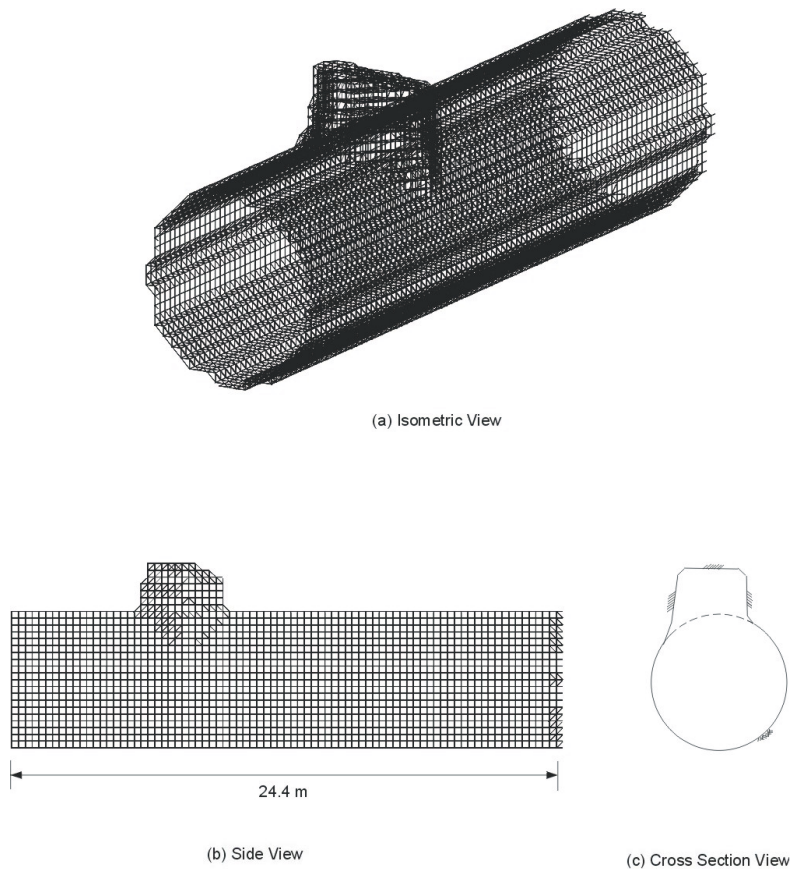
DTN: MO0109RDDAAMRR.003 [156306]

Figure 6.4-1.　　Emplacement Drift Profile for the Tptpmn Unit, Worst Case

(a) Isometric View

(b) Side View

24.4 m

(c) Cross Section View
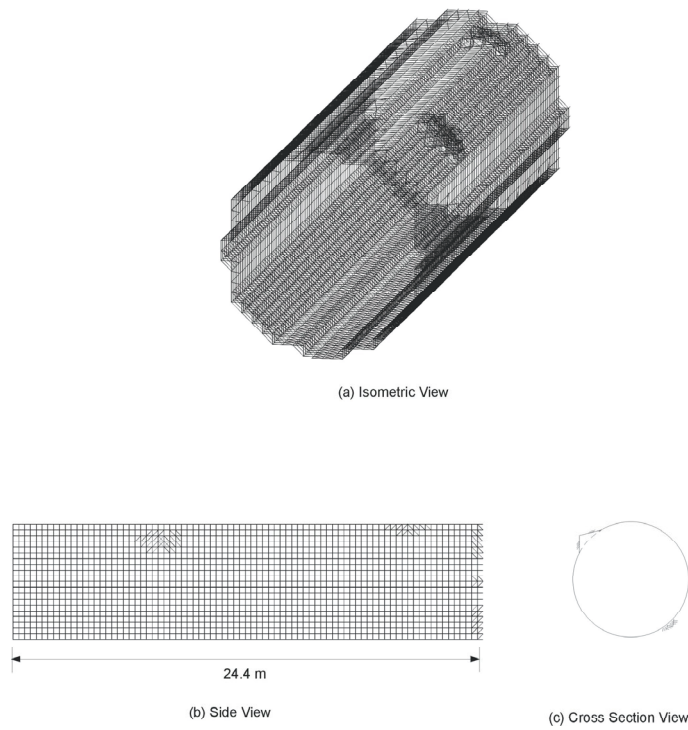
DTN: MO0109RDDAAMRR.003 [156306]

Figure 6.4-2.   Emplacement Drift Profile for the Tptpmn Unit, 75 Percentile Case

(a) Isometric View

(b) Side View

24.4 m

(c) Cross Section View
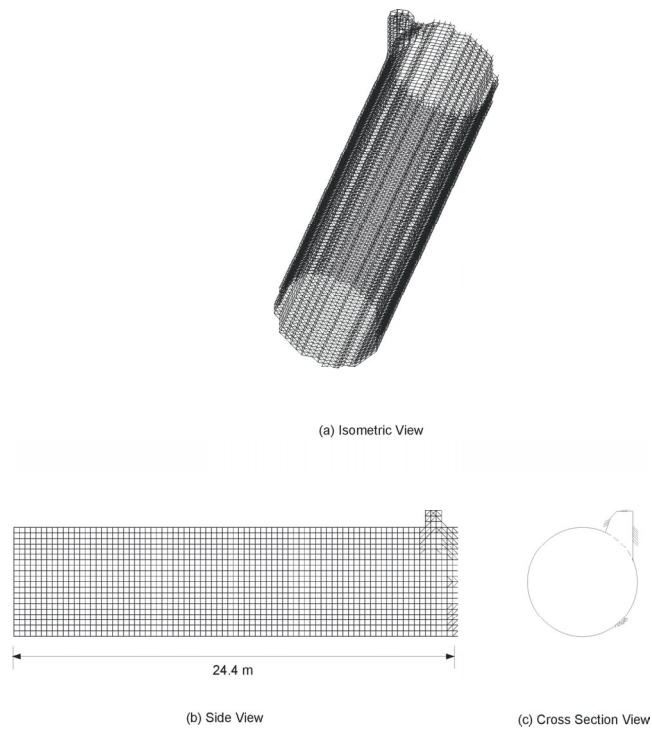
DTN: MO0109RDDAAMRR.003 [156306]

Figure 6.4-3.   Emplacement Drift Profile for the Tptpll Unit, Worst Case

(a) Isometric View

(b) Side View

24.4 m

(c) Cross Section View
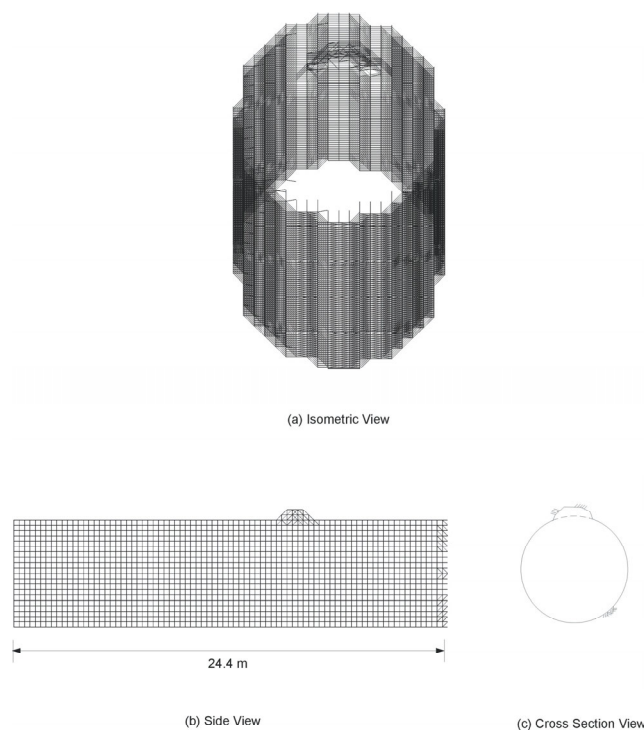
DTN: MO0109RDDAAMRR.003 [156306]

Figure 6.4-4.   Emplacement Drift Profile for the Tptpll Unit, 75 Percentile Case

Based on these discussions, four seepage models were designed to evaluate the impact of rockfall on seepage, and it is calculated for four alternative scenarios.

6.4.1.1.4   Results

Seepage percentage is defined as the ratio of liquid that seeped into the drift to the total liquid arriving on a cross-sectional area corresponding to the footprint of the drift. (Note that this term is defined differently in the seepage calibration model (CRWMS M&O 2001 [153045], Section 6.1.2), where it is defined in reference to the total water released in the liquid release tests). All results and the input/output files for the model computation are submitted to TDMS under DTNs LB0104AMRU0185.011 and LB0104AMRU0185.003, respectively. The SN supporting this work is Bodvarsson (2001 [156334], YMP-LBNL-CFT-GL-2, pp. 22–67).

Table 6.4-2 presents seepage percentages for three realizations for parameter Set A (Section 6.4.1.1.2) and four percolation rates.

Table 6.4-2.   Seepage Percentage (%) for Alternative Drift Degradation Scenarios, for parameter Set A

Q_p (mm/yr)		14.6	73.2	213.4	500
Base Case	R1	0.0	0.0	0.46	5.69
	R2	0.0	0.0	0.82	11.04
	R3	0.0	0.0	0.15	10.71
	Average	0.0	0.0	0.48	9.15
Worst Case	R1	0.0	0.0	0.48	8.97
	R2	0.0	0.0	0.86	13.99
	R3	0.0	0.0	0.34	12.58
	Average	0.0	0.0	0.56	11.85
75 % Case	R1	0.0	0.0	2.87	1.63
	R2	0.0	0.0	3.39	17.53
	R3	0.0	0.0	2.36	16.50
	Average	0.0	0.0	2.87	14.89

DTN: LB0104AMRU0185.011
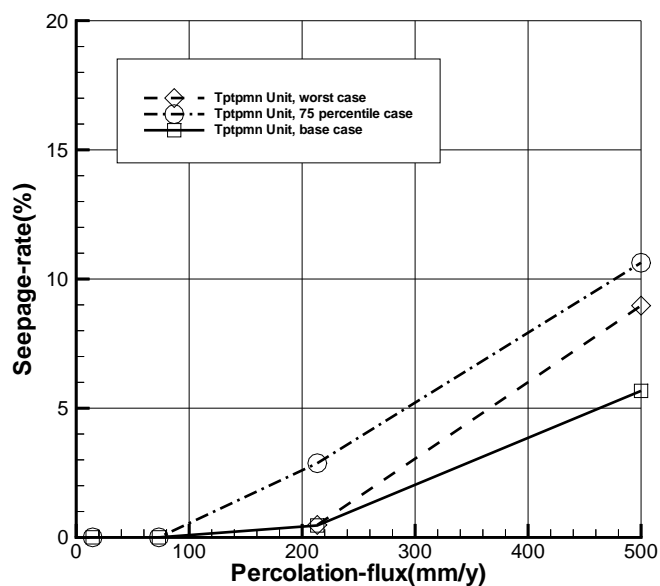
DTN: LB0104AMRU0185.011

Figure 6.4-5.   Seepage Percentage as a Function of Percolation Flux Q_P for the Two Degradation Scenarios for Parameter Set A, Realization 1
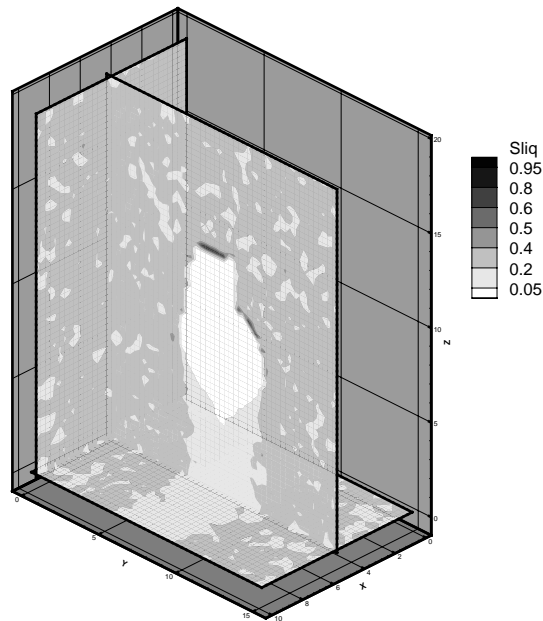
DTN: LB0104AMRU0185.011

Figure 6.4-6.   Saturation Distribution around a Drift for the Worst Case in the Tptpmn with Parameter Set A, Realization 1
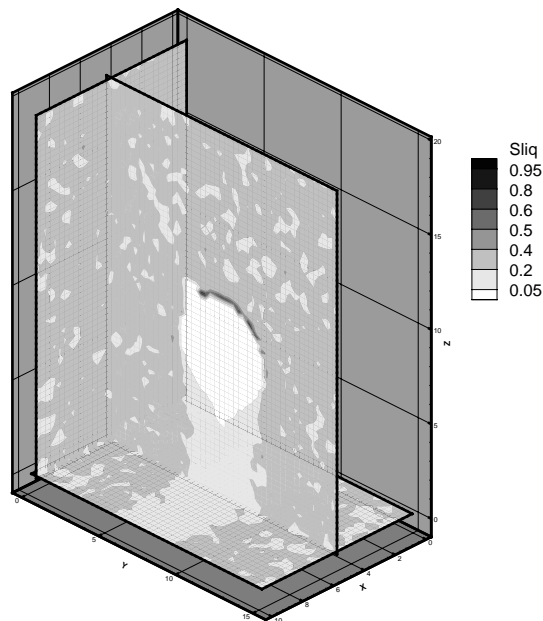
DTN: LB0104AMRU0185.011

Figure 6.4-7.   Saturation Distribution around a Drift for the 75 Percentile Case in the Tptpmn with Parameter Set A, Realization 1
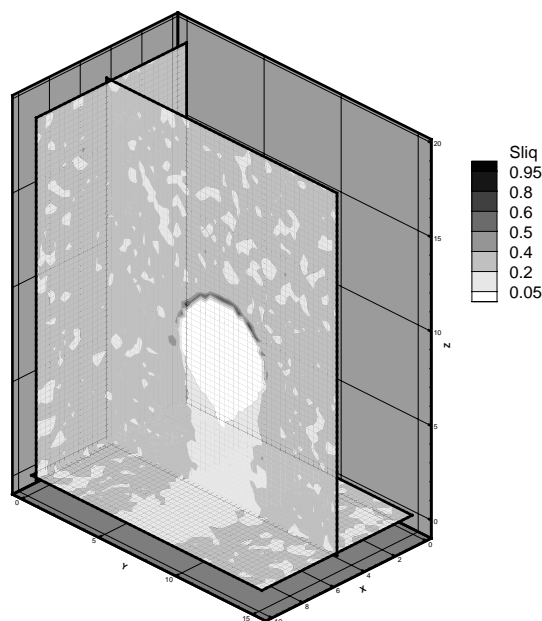
DTN: LB0104AMRU0185.011

Figure 6.4-8.   Saturation Distribution around a Drift for No-Degradation Case in the Tptpmn with Parameter Set A, Realization 1

The results in Table 6.4-2 show that the effect of rockfall on seepage into drift for the Tptpmn unit (parameter Set A). A series of percolation flux values were used up to 500 mm/yr to explore the effect of drift degradation on seepage threshold. Figure 6.4-5 shows the calculated seepage percentage as a function of percolation flux Q_p, Realization 1. It is seen in this figure that the effect of drift degradation for the scenarios decreases with decreasing Q_p, so that its impact on seepage threshold is relatively small. This can perhaps be explained by the fact that, under vertical percolation flux, the seepage threshold depends significantly on the horizontal cross section (footprint) of the drift, so that, if the cross-sectional area does not change very much, the seepage threshold also will not change very much.

The results of Realization 1 also indicate that seepage enhancement ranges from 0–5 percentage points for Q_p up to 500 mm/yr due to drift degradation for the worst case and 75 percentile case. The enhancement does not seem to be dependent on whether it is worst case (i.e., largest rockfall) or 75 percentile. The shape of the cavity in the ceiling may be more important than the volume. Confirming calculations were performed by using a homogeneous medium and it shows that more seepage obtained for the 75 percentile case.

Figures 6.4-6, 6.4-7, and 6.4-8 illustrate the saturation profile around the drift for two degradation scenarios and the no-degradation case in the Tptpmn unit with parameter Set A, Realization 1. The figures clearly show the degradation effect on the seepage into the drift.

Table 6.4-3 presents the seepage percentages of three realizations for parameter Set B′ representing the lower lithophysal unit with drift degradation modes, worst degradation case and

degradation at 75 percentile, and compares them with the no-degradation case. Here, because of the low seepage, values of Q_p up to 2500 mm/yr were needed.

Table 6.4-3.   Seepage Percentage (%) for Alternative Drift Degradation Scenarios, for Parameter Set B′

Q_p (mm/yr)		500	1000	1500	2000	2500
Base Case	R1	0.0	0.0	0.33	0.55	0.83
	R2	0.0	0.0	0.50	1.05	2.09
	R3	0.0	0.0	0.0012	1.03	2.86
	Average	0.0	0.0	0.28	0.88	1.93
Worst Case	R1	0.0	0.2	0.65	1.42	2.41
	R2	0.0	0.0	1.50	3.04	4.56
	R3	0.0	0.0	0.11	1.94	4.25
	Average	0.0	0.07	0.75	2.13	3.74
75 % Case	R1	0.0	0.0	0.33	0.59	1.24
	R2	0.0	0.0	0.50	1.06	2.32
	R3	0.0	0.0	0.33	1.36	3.10
	Average	0.0	0.0	0.39	1.00	2.22

DTN: LB0104AMRU0185.011
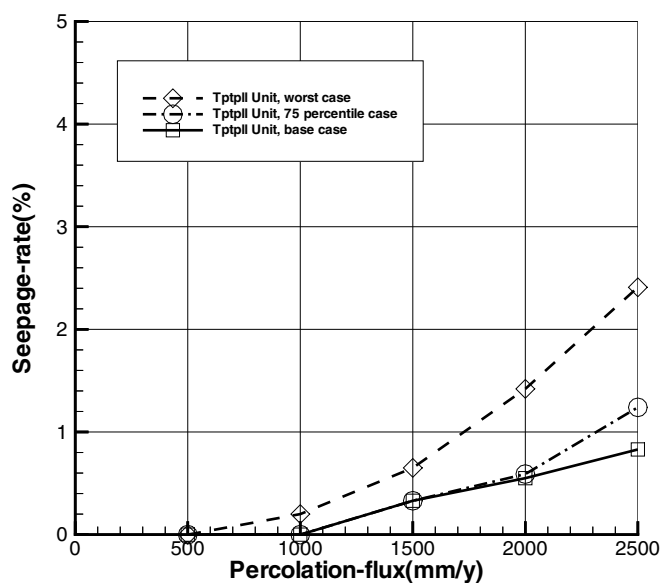
DTN: LB0104AMRU0185.011

Figure 6.4-9.   Seepage Percentage as a Function of Percolation Flux Q_P for the Two Degradation Scenarios for Parameter Set B′, Realization 1
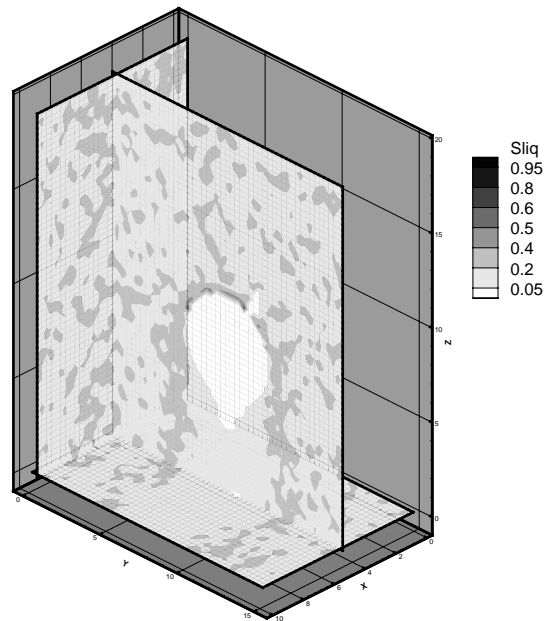
DTN: LB0104AMRU0185.011

Figure 6.4-10.   Saturation Distribution around a Drift for the Worst Case in the Tptpll with Parameter Set B′, Realization 1
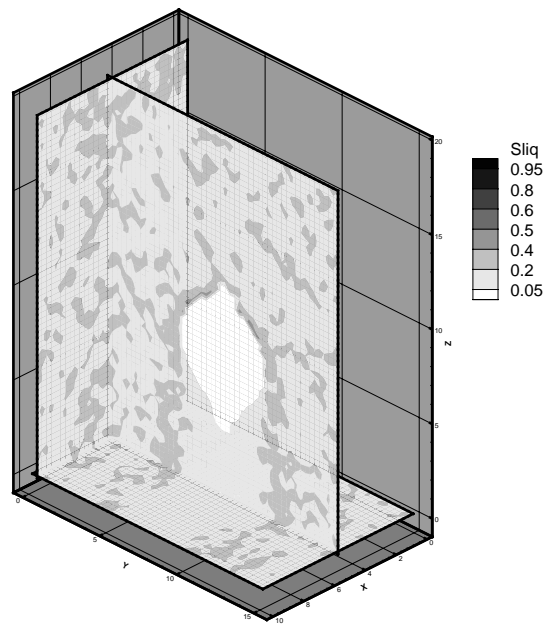
DTN: LB0104AMRU0185.011

Figure 6.4-11.   Saturation Distribution around a Drift for the 75 Percentile Case in the Tptpll with Parameter Set B′, Realization 1
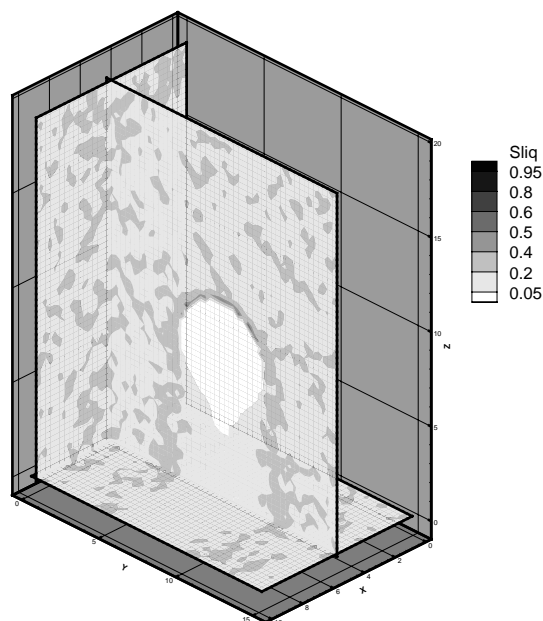
DTN: LB0104AMRU0185.011

Figure 6.4-12.   Saturation Distribution around a Drift for No-Degradation Case in the Tptpll with Parameter Set B′, Realization 1

The results in Table 6.4-2 show the effect of rockfall on seepage into drift in the Tptpll unit. Figure 6.4-9 shows the calculated seepage percentage as a function of percolation flux Q_p, Realization 1. The results indicate that the seepage threshold is not significantly affected by drift degradation, up to two percentage points. Figures 6.4-10, 6.4-11, and 6.4-12 illustrate the saturation profile around the drift for two degradation scenarios and the no-degradation case in the Tptpll unit with parameter Set B′, Realization 1.

Figures 6.4-13 and 6.4-14 show the spread of the drift seepage in the Tptpmn and Tptpll units from the three realizations. For the base case, the 75th percentile case, and the worst case, with the percolation flux value of 500 mm/yr, the seepage spread is between 5 and 7 percentage points in the Tptpmn and around 2 percentage points in the Tptpll unit.
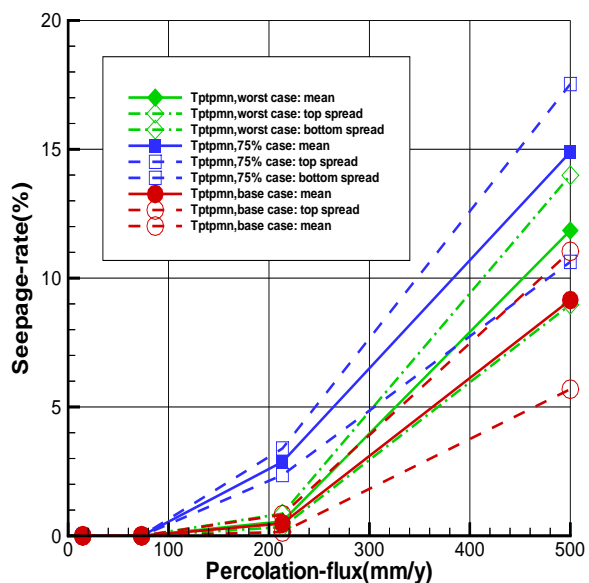
DTN: LB0104AMRU0185.011

Figure 6.4-13.   Seepage Spread from Three Realizations in the Tptpmn Unit
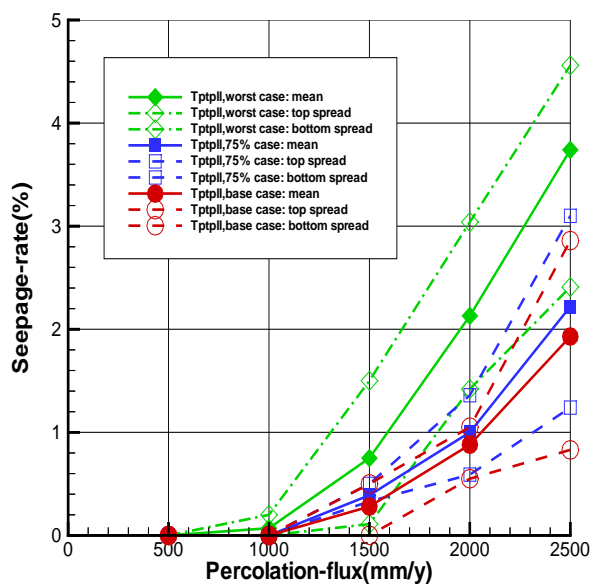
DTN: LB0104AMRU0185.011

Figure 6.4-14.   Seepage Spread from Three Realizations in the Tptpll Unit

Calculations were also made with parameter Set B that resulted in zero seepage for all cases with the percolation flux up to 2500 mm/yr, with or without drift degradation.

6.4.1.1.5   Conclusions

Four scenarios of detailed degraded drift profiles, calculated using a discrete region key-block analysis (CRWMS M&O 2000 [151635]; DTN: MO0109RDDAAMRR.003 [156306]), were selected for conducting seepage calculations. The model has been refined over previous studies (CRWMS M&O 2000 [153314]) both by use of 3-D key-block analysis (replacing prior schematic 2-D rock-failure profiling), and by incorporation of a revised set of calibrated mean parameters for the Tptpll unit.

Results in this section are based on seepage calibration model results and a review of available *in situ* field results appropriate to the Tptpmn lithostratigraphic unit and one set of data for the Tptpll unit. As more data from these units (where the potential repository resides) are obtained in field measurements, parameter values (with their uncertainties and probability weightings) should be developed and then seepage predictions from tables in this AMR can be used in PA to obtain the best estimates (with uncertainty ranges) for Yucca Mountain.

Uncertainty associated with geostatistics is evaluated through calculations using three realizations for each case. Results are shown in Tables 6.4.1.1-2 and 6.4.1.1–3. The spread of results from the three realizations gives an indication of geostatistical variation.

In summary, this section demonstrates that the impact of drift degradation and flow-field heterogeneity can be evaluated. Generally, for both the Tptpmn and Tptpll units, simulated seepage enhancement because of drift degradation is calculated, with larger effects for larger percolation flux values. Seepage enhancement resulting from rockfall is between 0 and 5 percentage points in all three realizations for the Tptpmn unit, and less than 2 percentage points for the Tptpll unit. The enhancement does not seem to be dependent on whether it is worst case (i.e., largest rockfall) or 75 percentile. The shape of the drift cavity may be more important to drift seepage than the volume of rockfall. These scoping calculations confirm that the approach used for seepage enhancement due to drift degradation in TSPA-SR (CRWMS M&O 2000 [153246]) is conservative.

6.4.1.2   The Effect of Rock Bolts on Seepage

Using grouted rock bolts is one proposed method of ground support for the emplacement drifts in the Tptpmn. Rock bolts are lengths of steel that are grouted into a borehole normal to the drift wall. They accomplish two purposes: (1) binding the mass of rock above the drift to prevent large rockfalls, and (2) providing an anchoring point for a steel mesh, which is placed against the drift wall to prevent raveling (small rock falls).

Rock bolts present a concern with respect to seepage because they may provide a direct flow conduit to the drift wall, and if so, they will increase the likelihood that a flowing fracture will be intersected and that flow will be diverted to the drift wall to become seepage. This simple model of the effect of rock bolts on seepage is illustrated in Figure 6.4-15. Flow along Path A, which may be considered a flowing fracture, is diverted around the drift, while flow along Path B intersects the rock bolt, which provides a direct conduit to the drift wall.
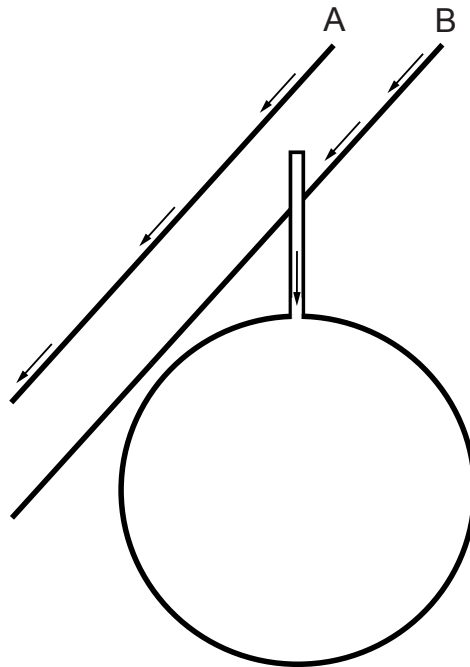
Figure 6.4-15.   Simple Model Schematic of Rock Bolt Impact on Seepage

6.4.1.2.1   Rock Bolt Model

A more complete model of the effect of rock bolts will consider several other factors, including:

- The properties of degraded grout and/or rock bolt material, including the case in which the rock bolt and grout are completely removed from the hole such that the rock-bolt hole is itself a capillary barrier

- The dimensions of the rock bolt and grout

- Uncertainty in the hydraulic properties of the formation

- A range of percolation rates

- The possibility for lateral diversion away from the rock bolt at or near the drift wall

- Rock bolt density and orientation(s).

Figure 6.4-16 shows a sketch of the conceptual model for rock bolt interaction with percolation, which may enhance seepage. Flow along a fracture may encounter a rock-bolt hole and either be diverted around the hole or enter the hole. How much enters the hole and how much is diverted around it depends on the dimensions of the hole, the angle of the fracture with respect to the hole, the rate of flow, channeling of flow in the fracture, the hydraulic properties of the grout (if any), filling the hole, and the local saturation of the grout. Flow that enters the hole will not necessarily result in seepage. The head (or reduction in capillary pressure) at the collar of the hole (i.e. where the hole intersects the drift wall) may not be sufficient to induce seepage,

especially if there are pathways for the water to flow back into the formation and be diverted around the drift. Similarly, if seepage would already be occurring without the presence of rock bolts, sufficient diversion capacity may exist such that the rock bolts will not increase seepage.
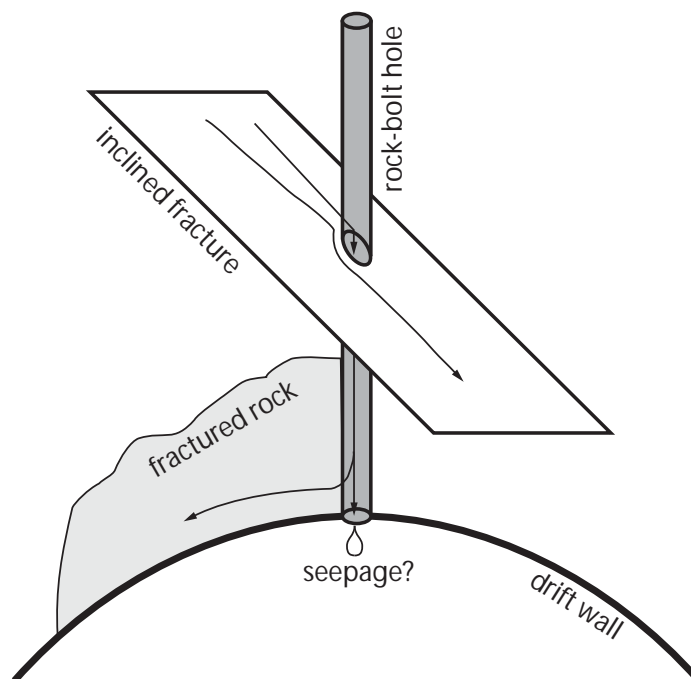
NOTE: Possible paths of percolating water are shown by arrows.

Figure 6.4-16.   Conceptual Model Schematic of Rock Bolt Impact on Seepage

Previous treatment of rock bolts as a seepage enhancing factor, documented in the AMR *Seepage Model for PA Including Drift Collapse* (CRWMS M&O 2000 [153314], Section 6.7), considered only an extremely simplified model for rock bolts in order to study their effect on seepage. The rock bolts were modeled as "needles" extending from the drift wall (the last grid node before the drift wall) vertically downward into the drift, unlike a bolt hole, which extends upward away from the drift. Because the "needle" is a single connection, no opportunity occurs for lateral flow away from the "needle" near the drift wall. The size and properties of this node were unmodified with respect to the surrounding grid. This is in contrast to an actual rock-bolt hole, which would have a significantly smaller horizontal cross section and, depending on the properties of the material in the hole (or lack thereof), might create a permeability or capillary barrier and divert flow. These simplifications are likely to significantly impact the results. Seepage enhancement was found to stabilize for a "needle" length of 0.15–0.25 m. The seepage enhancement for one needle was found to be 3%.

The proposed use of ground support is documented in the AMR *Ground Control for Emplacement Drifts for SR* (BSC 2001 [155187]). The proposed rock bolt and grout dimensions are 3 meters long (BSC 2001 [155187], Section 6.5.1.2.2), with a rock bolt diameter of 0.0254 m (1 inch) and a grout annulus thickness of 0.00635 m (¼ inch) (BSC 2001 [155187], Table 4-10). The rock bolts are proposed to be emplaced with a lateral spacing of 1.5 m (BSC 2001 [155187], Section 6.5.1.2.2). The properties and expected longevity of the rock bolt and grout system is

documented in (BSC 2001 [155667], Section 6.4.3.1). The design permeability of the newly emplaced grout is less than 10^{-19} m^2 (10^{-12} m/s) (BSC 2001 [155667], Section 6.4), and its expected life at that permeability is 300 years (BSC 2001 [155667], Section 6.4)

A refined model that includes a range of properties for the grout and the formation, as well as a range of percolation rates, has been prepared. Figure 6.4-17 shows a sketch of the model. The model uses a two-dimensional, radially symmetric grid with a vertical symmetry axis generated using the software iTOUGH2 V4.0 (LBNL 1999 [139918]). Grid size is 10 cm, with finer discretization, down to 0.1 mm, at the interface between the grout and the surrounding rock. Because this is a radially symmetric grid, the drift opening, created using the routines MoveMesh V1.0 (LBNL 2000 [152824]) and CutNiche V1.3 (LBNL 2000 [152828]), is spherical instead of cylindrical. Knight et al. (1989 [154293], p. 37) find that seepage exclusion from a cylindrical cavity is similar to that of a spherical cavity of twice the radius. This is explained by relating the seepage exclusion potential of an opening to the total curvature of the boundary of the opening. For a cylindrical cavity, the curvature is infinite along the axis of the cylinder and finite perpendicular to the axis. For a spherical cavity, the curvature is finite and equal in any direction. Thus, the equivalent radius of the spherical "drift" in the model is twice that of the design drift radius.
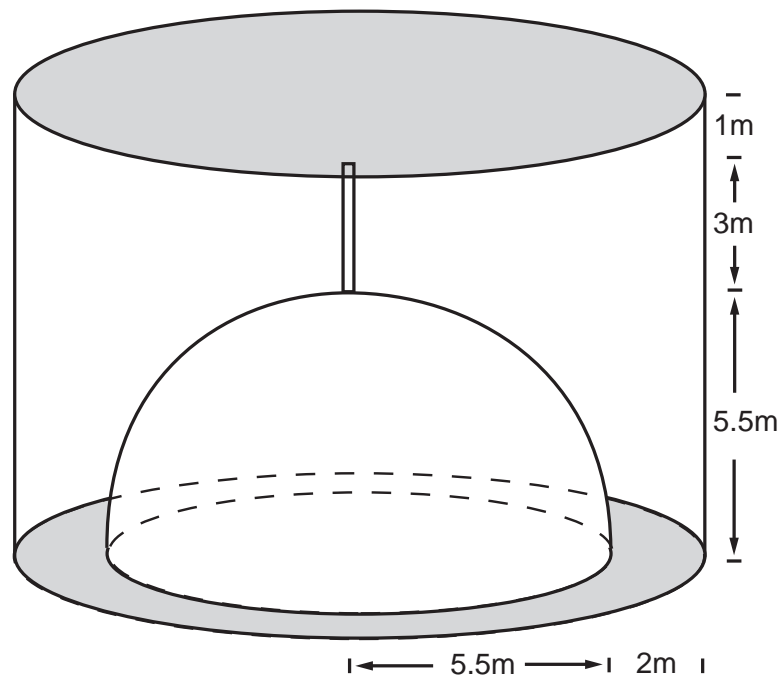
NOTE: The shaded areas represent the upper boundary where percolation is uniformly applied and the lower boundary where a gravity drainage condition is applied.

Figure 6.4-17.   Numerical Grid Dimensions

As a base case, seepage into the opening without any rock bolts is modeled. Percolation rates of 5, 14.6, 73.2, 213, and 500 mm/yr are applied uniformly to the upper model boundary as used in the AMR *Seepage Model for PA Including Drift Collapse* (CRWMS M&O 2000 [153314], Section 6.3.7). Parameter Set A from the same AMR (DTN: LB0010SCMREV01.002 [153393]) and the alternative $1/\alpha$ values of 400 and 200 Pa (CRWMS M&O 2000 [153314], Sections 6.3

and 6.3.4) are used for the formation. A constant zero capillary pressure is specified at the drift wall boundary, a gravity drainage condition at the lower boundary (assigned in the grid using the routine AddBound V1.0 (LBNL 2000 [152823])), and a no-flow condition on the lateral boundary, all of which are consistent with the current models of seepage at Yucca Mountain (CRWMS M&O 2001 [153045], Section 6.3.2.4; CRWMS M&O 2000 [153314], Section 6.3).

To investigate the impact of a rock bolt on seepage, only the case of a rock-bolt hole vertically upward from the crown of the drift is modeled. This case is sufficient to investigate whether there is any impact on seepage due to the presence of the rock-bolt hole. Three slightly different grids are prepared to explore diversion capacity away from the rock-bolt hole. Case 1 allows flow between the rock-bolt hole and the surrounding rock along the entire length of the bolt hole. Case 2 prevents flow between the bolt hole and the surrounding rock for 10 cm above the crown of the drift. Case 3 restricts flow between the bolt hole and the surrounding rock for 50 cm above the crown of the drift. Cases 2 and 3 represent scenarios where the first feature capable of carrying flow away from the bolt hole is found 10 cm or 50 cm, respectively, into the hole. A 0.0254 m (1 inch) radius bolt hole with a 0.0127 m (½ inch) radius rock bolt and a 0.0127 m (½ inch) grout annular thickness is modeled. These features are added to the grid using the routine AssignRock V1.0 (LBNL 2001 [154321]). The modeled grout annular thickness is twice as great as the design value (BSC 2001 [155187], Table 4-10); this results in a conservative model, because the modeled bolt hole has less potential as a capillary barrier to exclude in-flow, a larger surface area to intercept flow, and allow a greater opportunity to conduct flow to the drift wall.

Because the greatest impact of the rock bolts on seepage may come many thousands of years in the future after cool down and rewetting of the repository horizon and during wetter future climates, the grout is not likely to retain its design hydraulic properties. It may even completely disintegrate, leaving an open hole. So a range of properties for the grout is used. Figure 6.4-18 shows the parameter combinations evaluated. In the lower left combination, permeability equals 10^{-18} m^2 and $1/\alpha$ equals 10^7 Pa, corresponds to the design (or a slightly degraded) grout, while in the upper right combination, permeability equals 10^{-10} m^2 and $1/\alpha$ equals 10 Pa, essentially corresponds to an open bolt hole.

The details of the model and sensitivity study setup are found in Bodvarsson (2001 [156334], YMP-LBNL-DSM-CFA-1, pp. 62, 63, and 68–70). The sensitivity study uses the software TOUGH2 V1.5 (LBNL 2001 [154322]) to simulate unsaturated flow.
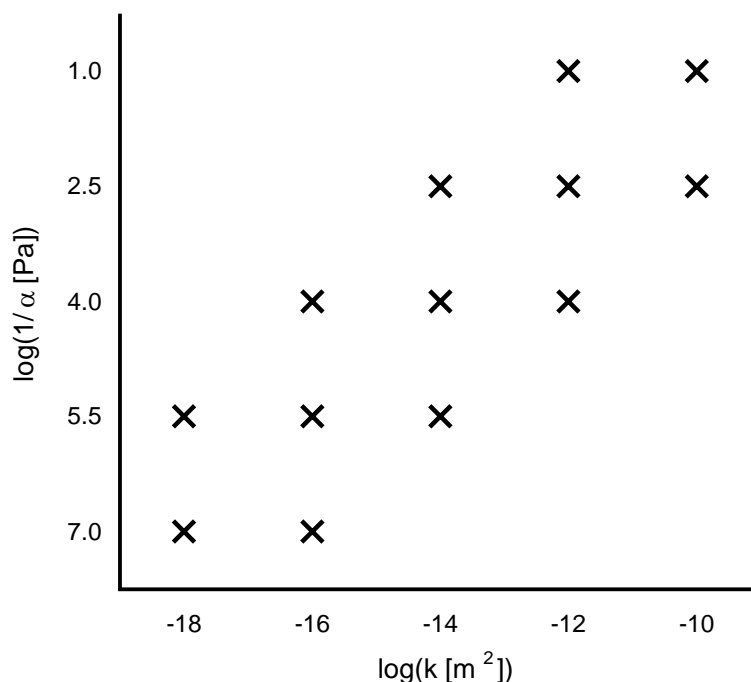
Figure 6.4-18.   Grout Parameter Combinations

6.4.1.2.2   Results of Rock Bolt Model

No seepage enhancement is predicted for any combination of the percolation rate, formation parameter, grout parameter, and numerical grid simulations. This result is very different from the previous "needle" calculation, where 3% seepage enhancement was shown for one rockbolt (CRWMS M&O 2000 [153314], Section 6.7). This result is understandable, especially considering two key points about the previous simulation:

1. The area onto which flow may be incident, if the lateral surfaces are considered, is 1.25 m^2 in the previous model as opposed to 0.24 m^2 in the current model, a ratio of 5 to 1. If only the horizontal surfaces are considered, the ratio increases to more than 100 to 1.

2. The parameters from the seepage calibration model, on which the seepage model for performance assessment is based, are predicated on the use of 5 cm connection distances between the drift wall and the first node adjacent to the drift wall (CRWMS M&O 2001 [153045], Sections 1, 6.3, 6.4.2.2). The previous calculation observed the seepage enhancement to be significant only when that connection was 3 to 5 times the recommended length, restricting the lateral flow away from the rock bolt.

6.4.1.2.3   Validation of Rock Bolt Model

Validation of the model for the intended use, i.e., evaluation of the seepage enhancement potential of rock bolts, can be judged by two criteria: 1) does the base case model using a spherical opening and a homogeneous permeability field provide comparable results to models previously used and validated for seepage calculations, and 2) do observations from Yucca Mountain contradict the results of the model.

A comparison of the seepage percentage predicted by this model with that predicted by the seepage model for performance assessment (SMPA) (CRWMS M&O 2000 [153314], Section 6.6.1), is shown in Figure 6.4-19. The SMPA uses a model with a cylindrical opening and a heterogeneous permeability field. For the formation parameters used, the two models perform similarly. There is more difference in the seepage percentage between the different formation parameters than there is between the models. Further, since the result of concern is seepage enhancement caused by rock bolts rather than seepage percentage, the use of a consistent model (i.e., one using a spherical opening and a homogeneous permeability field) for both the base-case simulations and the rock-bolt simulations is the important issue. The impact on seepage enhancement of using the spherical opening model with a homogeneous permeability field is considered a second-order effect. Thus, the model meets the first criterion listed above for validation.
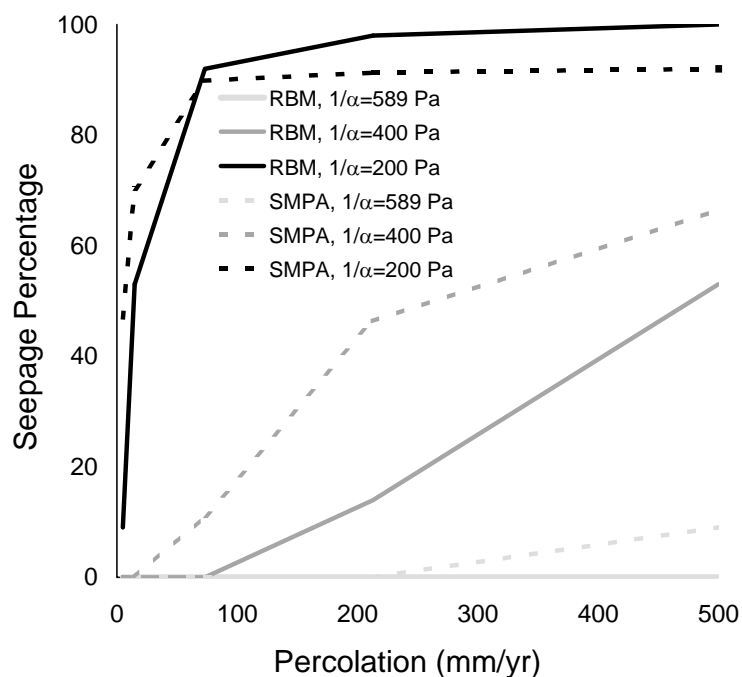
DTN: LB0104AMRU0185.004

SOURCE: (CRWMS M&O 2000 [153314], Section 6.6.1)

NOTE: For the SMPA cases with $1/\alpha$ equal to 400 and 200 Pa, the permeability is 0.9×10^{-12} m^2 rather than 1.4×10^{-12} m^2. No seepage is predicted for SMPA with $1/\alpha$ = 589 Pa.

Figure 6.4-19. Seepage percentage predicted by base case rock bolt model (RBM) compared to that for the seepage model for performance assessment (SMPA).

The model prediction of no seepage enhancement due to rock bolts appears to be counter to anecdotal evidence of occasional dripping at rock bolts in the ESF and associated tunnels (Note that there are no qualified data on seepage associated with rock bolts that could be used to directly validate this model). Several factors associated with the rock bolts in the ESF and adjacent tunnels suggest that the processes causing this dripping will not enhance seepage of background percolation. First, the type of rock bolt used in the ESF and associated tunnels is not

the same as will be used in the emplacement drifts. In the current tunnels, hollow steel "swellex" bolts are used. These bolts are expanded against the sides of the hole using water pressure (the end of the bolt is capped), which may leave behind water inside the bolt (which is available to drip out). Second, temperature, humidity, and pressure variations in the tunnels could lead to condensation inside the "swellex" bolts that would lead to dripping. Note that this water is not water from the formation but from the tunnel atmosphere because the bolt is impermeable. Third, water that has been used both in the mining of these tunnels and for drilling of the bolt holes may also be condensing and creating saturated conditions on the outside of the bolts, because the bolts are better thermal conductors than the surrounding rock. Thus, the model meets the second criterion listed above for validation.

The model results are not abstracted for TSPA-SR (BSC 2001 [155950], Section 4.3.3.6). Rather they are scoping calculations that provide confirmation of the conservatism of the models used and directly relied upon in TSPA-SR (CRWMS M&O 2000 [153246]; BSC 2001 [154659], Section 3.2.2.5). Because it meets the two criteria listed above, the model is valid for its intended use.

6.4.1.2.4   Alternative Rock Bolt Models

Alternative models for the investigation of seepage enhancement due to rock bolts include:

- Continuum models employing multiple realizations of heterogeneous permeability fields—The discussion in Section 6.4.1.2.3 suggests that a model of this type is unlikely to save significantly different results

- Discrete fracture models (Section 6.4.2)—The key element of the discrete fracture model, i.e., discrete features for flow into or out of the bolt hole, is adequately captured by the two current models in which the bolt hole is disconnected from the formation near the drift wall.

- Models that include inclined rock-bolt holes—The use of a vertical rock bolt rather than an inclined one minimizes the area onto which percolation is incident. However, the current simulations show that, for certain grout parameter combinations, flow enters even a vertical bolt hole from the sides, enhancing percolation through the grout with respect to the percolation around the bolt. The key to the lack of seepage enhancement is that the potential for sufficient lateral diversion at or near the drift wall exists, so that the flow in the bolt hole may be diverted away from the hole. For an inclined hole, there will exist even more diversion potential because the height of any "disconnected" length of the hole will be less and the diversion potential along the angled portion of the drift wall is much greater than at the crown of the drift. Thus, it is unlikely that a model including inclined rock bolts will give significantly different results.

6.4.1.2.5   Conclusions for Rock Bolt Models

The conclusion of this investigation of the potential for seepage enhancement caused by rock bolts is that there is no significant enhancement of seepage. These scoping calculations confirm

that the approach used for seepage enhancement due to drift degradation in TSPA-SR (CRWMS M&O 2000 [153246]) is conservative.

6.4.2 Focusing and Discrete Flow Paths in the TSw

The objective of this section is to investigate flow focusing and discrete paths that may occur through unsaturated fractures within the TSw unit. We developed a discrete fracture model that honors fracture data from these units, using a stochastic representation of fracture permeabilities. The model was then used to study flow allocation mechanisms and patterns and to assess the frequency and flux distributions of major water-bearing flow paths and transport pathways from the bottom of the PTn unit to the repository horizon.

6.4.2.1 Preferential Flow Phenomena

Field evidence at Yucca Mountain (for example, elevated levels of ^{36}Cl originating from atmospheric nuclear tests conducted in the 1950s and 1960s) found at several locations in the ESF (Fabryka-Martin et al. 1996 [144839], Section 9), suggests that preferential flow pathways may exist in the unsaturated rocks of Yucca Mountain. The focusing flow along these preferential paths or well-connected fracture networks may play an important role in controlling patterns of percolation through highly fractured tuffs, such as the TSw unit, and have a direct impact on seepage into drifts.

The mechanisms that control unsaturated flow and transport in fractured rocks may be very site-specific and are practically unknown. On the other hand, such detailed knowledge is necessary to accurately predict the degree of preferential flow and transport. In practice, accurate description of flow-focusing processes in unsaturated fractures is essential for accurate prediction of water seepage into emplacement drifts of the potential nuclear waste repository. The modeling studies on seepage into drifts showed that the amount of water that bypasses or breaks thorough a capillary barrier of an emplacement drift wall depends not only on the capillarity and permeability of the surrounding fracture system, but also on the heterogeneity of the water flux and flow paths (CRWMS M&O 2001 [153045], Section 6.5.2).

Several conceptual models have been proposed for handling water flow through the thick, fractured UZ at Yucca Mountain–from continuous fracture flow, such as indicated by the results of the dual-permeability model described in *UZ Flow Models and Submodels* (CRWMS M&O 2000 [122797]), to sparse discrete flow through a very small portion of the fracture network (Pruess et al. 1999 [117112]). Modeling approaches used in characterizing general fracture flow include (1) the continuum model (e.g., ECM and dual-permeability (Wu et al. 1999 [117161])) and (2) the discrete-fracture model (CRWMS M&O 2001 [153045], Section 6.5.1).

6.4.2.2 Modeling Approach and Model Description

The modeling studies of this section are based on a 2-D, vertical cross-sectional model that has the upper boundary at the bottom of the PTn and the lower boundary at the repository horizon. This cross section has a width of 100 m and is 150 m in vertical extent (Figure 6.4-20). The dimension of the model was considered adequate in the horizontal direction because the correlation length for variability in fracture permeability and spacing is on the order of 1 m. The 150 m vertical extent of the model corresponds to an average distance from the interface between

the PTn and TSw units to the repository horizon over the repository area. The bottom of the PTn was chosen as the upper boundary because this unit is believed to behave as a porous medium, with limited fracture flow. Both uniform and nonuniform percolation flux boundary conditions are prescribed at this upper boundary. The two side boundaries are treated as no-flux boundaries, whereas the bottom boundary allows for gravitational drainage out of the model.

Only the fracture continuum is modeled in this study because the matrix system is believed to play a limited role in carrying water. The matrix is also not expected to have a major impact on the development of preferential flow paths or weeps within the model boundaries because of its orders-of-magnitude lower permeability than fractures (CRWMS M&O 2000 [144426], Table 13). The properties of the fracture system are based on those from the *Calibrated Properties Model* (CRWMS M&O 2000 [144426]). Five different hydrogeologic layers (TSw31 to TSw35) within the 2-D model, are represented by different fracture properties (DTN: LB991121233129.001 [147328]).

Fracture permeability is prescribed stochastically, based on measured air-permeability data. Spherical semivariogram models (Deutsch and Journel 1992 [100567], p. 23) are used to represent the empirical log-permeability semivariograms. Details on the methodology of generating stochastic fracture permeability are discussed in the AMR *Seepage Calibration Model and Seepage Testing Data* (CRWMS M&O 2001 [153045], Section 6.4.2.1), which concludes that the fracture permeability near the potential repository is essentially random, without a noticeable or significant spatial correlation.

The fracture permeability distribution (defined using DTNs: LB990901233124.004 [123273], LB002181233124.001 [146878], LB0012AIRKTEST.001 [154586], LB00090012213U.001 [153141]) is generated by multiplying the mean fracture permeability of each hydrogeologic unit by randomly generated multipliers. The SISIM module of the GSLIB package (Specifically, GSLIB V1.0MSISIMV1.203 (LBNL 1999 [134136])) is used to generate the two-dimensional, spatially correlated permeability field multipliers for gridblocks of 0.25 m × 0.5 m, using a sequential-indicator simulator (Deutsch and Journal 1992 [100567], p. 151). The random permeability field takes into account the measured post-excavation air-permeability data. The resulting permeability fields are inserted into the 2-D numerical mesh for each permeability field realization using Perm2Mesh V1.0 (LBNL 2000 [152826]).

The cumulative distribution functions used for permeability field generation are documented in scientific notebooks (Bodvarsson 2001 [156334], YMP-LBNL-GSB-1.6.4, pp. 24–25; YMP-LBNL-YSW-4, pp. 25–27).

Figure 6.4-20 shows examples of the prescribed fracture permeability distributions over the model domain, using correlation lengths of 1 m and 3 m, respectively. The figure shows that fracture permeability varies nearly four orders of magnitude, between approximately 3×10^{-13} m^2 and 3×10^{-9} m^2. Each distribution has contrasting fracture permeability patterns, with upper regions (in TSw31, TSw32, and TSw33 units) having relatively high permeabilities extending 110 m vertically and the region just above the repository horizon boundary (in TSw34 unit) having lower permeability. The permeability structure (Figure 6.4-20 (a)) reflects the 1 m correlation length, which results in patches of high and low permeabilities extending over the correlation length in each direction. Figure 6.4-20 (b) shows a similar permeability structure

using a 3 m correlation length. Both permeability structures and the resulting simulation results are presented in this report. All other fracture properties besides fracture permeability are taken as constant over each hydrogeologic unit within the entire model domain (Table 6.4-4, DTN: LB991121233129.001 [147328]).

The work described here is further documented in Bodvarsson (2001 [156334], YMP-LBNL-YSW-KZ-1, pp. 7–23, YMP-LBNL-YSW-4, pp. 28–32).
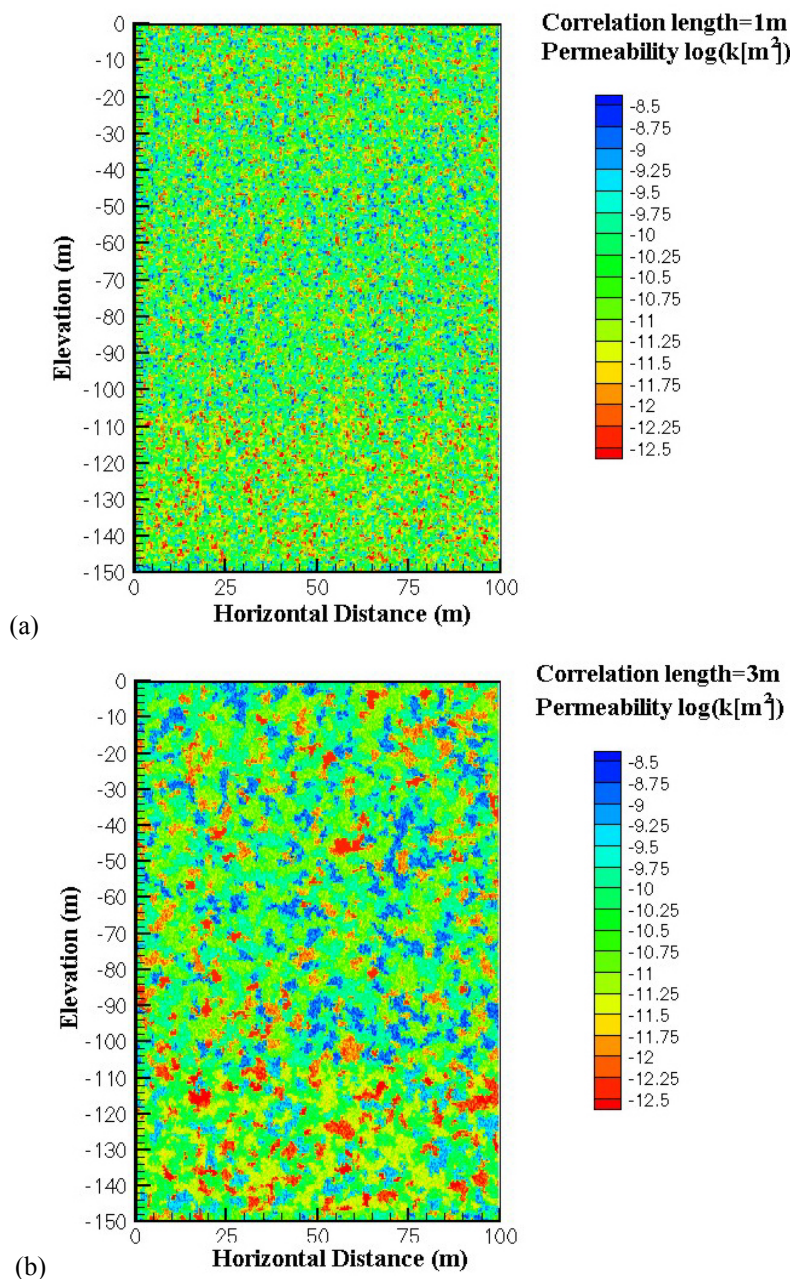
DTN: LB0104AMRU0185.005

Figure 6.4-20.   Spatially Correlated Fracture Permeability Fields [log (k(m^2))] Used in the Model Studies; (a) 1 m Correlation Length; (b) 3 m Correlation Length

Table 6.4-4.   Fracture Properties Used in the Model Studies

Model Layer	Permeability	van Genuchten parameters		Porosity	Residual saturation
	k_F (m^2)	α_F (1/Pa)	m_F (-)	ϕ_F (-)	S_{rf} (-)
Tsw31	3.21E-11	2.49E-4	0.566	5.5E-3	0.01
Tsw32	3.56E-11	1.27E-3	0.608	9.5E-3	0.01
Tsw33	3.86E-11	1.46E-3	0.608	6.6E-3	0.01
Tsw34	1.70E-11	5.16E-4	0.608	1.0E-2	0.01
Tsw35	4.51E-11	7.39E-4	0.611	1.2E-2	0.01

DTN: LB991121233129.001 [147328]

6.4.2.3   Model Results and Analyses

All the flow model results discussed below correspond to steady-state flow simulation results. Among these study cases, the realization (Realization #1) of fracture permeabilities with a correlation length of 1 m is considered as the base-case scenario. The upper boundary for the base-case modeling scenario is prescribed with uniform percolation flux of 5 mm/year for allocating flow to different fractures.

Model Results with 1 m Correlation Length: Figure 6.4-21 shows the distribution of simulated liquid mass flux magnitude within the 2-D domain with the base-case scenario. The figure shows clearly that a number of vertically high-flux, discrete flow paths develop for this flow scenario. In addition, Figure 6.4-21 indicates that about five to ten major pathways (or weeps) are present in the upper layer (above the elevation of –110 m). Considerably more pathways are present in the lower layer.

Figure 6.4-22 shows the vertical liquid mass flux at two different elevations. The first horizontal profile is for the depth of 25 m (Figure 6.4-22 (a)) and the second one at the bottom of the model domain (Figure 6.4-22 (b); at 150 m depth). At both elevations, the figure shows a significant variability in flux, with values ranging from practically 0 mm per year to almost 30 mm/year. The results shown in Figure 6.4-22 (a) and (b) indicate the development of some 50 weeps over the 100 m wide model domain, which average to about one major water pathway every 2 m. There appears to be little difference between the flow patterns in (a) and (b), suggesting that the water flow paths and their characteristics developed within tens of meters from the top of the model remain similar in statistics for the remaining 100 m vertical extent of the model. This similarity is clearly illustrated by Figure 6.4-23, which exhibits the normalized flux (with respect to mean infiltration rate on the top) on the horizontal axis and the flux frequency distribution on the vertical axis. The frequencies are generated by grouping the vertical flux results along an elevation, counting the total found in each group, and then calculating the percent contribution relative to the total horizontal distance (or area) in each category. Figure 6.4-23 compares statistical results at four different depths of the model: 25, 50, 100, and 150 m (bottom of the model). The figure shows very similar flux frequency distribution at all these elevations.
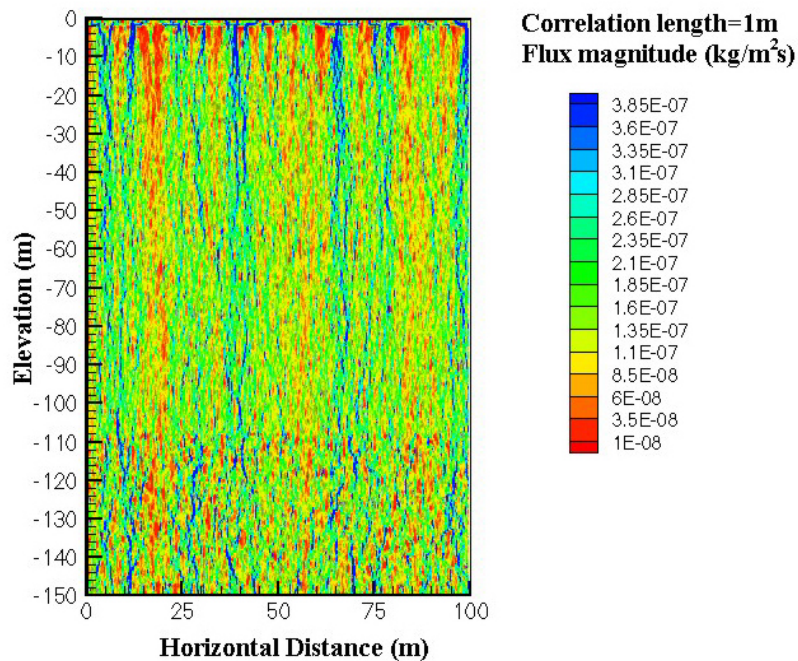
DTN: LB0104AMRU0185.005

Figure 6.4-21.   Distribution of Flux Magnitude within the 2-D Model Domain, Simulated Using the Base-Case Scenario with 1 m Correlation Length, Indicating Forming Several High-Flux Flow Paths (Realization #1)

(a)

(b)
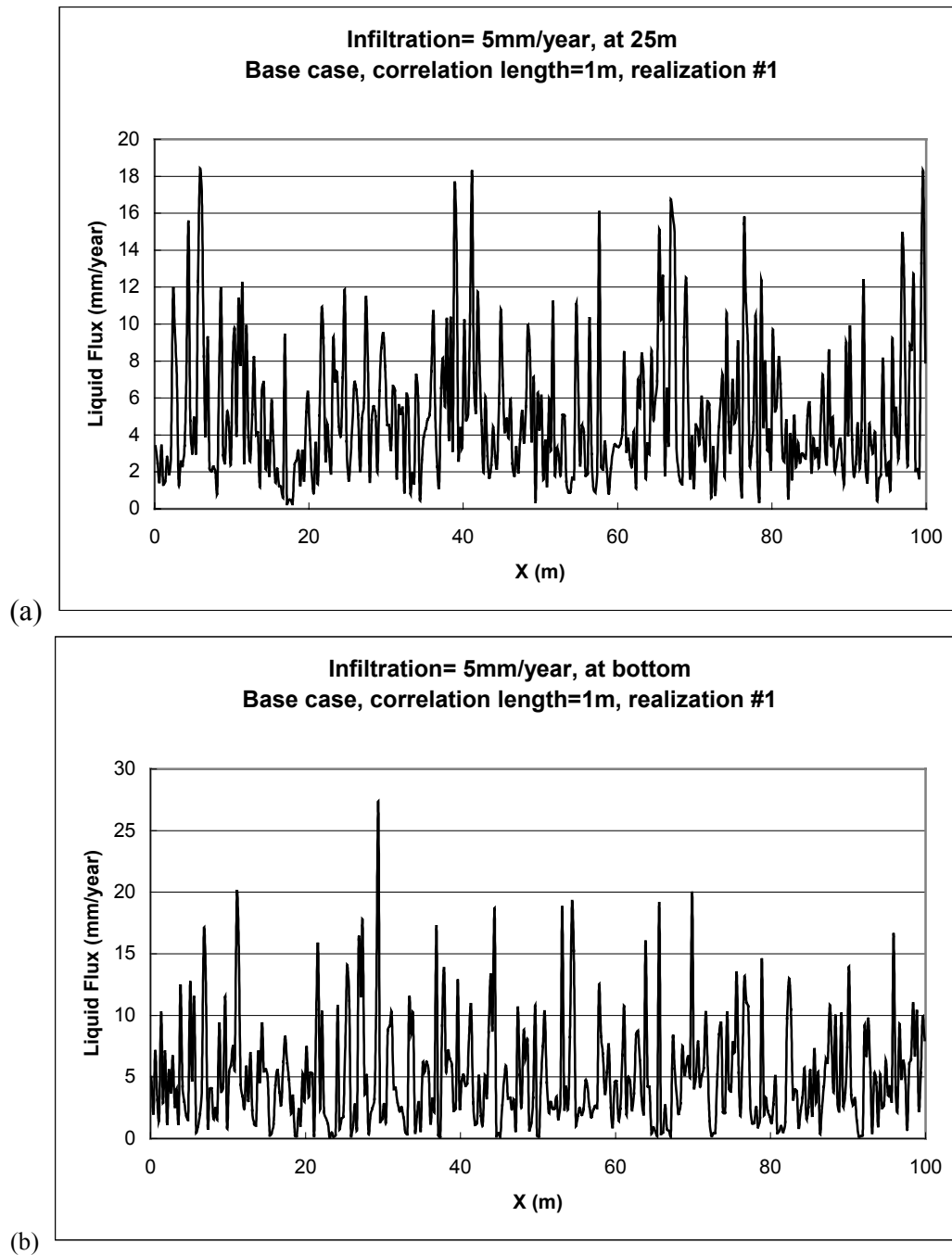
DTN: LB0104AMRU0185.005

Figure 6.4-22.   Distribution of Vertical Fluxes within the 2-D Model Domain, Simulated Using the Base-Case Scenario with 1 m Correlation Length, (a) at a Depth of 25 m; (b) at the Bottom

Infiltration=5mm/year
Base case, correlation length=1m, realization #1
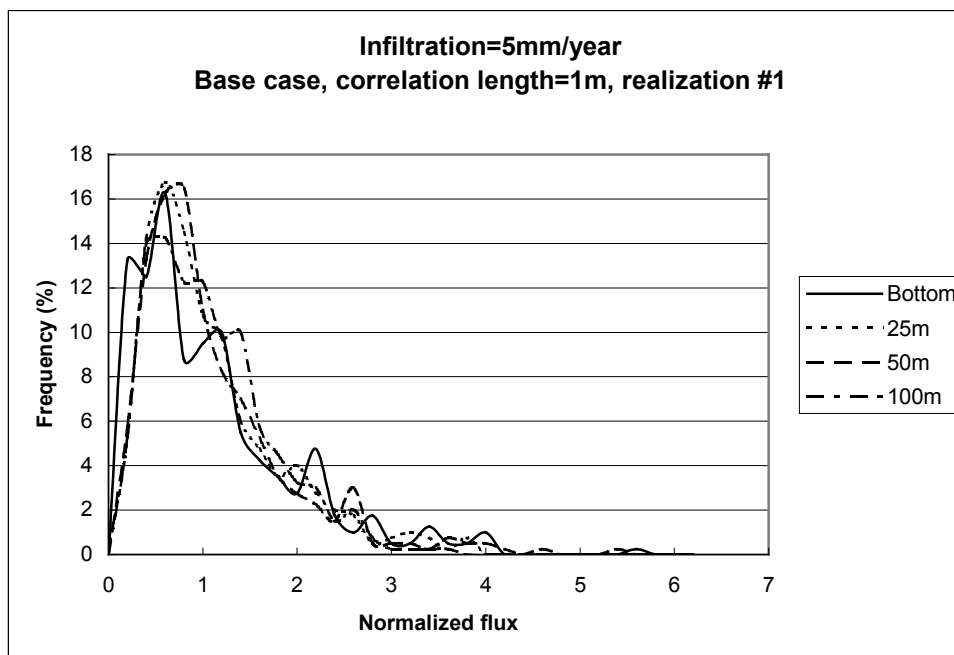
DTN: LB0104AMRU0185.012

Figure 6.4-23.   Comparison of Frequency Distribution of Simulated Fluxes at Different Elevations within the 2-D Model Domain, Simulated Using the Base-Case Scenario with 1 m Correlation Length

Several sensitivity analyses were performed using the base-case model. In particular, the flux values of the top boundary condition were varied from 1 to 500 mm per year. Figure 6.4-24 shows again the normalized flux plotted against the flux frequency for five distinct infiltration cases: 1, 5, 25, 100, and 500 mm/year. With percolation normalized to infiltration rates on the top, as shown in Figure 6.4-24, the flux frequency and distribution for all cases are statistically similar. The majority of normalized fluxes are in the range from zero to two, while the remaining high fluxes have low frequencies. The maximum flux that occurs in the system is generally about five to six times more than the prescribed infiltration rates at the upper boundary. This flow-focusing factor is considerably lower than what is currently assumed in the Total System Performance Assessment (TSPA) models, which assume flow focusing up to about 50 times the local percolation flux.
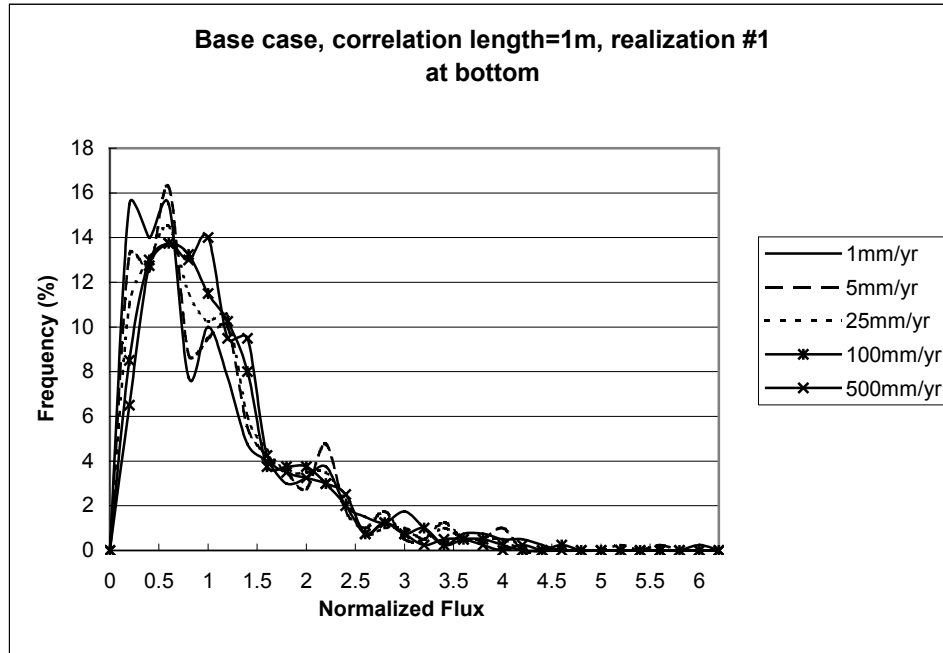
DTN: LB0104AMRU0185.012

Figure 6.4-24.   Frequency Distribution of Simulated Fluxes at Different Infiltration Rates within the 2-D Model Domain, Simulated Using the Base-Case Scenario with 1 m Correlation Length

A second realization (Realization #2) of fracture permeability, generated using a different random number (but otherwise using the same fracture properties and model domain with the same correlation length of 1 m), was also considered. The permeability distribution is found to be similar to that shown in Figure 6.4-20(a) and the resulting normalized flux versus frequency plot is shown in Figure 6.4-25. For this realization, three percolation fluxes were applied at the upper boundary at 1, 25, and 500 mm per year. The statistical results obtained are very similar to that shown in the first realization, as seen in the comparing of Figures 6.4-24 and 6.4-25. It therefore appears that the results shown in these figures can and should be used in future abstractions of flow focusing at the repository horizon.

**Base case, correlation length=1m, realization #2
at bottom**
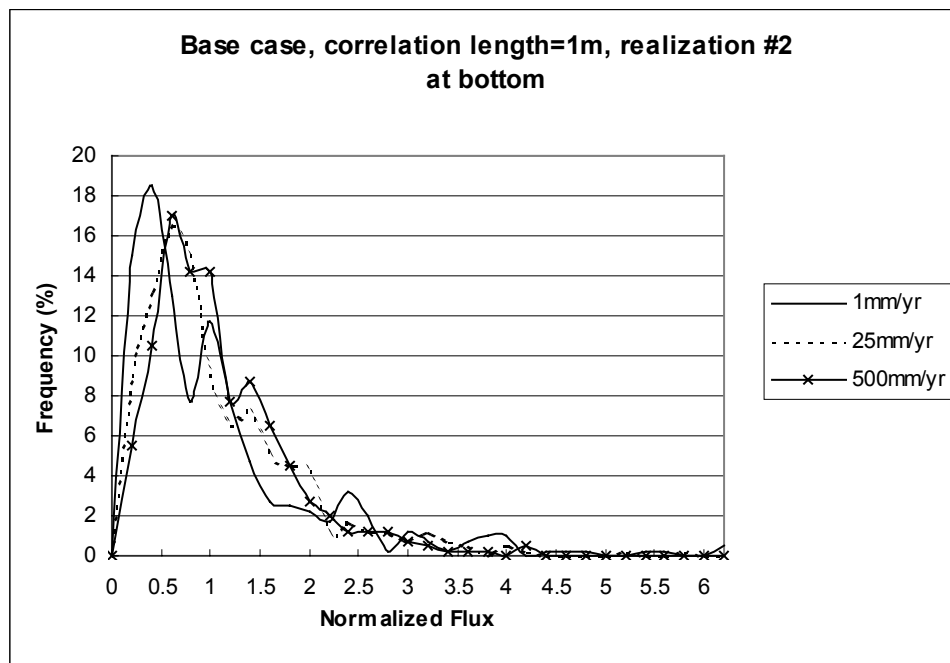
DTN: LB0104AMRU0185.012

Figure 6.4-25. Frequency Distribution of Simulated Fluxes at Different Infiltration Rates within the 2-D Model Domain, Simulated Using Realization #2 with 1 m Correlation Length

Model Results with 3 m Correlation Length: Simulations performed using a 3 m correlation length for the permeability field in the fracture network are presented below. Figure 6.4-20(b) shows the permeability spatial distribution with this realization. As expected, the patches or regions of high and low permeability are relatively larger, on the order of five to ten meters. The value range for fracture permeabilities is the same as other cases, from about 100 mD to over 100 D.

Figure 6.4-26 shows the distribution of simulated liquid flux across the 2-D domain with the 5 mm/year infiltration described on the top. Compared with the flow patterns on Figure 6.4-21 for the 1 m correlation length case, Figure 6.4-26 shows that fewer but wider discrete, high-flux flow paths (or weeps) are predicted with the 3 m correlation length scenario. Larger areas with similar high or low permeabilities (Figure 6.4-20(b)) result in larger higher and lower flow zones.

Figure 6.4-27 show vertical liquid fluxes at elevations of -25 m and -150 m (bottom), respectively. The figure shows that there are many more extended regions of low and high liquid flux for this case in comparison to the 1 m correlation length case (Figure 6.4-22). The extended regions of high or low flux cover on the order of tens of meters rather than just a few meters (as in the previous case). In addition, a comparison of Figures 6.4-27(a) and (b) shows different patterns at the two elevations. This indicates that the large correlation length (3 m) requires a longer vertical distance to reach the statistically similar flux distributions.

Figure 6.4-28 shows the normalized flux verses flux frequency distribution for the 3 m correlation length case under different infiltration rates at the upper boundary. Comparison of

Figures 6.4-24 and 6.4-28 indicates a rather similar behavior in spite of the large difference in correlation lengths. A more systematic shift occurs in the peak frequencies as a function of percolation flux for the 3 m correlation length case in this set of simulations.
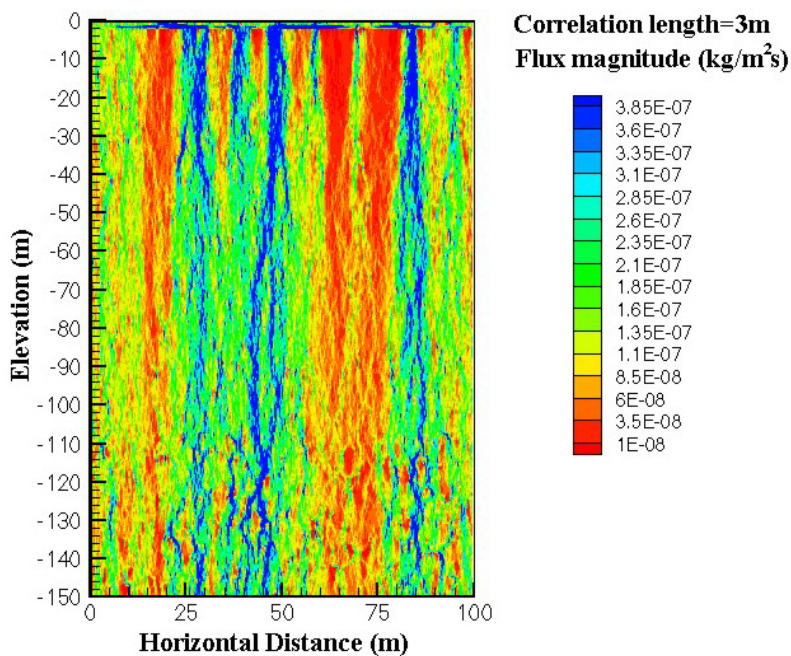
DTN: LB0104AMRU0185.005

Figure 6.4-26.   Distribution of Flux Magnitude within the 2-D Model Domain, Simulated Using with 3 m Correlation Length Case, Indicating Forming Large High- and Low Flux Flow Paths

Infiltration= 5mm/year, at 25m, correlation length=3m

Infiltration= 5mm/year, at bottom, correlation length=3m
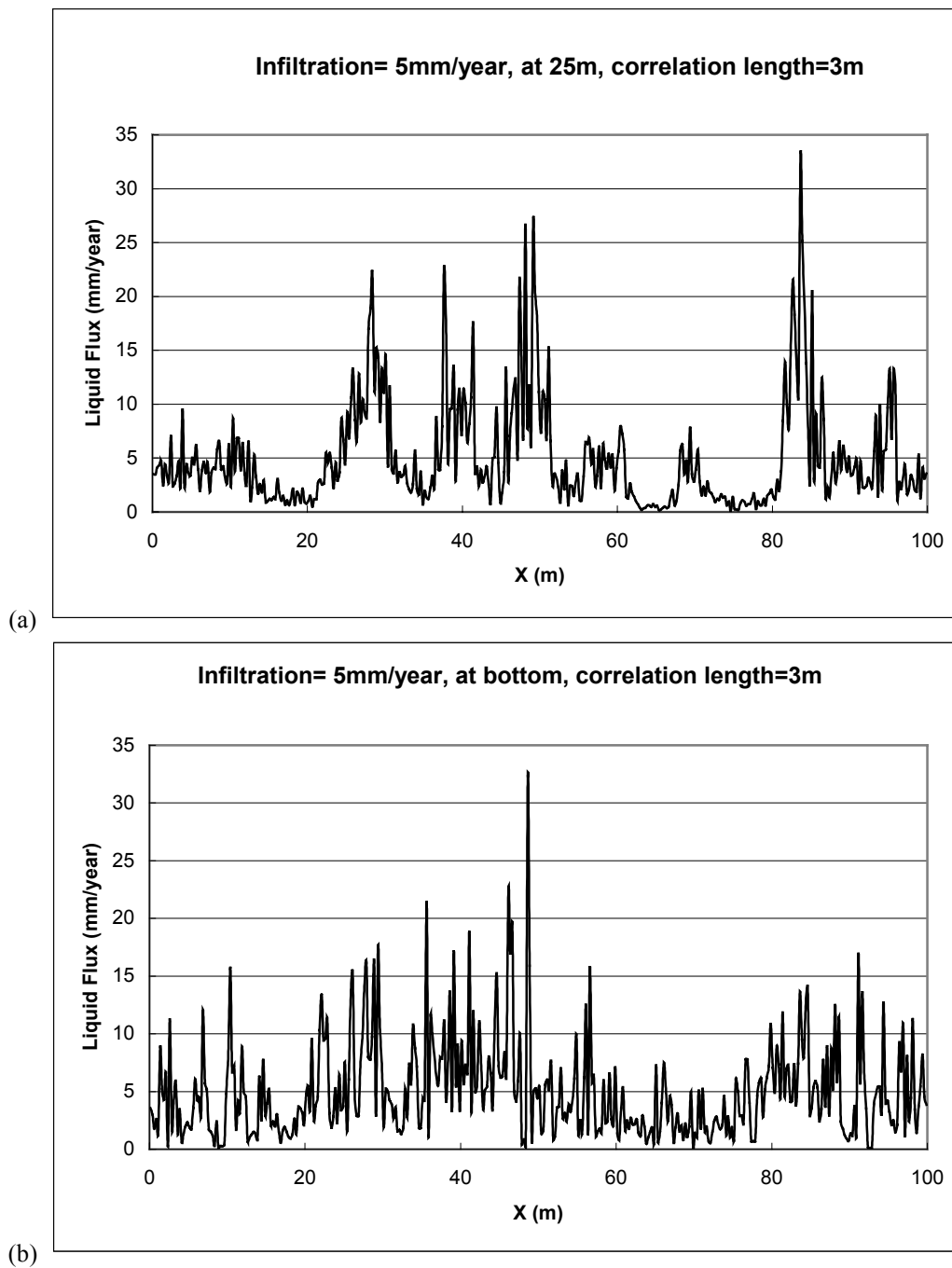
DTN: LB0104AMRU0185.005

Figure 6.4-27.   Distribution of Vertical Fluxes within the 2-D Model Domain, Simulated with the 3-m Correlation Length, (a) at a Depth of 25 m and (b) at the Bottom
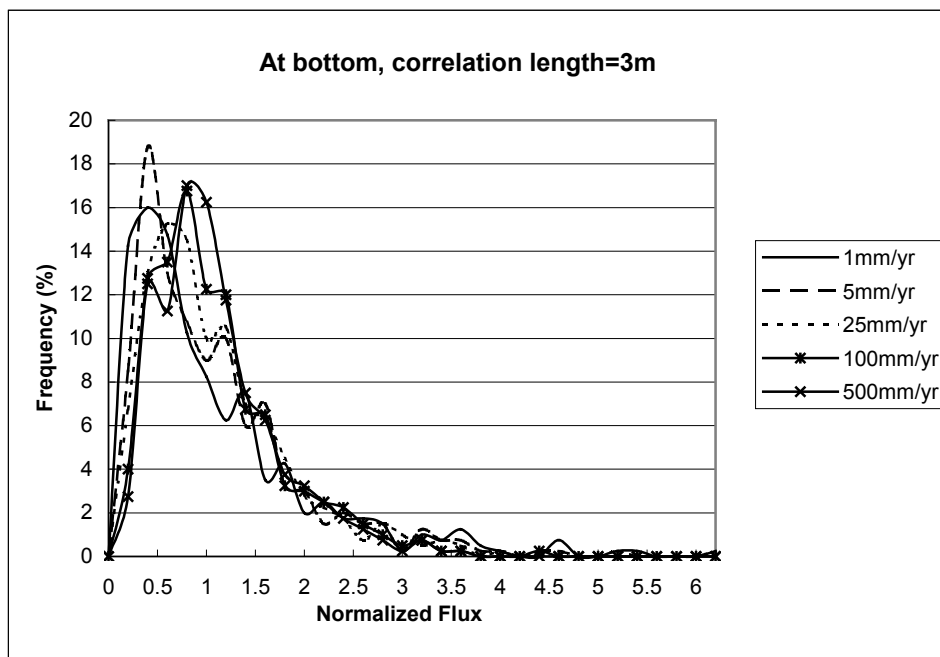
DTN: LB0104AMRU0185.012

Figure 6.4-28.   Frequency Distribution of Simulated Fluxes at Different Infiltration Rates within the 2-D Model Domain, Simulated with 1 m Correlation Length

Results with Nonuniform Infiltration: A sensitivity study on the effect of a nonuniform infiltration boundary condition at the upper boundary (at the bottom of the PTn), is given here. The case considered is that of water flux being injected at one point (pulse of 0.25 m wide) every 5 m along the top boundary. The total amount of injected mass flux is the same as that of the 5 m uniformly distributed infiltration. Thus, there are 20 discrete sources at the top of the model over the 100 m width of the model domain. Figure 6.4-29 shows the normalized flux versus frequency for this case at different elevations. Comparison of Figure 6.4-29 with Figure 6.4-23 shows that the results using uniform and nonuniform infiltration on the top boundary are very similar. This sensitivity analysis thus indicates that the flow patterns using a nonuniform infiltration flux behaves as if there were a uniform flux condition at the upper boundary.
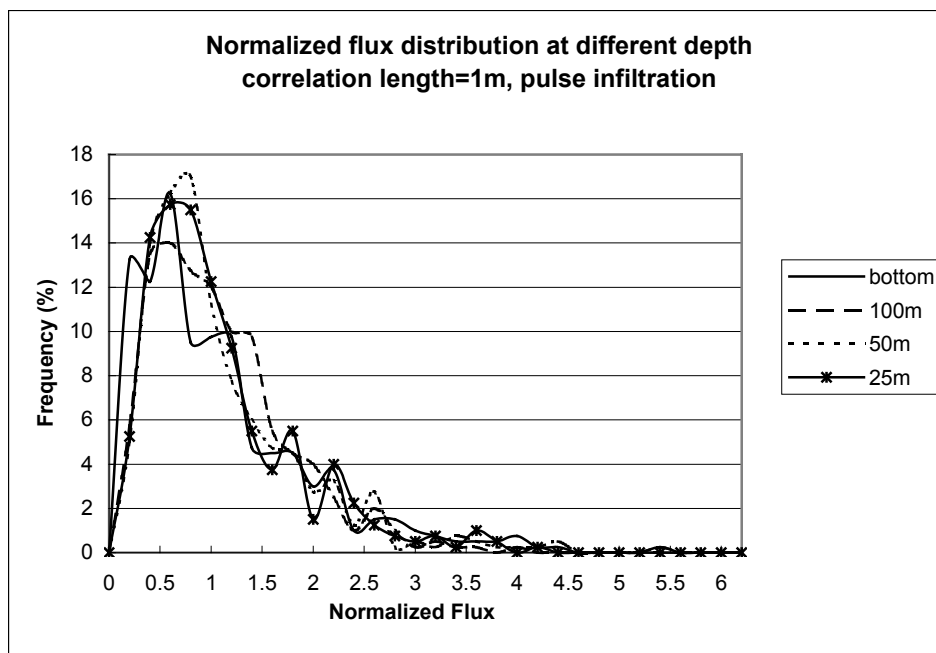
DTN: LB0104AMRU0185.012

Figure 6.4-29.   Frequency Distribution of Simulated Fluxes at Different Elevations with 5 m Pulse
Different Infiltration, Simulated with 1 m Correlation Length

Results with Tracer Transport: Tracer transport analyses with the 2-D model may provide additional insight into flow focusing and discrete paths. Here we discuss some of the transport modeling using the base-case flow model, i.e., uniform top infiltration flux and 1 m correlation length for fracture permeability. A conservative tracer (nonsorbing) with a molecular diffusion coefficient of $D_m = 3.2 \times 10^{-11}$ m^2/s (for technetium) constant concentration condition is prescribed for the top model boundary. Under steady-state flow conditions, the tracer starts to transport into the model domain from the top by advection and diffusion as time starts. Figure 6.4-30 shows the concentration contours in the model domains after one year of tracer release from the top boundary. Note that this time period (1 year) is considered short because all matrix blocks are omitted in these simulations, so that retardation due to matrix diffusion and sorption are implicitly neglected. Evaluation of the results in Figure 6.4-30 displays clearly that there exist several faster/fingering channels at this time, indicating very nonuniform, complex transport pathways. However, if compared with the high-flow paths of Figure 6.4-21, Figure 6.4-30 indicates that the faster transport pathways generally follow the faster flow pathways. Therefore, concentration distributions within the model domain serve as indicators of preferential flow.

Generalized Results for Seepage Abstraction: As Figure 6.4-24 demonstrates, the results of the analyses can be used to estimate the flow focusing factor for the seepage abstraction. The normalized flux distributions are similar, and it is reasonable to define a single distribution that applies to all expected percolation rates. A regression curve with confidence bands, summarizing the results of all the simulations, is shown in Figure 6.4-31.

DTN: LB0104AMRU0185.005
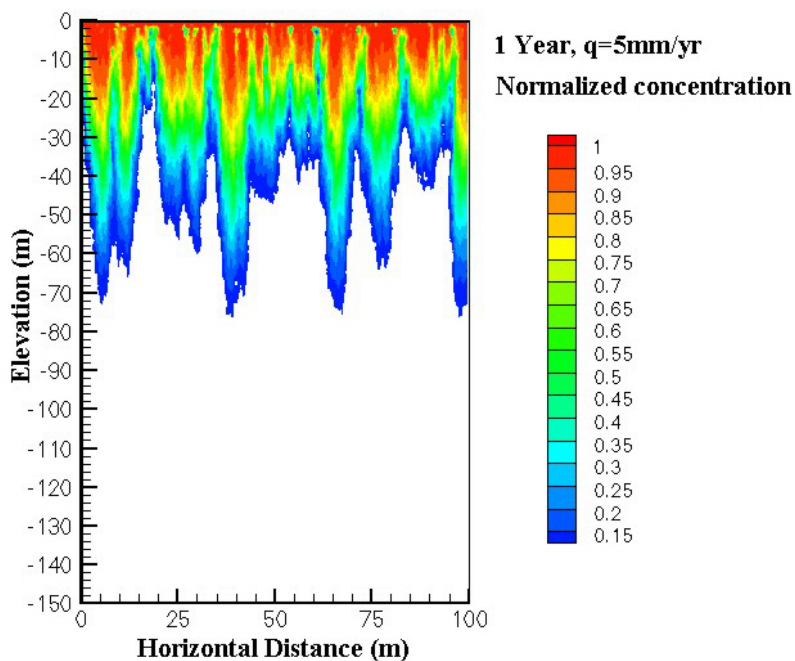
Figure 6.4-30.   Simulated Distribution of Tracer Concentration at One Year of Simulation Time within the Model Domain, Identifying Preferential Flow Pathways

DTN: LB0104AMRU0185.012
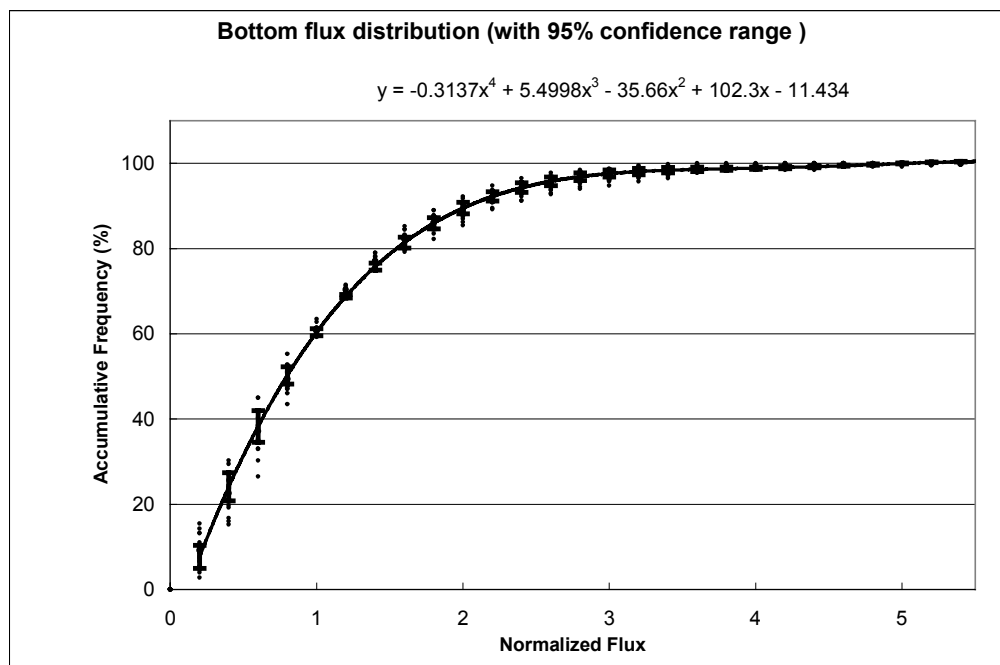
NOTE: Results averaged over all simulations. Regression: $y = -0.3137x^4 + 5.4998x3 + 35.66x2 + 102.3x - 11$. Range is given as the 95-percent confidence interval.

Figure 6.4-31.   Distribution and Range of Cumulative Flux as a Function of Percolation Flux for the Bottom of the Model Domain

6.4.2.4   Validation and Alternative Models

The intended use of the model for focusing and discrete flow paths in the TSw is to provide an estimate of the flow-focusing factor for seepage calculations. There are no sufficiently detailed data specific to focused flow and discrete flow paths in the TSw that can be used to validate this model. Validation of the model for the intended purpose is addressed through the criterion of comparison to analog studies and data. Analogous studies and data presented by Faybishenko et al. (2001 [156009]; 2000 [156010]) and Pruess et al. (1999 [117112]), which are published in the open literature, address the problems of modeling focused and discrete fracture flow using heterogeneous models similar to the one used here including modeling actual flow and transport experiments in fractured rock. This increases the confidence that the model used here is appropriate to address the problem at hand. A conservative approach is recommended here, i.e., applying a flow focusing distribution determined for the sub-meter scale to a drift-scale (multi-meter-scale) problem. More detailed models and/or alternative models (discussed below) are not likely to overcome this conservatism. Because the validation criterion is met, the model is valid for its intended use. However, the model results are not directly relied upon for TSPA-SR (CRWMS M&O 2000 [153246]). Rather, they are used for sensitivity studies (BSC 2001 [154659], Section 3.2.2.3) and provide confirmation of the conservatism of the models used and directly relied upon in TSPA-SR (CRWMS M&O 2000 [153246]).

Alternative approaches to the problem of modeling flow and transport in fractured media other than the high-resolution, heterogeneous continuum model used here are discussed in detail in Pruess et al. (1999 [117112]). Briefly, the alternative approaches include:

- macro-scale continuum models, which were the method previously used and are what are being improved upon in this study
- transfer functions and transit time distributions
- the weeps model
- chaos and fractal structures
- fracture network models
- percolation theory

All of these methods, except the fracture network models, attempt to use effective parameters and empirically observed phenomena to characterize in a simplified manner that is non deterministic (i.e., can produce probabilistic predictions but not specifics of where and when flow focusing will occur). The fracture network model, on the other hand, requires an immense amount of data and computational power that is generally infeasible, especially for a model of the scale described here.

6.4.2.5   Summary and Conclusions

A series of numerical studies have been conducted to evaluate flow focusing through fractures from the bottom of the PTn to the potential repository horizon. The studies were carried out using a 100 m wide and 150 m deep 2-D flow domain and covered the upper five different hydrogeologic units of the TSw at Yucca Mountain. Mean fracture parameters used in the simulations were those developed in the *Calibrated Properties Model* AMR (CRWMS M&O 2000 [144426]) as described in Section 6.4.2.2. The heterogeneous fracture permeability

distributions were generated using a stochastic approach. The studies considered various percolation fluxes, correlation lengths, and uniform and nonuniform percolation-flux boundary conditions. The results obtained provide a quantitative analysis of flow focusing and discrete path formation. All simulation results indicate that the flow-focusing factor is about an order of magnitude smaller than the conservative value used for TSPA-SR (CRWMS M&O 2000 [153246]) calculations. The frequency distributions of normalized flux are insensitive to magnitudes and spatial distributions of infiltration fluxes on the upper boundary, and to spatial correlation structures of the permeability fields within the UZ domains. The results of this model are used to support sensitivity studies for TSPA-SR (BSC 2001 [154659], Section 3.2.2.3).

6.4.3   Percolation Redistribution and Lateral Flow in the PTn

6.4.3.1   Introduction

The UZ system of Yucca Mountain has been the subject of intensive geological, hydrologic, and subsurface engineering studies. Main issues are the flow and transport pathways, and most importantly, the percolation flux through the system. The percolation distribution affects the waste-canister performance as well as solute travel times to the accessible environment. The long-term performance of the repository is determined by the timing of subsurface fluid percolation. Percolation distribution strongly depends on the infiltration rates and their spatial and temporal distributions. The conceptual model of net-infiltration spatial distribution (*Simulation of Net Infiltration for Modern and Potential Future Climates*, USGS 2001 [154674]) describes the effects of precipitation, runoff, evapotranspiration, and redistribution of water in the shallow UZ. The present-day mean infiltration rate over the potential repository footprint has been estimated to range from one millimeter per year to as high as hundreds of millimeters per year (USGS 2001 [154674], Table 6-10). Past climate changes have been used to estimate the possible range in infiltration rates in the future.

Geochemical data provide additional information to analyze the UZ system. Distribution of chemical constituents in both liquid and solid phases of the UZ system depends on many factors, such as hydrological and geochemical processes of surface precipitation, evapotranspiration, the fracture-matrix interactions of flow and transport, large-scale mixing via lateral transport, and history of climate changes and recharge. Naturally occurring and anthropogenic environment tracers provide a valuable interpretive resource of evaluating flow and transport processes over time and space scales. By synthesizing geochemical and geologic data, the model results provide insight into the validity of alternative hydrologic parameter sets, flow and transport processes, and the conceptual models.

The stratigraphic structure of the unsaturated zone of Yucca Mountain is comprised of alternating layers of welded and nonwelded volcanic tuffs that are tilted, uplifted, fractured, and faulted. Characterization of these units and their subunits has advanced as more information from field data become available (CRWMS M&O 2000 [144426]). The first major hydrologic unit below the surface is the Tiva Canyon welded tuff (TCw). The saturated matrix permeability of the TCw is relatively low, but the high degree of fracturing leads to a much higher bulk permeability. Below the TCw is the Paintbrush nonwelded tuff (PTn). The PTn matrix permeability is generally several orders of magnitude greater than that of the TCw, but PTn fracturing is substantially less, which results in a significantly lower bulk permeability. The

Topopah Spring welded tuff (TSw), below the PTn, is the horizon of the potential repository and much thicker than the TCw and PTn together. Matrix permeabilities in the TSw are low, but the bulk permeability is substantially greater resulting from a high degree of fracturing. Finally, between the TSw and the water table are the Calico Hills (CHn), Prow Pass, and Bullfrog nonwelded tuffs.

Below the zone of evapotranspiration, water can percolate through the UZ through a variety of pathways. Fracture flow is initiated in the upper welded tuff unit (TCw), and a transition from fracture-dominated flow to matrix-dominated flow occurs when the flow enters the PTn. In general, matrix flow in the PTn is expected to damp out seasonal climate variability. The questions concerning the conceptual models are: (1) what hydrogeologic features control isolated fast pathways through the PTn and (2) to what extent can the PTn damp extreme episodic infiltration pulses and to provide a uniform flux at the potential repository horizon.

In this study, chloride served as an interpretive natural tracer and measured pore-water chloride concentration data were used in conjunction with geologic interpretation and 3-D chemical transport simulations, to estimate lower and upper bounds on infiltration rates into the UZ system. Model results of chloride distributions matched the observed data better when the calibrated infiltration rates were used. Effects of PTn lateral flows on percolation and chloride redistribution were studied by 3-D simulations with increased horizontal permeability (i.e., anisotropy). The combined results from these scoping studies furnish alternative interpretations for matching the UZ model to chloride data. The relevant simulations runs are documented in the Scientific Notebook (Bodvarsson 2001 [156334], YMP-LBNL-UZ-JL-2.0, pp. 72–88).

6.4.3.2   Available Data

Measurements of pore-water chloride concentrations offer a unique spatially distributed data set for assessing unsaturated zone flow and transport processes and testing the conceptual models. The data available and applied were from samples collected at boreholes (USW NRG-6, USW NRG-7A, USW SD-6, USW SD-7, USW SD-9, USW SD-12, USW UZ-14, and UE-25 UZ#16), the ECRB tunnel, the Exploratory Studies Facility (ESF) tunnel, including South Ramp, North Ramp, and Main Drift (Data Sources: DTN: GS950608312272.001 [145617], DTN: GS990208312272.001 [146134], DTN: LA9909JF831222.004 [145598], DTN: LA0002JF12213U.002 [156281]). The detailed description of these data was given in several reports (Yang et al. 1998 [101441], Table 4, pp. 12–13; CRWMS M&O 1998 [104878], Sections 2 and 3). The water infiltration flux in the base-case study was from the present-day mean infiltration map (Figure 6.4-32). Combining the mean annual precipitation of about170 mm/year with a present day chloride surface flux of 106 mg/m^2 year yields a mean chloride concentration of about 0.62 mg/L (Sonnenthal and Bodvarsson 1999 [117127], p. 113). Chloride surface flux was obtained by applying the mean chloride concentration to precipitated water.

6.4.3.3   Modeling Approaches

The UZ consists of a series of welded and unwelded volcanic tuff layers with different hydrogeologic characteristics, including fracture density. The welded units are generally heavily fractured, with fracture flow considered the dominant mode of air and water movements. The unwelded units, however, have higher porosity and fewer fractures, and matrix flow is

prominent. A dual-permeability transient model is necessary to investigate fluid flow and chemical transport phenomena and represent the large spatial and temporal chemical variations (CRWMS M&O 2000 [141187]).

The system is modeled as two-phase isothermal flow conditions for water and air. The major chemical transport process taken into account were molecular diffusion. A three-dimensional dual-permeability model and the T2R3D V1.4 (LBNL 1999 [113942]) of the TOUGH2 code V1.4 (LBNL 2000 [146496]) were employed for the simulations. Simulation grids as well as basic hydrologic properties of rock matrix and fractures are the same as those used in the 3-D UZ nonperched water model described in CRWMS M&O (2000 [122797]), and are available under DTNs: LB991131233129.003 [147119]; LB990701233129.002 [125604]; LB997141233129.001 [104055]; LB990801233129.022 [156331]). Boundary conditions for chemical components were treated similarly to those for flow simulations, with mass fluxes described at the top boundary and no-flow and water table conditions at the lateral and bottom boundaries, respectively. The dispersivities for both fracture and matrix continua in the simulation were set to zero (Sonnenthal and Bodvarsson 1999 [117127], p. 129). Diffusion coefficients used were those for chemical ions at 25°C and infinite dilution in water (Lasaga 1998 [117091], p. 315, Table 4.1).

6.4.3.4   Model Calibration and Analyses

The complexity of the spatial and temporal patterns of infiltration make it difficult to correlate measurements taken at depths of a few hundred meters with observable surface features. Calibration was done by dividing the surface-infiltration area into nine regions (Figure 6.4-33) according to the availability and range of Cl data, the range of present-day mean infiltration data, and the hydrogeologic and hydrostructural features. The Cl field data were first assigned to the corresponding simulation cells based on the pore-water sample locations. The cell-water infiltration flux was then computed using the Cl net-infiltration flux and the assigned Cl concentration data at the cell. For cells where Cl data were unavailable, the net-infiltration flux was interpolated based on the already calculated infiltration flux in nearby cells in the same region and the cell surface area. The map of calibrated infiltration is shown in Figure 6.4-33. Averaged present-day mean net-infiltration was applied to regions where regional Cl data is unavailable (Regions I, II, and VIII). The overall and regional net-infiltration rates of the two infiltration schemes are compared in Table 6.4-5.

Table 6.4-5.   Infiltration Data by Region

Region	Area		Infiltration Volume by Calibration				Infiltration Rate by Calibration	
			Before		After		Before	After
	km^2	%	m^3/yr	%	m^3/yr	%	mm/yr	mm/yr
I	9.9	25.5	104435	58.9	104436	54.2	10.57	10.57
II	5.3	13.8	12317	6.9	12317	6.4	2.31	2.31
III	3.7	9.6	26266	14.8	20194	10.6	7.10	5.46
IV	3.6	9.4	8819	5.0	16267	8.4	2.43	4.48
V	4.6	11.9	12510	7.1	17534	9.1	2.71	3.80
VI	2.2	5.6	2479	1.4	5447	2.8	1.14	2.51
VII	1.8	4.6	3345	1.9	3345	1.7	1.88	1.88
VIII	3.0	7.7	2156	1.2	2156	1.1	0.73	0.73
IX	4.7	12.0	4996	2.8	11022	5.7	1.07	2.36
Overall	38.7	100.0	177323	100.0	192718	100.0	4.58	4.98

DTN: LB0104AMRU0185.006

Three-dimensional flow and Cl transport simulations were conducted using the present-day mean infiltration (Figure 6.4-32) and the calibrated present-day mean infiltration (Figure 6.4-33) to assess the two infiltration schemes. Figures 6.4-34 through 6.4-36 show the comparisons of model results of steady-state Cl concentrations with measured pore-water Cl concentration data along the stations in the ESF, ECRB, and borehole UE-25 UZ#16, respectively. Compared to the data, the model results using the present-day mean infiltration are higher at the North Ramp (0–2,000 m), South Ramp (6,400–8,000 m), northeast ECRB (left side of the figure), and borehole UE-25 UZ#16; and lower at southwest ECRB (right side of the figure). To examine the cause of these differences, we plotted the infiltration rates along the ECRB in Figures 6.4-37. As can be seen, higher model results at northeast ECRB correspond to very low infiltration rates, while extreme higher infiltration rates lead to lower model results at southwest ECRB. In Figure 6.4-38, with logarithmic scale, we plotted the distribution of Cl concentration in infiltrated water along the ECRB. The Cl infiltration concentrations vary significantly compared to the rather smooth concentration data at the same location. This inconsistency is not expected for a system dominated by vertical flow. Figure 6.4-39 shows the percolation fluxes at the ECRB station, using the present-day mean infiltration rates and the calibrated present-day mean infiltration rates. With the calibrated present-day mean infiltration rates, the percolation flux along the ECRB station is smoother than that by the present-day mean infiltration rates.

Model results at the same locations using the calibrated infiltration are closer to the Cl field data compared to those using present-day mean infiltration. Absolute differences between model results and measured field Cl data were calculated and shown in Figures 6.4-40. The differences by calibrated infiltration are in several smaller than those by present-day mean infiltration.
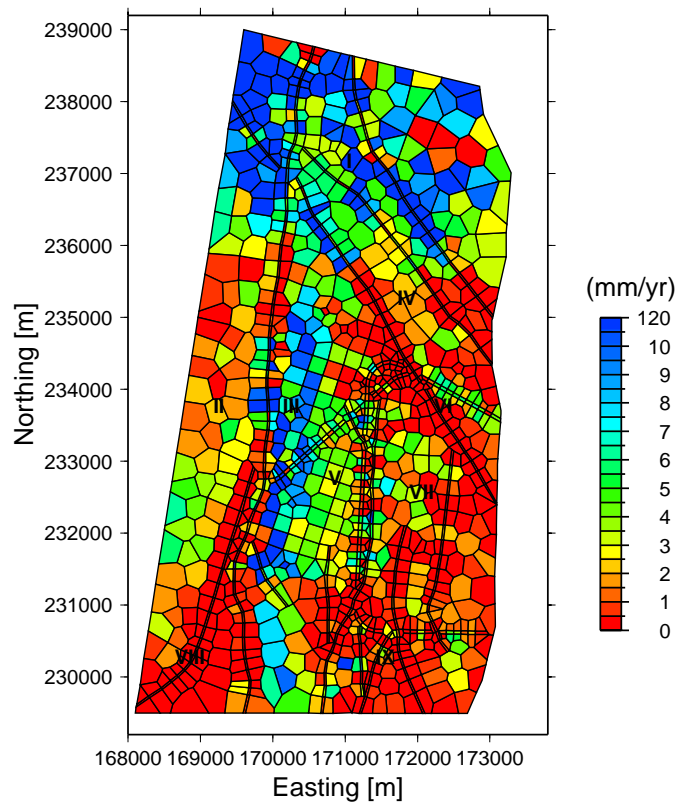
DTN: LB990801233129.022 [156331]

Figure 6.4-32.   Present-day Mean Infiltration

DTN: LB0104AMRU0185.006
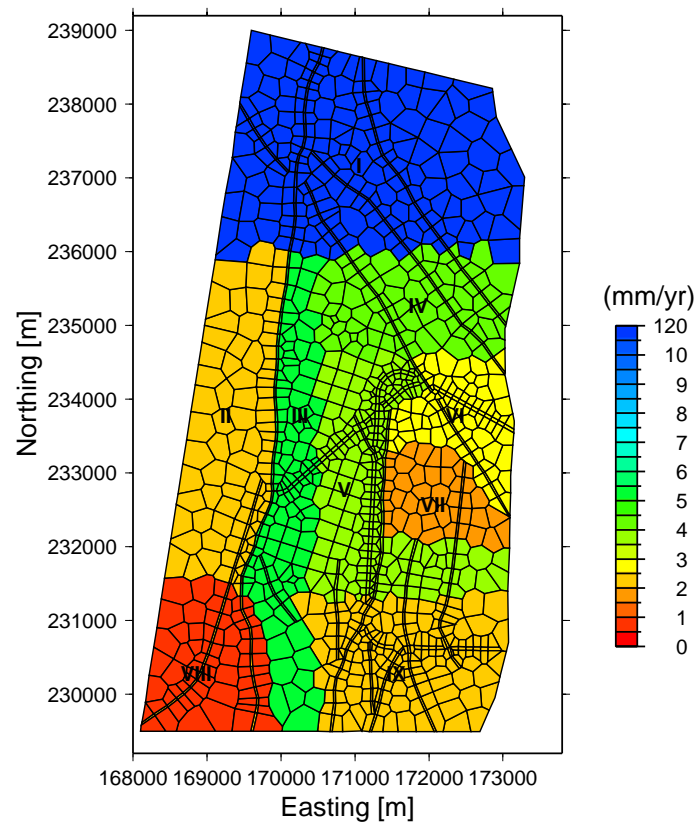
Figure 6.4-33.   Calibrated Present-day Mean Infiltration
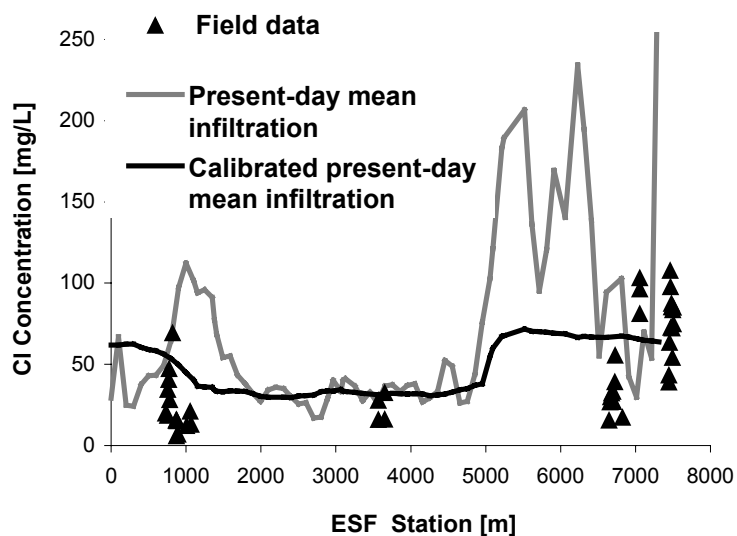
Source DTNs for Field Data: LA0002JF12213U.002 [156281]
Source DTN for Simulations: LB0104AMRU0185.006

Figure 6.4-34.   ESF Cl Model Results by Present-day and Calibrated Present-day Mean Infiltration
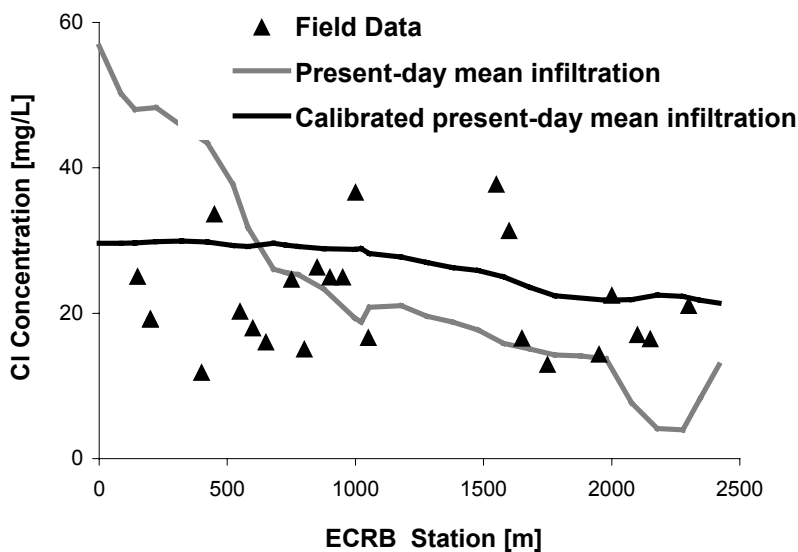
Source DTNs for Field Data: LA9909JF831222.004 [145598]
Source DTN for Simulations: LB0104AMRU0185.006

Figure 6.4-35.   ECRB Cl Model Results by Present-day and Calibrated Present-day Mean Infiltration
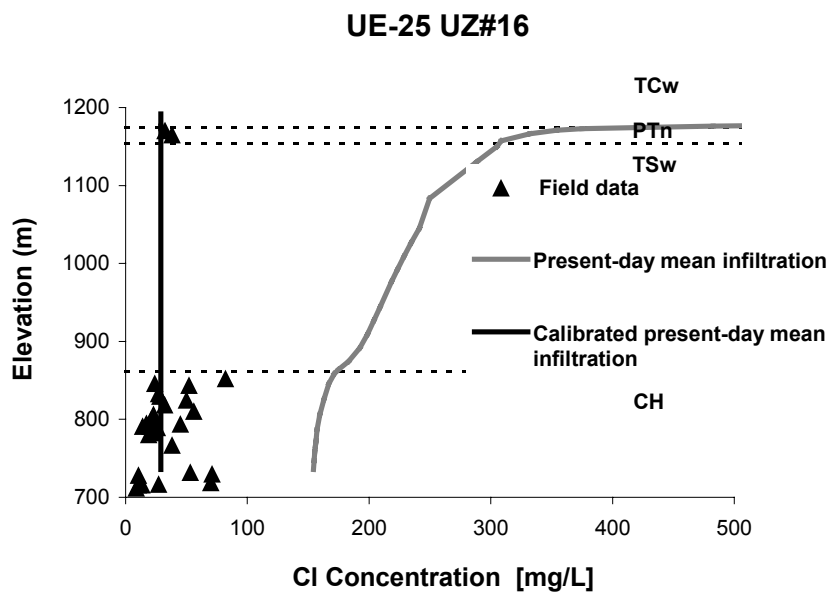
UE-25 UZ#16

Source DTNs for Field Data: GS950608312272.001 [145617]
                                                          GS990208312272.001 [146134]
Source DTN for Simulations: LB0104AMRU0185.006

Figure 6.4-36.   Borehole UE-25 UZ#16 Model Results by Present-day and Calibrated Present-day Mean Infiltration
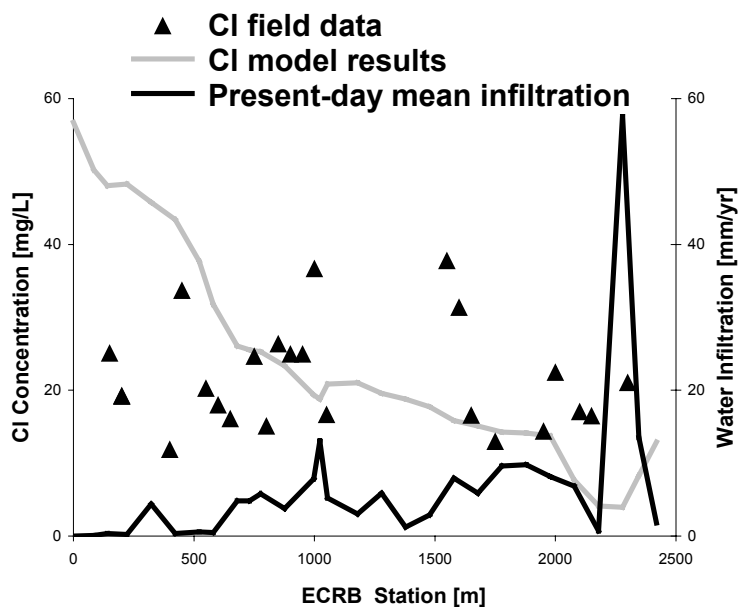
Source DTNs for Field Data: LA9909JF831222.004 [145598]
Source DTN for Simulations: LB0104AMRU0185.006

Figure 6.4-37.   ECRB Present-day Mean Infiltration
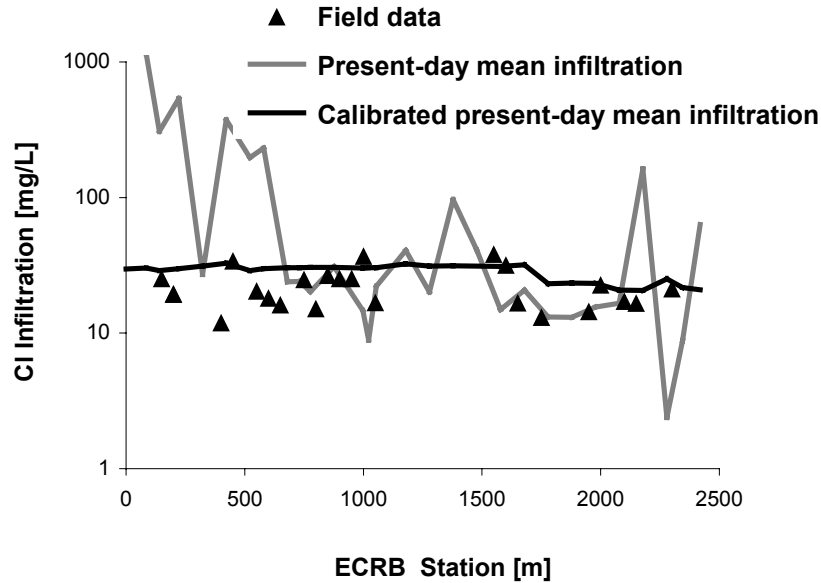
Source DTNs for Field Data: LA9909JF831222.004 [145598]
Source DTN for Simulations: LB0104AMRU0185.006

Figure 6.4-38.   ECRB Cl Infiltration Concentration by Present-day and Calibrated Present-day Mean Infiltration
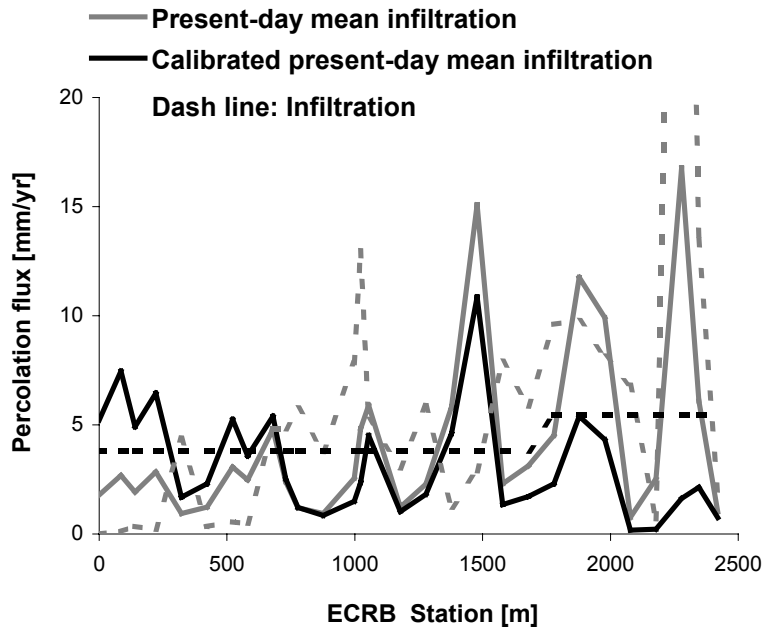
Source DTN for Simulations: LB0104AMRU0185.006

Figure 6.4-39.   ECRB Percolation Flux by Present-day and Calibrated Present-day Mean Infiltration
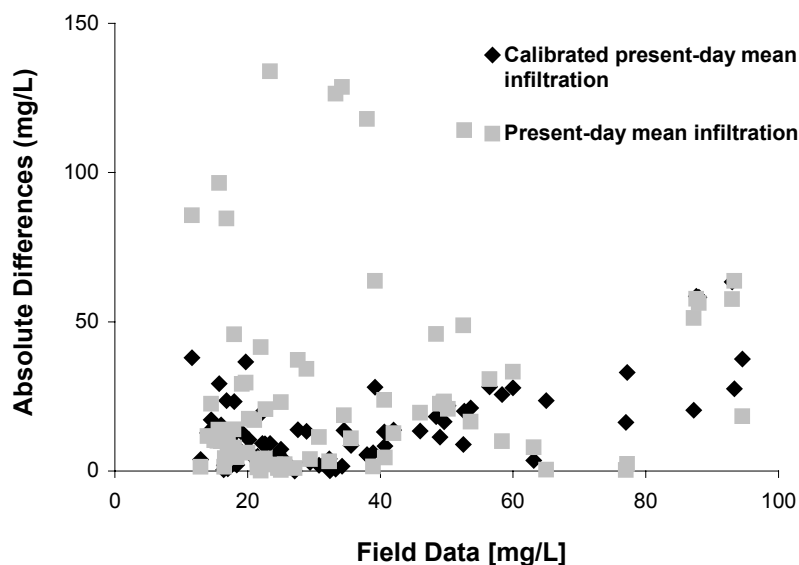
Source DTNs for Field Data:
GS950608312272.001 [145617]; GS990208312272.001 [146134];
LA9909JF831222.004 [145598]; LA0002JF12213U.002 [156281]
Source DTN for Simulations: LB0104AMRU0185.006

Figure 6.4-40. Differences Between Cl Model Results and Cl Data

6.4.3.5 PTn Lateral Flow Effects

A transition from fracture-dominated flow to matrix-dominated flow occurs when fluids flow from TCw into PTn. PTn layers have variable porosity and permeability. The transition to matrix flow in PTn is expected to damp out the variability in infiltration flux and produce a more uniform Cl distribution. Flow through this unit was believed to be primarily vertical, with some lateral flow occurring because of its layered structure and associated heterogeneities (Wu et al. 1999 [117161]). To study the effect of PTn lateral flow on the degree of damping and Cl distribution, 3-D simulations were run with increased PTn horizontal permeability, which gave ratios of horizontal permeability to vertical permeability of 10:1 and 100:1, respectively. Figures 6.4-41 through 6.4-43 show the model results of Cl concentrations at ESF and ECRB, and borehole UE-25 UZ#16. The degrees of damping effects vary in different locations. They were observed at North Ramp, south Main Drift, and northeast ECRB. As horizontal permeability increased, the simulated Cl concentrations in borehole UE-25 UZ#16 below PTn units are decreased and are closer to the measured Cl data from pore water samples. Decreased Cl concentrations were also observed at boreholes USW NRG-6, USW NRG-7A, USW SD-7, USW SD-12, and UE-25 UZ#4 as PTn permeability altered. Little change was found, however, at boreholes USW SD-9 and USW UZ-14. Figure 6.4-44 gives the simulated percolation flux at the ECRB. A smoother and smaller percolation flux than that of the base case is observed as the PTn horizontal permeability is increased.
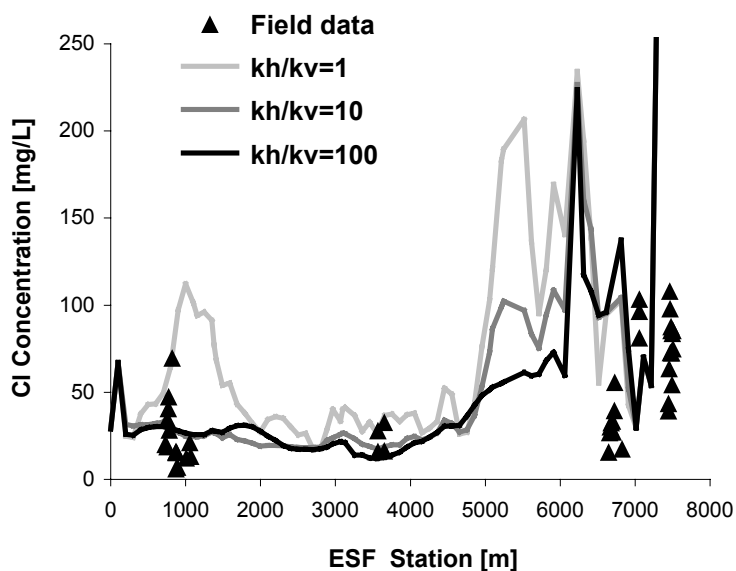
Source DTNs for Field Data: LA0002JF12213U.002 [156281]
Source DTN for Simulations: LB0104AMRU0185.006

Figure 6.4-41.   ESF Cl Model Results by Increased PTn Horizontal Permeability
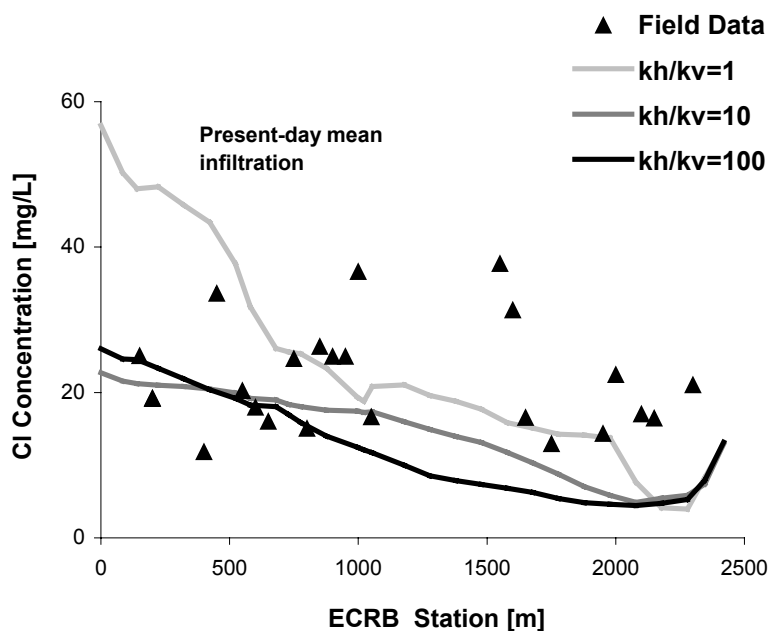
Source DTNs for Field Data: LA9909JF831222.004 [145598]
Source DTN for Simulations: LB0104AMRU0185.006

Figure 6.4-42.   ECRB Cl Model Results by Increased PTn Horizontal Permeability
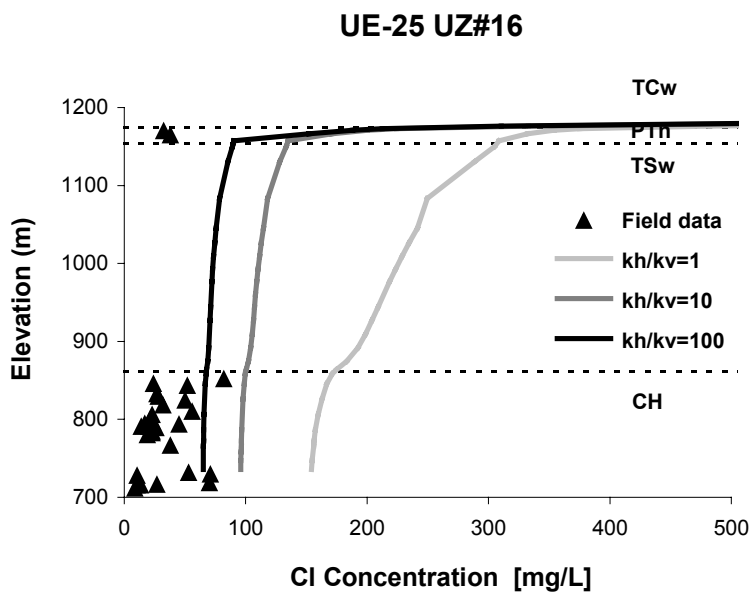
UE-25 UZ#16

Source DTNs for Field Data: GS950608312272.001 [145617]
GS990208312272.001 [146134]
Source DTN for Simulations: LB0104AMRU0185.006

Figure 6.4-43.   Borehole UE-25 UZ#16 Cl Model Results by Increased PTn Horizontal Permeability
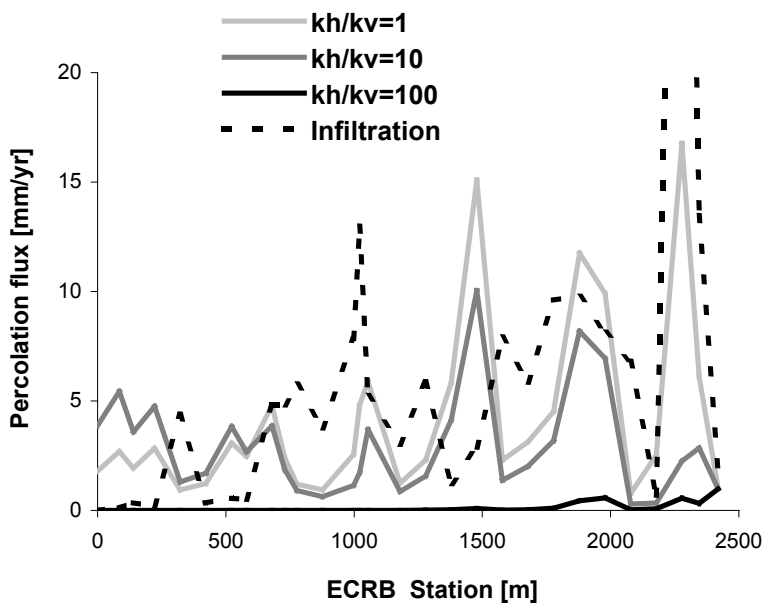
DTN: LB0104AMRU0185.006

Figure 6.4-44.   ECRB Percolation Flux by Increased PTn Horizontal Permeability

6.4.3.6   Conclusions

Percolation flux affects both waste-canister performance and solute travel times to the accessible environment. Percolation distribution strongly depends on infiltration rates and their spatial and temporal distributions. The present-day mean infiltration in the Yucca Mountain flow and transport models was calibrated, and percolation distribution analyzed, using pore-water Cl concentration data. The surface-infiltration area was divided into regions according to the availability and range of Cl data, the range of present-day mean infiltration data, and hydrostructural and hydrogeologic features. Infiltration rates in each region were calculated based on the pore-water Cl concentration data and Cl infiltration flux. Results of the three-dimensional simulation using the calibrated infiltration map match the Cl data better than when using an uncalibrated infiltration map.

PTn lateral flow effects on percolation and Cl distribution were studied by 3-D simulation with increased horizontal permeability. The degree of the effects varied by locations. As expected, a more uniform Cl distribution under PTn was observed in most places when lateral-flow effects increased. Further calibration can be done by adjusting layer heterogeneity and anisotropic permeability in different regions, based on the hydrostructural features, percolation fluxes, and distribution of geochemical data.

This scoping study suggests that several approaches may be used to obtain UZ model results consistent with chloride data.

6.4.4   The Effect of Episodic Percolation on Seepage

Episodic percolation has been shown to enhance seepage. The AMR *Seepage Model for PA Including Drift Collapse* (CRWMS M&O 2000 [153314], Section 6.6.6) considers an example of episodic flow. Each year's worth of infiltration is concentrated into two months of percolation at the repository level, and there is no percolation the other ten months. This model shows that for this limited case, the expected peak seepage percentage for episodic flow is the same as that for continuous percolation at the same rate.

The AMR *Abstraction of Drift Seepage* (CRWMS M&O 2001 [154291], Section 5) neglects the effects of episodic flow on seepage because it is generally believed that the PTn effectively damps out most, if not all, episodic flow from the TCw. However, portions of the western margin of the proposed repository are near the western escarpment of Yucca Crest above Solitario Canyon and the PTn and TSw outcrop in several places along that escarpment. At these locations, the TSw is exposed to episodic infiltration with very little to none of the moderating influence of the PTn. If this episodic infiltration is diverted laterally to the east, it may intersect emplacement drifts, with the possibility of enhancing seepage.

6.4.4.1   Episodic Percolation Model

To investigate the potential for lateral flow of transient percolation, a model that includes the details of the PTn and TSw outcrops on the western escarpment of Yucca Crest and a transient infiltration boundary condition is used.

A simple, two-dimensional, rectilinear model is generated with lateral grid size of 10 meters and maximum vertical grid size of 10 meters. Where layers are thinner than 10 m, the grid size is equal to the layer thickness. Layer thicknesses are constant and are defined by data from borehole USW SD-6 (CRWMS M&O 2000 [114277], Attachment III, Table III-1). The dip of the layers is defined by average layer dip between boreholes USW SD-6 and USW SD-12, which is 7° below horizontal to the southeastward.

A single continuum fracture-only model is used to simplify calculations and to provide a conservative approach to determining whether the potential for transient percolation exists. Representation of the matrix in the model would provide more storage and thus more damping capacity for both vertical and lateral transient flow. The software iTOUGH2 V4.0 (LBNL 1999 [139918]) is used to generate the grid. The routine AssignRock V1.0 (LBNL 2001 [154321]) is used to assign material properties, including TSw fault properties to the columns next to the no-flow lateral boundaries. The routine AddBound V1.0 (LBNL 2000 [152823]) is used to add a gravity-drainage boundary condition to the lower boundary of the model.

The cross-sectional alignment is defined by SD-6 and SD-12 so that the cross section crosses the western escarpment of Yucca Crest where the Tptrv, Tptrn, and Tptpul outcrop and the proposed repository footprint comes closest to these outcrops. The bedrock surface, extracted from GFM3.1 (DTN: MO9901MWDGFM31.000 [103769]) using EarthVision V5.1 (Dynamic Graphics 1998 [152614]), is used to manually clip the surface of the rectilinear grid. A schematic of the resulting grid is shown in Figure 6.4-45. Grid generation details are found in Bodvarsson (2001 [156334], YMP-LBNL-UZ-CFA-1, pp. 19, 29–35) and Hinds (2001 [155955], p. 152).
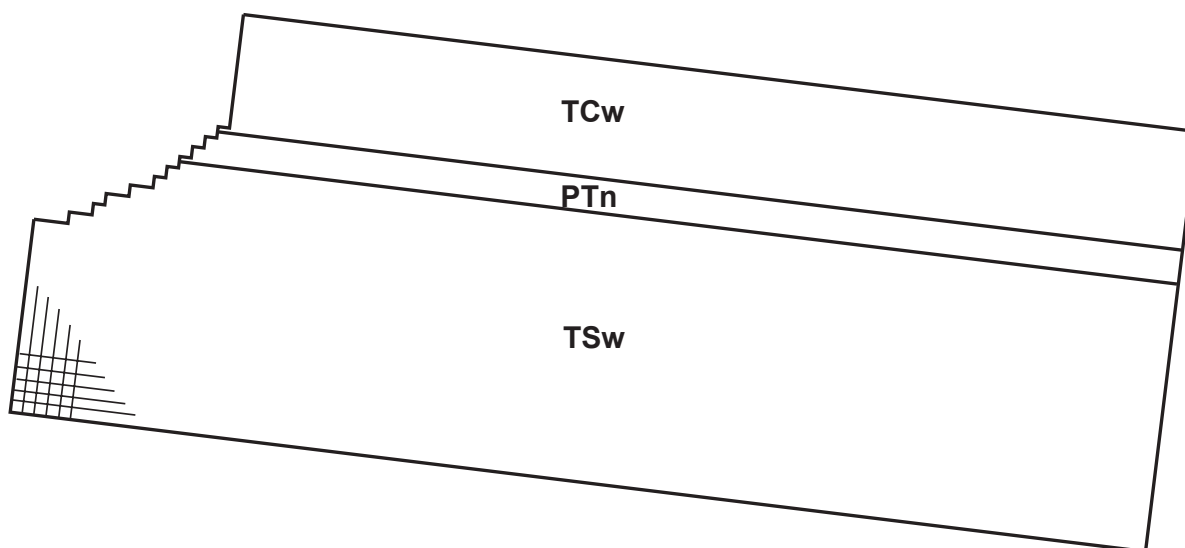
Figure 6.4-45.   Schematic of Numerical Grid

The upper-bound glacial-average infiltration map (ITN: 00316.T) is used to define the infiltration condition at the upper boundary. Steady-state infiltration rates are calculated for each upper-boundary node, using routine RoutineRick1 V1.1 (LBNL 2001 [156137]). Transient infiltration rates are calculated by assuming that infiltration happens only 1 week per year. Transient infiltration is applied only to the upper boundary nodes where the TSw outcrops, so

that possible transient-infiltration effects from other areas do not mask or complicate the interpretation of possible transient percolation below and/or just to the east of the TSw outcrop. These calculations are documented in Bodvarsson (2001 [156334], YMP-LBNL-UZ-CFA-1, pp. 19, 29–35) and Hinds (2001 [155955], pp. 122–123).

Fracture properties are from the AMR *Calibrated Properties Model* (CRWMS M&O 2000 [144426], Section 6; DTN: LB997141233129.001 [104055]; DTN: LB991091233129.004 [126111]).

The model is first used to simulate steady-state conditions, using a steady-state infiltration boundary condition everywhere on the upper boundary. Then 100 years of transient infiltration is simulated using the steady-state conditions as initial conditions. All the simulations are performed with the software TOUGH2 V1.5 (LBNL 2001 [154322]). These simulations are documented in Bodvarsson (2001 [156334], YMP-LBNL-UZ-CFA-1, pp. 19, 29–35).

6.4.4.2   Results of Episodic Percolation Model

The results are contained in DTN: LB0104AMRU0185.007. These results indicate that transient percolation is damped out by the time it reaches the interface between the Tptpul and Tptpmn, and that lateral diversion of transient percolation is not at all significant. These results are not unexpected because:

- Gravity drainage is expected to dominate a system with such high permeabilities, from 10×10^{-12} to 100×10^{-12} m^2.

- The capillarity and storage of the fracture system damp out the transient infiltration rapidly. Even where the bedrock surface is only 40 meters above the interface between the Tptpul and Tptpmn, the transient percolation is effectively damped out.

6.4.4.3   Validation of Episodic Percolation Model

Validation of this model against observations is not possible because no data exist on large-scale fracture flow in the TSw. However, validation for intended use can be achieved by using the criterion that a negative result is predicted using a conservative model. The conservatism built into this model (i.e., using a fracture-only model, using the upper-bound glacial-average infiltration map, and putting all the infiltration into a short, transient pulse) build confidence in the model finding of no episodic percolation at the western margin of the repository and meet the criterion for validation listed above. The model is valid for its intended purpose, i.e., as confirmation of the abstraction approach for TSPA-SR that does not include episodic percolation as a seepage enhancing factor (CRWMS M&O 2001 [154291], Section 6.4.4; BSC 2001 [154659], Section 3.2.2.4).

6.5   PROCESSES AFFECTING UNSATURATED ZONE FLOW AND TRANSPORT BELOW THE REPOSITORY

Flow and transport through the UZ below the repository is important because these are the processes by which radionuclides may be carried to the water table. However, the sparsity of data from below the repository horizon, particularly in the CHn and CFu, makes discrimination

between alternative models difficult. In some cases, it also makes parameter estimation highly uncertain. In this section, scoping of alternative models is used to document whether the choice of model impacts transport simulations significantly. As an alternative to the previously used conceptual model that fractures and fracture flow are continuous through the vitric CHn, the conceptual model that the fractures and fracture flow through the vitric CHn is discontinuous, and thus flow is carried wholly through the matrix, is used and is presented in Section 6.5.1. Also presented in this section is the calibration of vitric CHn hydrologic properties for the UZ Flow and Transport Model based on this alternative conceptual model. In Section 6.5.2, uncertainty in perched water models and resulting percolation and tracer breakthrough patterns at the water table are addressed by investigating impact of different perching zone permeabilities and configurations. In Section 6.5.3, uncertainty in fault parameters for the CHn and CFu are investigated by a study of the sensitivity of transport results to variations of fault parameters. In Section 6.5.4, the impact of releasing radionuclides directly to the matrix continuum below the waste emplacement drift, rather than to the fracture continuum, is studied. None of the results of studies documented in this section are used for TSPA.

6.5.1   Fracture Flow in the Vitric Calico Hills Formation

Relatively unaltered (vitric), nonwelded tuff exists beneath the potential repository horizon within the Calico Hills Formation, as indicated in Figure 6.5-1. Flow and transport behavior within this unit may have important effects on the overall performance of the potential repository. This section presents a modeling study of flow and transport processes within the vitric tuff, based on a new conceptual model and additional rock property data from the Busted Butte test site. Effects of the conceptual model and property changes on simulated flow and transport processes (from the potential repository to the water table) will also be discussed. Note that fracture flow and matrix flow herein refer to water flow occurring in fractures and in the rock matrix, respectively.

6.5.1.1   Conceptual Models

Two conceptual models can be used for describing flow and transport in the vitric Calico Hills Formation, as indicated in Figure 6.5-1. One conceptual model, (a), hypothesizes that flow occurs both in fractures and in the rock matrix, while the other, (b), hypothesizes no fracture flow under unsaturated conditions. The current flow and transport models of the UZ are based on the first conceptual model and predict about 20% of liquid water flow occurring in fractures within this unit, as discussed in *Unsaturated Zone Flow and Transport Model Process Model Report* (CRWMS M&O 2000 [151940], Figure 3.6-9). However, the Unsaturated Zone Transport Test (UZTT) at Busted Butte strongly supports the second conceptual model, (b).
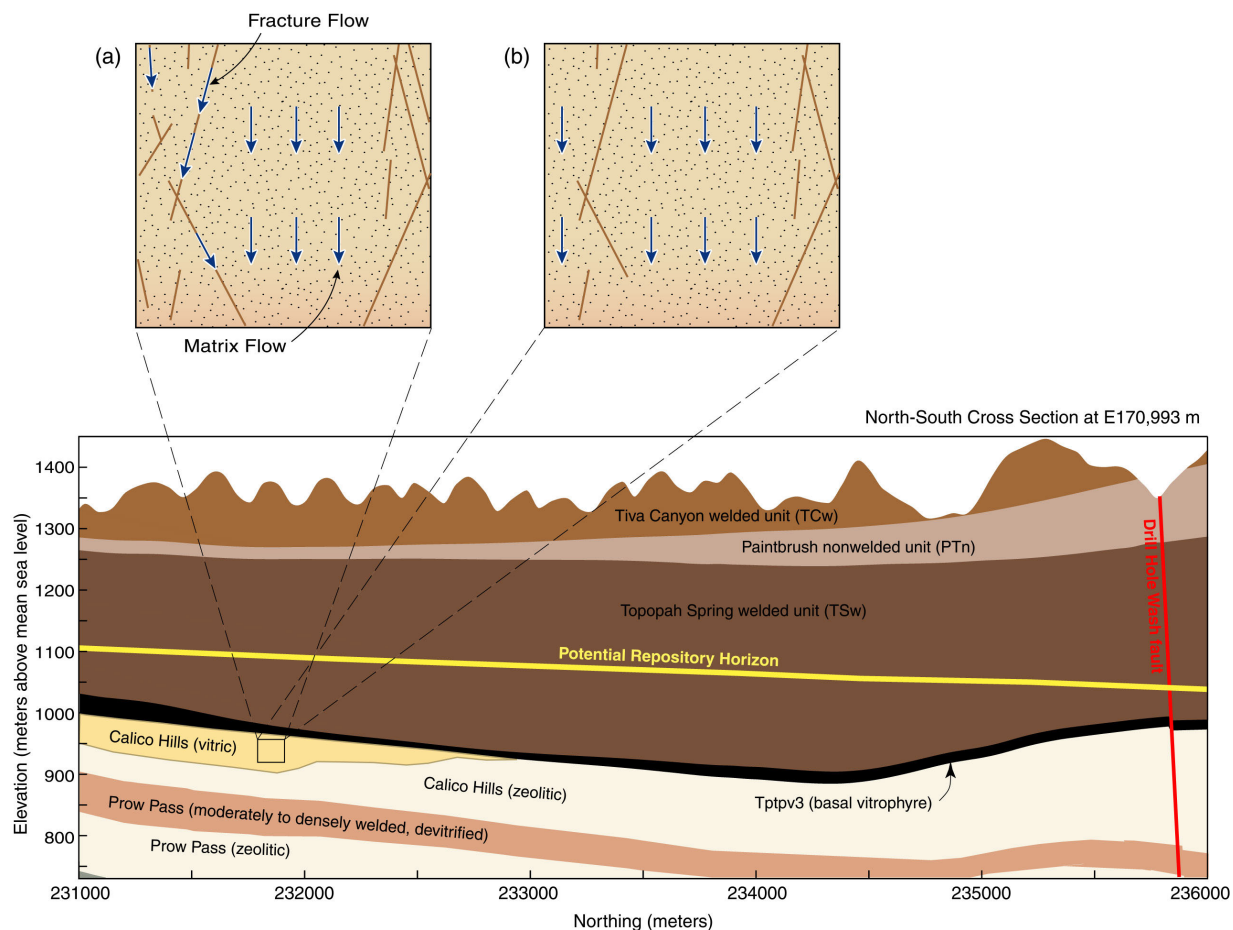
NOTE: Conceptual model (a) hypothesizes that flow occurs both in fractures and in the rock matrix, while model (b) hypothesizes no fracture flow under unsaturated conditions.

Figure 6.5-1.   A North-South Cross Section of Yucca Mountain Showing Two Conceptual Models for Water Flow in the Vitric Calico Hills

Busted Butte is located approximately 8 kilometers southeast of the potential repository area at Yucca Mountain (Figure 6.5-2). The underground test facility at Busted Butte exposes portions of the Topopah Spring Tuff (Tpt) and the Calico Hills Formation (Tac) lithostratigraphic units, which represent a distal extension of the rocks located directly beneath the potential repository. As discussed in the AMR *Unsaturated Zone and Saturated Zone Transport Properties (U0100)* (CRWMS M&O 2001 [154024], Section 6.8), tracer transport testing at Busted Butte has focused on three specific lithostratigraphic units at the contact between Topopah Spring welded unit and Calico Hill nonwelded unit: the moderately welded (Tptpv2) and non- to partially welded (Tptpv1) vitric tuffs at the base of the Topopah Spring Tuff, and the largely unaltered (vitric) upper portion of the Calico Hills Formation.
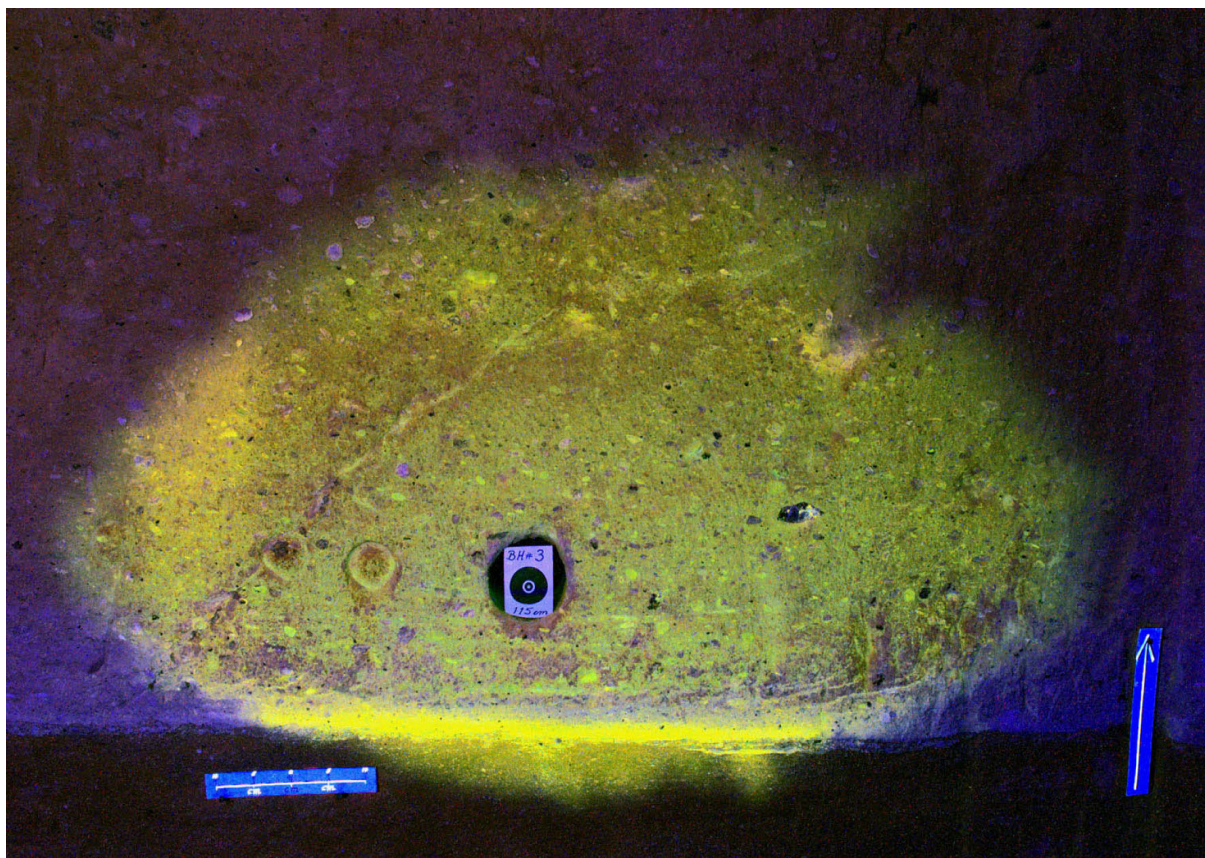
Tracer Plume from Injection in the Side Wall of the Main Adit,
Opposite to the Test Alcove (Phase 1A)

Source: modified from CRWMS M&O 2000 [151940], Figure 2.2-12(c)

Figure 6.5-2.   Busted Butte Test Site and Observed Tracer Plume from the Phase 1A Test

In Phase 1A testing at the Busted Butte site, the tracer was injected from a point. The observed tracer plume from this testing clearly indicates that flow and transport occurs only in the matrix within the vitric Calico Hills Formation (Figure 6.5-2). During Phase 1B testing in which liquid was injected immediately adjacent to a fracture, water imbibed quickly into the surrounding matrix, as discussed in the AMR *Unsaturated Zone and Saturated Zone Transport Properties (U0100)* (CRWMS M&O 2001 [154024], Section 6.8.9). This is also consistent with observed relatively high matrix permeabilities and matrix porosities, and small fracture densities compared to welded units (CRWMS M&O 2000 [145771], Tables 6 and 7), which are expected to essentially prevent flow and transport processes from occurring in fractures because of the large storage and strong capillary force within the matrix. These arguments strongly support the validity of conceptual model (b), in which flow and transport occurs only in the matrix. This conceptual model is considered more realistic and is used in this study. Use of conceptual model (a) (where some flow occurs in fractures of the vitric Calico Hills Formation) might underestimate the water and radionuclide travel times through the vitric Calico Hills Formation.

6.5.1.2 Determination of Rock Properties

Conceptual model (b), in which flow and transport occur only in the matrix, is incorporated into the site-scale model by removing the fracture continuum from model layers corresponding to the vitric portions of the Calico Hills Formation. Rock properties have been updated to be consistent with this conceptual model change and to incorporate new rock-property data from the Busted Butte site. The determination of updated rock properties is documented in the Scientific Notebook (Liu 1999 [155675], pp. 90–94).

Determination of rock properties consists of two steps. First, small-scale rock property data are analyzed to develop average hydrological properties for the UZ model layers. Because of scale issues and uncertainties in property-estimation methods, properties developed from this step may not be reliable for use in the flow and transport models of the UZ. Therefore, the second step is to refine hydrological properties for the UZ model layers based on model calibration, which is a procedure to adjust hydrological properties such that simulated results are consistent with field observations, including matrix water saturation and potential data. The estimated properties from the first step are used in model calibration as prior information and initial guesses to constrain the property values that are to be determined. While detailed descriptions of methodologies used in these two steps are given in two AMRs, *Analysis of Hydrologic Properties Data* (CRWMS M&O 2000 [145771]) and *Calibrated Properties Model* (CRWMS M&O 2000 [144426]), a brief introduction to these methodologies is provided here.

6.5.1.2.1 Available Data

Since the fracture continuum is removed from only the vitric portion of the Calico Hills Formation, only properties corresponding to this unit are updated while other properties remain the same as those in the base case mountain-scale property set reported in AMR *Calibrated Properties Model* (CRWMS M&O 2000 [144426], Table 13). Relations between the lithostratigraphy of the Geologic Framework Model (GFM3.1) and the UZ model layers are given in Table 6.5-1 (CRWMS M&O 2000 [114277], Table 10).

Table 6.5-1.   GFM3.1 Lithostratigraphy, UZ Model Layer, and Hydrogeologic Unit Correlation (CRWMS M&O 2000 [114277], Table 10)

Major Unit	GFM3.1* Lithostratigraphic Nomenclature	Fiscal (FY) 99 UZ Model Layer	Hydrogeologic Unit
Tiva Canyon welded (TCw)	Tiva_Rainier	tcw11	CCR, CUC
	Tpcp	tcw12	CUL, CW
	TpcLD		
	Tpcpv3	tcw13	CMW
	Tpcpv2		
Paintbrush Tuff nonwelded (PTn)	Tpcpv1	ptn21	CNW
	Tpbt4	ptn22	BT4
	Tpy (Yucca)		
		ptn23	TPY
		ptn24	BT3
	Tpbt3		
	Tpp (Pah)	ptn25	TPP
	Tpbt2	ptn26	BT2
	Tptrv3		
	Tptrv2		
Topopah Spring welded (TSw)	Tptrv1	tsw31	TC
	Tptrn		
		tsw32	TR
	Tptrl, Tptf	tsw33	TUL
	Tptpul		
	Tptpmn	tsw34	TMN
	Tptpll	tsw35	TLL
	Tptpln	tsw36	TM2 (upper 2/3 of Tptpln)
		tsw37	TM1 (lower 1/3 of Tptpln)
	Tptpv3	tsw38	PV3
	Tptpv2	tsw39	PV2

Calico Hills nonwelded (CHn)	Tptpv1	ch1 (vit, zeo)	BT1 or BT1a (altered)
	Tpbt1		
	Tac (Calico)	ch2 (vit, zeo)	CHV (vitric) or CHZ (zeolitic)
		ch3 (vit, zeo)	
		ch4 (vit, zeo)	
		ch5 (vit, zeo)	
	Tacbt (Calicobt)	ch6	BT
	Tcpuv (Prowuv)	pp4	PP4 (zeolitic)
	Tcpuc (Prowuc)	pp3	PP3 (devitrified)
	Tcpm (Prowmd)	pp2	PP2 (devitrified)
	Tcplc (Prowlc)		
	Tcplv (Prowlv)	pp1	PP1 (zeolitic)
	Tcpbt (Prowbt)		
	Tcbuv (Bullfroguv)		
Crater Flat undifferentiated (CFu)	Tcbuc (Bullfroguc)	bf3	BF3 (welded)
	Tcbm (Bullfrogmd)		
	Tcblc (Bullfroglc)		
	Tcblv (Bullfroglv)	bf2	BF2 (nonwelded)
	Tcbbt (Bullfrogbt)		
	Tctuv (Tramuv)		
	Tctuc (Tramuc)	tr3	Not Available
	Tctm (Trammd)		
	Tctlc (Tramlc)		
	Tctlv (Tramlv)	tr2	Not Available
	Tctbt (Trambt)		

NOTE: * GFM3.1 refers to the Geologic Framework Model Version 3.1.

Core measurements from surface-based boreholes and from the Busted Butte site include matrix saturated hydraulic conductivity, matrix porosity, matrix relative unsaturated hydraulic conductivity as a function of saturation, and capillary pressure as a function of saturation. The "averaged" properties determined based on core measurements from surface-based boreholes were reported in the AMR *Analysis of Hydrologic Properties Data* (CRWMS M&O 2000 [145771], Section 6.2) (DTN: LB990501233129.001 [106787]). These properties need to be updated, however, to incorporate core measurements from Busted Butte (DTNs: GS990308312242.007 [107185] and GS990708312242.008 [109822]) made available after the analysis of hydrologic properties was completed. In this case, both data from Busted Butte and surface-based boreholes are used for updating rock properties for the relevant model layers.

Correlation between location of a core sample from Busted Butte and the appropriate UZ model layer is determined from geological information of the core sample (CRWMS M&O 2000 [154123]).

The Busted Butte underground facility provides access to the lower Topopah Spring Tuff (crystal-poor, vitric subzones, Tptpv2 and Tptpv1) and the upper Calico Hills Formation (Tac). This lithostratigraphic sequence is marked by a downward gradation from moderately welded tuffs (upper Tptv2) to nonwelded tuffs (Tptpv1 and Tac). Samples from the lower part of layer Tptpv2, layer Tptpv1, and the upper part of layer Tac have been collected and analyzed to determine matrix hydrologic characteristics. Average matrix permeabilities of Busted Butte samples from the lower Topopah Spring Tuff and upper Calico Hills Formation are higher than those from surface-based boreholes near or within the potential repository area at Yucca Mountain. This may result from a possible difference in degree of alteration, but it more likely reflects a biasing of the samples collected from the surface-based drilling toward those that are less friable (those with a greater degree of welding or increased clay or zeolite content). Matrix permeability data from Busted Butte are also available for the Tptpv2 lithostratigraphic unit, corresponding to UZ model layer tsw39. However, these data are significantly different from those collected from surface-based boreholes. For example, the average matrix permeability from the Busted Butte site is about three orders of magnitude higher than that determined using core measurements from surface-based boreholes. Even the smallest matrix porosity for this layer observed at Busted Butte (0.28) is larger than the average porosity obtained from surface-based boreholes (0.17) (DTN: LB990501233129.001 [106787]), suggesting almost no overlap between observed porosity values from these two sources. This apparent discrepancy may reflect vertical differences in sampling locations within the Tptpv2 lithostratigraphic unit, which is characterized by a welding transition. Core samples from surface-based, vertical boreholes may have been biased to the upper, more welded part of the Topopah Spring-Calico Hills transition (which has lower porosity), while samples from Busted Butte were taken near the base of this transition, where it exhibits a lesser degree of welding (therefore, higher porosity). Further investigation may be needed to determine if the Busted Butte data are representative of the vitric Topopah Spring-Calico Hills welding transition below the potential repository. In this study, these data for Tptpv2 were not used.

Although unsaturated matrix relative permeability (unsaturated hydraulic conductivity) data are available, they are not used in this study, because the water potential versus saturation relationship enables successful prediction of the relative permeability relationship based on van Genuchten's (1980 [100610], pp. 892–893) model (Flint et al. 1999 [107377], pp. 297–298). Note that van Genuchten (1980 [100610], pp. 892–893) relations are used in this study for describing unsaturated flow in the matrix.

In addition to hydrological property data, observed matrix saturation and *in-situ* water potential data, infiltration rates and developed numerical grids are used for model calibration. These data have been incorporated into model input files for the Calibrated Properties Model (CPM) (DTN: LB991091233129.001 [125868]) that is used in this study. A detailed discussion of these data in terms of their use for model calibration can be found in the AMR *Calibrated Properties Model* (CRWMS M&O 2000 [144426], Section 4).

6.5.1.2.2 Analysis of Hydrological Properties Data

Small-scale rock property data need to be analyzed to develop average hydrological properties for UZ model layers, as previously discussed. Matrix permeability is considered to be a log-normally distributed quantity (CRWMS M&O 2000 [145771], Section 6.2.1). Therefore the geometric mean is used to represent the average permeability of a model layer. Measured data are presented in terms of saturated hydraulic conductivity (m/s) and the need to be converted to permeability (m^2) (CRWMS M&O 2000 [145771], Section 6.2.1). For a given model layer, the geometric mean can be very different from the effective matrix permeability used to represent large-scale water flow and solute transport due to scale effects (Paleologos et al. 1996 [105736], Figure 4, p. 1337). While many upscaling schemes are available in the literature, a scheme for highly heterogeneous porous media is described by the following expression (Paleologos et al. 1996 [105736], p. 1336, Equation 26):

$$k_e = k_g \exp[\sigma_{\ln(k)}{}^2 (\frac{1}{2} - D)] \qquad \text{(Eq. 6.5.1.1)}$$

where k_e is the large-scale effective permeability, k_g is the geometric mean of small (core) scale permeability, $\sigma_{\ln(k)}{}^2$ is the variance of the natural log transformed permeability, and D is a function of spatial dimensional (e.g. 2-D and 3-D) and the correlation scale of ln(k). For a 3-D isotropic problem, D = 1/6 when the characteristic size of a flow domain under consideration (a model layer for example) is much larger than the correlation length (Paleologos et al. 1996 [105736], p. 1336). For a site-scale model layer, these conditions are approximately satisfied. In this case, Equation 6.5.1.1 can be rewritten as:

$$\log(k_e) = \log(k_g) + 0.38\sigma_{\log(k)}{}^2 \qquad \text{(Eq. 6.5.1.2)}$$

where $\sigma_{\log(k)}{}^2$ is the variance of the log transformed permeability.

Matrix porosity is considered a normally distributed quantity, so the arithmetic mean of core measurements is used to determine the porosity for a model layer. These core measurements were obtained after drying samples in a $105^{\circ}C$ oven for at least 48 hours to obtain a standard dry weight (Flint 1998 [100033], p. 17).

Matrix van Genuchten parameters are satiated saturation (S_s), residual saturation (S_r), α and m. Satiated saturation is assumed to be one (there is no residual gas saturation). Residual saturation is determined from relative-humidity (RH) porosity and total porosity. With satiated and residual saturations fixed, α and m are obtained for a model layer by fitting combined water-potential and saturation data for all samples located within the model layer, and their uncertainties (standard error) are calculated as diagonal terms of the covariance matrix associated with the fitting procedure. Because the data used to estimate α and m are from laboratory desaturation experiments, the estimate of α represents a low bound of the average wetting and drying behavior. Therefore, the estimated α values need to be corrected by forcing the water potential curve through saturation and *in situ* water potential data representing field conditions. A detailed description of the procedures to estimate matrix van Genuchten parameters can be found in the AMR *Analysis of Hydrologic Properties Data* (CRWMS M&O 2000 [145771], Section 6.2.3).

Table 6.5-2 shows estimated matrix properties for the vitric Calico Hills Formation layers. Note that for the case without considering Busted Butte data, the property values are directly from DTN: LB990501233129.001 [106787]. For the case considering the Busted Butte data, detailed calculations for estimating the properties are documented in the Scientific Notebooks (Ahlers 2000 [155853], pp. 81–83; and Liu 1999 [155675], pp. 90–94).

Table 6.5-2.   Uncalibrated Matrix Hydrological Properties for Model Layers Corresponding to the Vitric Calico Hills Formation

UZ Model Layer	Permeability (m^2)		Porosity (-)	Van Genuchten Parameters				
	k	SE$_{log(k)}$	ϕ	α (Pa^{-1})	m (-)	SE$_m$[a]	S$_r$	S$_s$
Parameter set without considering the Busted Butte data (DTNs: LB990501233129.001 [106787])								
ch1v	2.6E-14	0.269	0.273	2.91E-5	0.337	0.035	0.03	1
ch(2-5)v	8.9E-14	0.335	0.345	7.20E-5	0.220	0.057	0.07	1
New parameter set considering the Busted Butte data								
ch1v	2.30E-13	0.201	0.327	9.08E-5	0.240	0.011	0.04	1
ch(2-5)v	1.19E-12	0.247	0.348	1.73E-4	0.178	0.010	0.06	1

[a] SE refers to the standard error and is related to standard deviation (σ) by SE = $\sigma/N^{0.5}$, where N is number of samples.

DTN: LB0103CHVUPROP.001

6.5.1.2.3   Calibrated Hydrological Properties

One-dimensional data inversion is carried out for a number of vertical columns corresponding to boreholes UE-25 NRG#5, USW NRG-6, USW NRG-7a, USW SD-7, USW SD-9, USW SD-12, UE-25 UZ#4, USW UZ-14, UE-25 UZ#16 and USW WT-24 (CRWMS M&O 2000 [144426], Section 6.1.1). Matrix saturation and/or *in situ* water potential data are available for these boreholes. The vitric Calico Hills Formation occurs only in columns corresponding to boreholes USW SD-6, USW SD-7, and USW SD-12. Therefore, the fracture continuum was removed from these columns for UZ model layers ch1v and ch(2-5)v. One-dimensional data inversion (based on inverse modeling) was used because inverse modeling involves many forward runs, and it is not computationally feasible to use 3-D site-scale model directly.

The EOS9 module (Richard's equation) of iTOUGH2 V3.2 (LBNL 1999 [154337]) is used for model calibration. For this study, only the base-case infiltration scenario is considered. Uncalibrated hydrological property values for matrix permeability and van Genuchten parameters excluding residual and satiation saturations (Table 6.5-2) are used as prior information and initial parameter guesses during inverse modeling. The optimized (calibrated) parameter values are obtained when the objective function reaches the minimum, as determined automatically by the ITOUGH2 code.

Table 6.5-3 gives the calibrated hydrological properties for UZ model layers ch1v and ch(2-5)v. As previously indicated, property values for other UZ model layers remain the same as those in the base-case parameter set (CRWMS M&O 2000 [144426], Table 13). As an example, Figure 6.5-3 shows the match between the simulation results achieved with the calibrated parameter set (incorporating the Busted Butte data) and the observed matrix saturation data for USW SD-7.

DTNs: LB991091233129.001 (observations) [125868]
LB0103CHVUPROP.002 (simulations)
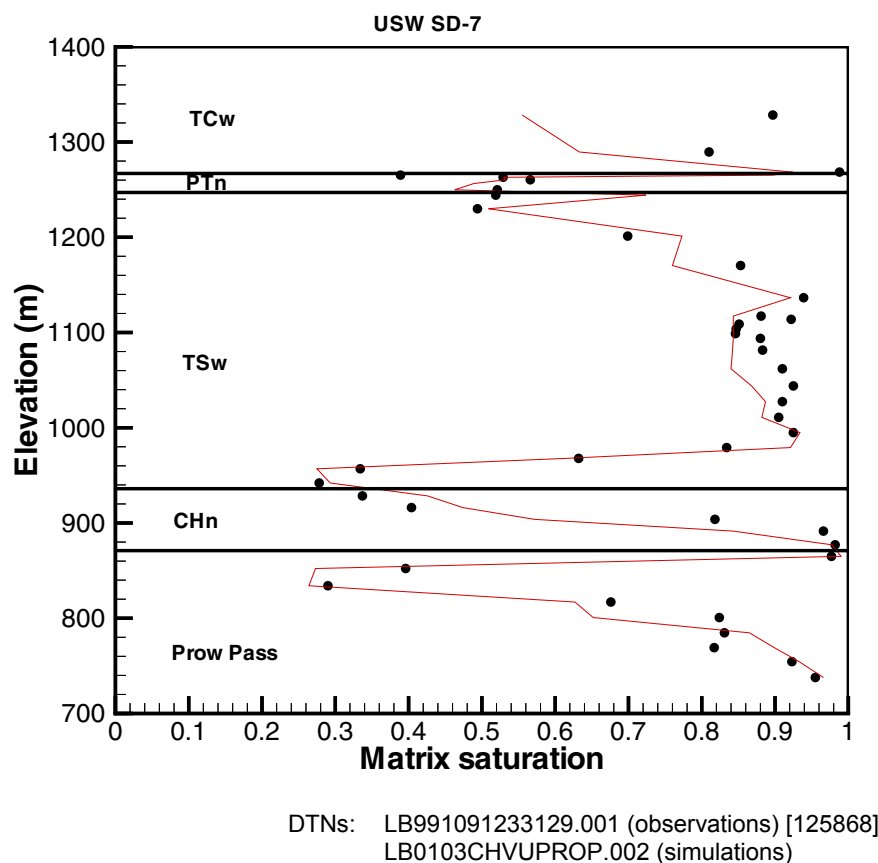
Figure 6.5-3.   Match Between the Simulation Results (solid curve) Achieved with the Calibrated Parameter Set (incorporating the Busted Butte data) and the Observed Matrix Saturation Data for USW SD-7

Comparison between the calibrated and uncalibrated property values (Tables 6.5-2 and 6.5-3) indicates that calibrated matrix permeability values are consistently larger than uncalibrated ones. This may result from the scale-dependent behavior of matrix permeability, although this behavior is approximately considered when determining uncalibrated permeability values (Equation 6.5.1.1). The calibrated matrix α and m values are consistently smaller and larger, respectively, than the uncalibrated ones. This suggests that a systematic bias may exist in our procedure to determine the uncalibrated values for these parameters, which is removed by using the model calibration. Note that the above discussion cannot be extended to other model layers characterized by the dual-continuum. Also, a reliable upscaling procedure, directly based on small-scale measurements and without using model calibration, is not available at this stage (Looney and Falta 2000 [153458]). Therefore, the two-step procedure mentioned above provides a practical and reliable approach to estimating large-scale unsaturated flow and transport parameters (Looney and Falta 2000 [153458], pp. 685–690).

Table 6.5-3.   Calibrated Matrix Hydrological Properties for Model Layers Corresponding to the Vitric Calico Hills Formation

UZ Model Layer	Permeability (m^2)	α (Pa^{-1})	m
Parameter set without considering Busted Butte data			
ch1v	1.50E-13	2.46E-5	0.374
ch(2-5)v	2.58E-13	3.87E-5	0.270
Parameter set considering Busted Butte data			
ch1v	2.95E-12	5.57E-5	0.291
ch(2-5)v	1.42E-12	4.41E-5	0.254

DTN: LB0103CHVUPROP.001

6.5.1.3   Site-Scale Modeling Results

This section presents and analyzes 3-D modeling results for site-scale flow and transport, using the UZ 3-D TSPA grid, present-day and mean infiltration scenario, and the modified vitric conceptual model parameters, as discussed in the previous section. The simulations are also based on perched water Conceptual Model #1 (see Section 6.5.3 for details), and the results are compared to those without considering the vitric zone model modification (conceptual model (a) in Figure 6.5-1). The details on numerical modeling procedures are the same as those in the AMR *UZ Flow Models and Submodels* (CRWMS M&O 2000 [122797]). The relevant simulations runs are documented in the Scientific Notebook (Wu 2001 [155676], pp. 216–254)

Two sets of 3-D flow and transport simulations are carried out, using the new parameters for the Calico Hills Formation vitric zones, estimated in the previous sections, with and without incorporating the Busted Butte data. The two sets of flow simulation results have been checked against the field observed data of matrix liquid saturations, water potentials (when available), and perched water elevations—with reasonable agreements. Flow and transport simulations use TOUGH2 V1.4 (LBNL 2000 [146496]) and T2R3D V1.4 (LBNL 1999 [113942])

6.5.1.3.1   Comparison of Percolation Fluxes at Water Table

Figures 6.5-4 – 6.5-6 show the simulated percolation fluxes at the water table using the two simulation results as well as the original flow field without the vitric-zone properties modification (CRWMS M&O 2000 [122797], Section 6.6). By comparing these with the percolation fluxes at the water table for the two vitric-zone conceptual models and three parameter sets, we find the following:

- As expected, model results using the original conceptual model indicate faster vertical flow through vitric zones than model results based on the newer conceptual model, which assumes no fracture flow in the vitric Calico Hills. The vitric area is limited in extent to the southern part of the model domain below the potential repository horizon (as discussed in *Unsaturated Zone Flow and Transport Model Process Model Report* (CRWMS M&O 2000 [151940], Section 3.2.4)). In areas of the model domain where vitric tuffs have been altered to zeolites, the calibrated percolation flux at the water

table is the same for both conceptual models because the model parameters are unchanged in these areas.

- Simulations based on the new conceptual model (i.e., no vitric fracture flow), with and without incorporation of the Busted Butte data, show similar flow patterns at the water table. This indicates that inclusion of Busted Butte data has an insignificant effect on model results.
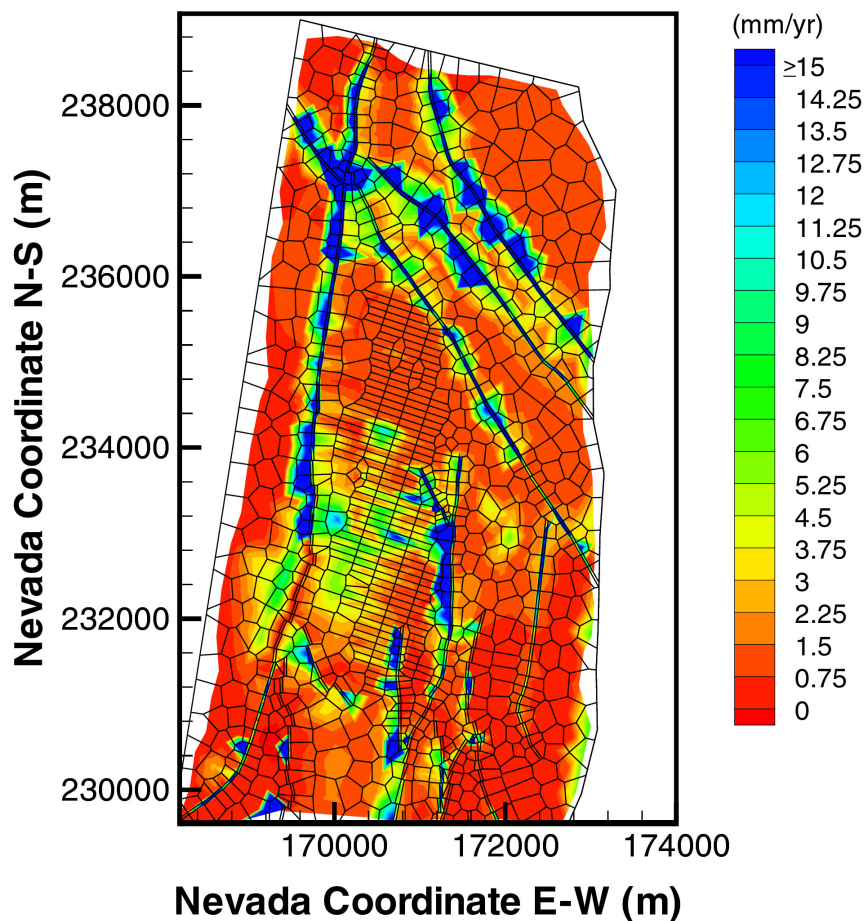
Source: CRWMS M&O 2000 [122797], Figure 6-45, based on DTN: LB990801233129.003 [122757]

Figure 6.5-4.   Simulated Percolation Fluxes at the Water Table Under Present-day, Mean Infiltration Using the Results of the Base-Case Conceptual Model (a)

TOTAL FLUX AT WATER TABLE

Exp-m1/wt/CH

DTN: LB0104AMRU0185.013
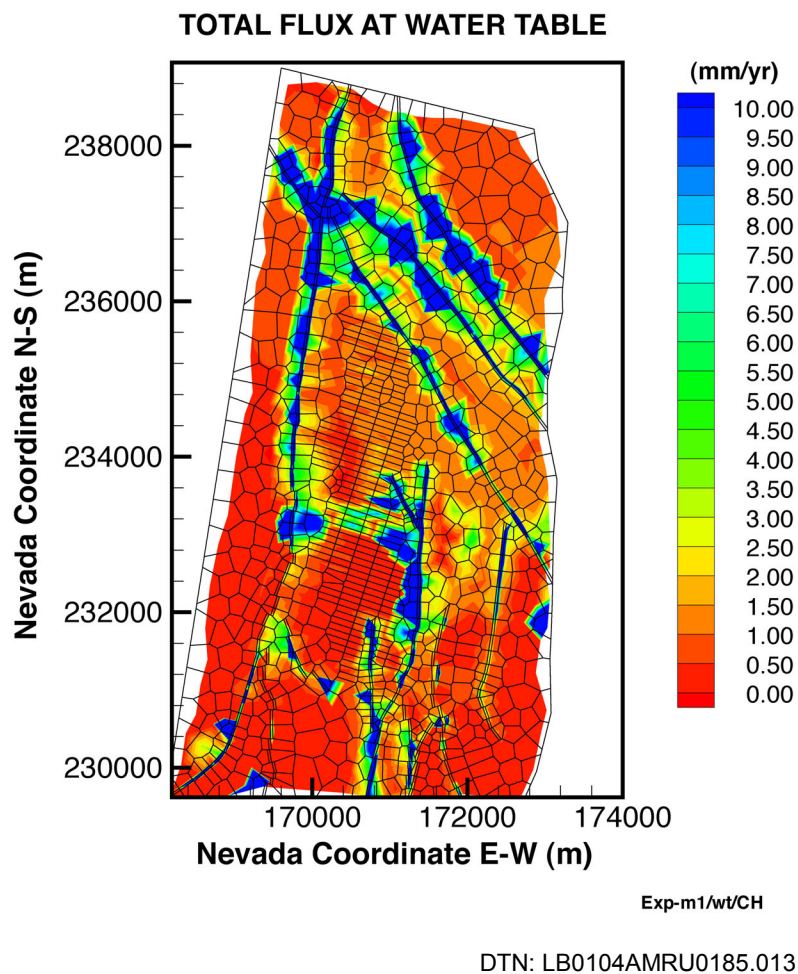
Figure 6.5-5.   Simulated Percolation Fluxes at the Water Table Under Present-day, Mean Infiltration, for Conceptual Model (b) and the New Vitric Properties Without Incorporation of the Busted Butte Data

TOTAL FLUX AT WATER TABLE

ebb-m1/wt/CH

DTN: LB0104AMRU0185.013
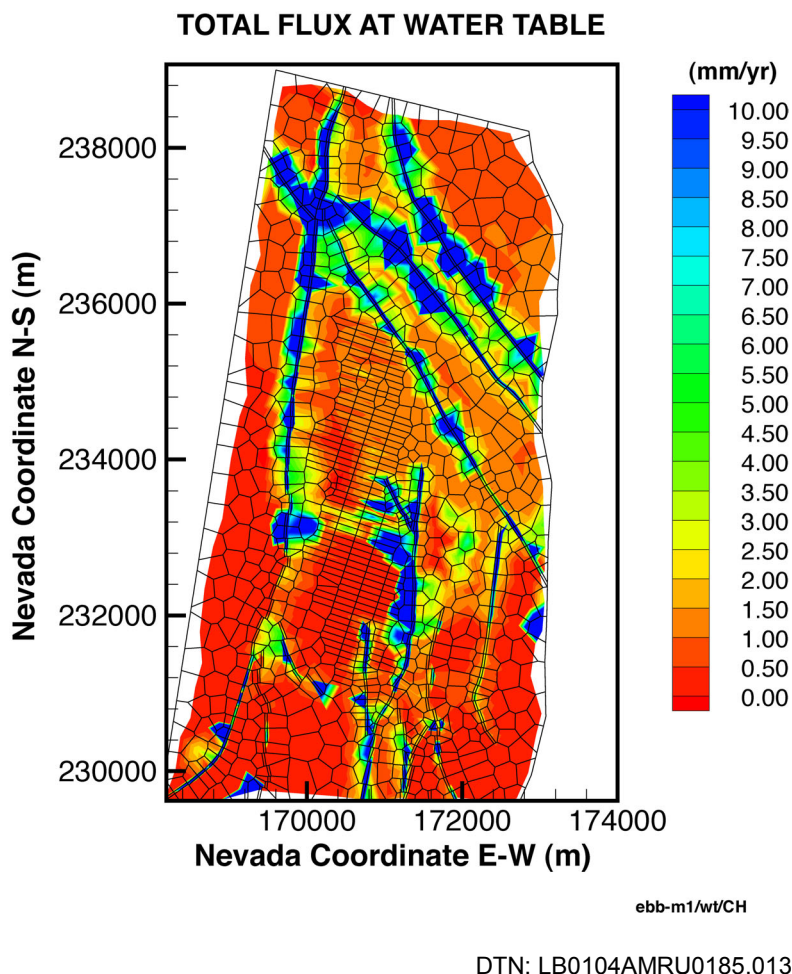
Figure 6.5-6.   Simulated Percolation Fluxes at the Water Table Under Present Day, Mean Infiltration, for Conceptual Model (b) and the New Vitric Properties With Incorporation of the Busted Butte Data

6.5.1.3.2   Comparison of Tracer Transport Times

For each of the three flow simulations, one transport run was made for a conservative tracer. Tracer migration times since release from the potential repository to the water table estimated from these transport simulations are compared in Figure 6.5-7. In this figure, the fractional mass breakthrough curve for the conservative tracer is defined as the cumulative mass of the tracer arrived at the water table over the entire bottom model boundary at the time, normalized by the total initial mass at the potential repository.

Figure 6.5-7 shows that the new conceptual model slightly increases transport times. Without fracture effects (i.e., conceptual model (b) rather than (a), see Section 6.5.1.1), the vertical flow through the vitric zones is reduced, and as a result, the early breakthrough (20% or less) time for a conservative tracer is a little longer. Similar to flow results, the transport simulations with and without incorporating the Busted Butte data give the same transport times.
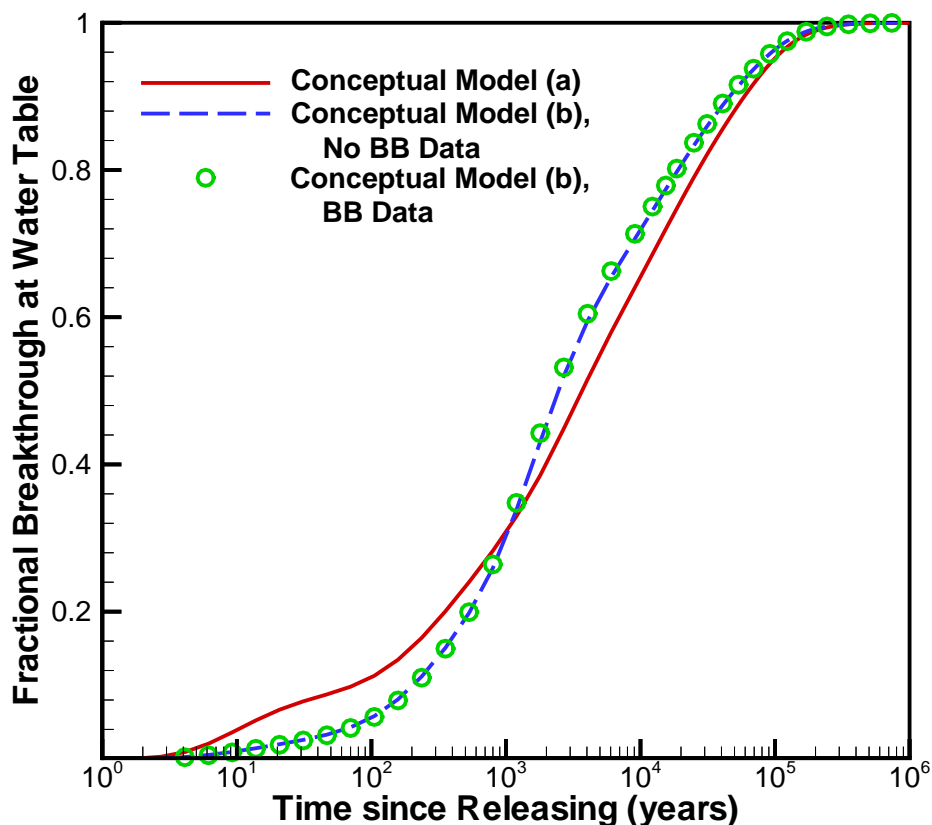
NOTE: In this figure, "BB" refers to Busted Butte.

Figure 6.5-7.   Comparison of Simulated Cumulative Breakthrough Curves of Conservative Tracer Mass Arriving at the Water Table Since Release from the Potential Repository, using the Different Vitric-Zone Conceptual Models

6.5.1.4   Model Validation and Alternative Models

Validation of the data inversion for model parameter estimation can be addressed by evaluating four criteria given by CRWMS M&O (2000 [144426], Section 6.4):

1.   Calibration within experimental data sets.

2.   Comparison of predictions using the calibrated property sets and the UZ Flow and Transport Model to data not used in the calibration process.

3.   Review of model calibration parameters for reasonableness, or consistency in explanation of all relevant data

> *4.   Technical review through publication in the open literature.*

Criteria 1, 3, and 4 are considered partially met by the same rationale given in CRWMS M&O (2000 [144426] Section 6.4). It is not possible to evaluate criterion 2 with respect to this model because there are no data relevant to mountain-scale processes that allow discrimination between a vitric CHn model with or without fractures. However, the evidence presented above in Section 6.5.1.1 and shown in Figure 6.5-2 does suggest that at the meter scale, flow is completely matrix dominated. Note that for the Calibrated Properties model, the intended use is the broad goal of providing estimated model parameters for the UZ Flow and Transport model and other models. For this model, the intended use is the much more limited goal of providing model parameters for presenting an alternative model for flow through the vitric CHn. Moreover, this alternative model is not used for TSPA-SR (CRWMS M&O 2000 [153246]), but does provide confirmation of the conservatism of the models used and directly relied upon in TSPA-SR. Based on this limited goal, the above criteria are applied less rigorously, and based on the evidence above, this model is valid for its intended use.

An alternative to the two conceptual models presented in Section 6.5.1.1 is that fractures exist in the non-welded layers (PTn, vitric and zeolitic CHn, and non-welded portions of the CFu) at multiple scales but only form continuous flow paths capable of supporting unsaturated flow at larger scales. In this model, small-scale fractures would not support large-scale, continuous flow through the non-welded layers because of insufficient fracture length and density. Though it would be possible for the small-scale fractures to contribute some secondary permeability to the non-welded layers. The larger-scale fracturing, generally due to tectonics, would provide continuous flow paths through the non-welded layers, but would support liquid flow only under large transient percolation conditions or saturated conditions. This model would be consistent with the bomb-pulse ^{36}Cl and ^{3}H data from the TSw (see Section 6.2.1.3) and the pneumatic data from the TSw (CRWMS M&O 2000 [144426], Section 6.1.2) which both suggest larger permeability through the PTn than can be accounted for by the matrix alone. Through analogous treatment of all non-welded layers, this model would allow the much more substantial data with respect to the PTn to be applied to the non-welded layers below the TSw while still being consistent with the vitric CHn specific data indicating completely matrix dominated flow. However, analogous treatment of all non-welded layers should not be considered a substitute for collection of data that would allow development of a more robust model (or discrimination between the proposed models) for flow and transport in the non-welded vitric and zeolitic layers below the TSw.

6.5.1.5   Conclusions and Recommendations

This section presents the incorporation of newly available data on the vitric CHn into the UZ Flow and Transport Model. The data, from the Busted Butte test site, suggest higher matrix permeability and lower matrix capillarity than the previously used data indicate. Further, tests at Busted Butte suggest that unsaturated flow and transport in the vitric CHn is completely matrix dominated. A new conceptual model in which fractures are not present in the vitric CHn is used, and new model parameters for these layers are estimated based prior information about the layer properties updated with the Busted Butte data. Mountain-scale, three-dimensional simulations using this updated model show lower percolation fluxes at the water table directly under the vitric portion of the CHn and longer initial-breakthrough times for contaminants from the

repository horizon at the water table. Direct validation of this model of the vitric CHn (with no fractures) is not possible because there are no relevant data against which to compare model predictions. However, the use of calibration, review of the estimated parameters for reasonableness, and technical review of the calibration approach through open literature as well as consistency with the Busted Butte test results make the model valid for its intended use of presenting an alternative model for flow and transport through the vitric CHn. At this time, further development of alternative models is not warranted. Rather, more data on flow and transport through the layers between the bottom of the TSw and the water table is needed in order to discriminate between alternative models and allow development of a single robust model.

6.5.2 Fault Characteristics

6.5.2.1 Introduction

Yucca Mountain is a structural complex of Tertiary volcanic rock. Faults at Yucca Mountain were categorized by Day et al. (1996 [102757]) into three types: (1) north-striking block bounding faults such as the Solitario Canyon and Bow Ridge faults, (2) northwest-striking faults such as Drill Hole Wash, Sever Wash, and Pagany Wash faults, and (3) intrablock faults. Block-bounding faults are key structural features that dip steeply to the west and have large cumulative displacements. Intrablock faults tend to be shorter and more discontinuous than block-bounding faults, and, with the exception of the Ghost Dance fault, generally have minor displacements. Displacement along northwest-striking faults varies from small to moderate. Figure 6.5-8 shows the location of the major faults and boreholes at Yucca Mountain.

Major faults may play a large role in shaping the ambient hydrogeologic system. The hydrologic properties within and near fault zones are expected to be different than in areas without faulting. In brittle, densely welded tuffs, fracture intensities may be high within and adjacent to major faults. Increase in fracture aperture associate with faulting can result in increased permeability and decreased capillarity. However, mineral precipitation along flow pathways or development of fault gouge may effectively reduce fault zone permeability. Nonwelded intervals are less likely to develop intensely fractured zones associated with faulting because of their more ductile properties.

The main area of the potential repository is located in a relatively undeformed section bounded by long, north-trending, normal faults. That faults may provide a direct path from the repository horizon, through the Calico Hills, (CHn), the Crater Flat, (CFu), Prow Pass, Bullfrog and Tram nonwelded tuffs, to the water table is particularly significant to the problem of waste isolation, because radionuclides released from the potential repository could bypass altered, zeolitic layers within the CHn where sorption could occur. Consequently, dissolved radionuclides could enter the saturated zone where hydrologically significant faults and the water table intersect.

Very few direct measurements of fault properties have been made. The relative lack of data with respect to faults makes prediction of their effects on the ambient system and on future potential repository performance challenging. There are no fault data, other than the prior information, for the lower fault layer, CHn/CFu. Sensitivity studies with respect to CHn and CFu fault properties

could help to investigate the effects of hydrogeologic parameters on transport between the potential repository and the water table and reduce uncertainty in these parameters.

Sensitivity studies were conducted for this study using the 3-D site-scale flow and transport model. The results indicate that cumulative transport fluxes at the water table are not sensitive to variations in fracture permeability and capillary pressure parameters used to describe the CHn and CFu faults. Among major faults, transport fluxes mainly go through Drill Hole Wash, Sundance, and Ghost Dance faults from the potential repository to the water table.
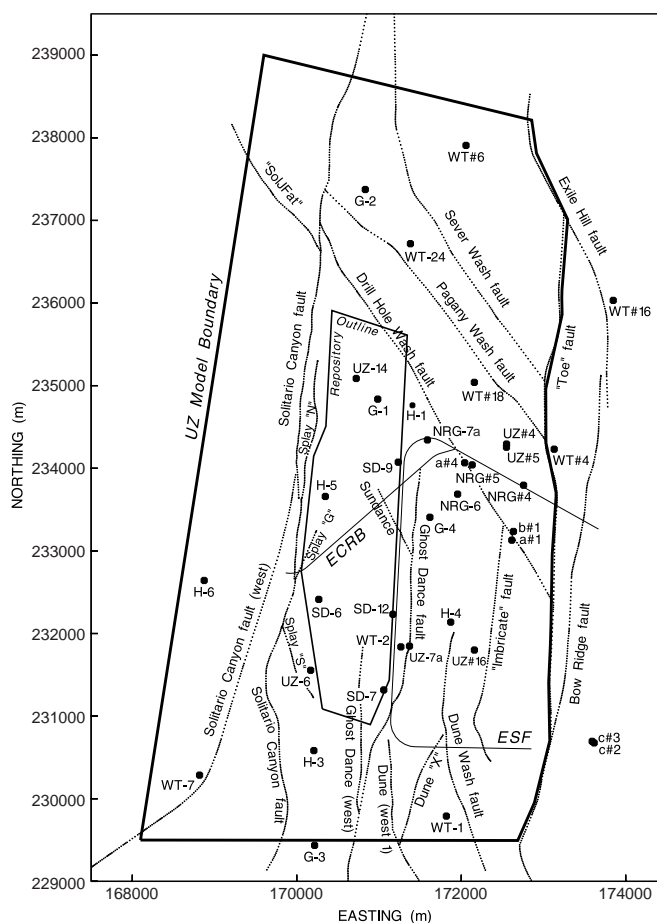
SOURCE: CRWMS M&O 2000 [114277]

Figure 6.5-8.   Location of the Major Faults and Boreholes at Yucca Mountain

6.5.2.2   Conceptual Model

Fluid flow in faults has been described using various conceptual models based on several factors, including the type of rock, the proximity of a region of the fault zone to the surface and/or the water table, and the degree of offset along the fault.

Because there are no fault data for units below TSw, they are taken as analogous to those of PTn. In some respects, the rocks below the TSw will behave like the PTn in the fault zone. The more plastic character of the rocks will reduce the intensity of fracturing in comparison to the densely

welded rocks. Gouge formation is also expected to be important for mountain-scale flow in these nonwelded units. However, in some places, most notably east of the Solitario Canyon Fault, the Bullfrog and Tram units are above the water table. These units are more welded and therefore, where they are faulted, they are expected to behave more like the TCw and TSw with very intense fracturing. All of the units below the TSw are near the present water table and are therefore likely to have undergone hydrothermal alteration in the past under higher water table conditions. Hydrothermal alteration will serve to reduce the permeability of the fault zone. The reduced permeability of fault zones below the TSw will aid the formation of perched water at the base of the TSw where structural traps are formed by fault offset. The fault zones are likely to be more permeable than the surrounding altered rock, and thus will still form the main drain from perched water zones.

Characterization of the hydrogeologic setting at Yucca Mountain is complicated by the presence of numerous faults. Other than geologic-mapping studies, limited data have been collected to characterize faults at Yucca Mountain. Types of data available include pneumatic pressure monitoring, air-injection and tracer-testing data, core sample measurements of water potential and saturation, *in situ* measurements of water potential, fracture characteristics and temperature and geochemical data. An east-west vertical cross section model through borehole USW UZ-7a was used to calibrate parameters for the faults (CRWMS M&O 2000 [144426], Section 6). Data from USW UZ-7a are the most comprehensive with respect to faults. Saturation, water potential, and pneumatic pressure data are available within the Ghost Dance fault zone from the surface to the upper layers of the TSw. Because data are limited, it is best to characterize one fault (Ghost Dance fault) as completely as possible and apply these properties to all other faults. Heterogeneity in faults is considered a function of major hydrogeologic units. The limited data were separated into four layers (TCw, PTn, TSw, and CHn/CFu) to reduce the number of calibration parameters. Data for inversion are only available for the first three layers. Fracture permeability for the CHn unit is based on only one measurement in the CHn (CRWMS M&O 2000 [145771], Table 5). Fracture permeability for the TCw and TSw fault layers is given by the crosshole air-injection tests. Permeability for the PTn and CHn/CFu fault layers is calculated by scaling the weighted average bulk-rock fracture permeability. Equivalent fracture permeability is calculated for all four fault layers using the weighted harmonic mean of permeabilities for the corresponding non-fault model layers. The average ratio of the measured permeability to the calculated equivalent permeability for layers TCw and TSw is calculated. This factor multiplies the calculated equivalent permeability of the PTn and CHn/CFu layers to scale them up. Fracture porosity is determined by scaling the weighted arithmetic mean of bulk rock fracture porosity. The scaling factor is the ratio of fault fracture aperture to mean bulk rock fracture aperture. The fracture-to-matrix connection area for the faults is approximated as the weighted arithmetic mean of bulk rock fracture to matrix connection area. The process is explained in *Analysis of Hydrologic Properties Data* (CRWMS M&O 2000 [145771]). Calibrated data sets are used in the base case of this study.

6.5.2.3   Model Setup and Sensitivity Studies

Fluid flow in faults has been simulated using many different conceptualizations including a fractured medium, a seepage face, a single- or double-porosity medium, and a dual-permeability medium.

Sensitivity studies were conducted in this work to consider the impact of varying (i.e., increasing and decreasing) CHn and CFu fault fracture permeability and van Genuchten curve-fitting α parameter on transport fluxes from the potential repository to the water table.

A three-dimensional dual-permeability model, T2R3D V1.4 (LBNL 1999 [113942]), and TOUGH2 V1.4 (LBNL 2000 [146496]) were employed for the sensitivity studies described herein. Simulation grids, basic hydrologic properties of rock matrix, and fractures are the same as those used in the 3-D UZ perched water model (DTN: LB990801233129.003 [122757], DTN: LB990701233129.001 [106785]). The T2R3D module simulates transport of radionuclides in 3-D multiphase subsurface systems. A conservative liquid tracer applied at the potential repository is observed using bot_sum.f V1.0 (LBNL 2000 [153471]) to study the effect of fault parameters on tracer flow in a steady-state flow field. The dual-permeability formulation was used for all simulations to describe fracture and matrix continua within and outside of the fault zones.

For each sensitivity run, fault properties were changed throughout the CHn and CFu layers. The base-case values of fracture permeability and van Genuchten curve-fitting parameter α for matrix and fracture are 0.36×10^{-12} m^2, 0.979×10^{-6} Pa^{-1}, and 0.23×10^{-2} Pa^{-1}, respectively. For the sensitivity studies, permeability is increased and decreased by two orders of magnitude, and α is increased and decreased by one order of magnitude. This range is appropriate considering the limited available data.

The top model boundary represents the ground surface of the mountain or, where present, the bottom of the alluvium. The bottom boundary of the model represents the water table, which is a relatively flat, stable surface. Lateral boundaries are treated as no-flow boundaries. The spatial distribution of net infiltration along the top ground surface boundary was described in *UZ Flow Models and Submodels* (CRWMS M&O 2000 [122797]; DTN: LB990801233129.003 [122757]).

6.5.2.4   Results

Sensitivity-study results can be evaluated considering both the distribution of instantaneous and cumulative tracer fluxes at the water table. Figure 6.5-9 shows the changes in the total cumulative tracer fluxes at the water table to the base case as a result of increasing and decreasing fracture permeability and van Genuchten parameter α. There are basically no differences in these curves in terms of both breakthrough times and amount of tracer fluxes, indicating that the model is not sensitive to the order-of-magnitude changes in these flow parameters. The results of an impermeable-fault case are also shown in this figure, and again with little difference compared to other cases. Table 6.5-4 lists the percentages of cumulative tracer fluxes going through each major fault relative to the total cumulative tracer flux at the water table at a simulation time of 1 million years. For all scenarios, the total tracer flux through faults is approximately 20%, with the Drill Hole Wash fault containing the majority of that flux (about 15%). The Sundance and Ghost Dance faults account for most of the remaining 5% of the total flux, while the other modeled faults do not significantly participate in tracer transport. Except for the high capillarity (low α) case, which results in a 3–4% increase in total flux, there are no notable differences among the different simulation scenarios. Figures 6.5-10 through 6.5-12 show the distributions of cumulative tracer fluxes along the three faults with the higher percentages. The results are consistent with those given in the table. For Sundance and Ghost

Dance faults, the case with higher capillary pressure gives a slightly higher cumulative tracer flux, but this difference was not observed in Drill Hole Wash fault. Figure 6.5-13 show the cumulative tracer fluxes along an east-west cross section that crosses the faults of Solitario Canyon, Splay, Ghost Dance (west), Ghost Dance, Dune Wash, and Imbricate and goes through borehole USW UZ-7a. Higher tracer fluxes can be observed around fault zones.

Table 6.5-4.   Cumulative Tracer Fluxes Reaching Water Table through Major Faults after One Million Years as a Percentage of Total Flux

Faults	Base Case	High Permeability	Low Permeability	High Capillary Pressure (low α)	Low Capillary Pressure (high α)	Impermeable Case
Drill Hole Wash	15.05	15.20	14.86	16.26	14.78	0.00
Sundance	2.18	2.23	2.09	2.80	2.11	0.00
Ghost Dance	1.63	1.68	1.55	2.80	1.54	0.00
Ghost Dance West	1.06	1.15	0.79	1.67	1.00	0.00
Solitario Canyon	0.08	0.08	0.07	0.09	0.07	0.00
Splay	0.01	0.01	0.01	0.01	0.01	0.00
Dune Wash, Dune west, Dune X	0.00	0.00	0.00	0.00	0.00	0.00
Imbricate	0.00	0.00	0.00	0.00	0.00	0.00
Pagany Wash	0.00	0.00	0.00	0.00	0.00	0.00
Sever Wash	0.00	0.00	0.00	0.00	0.00	0.00
Solitario Canyon West	0.00	0.00	0.00	0.00	0.00	0.00
Solj Fat	0.00	0.00	0.00	0.00	0.00	0.00
Total	20.0	20.4	19.4	23.6	19.5	0.00
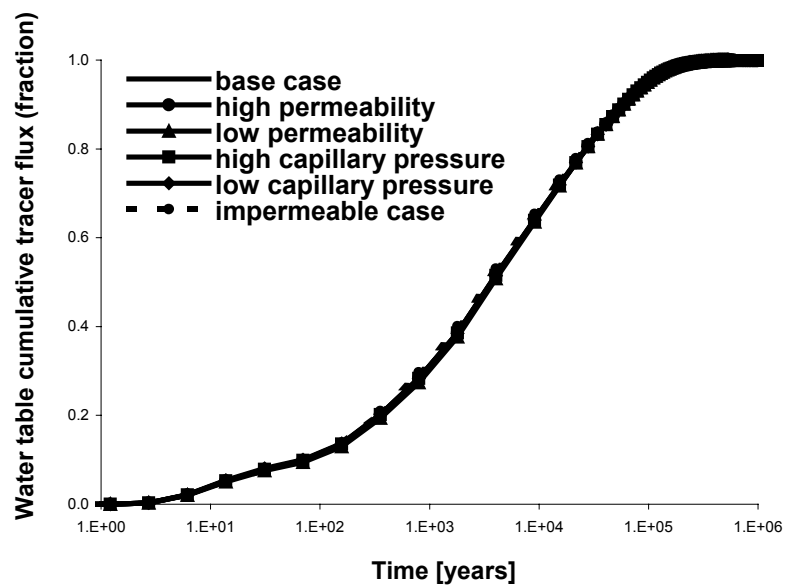
DTN: LB0104AMRU0185.008

Figure 6.5-9.   Cumulative Tracer Fluxes at the Water Table
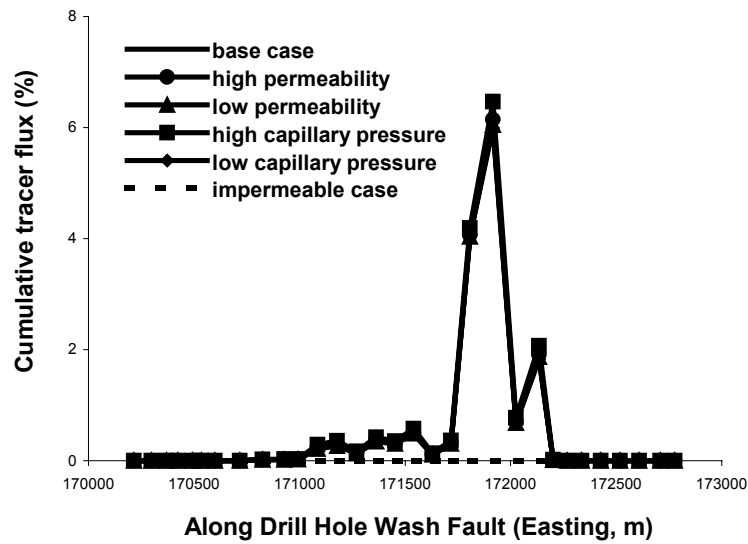
DTN: LB0104AMRU0185.013

Figure 6.5-10.   Cumulative Tracer Fluxes along the Drill Hole Wash Fault
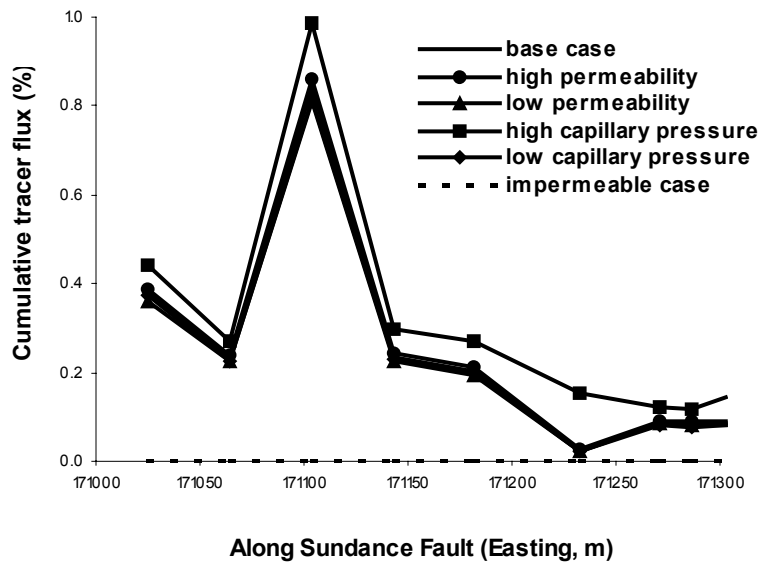
DTN: LB0104AMRU0185.013

Figure 6.5-11.   Cumulative Tracer Fluxes along the Sundance Fault
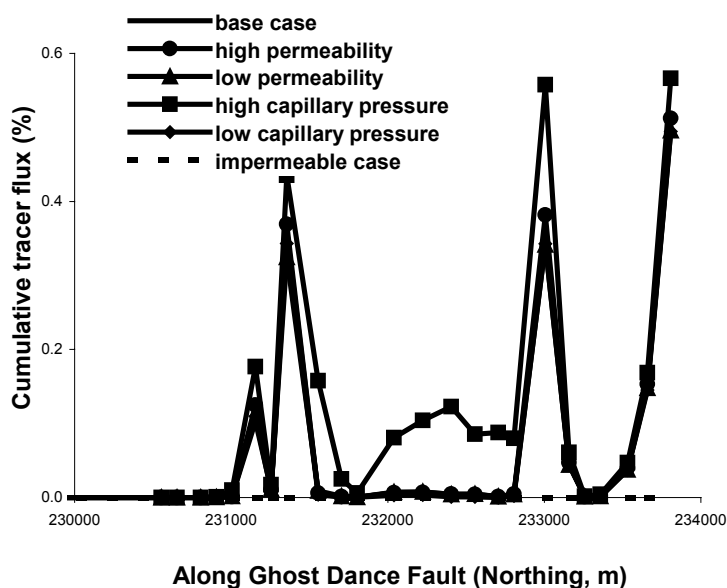
DTN: LB0104AMRU0185.013

Figure 6.5-12.   Cumulative Tracer Fluxes along the Ghost Dance Fault
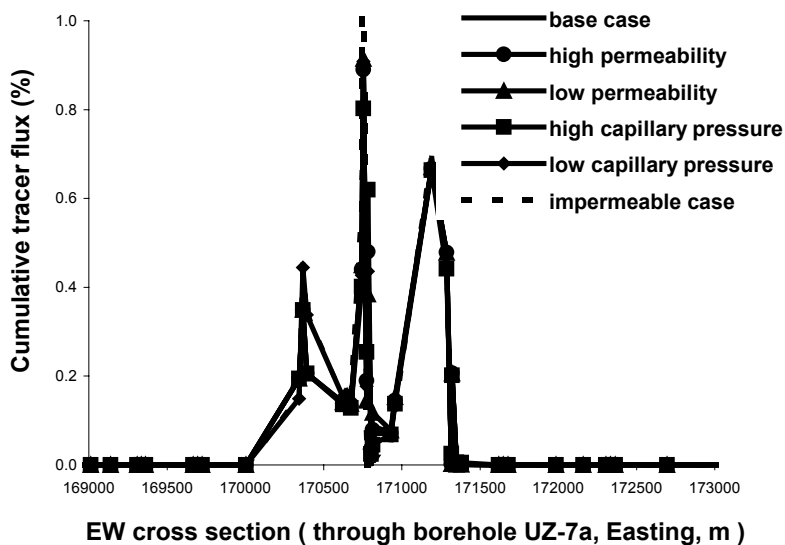
DTN: LB0104AMRU0185.013

Figure 6.5-13.   Cumulative Tracer Fluxes along EW Cross Section (through borehole USW UZ-7a)

6.5.2.5   Summary and Conclusions

The role of major faults in the vicinity of the potential repository area in flow and transport processes within the UZ is uncertain, given the absence of information about fault hydrological properties below the Topopah Spring Tuff. Sensitivity of modeled flow and transport behavior to changes in certain key hydrological parameters assigned to major faults below the potential repository horizon has therefore been evaluated. Results of this study indicate that changes in fracture permeability within the fault zones (increased and decreased by two orders of magnitude) and van Genuchten parameters α for both fractures and matrix within fault zones (increased and decreased by one order of magnitude) have little impact on tracer transport from the potential repository horizon to the water table. Of the total cumulative tracer fluxes through the water table, about 15% go through the Drill Hole Wash fault, followed by Sundance and Ghost Dance faults, which combined contribute about 5%. The total tracer fluxes through faults are about 20%, and the case with higher capillary pressure gives about 3% higher tracer fluxes.

It is therefore concluded that, with the current infiltration rate and conceptualization of fault zones and perched water, flow and transport between the potential repository horizon and the water table are not sensitive to these fault-zone parameters. The analysis conducted here used only one infiltration scenario, with the flow-through perched-water model. To explore all the uncertainties in the CHn/CFu flow and transport behavior, further studies need to be performed considering the combined factors of fractured or unfractured vitric CHn, permeable or impermeable faults, and flow-through or lateral-flow perched-water model. What may be more important is the percolation flux occurring within major fault zones, which is affected by infiltration rates and potential flow focusing within faults.

6.5.3   Perched Water Models

The objectives of this section are: (1) to summarize the available data for perched water; (2) to review the current perched water conceptual models and the related issues affecting potential repository performance; (3) to evaluate effects of different perched water conceptual models on flow and transport processes; and (4) to discuss several more likely scenarios of perched water models.

6.5.3.1   Available Data

Perched water has been encountered in a number of boreholes at Yucca Mountain, including boreholes USW UZ-14, USW SD-7, USW SD-9, USW SD-12, USW NRG-7a, USW G-2, and USW WT-24 (see Figure 6.5-14 for the borehole locations). These perched water observations were made during borehole drilling (Rautman and Engstrom 1996 [101008], p.8; Rautman and Engstrom 1996 [100642], p.8; Rousseau et al. 1999 [102097], pp. 170–183; and DTN: GS980508312313.001 [109746]). The most recent perched water data were collected found from borehole USW WT-24 (DTN: GS980508312313.001 [109746]). The observed perched water data in boreholes at Yucca Mountain have been used for developing the UZ Flow Model (CRWMS M&O 2000 [122797]).

Several field hydraulic pumping tests on perched water were conducted at the site. Boreholes tested include USW UZ-14 (DTN: GS960308312312.005 [107230]) and USW G-2 (DTN:

GS970208312312.003 [119786]). Some of these tests were successful and have been used to estimate perched water bodies and local rock permeabilities (Wu et al. 1999 [117167], pp. 178–180).

In addition to the observation of perched water at boreholes, a wide range of chemical and isotopic data was obtained from the perched water and matrix pore waters of the UZ. These data include tritium (^{3}H), Carbon-14 (^{14}C), chloride (Cl$^-$) concentration, delta Carbon-13 (δ^{13}C), and other geochemical and isotopic compositions of pore water samples (Yang et al. 1996 [100194], pp. 34–39, Table 7, Figure 20; Rousseau et al. 1999 [102097], Table 4.2.4-1).

6.5.3.2   Current Perched Water Models

Since the mid-1980s, the U.S. Department of Energy has pursued a program of site-characterization studies designed to characterize the geological, hydrological, and geothermal conditions in the UZ and SZ of Yucca Mountain. During these field investigations, several perched water zones have been encountered (Rautman and Engstrom 1996 [101008], p.8; Rautman and Engstrom 1996 [100642], p.8; Rousseau et al. 1999 [102097], pp. 170–183; and DTN: GS980508312313.001 [109746]). The presence of perched water bodies within Yucca Mountain may have important implications for flow paths and transport times of water and radionuclides through the UZ and therefore could have a possible impact on the performance of the potential repository.

Perched water may accumulate where adjacent formation units have disparate hydraulic conductivities, such as when water migrating downward through a more permeable tuff reaches a much-less-permeable rock through which flow paths are limited. It may occur in a permeable layer overlaying a relatively impermeable layer or in a well-connected fractured unit overlaying a locally unfractured or poorly globally connected fractured unit. Perched water may also form along a dipping, low-permeability layer that is adjacent to a fault that acts as a capillary barrier to retard down-dip water flow.

In general, the presence of perched water indicates that vertical percolation flux locally exceeds the saturated hydraulic conductivity of the perching layers. It also suggests that flow paths may not be completely vertical through the CHn to the water table. Instead, the water may be partially diverted laterally to a fault zone or other high-permeability channel that may serve to focus flow downward to the water table. A concern is that perched water zones may divert water around low-permeability zeolitic layers of a CHn formation unit underlying the potential repository horizon. Bypassing of these units, which have substantial capacity to retard radionuclide transport, could have an impact on the capability of the geologic system to retard radionuclide releases to the water table.

In terms of groundwater flow paths, travel times, and radionuclide transport from the potential repository level, perched water zones and the CHn, which separates the potential repository horizon from the SZ, may play an important role. The predominantly nonwelded CHn, consisting mainly of high-porosity vitric tuffs and low-permeability zeolites, creates complex, heterogeneous flow paths within this unit. In addition, the existence of perched water bodies within the CHn further complicates assessment of the flow patterns and transport processes in the unit.

The current perched water conceptual models are based on the UZ Flow Model (CRWMS M&O 2000 [122797]), which is in turn built on the numerical model grids (CRWMS M&O 2000

[114277]) and *Calibrated Properties Model* (CRWMS M&O 2000 [144426]). In the UZ Flow Model, the UZ of Yucca Mountain is represented using two numerical discrete grids (3-D UZ Calibration and TSPA grids) for investigating flow and transport processes using a numerical modeling approach. The model domain and the associated 3-D grid are shown in Figure 6.5-14. Vertically, the model extends from the ground surface to the water table. Within the UZ Flow Model, the CHn is represented with fourteen 3-D model layers in general, based on lithostratigraphy and available hydrogeologic properties, as discussed in (CRWMS M&O 2000 [114277]).

The genesis of perched water at Yucca Mountain is much debated among Yucca Mountain Project scientists, and several conceptual models have been discussed (e.g., Wu et al. 1999 [117167], pp. 163–164). At Yucca Mountain, occurrence of perched water is found to be associated with low-permeability zeolites in the CHn or the densely welded basal vitrophyre of the TSw. The current conceptual model of the UZ Flow Model relies on a permeability-barrier concept for perched water occurrence. Related modeling studies (Wu et al. 1999 [117167] and CRWMS M&O 2000 [122797], Sections 6.2 and 6.6) concluded that this conceptual water-perching model is able to match the observation data of perched water at the site. The perched water conceptual model of the UZ Flow Model consists of two permeability-barrier scenarios. One (Conceptual Model #1) uses reduced fracture permeabilities within zeolitic layers (beneath the basal vitrophyre) as well as within the basal vitrophyre of the TSw unit and is called the permeability-barrier model. The other scenario (Conceptual Model #2) (called the unfractured zeolite model) presumes that the occurrence of perched water at Yucca Mountain results mainly from the lack of globally connected fractures within zeolitic units and that a water-perching mechanism is controlled by the low-permeability zeolitic matrix only (i.e., the effects of fractures in zeolites are ignored).

In the UZ Flow Model and submodels, the perched water occurrence is assumed to follow these two conceptual models (the permeability-barrier and unfractured zeolite models). In addition to the two conceptual models, a third alternative scenario considered in the UZ Flow Model is a nonperching model, which provides an extreme case using the 1-D calibrated properties. This model ignores perched zones and their effects, and provides maximum and rapid vertical flow through all the layers in the CHn.
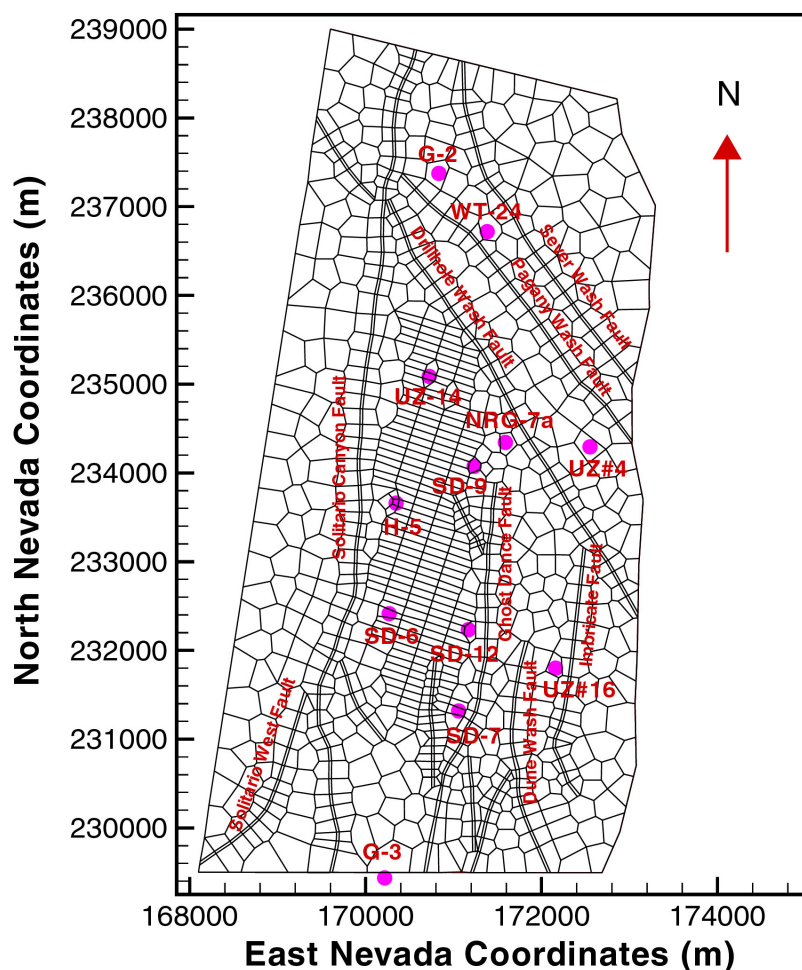
Figure 6.5-14.   Plan View of the 3-D UZ TSPA Model Grid, Showing the Model Domain, Faults Incorporated, and Borehole Locations

While several mechanisms may be responsible for the occurrence of perched water in the formation below the potential repository, the main concern with respect to PA is the impact of perched water on radionuclide transport from the potential repository to the water table. Evaluation of perched water effects on radionuclide transport depends, among other factors, on perched water conceptual models. Modeling studies in *UZ Flow Models and Submodels* (CRWMS M&O 2000 [122797]) indicate that for sorbing (reactive) radionuclides, the current perched water conceptual model is very conservative. This is because the current model predicts significant lateral flow over or within the zeolitic units of the CHn, which therefore reduces the amount of water flowing through the zeolites. As a result, the potential of highly sorbing or retardation effects of these zeolitic rocks is not sufficiently utilized, and a large mount of bypassing water, carrying radionuclides, goes through lower-sorbing vitric zones, faults, and/or high-permeability fractures.

For nonsorbing (conservative) radionuclides, without the benefit of adsorption on rocks, the major factor to determine transport times under steady-state percolation condition is matrix diffusion and/or liquid dilution for a pulse release of radionuclides from the potential repository neither of

which are related to the perched water conceptual models. In this case, transport times of conservative radionuclides are determined by several competing factors, which also depend on how much water flows through vertically and how much is diverted laterally. On the one hand, a large amount of water rapidly flowing through fractures in the underlying zeolites will leave little time for matrix diffusion and liquid dilution. This would result in very short radionuclide breakthrough times at the water table (conservative model results). However, the modeling studies indicate that this is a very unlikely scenario because the observed perched water occurrence cannot be matched by this model. On the other hand, if a large amount of water is significantly diverted laterally, the resulting groundwater travel distance or travel times along these diverted flow paths will be longer, compared to paths with rapidly vertical flow. However, intensive lateral diversion over perched water zones and significantly focused flow over small areas of faults or fractured channels will decrease the amount of water seeping through perched bodies and low-permeability zeolites. This will significantly reduce contact between flowing water (carrying radionuclides) and rock matrix blocks and will result in a minimum benefit of matrix diffusion and liquid dilution for retarding the radionuclide migration. Therefore, even with the longer lateral travel distance, less vertical flow through reduces interaction with low permeability zeolites and as a result may lead to shorter overall transport time.

6.5.3.3   Alternative Perched Water Conceptual Models

Conceptual models involving perched water occurrence in the UZ below the potential repository horizon are of particular interest in assessing nature-system performance of the potential repository. Waste isolation strategies at the potential repository depend in part on sorption within the zeolitically altered CHn and on groundwater travel times between the potential repository horizon and the water table.

There are several alternative conceptual models regarding the formation of perched water bodies. One of them is called the fault-controlled perching model. This conceptual model was proposed by USGS scientists to explain the thick perched body present in USW UZ-1 and USW UZ-14 of the North Ramp (Rousseau et al. 1999 [102097], pp. 170–183). In this hypothesis, the water perching in this area may result from the presence of a northeast trending fault that forms a barrier to lateral water flow. In the UZ, faults may play an important role in forming localized perched water bodies and were considered as a possible perching mechanism (Montazer and Wilson 1984 [100161], Figure 14, p. 45) for Yucca Mountain. However, lack of detailed characterization studies of faults and, in particular, limited knowledge of fracture and matrix properties within and near faults make it very difficult to test this conceptual model using the 3-D site-scale model.

Three possible conceptual explanations for water perching are illustrated in Figures 6.5-15, 6.5-16, and 6.5-17, for the northern part of the UZ model domain. The geological information along the cross section is closely based on the current geological framework model. Figure 6.5-15 presents a very simplified scenario for the non-water perching model. This model assumes that fractures in the basal vitrophyre and in the CHn are so extensive that no large or significant perched bodies can form and perched water effects can be ignored. Another extreme case, shown in Figure 6.5-16, is that extensive, continuous perched water zones exist, leading to significant, large-scale lateral flow and a small percentage of vertical flow through. Figure 6.5-17 presents a water-perching scenario

between the two extremes, with discontinuous but quite large perched bodies and moderate lateral flow, mainly within the perched zones.

Non-Water Perching

East-West Cross Section at N235,087 m
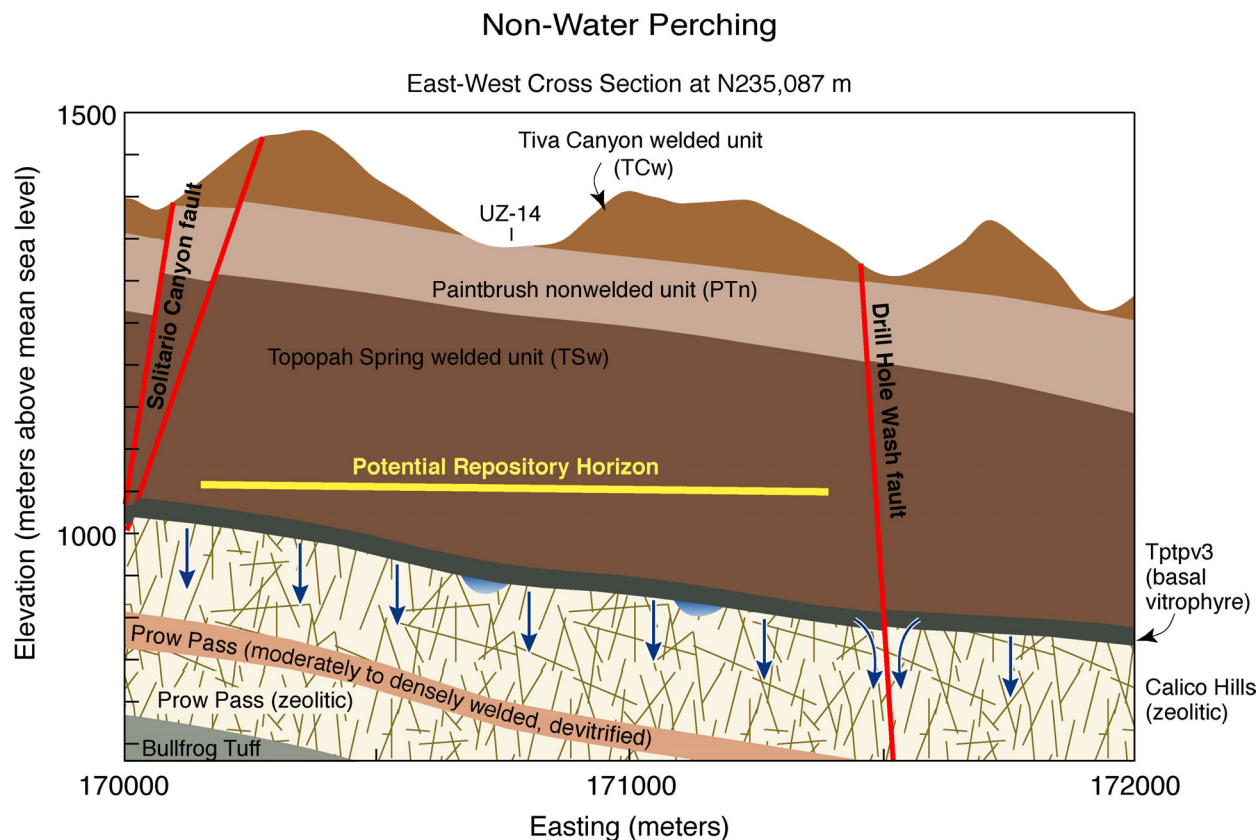
Figure 6.5-15.   Schematic of Non-Water Perching Model in the Northern Part of the UZ Flow Model Domain with Extensive Globally Connected Fractures, Ignoring Perched Water Effects with Little Lateral Diversion
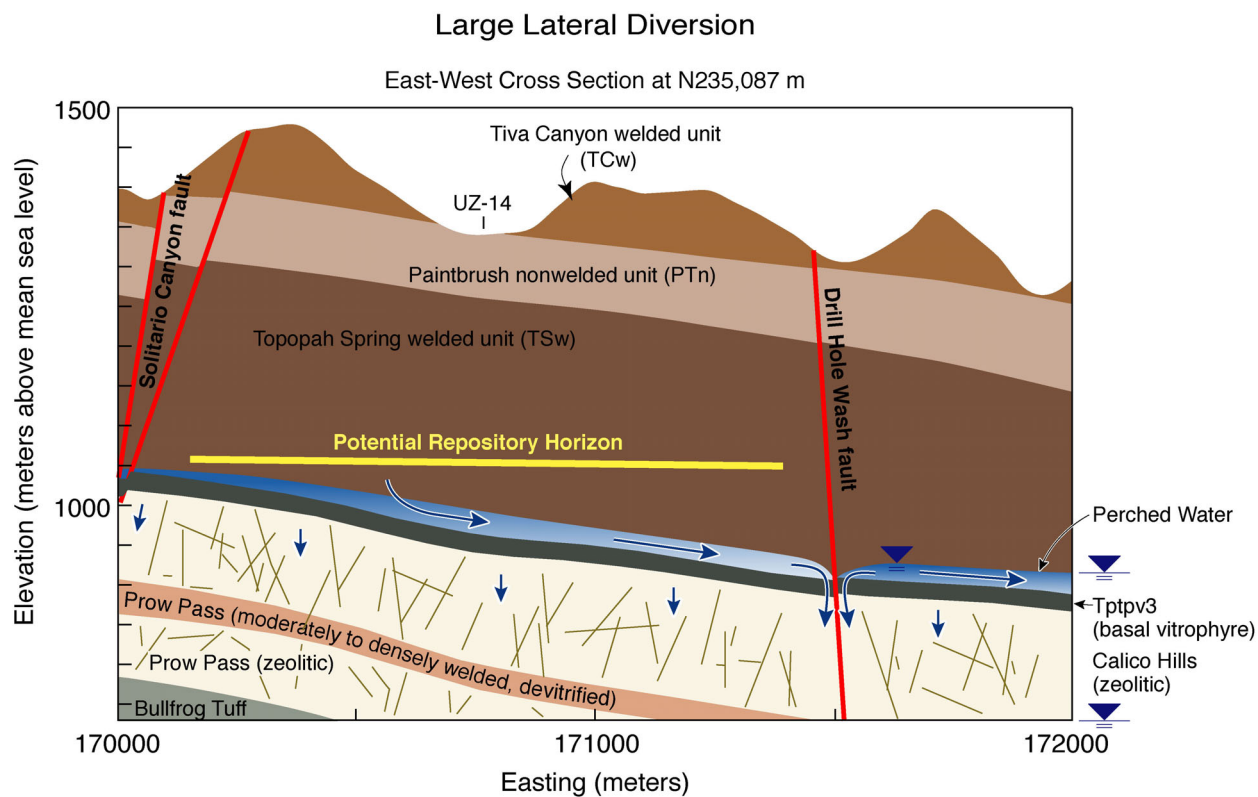
Figure 6.5-16. Schematic of Permeability-Barrier Model (Conceptual Model #1) in the Northern Part of the UZ Flow Model Domain with Additional Conceptual Model Element of Few Globally Connected Fractures. This Model Results in Large, Continuous Perched Water Bodies, Limited Vertical Flow under the Perched Water Bodies, and Extensive Lateral Flow to Faults

Perched Water

East-West Cross Section at N235,087 m
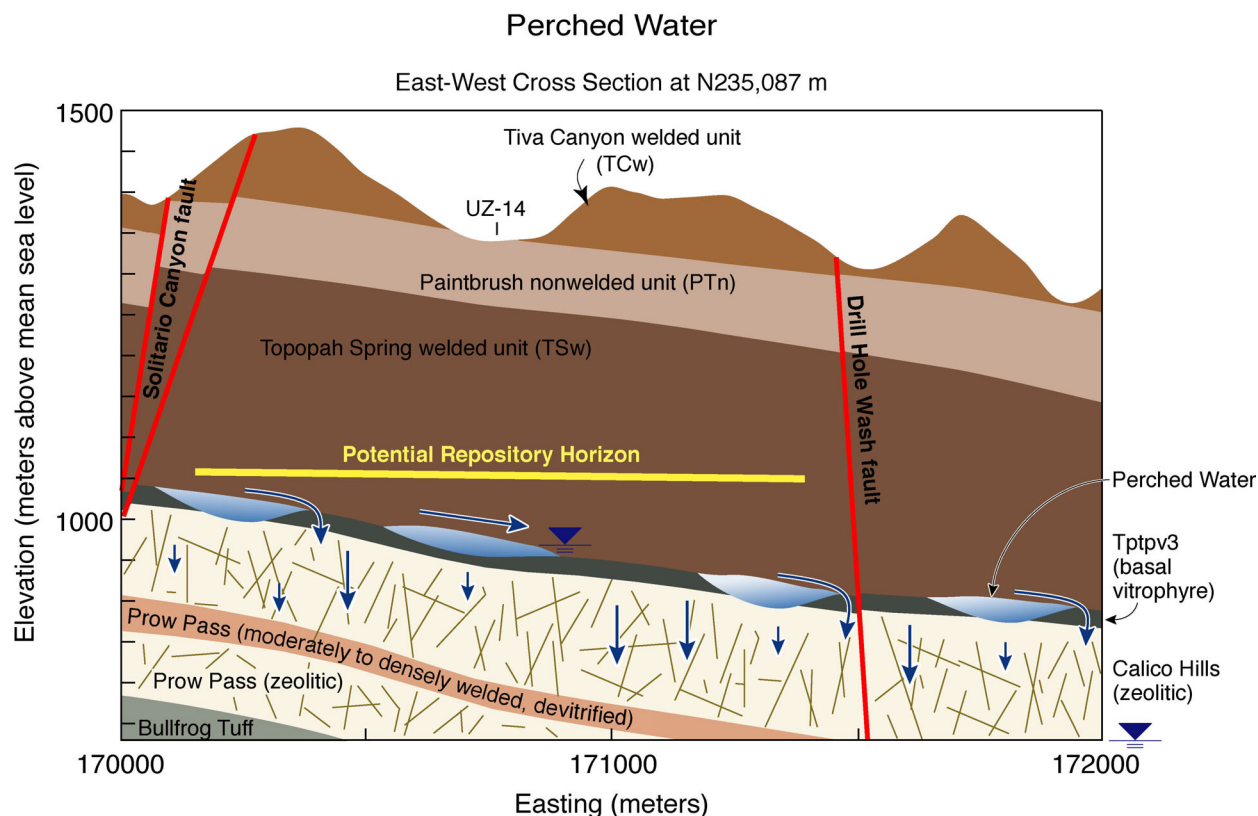
Figure 6.5-17.   Schematic of Permeability-Barrier Model (Conceptual Model #1) in the Northern Part of the UZ Flow Model Domain with Additional Conceptual Model Element of Some Globally Connected Fractures. This Results in Discontinuous Perched Water Bodies, Limited Vertical Flow only Directly under Perched Bodies, Limited Lateral Flow to Faults and Areas between Perched Water Bodies.

The identification of controlling mechanisms for perched water occurrence at Yucca Mountain is complicated by the lack of field data, as well as by large uncertainties about the exact locations of many of the key geological formations and the past infiltration history. The conceptual models for water perching, as discussed above, need to be further investigated before a better understanding can be obtained of the perched water conditions at Yucca Mountain.

6.5.3.3.1   Results and Analyses

This section analyzes and compares modeling results of six 3-D simulations of flow and transport, respectively, using the UZ 3-D TSPA grid and present-day, mean infiltration scenario. The simulations are based on perched water Conceptual Models #1 and #2, with modifications to the vitric zone conceptual models and fracture properties in the zeolites associated with perched water bodies. The details on the numerical method, modeling approach, boundary, and initial condition specifications are the same as those in *UZ Flow Models and Submodels* (CRWMS M&O 2000 [122797]).

The simulation scenarios of flow and transport, which use TOUGH2 V1.4 (LBNL 2000 [146496]) and T2R3D V1.4 (LBNL 1999 [113942]), are listed in Table 6.5-5. This table summarizes the simulation cases, associated conceptual models/grids, and parameter sets. As shown in Table 6.5-5, two (pa_pchm1 and pa_pchm2) of the six flow scenarios are directly taken from the work on the UZ Flow Model (CRWMS M&O 2000 [122797]). The three new simulations (exp_m1, exp_m2 and exp_m3) implement the new estimated parameters, which ignore fracture-flow effects within vitric zones, as discussed in Section 6.5.1. Fracture parameters for the grid are modified using vf_con.for V1.0 (LBNL 2001 [154345]). In addition, fracture permeabilities are increased by a factor 10 and 100, respectively, for potentially water perching zeolites to investigate effects of large vertical flow through perched water bodies.

Table 6.5-5. Six Flow and Transport Simulation Scenarios: INPUT Files, Conceptual Models/Grids, with Present-Day, Mean Infiltration Rate

Designation/ Flow Simulation	Designation/ Transport Simulation	Perched Water Conceptual Model/Numerical grid	Description/ Parameter DTN
pa_pchm1 DTN: LB990801233 129.003 [122757]	pam1_tr1 pam1_tr2 DTN: LB9908T12331 29.001 [147115]	#1 permeability-barrier model/ 3d2kpa_pc1.mesh DTN: LB990701233129.001 [106785]	Taken from the AMR on *UZ Flow Models and Submodels* (CRWMS M&O 2000 [122797]) (DTN: LB991121233129.001 [147328])
exp_m1	expm1_tr1 expm1_tr2	#1 permeability-barrier model/ 3d2knvf_pc1.mesh DTN: LB0104AMRU0185.009	New simulation, modifying parameter set (DTN: LB991121233129.001 [147328]) with unfractured CHn vitric unit (DTN: LB0103CHVUPROP.001)
exp_m2	expm2_tr1 expm2_tr2	#1 permeability-barrier model/ 3d2knvf-pc1.mesh DTN: LB0104AMRU0185.009	New simulation, modifying parameter set (DTN: LB991121233129.001 [147328]) with unfractured CHn vitric unit (DTN: LB0103CHVUPROP.001) and increasing fracture permeabilities in potentially perched zeolites by a factor of 10
exp_m3	expm3_tr1 expm3_tr2	#1 permeability-barrier model/ 3d2knvf_pc1.mesh DTN: LB0104AMRU0185.009	New simulation, modifying parameter set (DTN: LB991121233129.001 [147328]) with unfractured CHn vitric unit (DTN: LB0103CHVUPROP.001) and increasing fracture permeabilities in potentially perched zeolites by a factor of 100
pa_pchm2 DTN: LB990801233 129.004 [117129]	pchm2_tr1 pchm2_tr2 DTN: LB9908T12331 29.001 [147115]	#2 unfractured zeolitic model/ 3d2kpa_pc2.mesh DTN: LB990701233129.001 [106785]	Taken from the AMR on *UZ Flow Models and Submodels* (CRWMS M&O 2000 [122797]) (DTN: LB991121233129.002 [147334])
exp_pch2	expch2_tr1 expch2_tr2	#2 unfractured zeolitic model/ 3d2knvf_pc2.mesh DTN: LB0104AMRU0185.009	New simulation, modifying parameter set (DTNs: LB991121233129.002 [147334]; with unfractured CHn vitric unit (DTN: LB0103CHVUPROP.001)

In Table 6.5-5, *_tr1 represents transport simulations for conservative/nonsorbing tracer/radionuclide and *_tr2 for reactive/sorbing tracer transport. Transport properties for non-sorbing and sorbing tracers correspond to those of technetium (^{99}Tc) and neptunium (^{237}Np) (CRWMS M&O 2000 [122797]), when not explained.

Examination of Flow Model Results: The two flow and transport scenarios of Table 6.5-5, corresponding to flow scenarios "pa_pchm1" and "pa_pchm2", were developed in the AMR *UZ Flow Models and Submodels* (CRWMS M&O 2000 [122797]), and the results have already been checked. For the rest of the four flow fields, we have compared the model results with the field observed data of matrix liquid saturation and water potentials (when available) (DTNs: MO0109HYMXPROP.001 [155989], GS980808312242.014 [106748], GS980708312242.010 [106752]), and perched water elevations (see DTNs given in Section 6.5.3.1), and reasonable agreement is observed (Wu 2001 [155676], pp. 216–254; Bodvarsson 2001 [156334], YMP-LBNL-YSW-4, pp. 7–20; Zellmer 2001 [155956], pp. 9–13, 39–48, 85).

Comparisons with Measured Chloride Data: Geochemical data provide additional information to analyze the UZ flow process and history. Here pore-water chloride chemical concentration data are used to examine the perched water model and resultant flow fields. Distribution of chemical constituents in both liquid and solid phases of the UZ system depends on many factors, such as hydrological and geochemical processes of surface precipitation, evapotranspiration, the fracture-matrix interactions of flow and transport, large-scale mixing via lateral transport, and the history of climate changes and surface recharge.

The results of three-dimensional chemical transport simulations using the steady-state flow field, exp_m2, have been compared with measured pore-water chloride concentration data in this study. (The data available and applied are from samples collected from boreholes (USW NRG-6, USW NRG-7a, USW SD-6, USW SD-7, USW SD-9, USW SD-12, USW UZ-14, and UE-25 UZ#16); the ECRB tunnel; and the Exploratory Studies Facilities tunnel, including South Ramp, North Ramp, and Main Drift (Data Sources: DTN: GS950608312272.001 [145617], DTN: GS990208312272.001 [146134], DTN: LA9909JF831222.004 [145598], DTN: LA0002JF12213U.002 [156281]).) Detailed descriptions of these data are given in reports by Yang et al. (1998 [101441]) and Fabryka-Martin et al. (1997 [100145]). Chloride surface flux is obtained by applying a mean chloride concentration to precipitated water. Combining the mean annual precipitation of about 170 mm/year (Flint et al. 1996 [100147]) with a present-day chloride surface flux of 106 mg/m^2/year (Flint et al. 1996 [100147]) yields a mean chloride concentration of about 0.62 mg/L (Fabryka-Martin et al. 1997 [100144]; Sonnenthal and Bodvarsson 1999 [117127]). The system is assumed to be under two-phase isothermal flow conditions for water and air. Major chemical transport processes taken into account are advection and molecular diffusion.

Model and basic hydrologic properties of rock matrix and fractures are the same as those used in the flow model. Boundary conditions for chemical components of chloride are treated similarly to those for flow simulations, with mass fluxes described at the top boundary and no-flow and water table conditions at the lateral and bottom boundaries, respectively. Diffusion coefficients used were those for chemical ions at 25°C and infinite dilution in water (Lasaga 1998 [117091]).

Simulated chloride concentrations from the 3-D transport model are compared with measured chloride concentrations at boreholes USW SD-7, USW SD-9, USW SD-12, USW UZ-14, and UE-25 UZ#16 as well as along the ECRB and ESF tunnels. The model results are found in reasonable agreement with the field (Bodvarsson 2001 [156334], YMP-LBNL-YSW-4, pp. 13–17).

Percolation Fluxes at the Potential Repository and the Water Table: Percolation fluxes at the potential repository horizon, simulated using the present-day, mean infiltration map, are almost the same for the six flow fields. This is because the only difference between the six models is in the flow properties and conceptualization for the CHn and the bottom portion of the TSw, which has little effect on the upstream flow condition in an upper elevation (at the potential repository horizon). One example of percolation fluxes at the potential repository level is shown in Figure 6.5-18, indicating a very nonuniform distribution (with high percolation fluxes) located mainly at the northern part, over the potential repository area along the mountain ridge, and the Solitario Canyon Fault in the middle-to-south portion of the model domain.

TOTAL FLUX AT REPOSITORY LEVEL (mm/year)

exp-m1/REP/CH
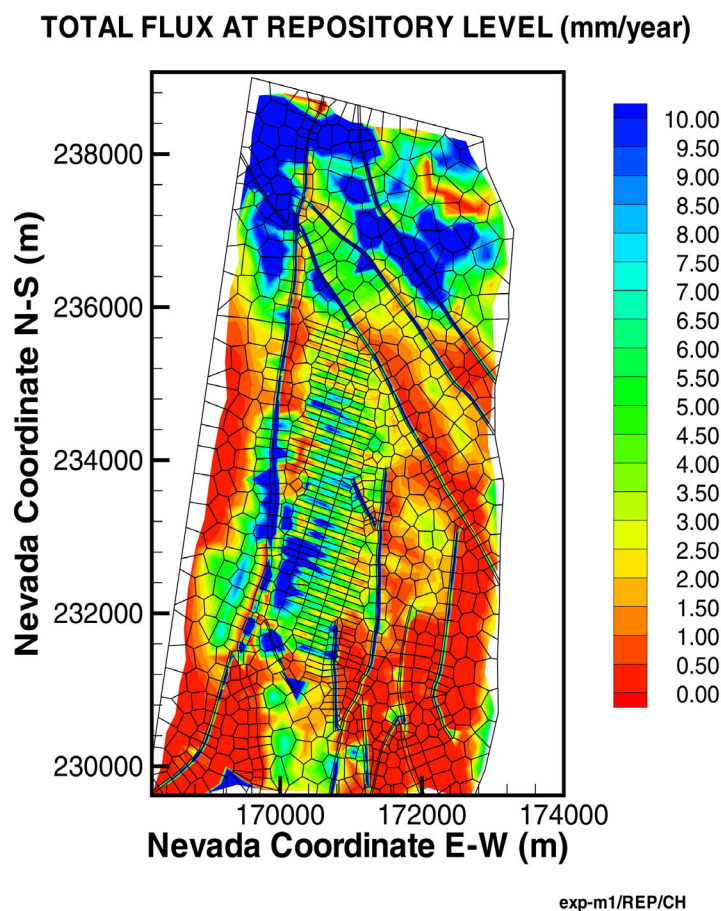
DTN: LB0104AMRU0185.009

Figure 6.5-18.   Simulated Percolation Fluxes at the Potential Repository Horizon under Present-Day, Mean Infiltration Using the Results of Simulation exp_m1

A comparison of the simulated percolation fluxes at the water table with the six simulations (Figures 6.5-19 to 6.5-24) for the perched water, vitric, and zeolitic fracture conceptual models, reveals the following:

- Conceptual Model #1 predicts the least flow-through or maximum bypassing over perched water zones or zeolites in the northern part of the model domain. In the area directly below the potential repository or vitric zones in the southern part of the model domain, this model results in a large vertical flow-through (Figure 6.5-19).

- Conceptual Model #1 with unfractured vitric zone modification shows the least vertical flow-through in the southern part of the model domain, the vitric zones below the potential repository (Figures 6.5-20).

- Conceptual Model #1, with reduced fracture permeability in potential water perching zeolites, as well as unfractured vitric zone modification, predicts significantly more vertical flow-through in the northern part of the model domain and less lateral diversion (Figures 6.5-21 and 6.5-22) than the original scenario.

- Conceptual Model #2, with (Figures 6.5-23) or without (Figure 6.5-24) unfractured vitric zone modification, predicts similar vertical flow patterns through the CHn below the potential repository, but significantly less vertical flow-through in the northern part of the model domain, compared with Conceptual Model #1.

TOTAL FLUX AT WATER TABLE

pa-pchm1/wt/CH
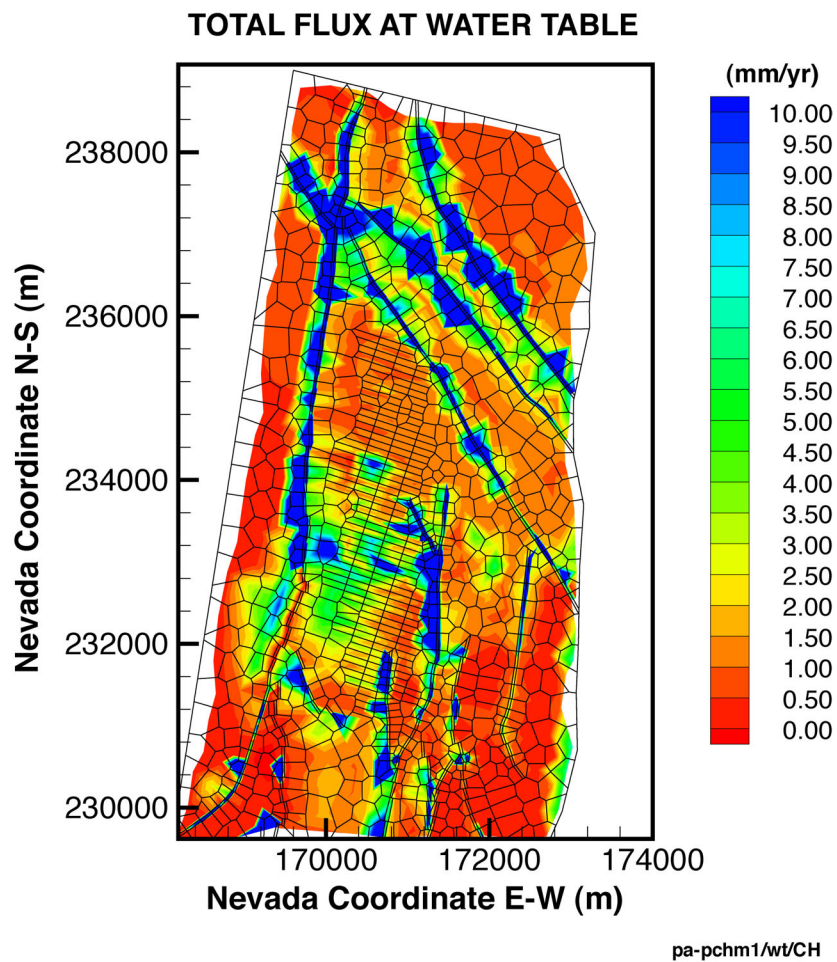
DTN: LB990801233129.003 [122757]

Figure 6.5-19.   Simulated Percolation Fluxes at the Water Table under Present-Day, Mean Infiltration Using the Results of Simulation pa_pchm1, Conceptual Model #1
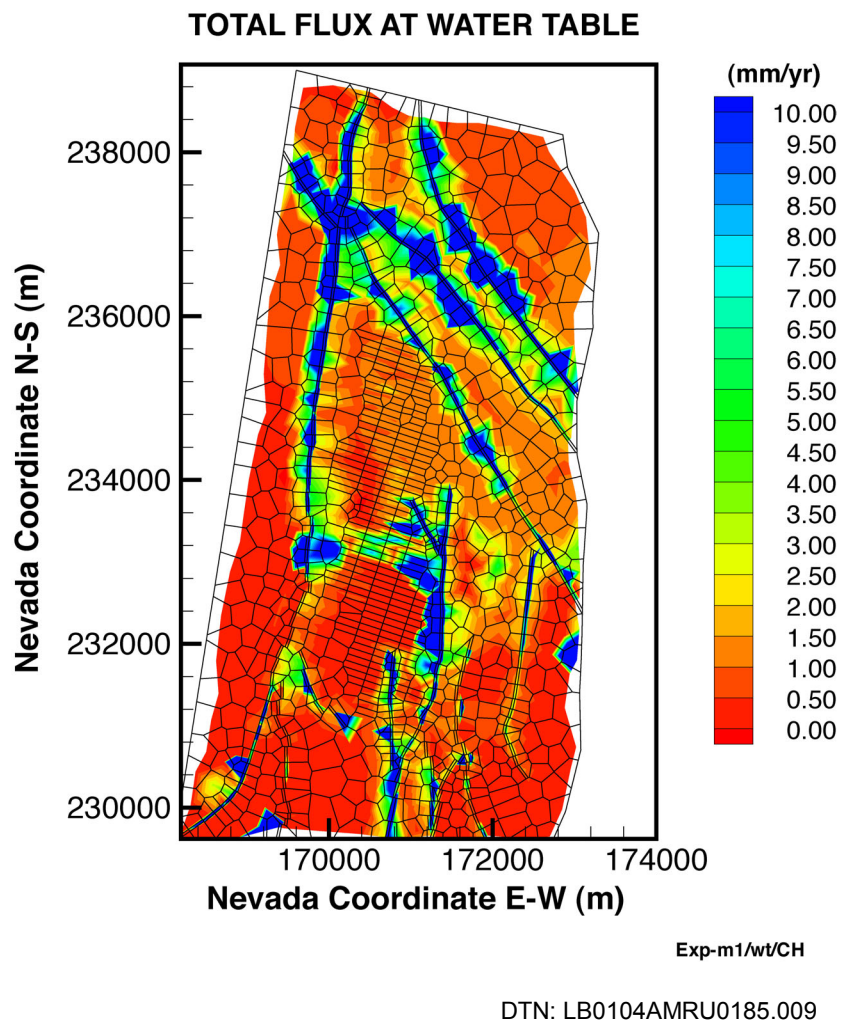
Figure 6.5-20. Simulated Percolation Fluxes at the Water Table under Present-Day, Mean Infiltration Using the Results of Simulation exp_m1, Conceptual Model #1 with Unfractured Vitric Zones
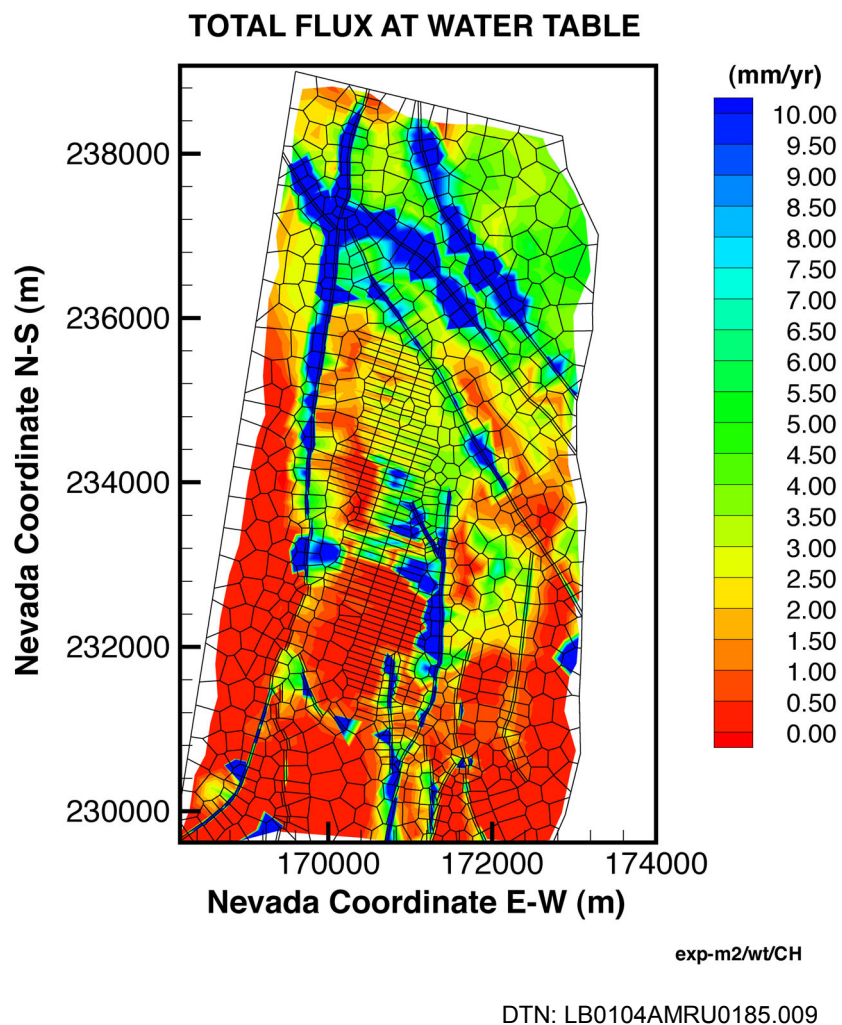
Figure 6.5-21.   Simulated Percolation Fluxes at the Water Table under Present-Day, Mean Infiltration Using the Results of Simulation exp_m1, Conceptual Model #1 with Unfractured Vitric Zones and Reduction of a Factor 10 for Fracture Permeability in Potential Water Perching Zeolites

TOTAL FLUX AT WATER TABLE

exp-m3/wt/CH

DTN: LB0104AMRU0185.009
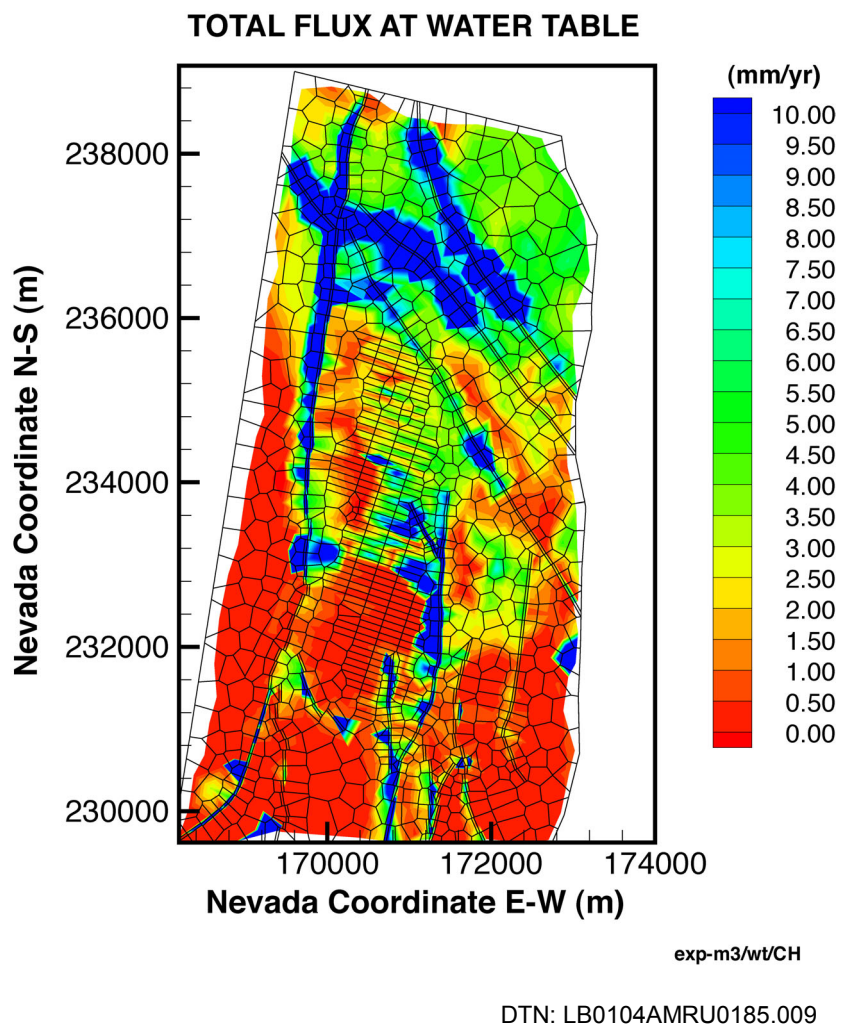
Figure 6.5-22.   Simulated Percolation Fluxes at the Water Table under Present-Day, Mean Infiltration Using the Results of Simulation exp_m1, Conceptual Model #1 with Unfractured Vitric Zones and Reduction of a Factor 100 for Fracture Permeability in Potential Water Perching Zeolites

TOTAL FLUX AT WATER TABLE
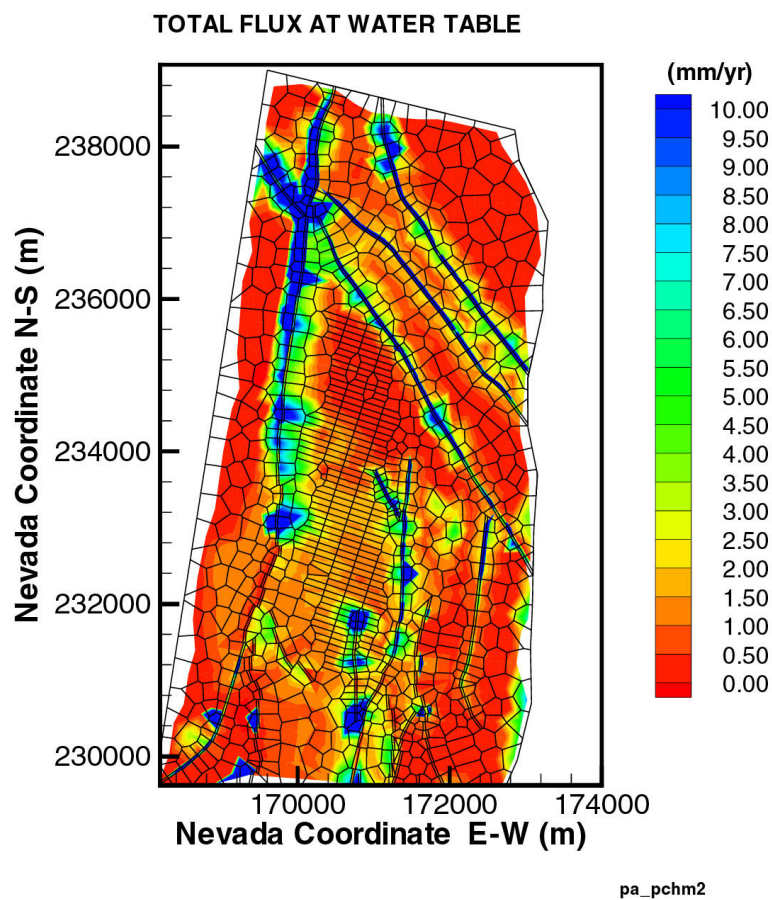
pa_pchm2

DTN: LB0104AMRU0185.009

Figure 6.5-23.   Simulated Percolation Fluxes at the Water Table under Present-Day, Mean Infiltration Using the Results of Simulation pa-pchm2, Conceptual Model #2

TOTAL FLUX AT WATER TABLE
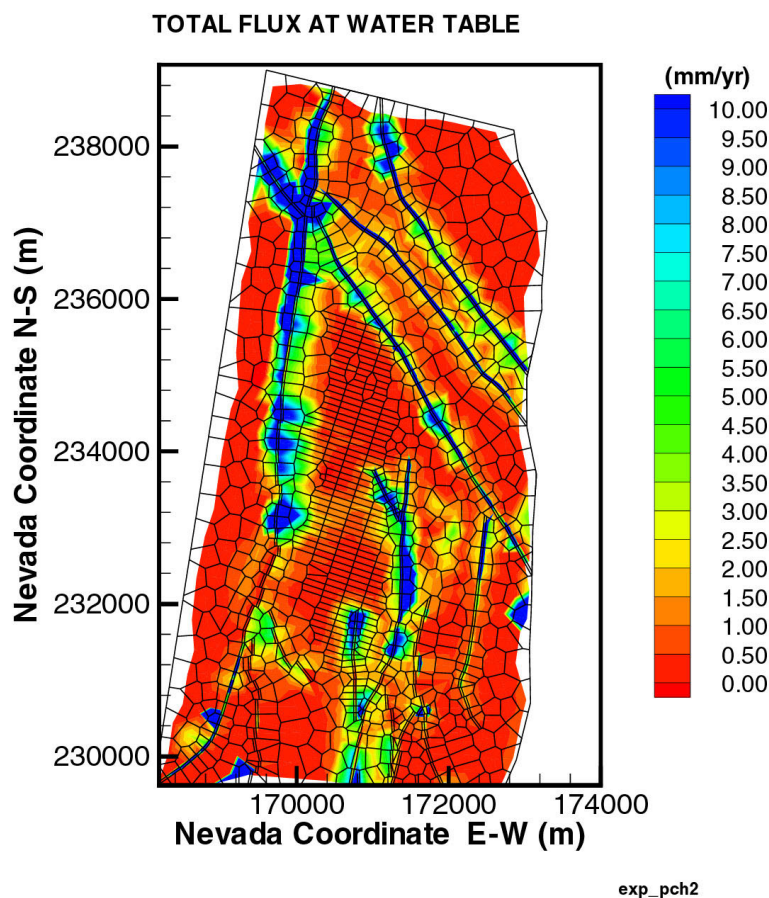
exp_pch2

DTN: LB0104AMRU0185.009

Figure 6.5-24.   Simulated Percolation Fluxes at the Water Table under Present-Day, Mean Infiltration Using the Results of Simulation exp_pch2, Conceptual Model #2 with Unfractured Vitric Zones

Flow Through versus Bypassing in Perched Water Zones: The percentage of water flowing through or bypassing perched water bodies below the potential repository may have an impact on groundwater flow paths and travel times. This can, in turn, affect the amount of radionuclides that can sorb on to sorptive materials or diffuse into low-permeability rock matrixes. As a result, the percentage of the percolation flux through highly sorptive rock matrix over the total percolation fluxes will have a direct impact on performance of the potential repository. The percentage of flow-through or bypassing of perched bodies can be further analyzed using the 3-D model results. Figure 6.5-25 shows vertical flow distributions at locations near USW UZ-14 from the six model results. The location of USW UZ-14 is shown in Figure 6.5-14, which is located in the north of the potential repository.

Figure 6.5-25 shows that at the location near USW UZ-14, vertical fluxes through the perched water or zeolitic zones vary significantly with conceptual models. The simulations with non-water perching and high fracture permeability (by a factor of 100) predict the highest vertical flow-through. As fracture permeability in zeolites decreases, vertical flow decreases and indicates

more lateral diversion. The original Conceptual Model #1 gives very low vertical flow and Conceptual Model #2, or unfractured zeolitic zone model, predicts the lowest vertical flux at this location.

UZ-14
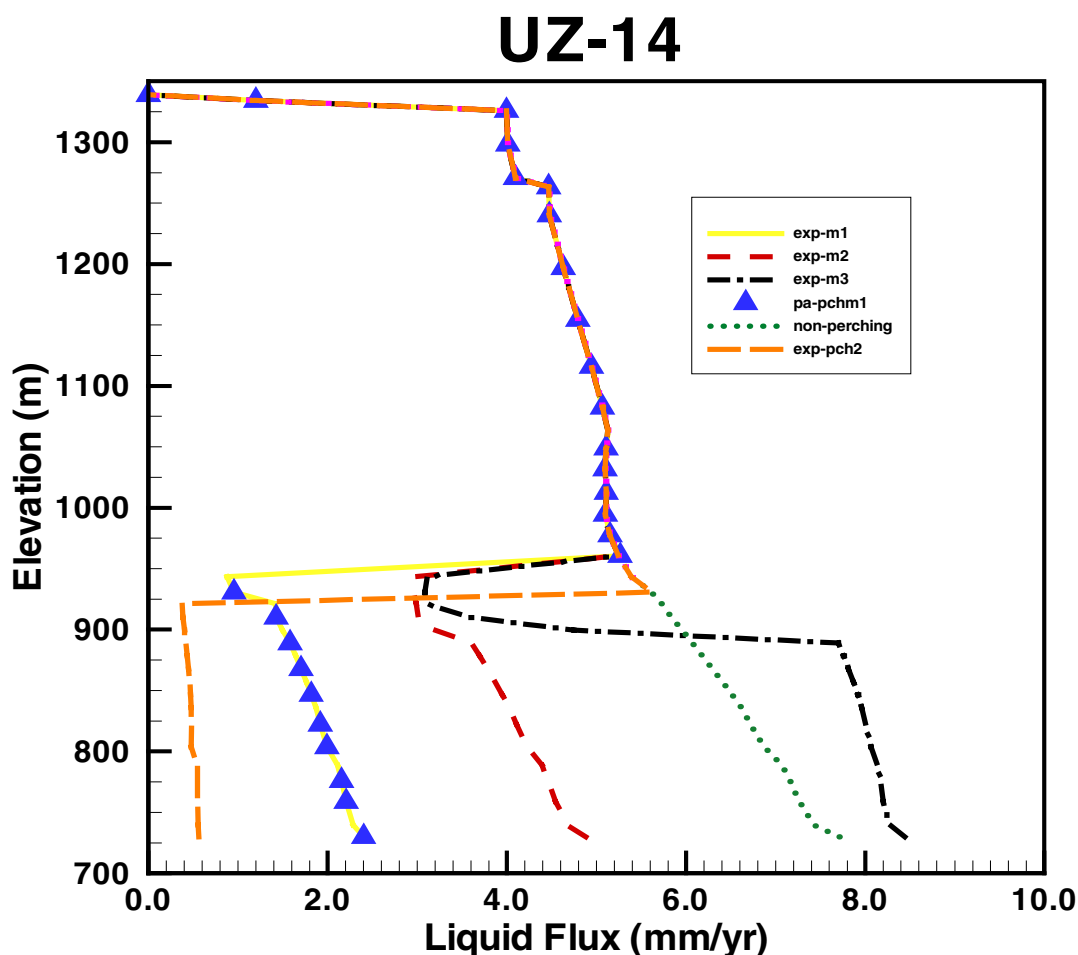
NOTE: See Table 6.5-5 for key to legend

DTN: LB0104AMRU0185.009, except for pa-pchm1 DTN: LB990801233129.003 [122757]
and non-perching DTN: LB990801233129.019 [144659]

Figure 6.5-25.   Comparisons Between Simulated Vertical Percolation Fluxes at the Location of USW UZ-14 Using Different Perched Water, CHn Vitric and Zeolitic Fracture Permeabilities

Effects on Tracer Transport Times: For each flow simulation, as listed in Table 6.5-5, two transport runs (in general) were carried out for conservative and reactive tracer transport, respectively. Tracer or radionuclide migration times since its release from the potential repository to the water table can be analyzed using a cumulative or fractional-mass curve. Figures 6.5-26 and 6.5-27 present the fractional-mass breakthrough curves for conservative and reactive tracers (i.e., nonsorbing and sorbing), respectively, using perched water Conceptual Model #1. Figure 6.5-28 shows the results for perched water Conceptual Model #2. In these figures, fractional mass breakthrough is defined as the cumulative mass of tracer or radionuclide arriving at the water table over the entire bottom of the model boundary at the time, normalized by the total initial mass at the potential repository.

Figure 6.5-26 shows that different CHn vitric and zeolitic fracture properties with perched water Conceptual Model #1 have a large impact only for early breakthrough (30% or less) of a conservative tracer (nonsorbing) tracer or radionuclide. For reactive tracer transport, effects of different perched CHn conceptual models under study seem insignificant (Figure 6.5-27). Under perched water Conceptual Model #2, Figure 6.5-28 shows that excluding fractures from the vitric CHn units has little impact on the early breakthrough times of both sorbing (up to 10,000 years) and nonsorbing (up to 1,000 years) tracer transport. Notable effects can be seen in the later times for both tracers, with the unfractured vitric model giving shorter travel times in both cases.
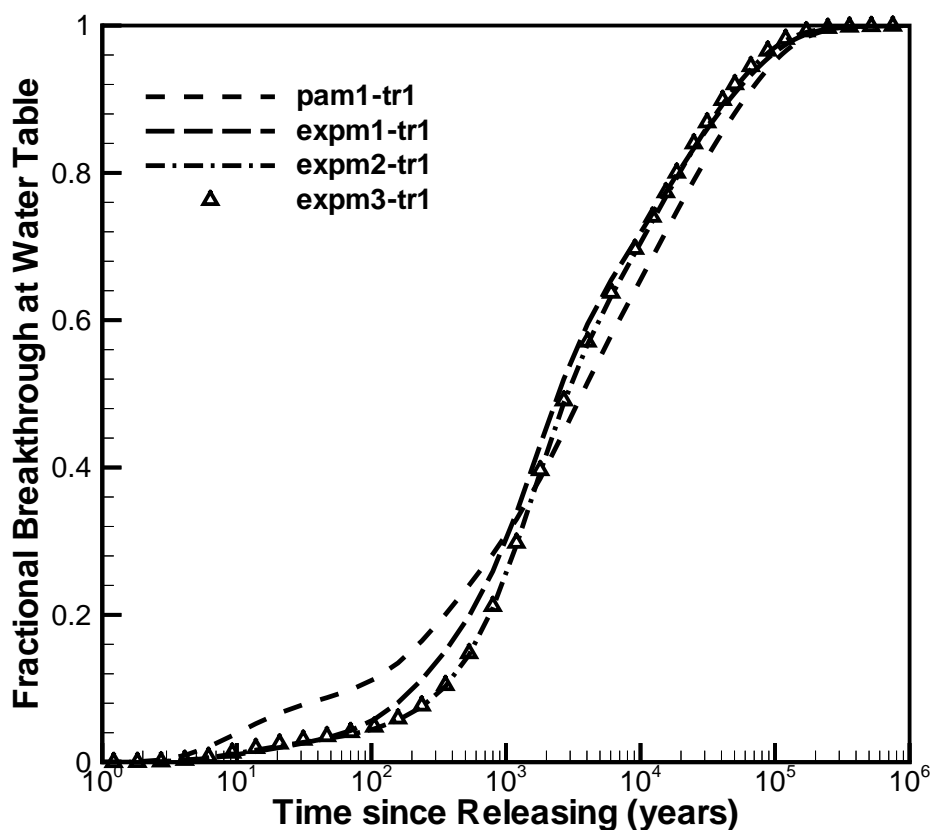
NOTE: See Table 6.5-5 for key to legend

DTN: LB0104AMRU0185.009, except for pam1-tr1 DTN: LB9908T1233129.001 [147115]

Figure 6.5-26.   Simulated Cumulative Breakthrough Curves of Conservative Tracer/Radionuclide Mass Arriving at the Water Table, Using Different CHn Vitric and Zeolitic Fracture Permeabilities with Perched Water Conceptual Model #1
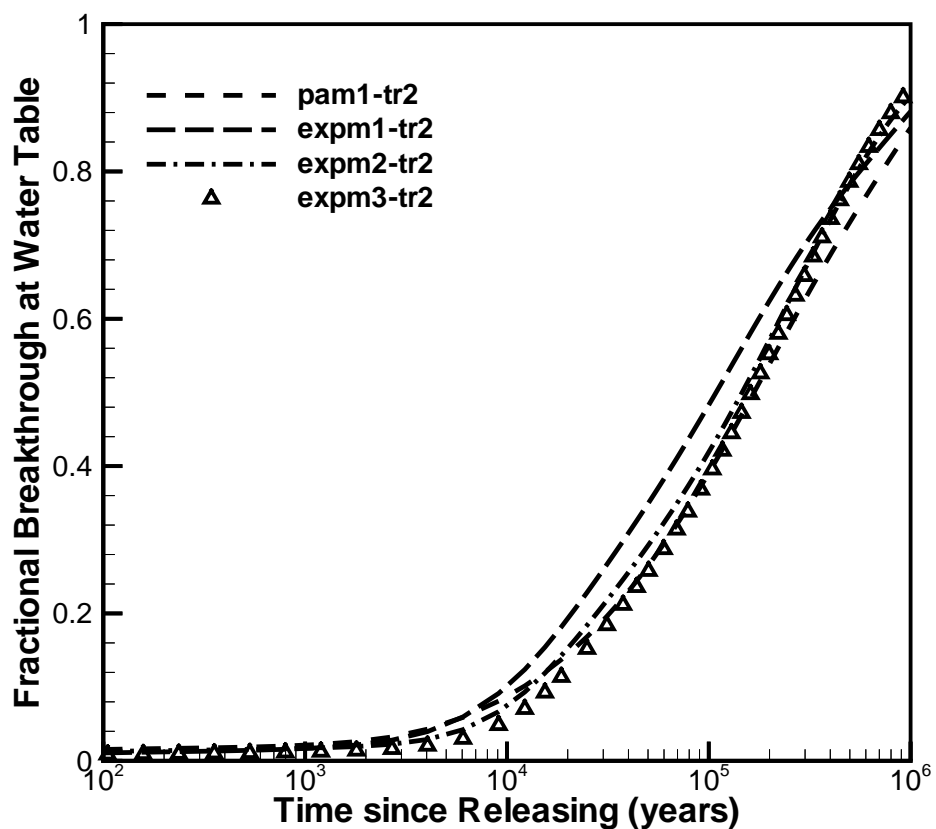
NOTE: See Table 6.5-5 for key to legend

DTN: LB0104AMRU0185.009, except for pam1-tr2 DTN: LB9908T1233129.001 [147115]

Figure 6.5-27.   Simulated Cumulative Breakthrough Curves of Reactive Tracer/Radionuclide Mass Arriving at the Water Table, Using Different CHn Vitric and Zeolitic Fracture Permeabilities with Perched Water Conceptual Model #1

NOTE: See Table 6.5-5 for key to legend

DTN: LB0104AMRU0185.009, except for pchm2-tr1 and pchm2-tr2 DTN: LB9908T1233129.001
[147115]

Figure 6.5-28.   Simulated Cumulative Breakthrough Curves of Conservative and Reactive
                     Tracer/Radionuclide Mass Arriving at the Water Table, Using Different CHn Vitric
                     Models with Perched Water Conceptual Model #2

For transport of a nonsorbing tracer, Figure 6.5-26 indicates that the original Conceptual Model #1 (pa_pchm1), which considers fracture effects in vitric zones, results in shortest early travel times due to the large lateral flow over perched water zones. By ignoring fracture flow in vitric zones, breakthrough (exp_m1) improves a little bit during early times. If more flow through the zeolites or an increase in contacts is allowed in order to increase vertical flowing water and matrix blocks for enhancing matrix diffusion and liquid dilution effects, the simulation results (exp_m2 and exp_m3) show a further improvement (slightly longer early travel times).

For transport of a sorbing tracer, Figure 6.5-27 displays very similar breakthrough behavior for the four flow fields with different CHn vitric and perched water conceptualizations of Conceptual Model #1, until 10,000 years after release from the potential repository. After that, breakthrough curves show some differences (by a factor of 2), with the more flow-through models (exp_m2 or exp_m3) predicting longest travel times.

6.5.3.3.2   Likely Scenarios

The existence of perched water bodies in the UZ of Yucca Mountain, as observed in the field investigations, should be considered in UZ flow modeling studies as well as in TSPA analyses. Different perched water conceptual models, as discussed in the previous section, may have significant impact on flow paths and lateral diversion in the CHn. In terms of affecting tracer/radionuclide transport, however, perched water conceptual models are found to have a large impact only for early breakthrough times of a conservative or nonsorbing tracer with Conceptual Model #1. These results should be taken into account when discussing the most likely scenario of perched water conceptual models.

Conceptual Model #1 (permeability-barrier model) in the UZ Flow Model (CRWMS M&O 2000 [122797]) could match observed perched water data, as well as moisture data. However, at the base of this model (without modification in fracture permeability in potential perching zeolites) are low-permeability layers of fracture and matrix in zeolitic zones, which are continuous on a 1,000 m scale without being intersected by vertical high permeability. This may not be very realistic, given the highly fractured nature of the tuffs of the basal vitrophyre as well in the CHn. At the site, extensive lateral flow along perched water and zeolitic zones, as predicted by this model, may not occur.

A more likely model of water perching is considered here to be the case of simulation scenarios exp_m2 or exp_m3, with schematic shown in Figure 6.5-17. Even though these two simulations are also based on perched water Conceptual Model #1 or the permeability-barrier concept, they allow for more vertical flow because of an increase in fracture permeability or connectivity crossing the potential water-perching zeolites. This addresses the fact that large-scale fractures and faults may cross certain portions of basal vitrophyre and/or zeolitic zones, and should be considered in conceptual models. In addition, these modified permeability-barrier conceptual models can also match the field observation data reasonably well, which supports the argument that they are the more likely scenarios.

Under ambient moisture conditions of the unsaturated zone of the mountain, recent radionuclide transport modeling studies (CRWMS M&O 2000 [122797]) identify that the two most important parameters impacting radionuclide transport are percolation fluxes and sorbing effects. In addition, matrix diffusion has also been found to have significant effects on nonsorbing tracer transport (CRWMS M&O 2000 [144331]). Therefore, a reliable transport model should incorporate the most representative matrix diffusion coefficients. Figure 6.5-29 presents a comparison of transport simulation results using two different matrix diffusion coefficients with the original and modified permeability-barrier conceptual models.
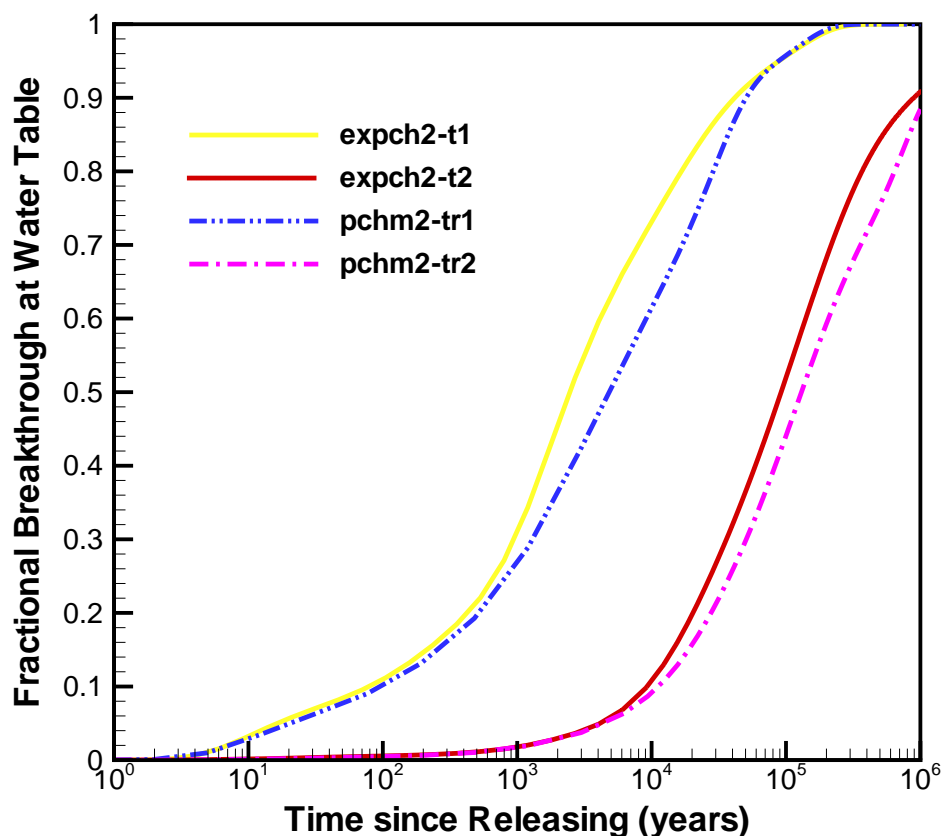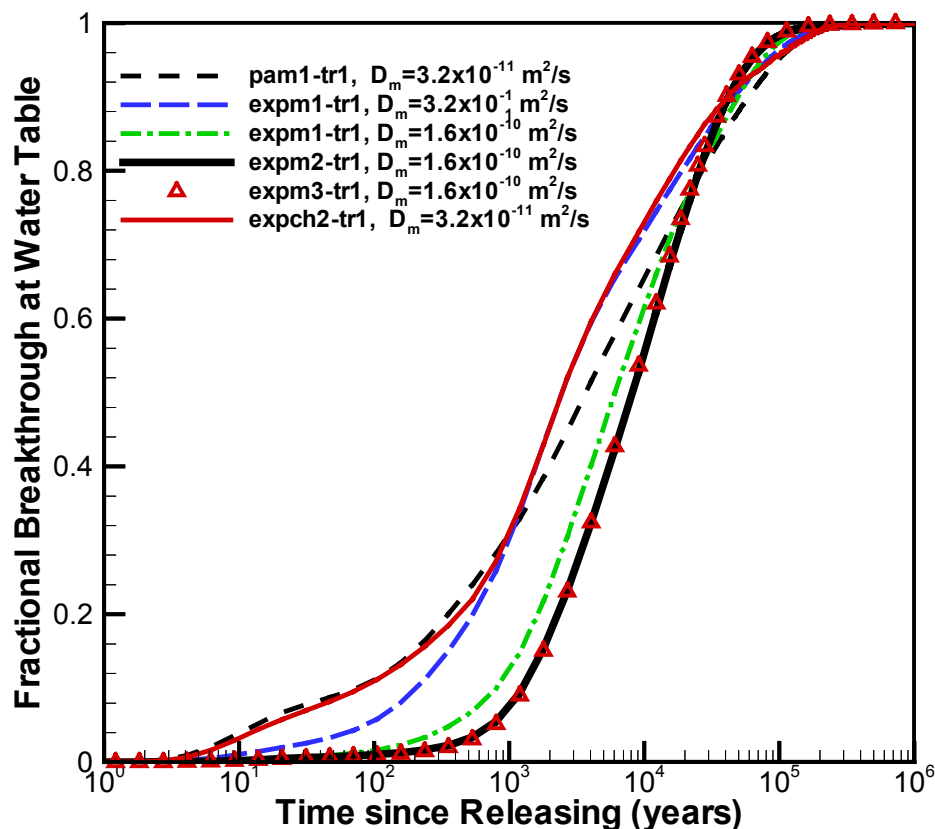
DTN: LB0104AMRU0185.009

Figure 6.5-29.   Comparison of Simulated Cumulative Breakthrough Curves of Conservative Tracer/Radionuclide Mass Arriving at the Water Table, Since Releasing from the Potential Repository, Using the Different Matrix Diffusion Coefficients and Perched Water Conceptual Models

In Figure 6.5-29, the first two simulations (pam1_tr1 and expm1_tr1) uses a molecular diffusion coefficient of $D_m = 3.2 \times 10^{-11}$ (m^2/s) for technetium. This value may not be very representative (in general) for a common nonsorbing tracer or radionuclide to diffuse in water phase. A value of $D_m = 1.6 \times 10^{-10}$ (m^2/s) is within a range of tritiated water diffusion coefficient ($D_m = 2.236 \times 10^{-9}$, m^2/s) (Mills 1973 [133392]), multiplied by a tortuosity of matrix porosity, as estimated in the AMR on ambient transport (CRWMS M&O 2000 [144331]). This modified effective molecular diffusion coefficient is also equivalent to the molecular coefficient measured for tritium (^{3}H) transport (DTN: LA000000000034.001 [148602]; BSC 2001 [154874]). Using this modified, more representative matrix diffusion coefficient, the last three simulations, using the same flow fields, show much longer travel times in cumulative breakthrough curves for non-sorbing tracer transport. The reduction in fractional breakthrough is more significant during early times up to 60% breakthrough. Note that there is little difference in the transport results among those three simulations whether the fracture permeability is increased by a factor of 10 or 100. Among the three transport simulations (exp_m1, exp_m2 and exp_m3) with unfractured vitric CHn zone

modifications, exp_m2 is considered in this study to be the most likely case for explaining perched water occurrence.

6.5.3.3.3 Testing to Reduce Uncertainty

Testing to discriminate between alternative different perched water conceptual models is currently difficult and costly. One economical way is to make use of the existing boreholes in which perched water is observed to conduct further tests. A disadvantage is that this may measure only the disturbed conditions of perched water. Nevertheless, multiborehole interference tests, such as air-permeability, tracer or pumping tests (conducted using the existing boreholes in the northern part of the model domain by measuring pressure responses at different layers/elevation of the CHn), may provide critical information regarding global connections of fractures/faults. Another potential testing program could be conducted to extend a tunnel from the ESF to the lower CHn in the northern part of the potential repository, near borehole USW UZ-14. Through this extension direct measurements of perched water under *in situ* conditions and of fracture connection data could be made.

6.5.4 Consideration of Radionuclide Release into Matrix Rock

This subsection presents a modeling assessment of effects of radionuclide release from drifts into the rock matrix on UZ transport. The objective of this study is to evaluate potential repository performance under the rock matrix release scenario, rather than fractures, with the present-day, mean infiltration rate using the expected flow and perched water models.

6.5.4.1 Model Description

Most analyses of UZ radionuclide transport consider that radionuclides be released directly into fractures below repository drifts (CRWMS M&O 2000 [122797]; CRWMS M&O 2000 [144331]). These release-to-fracture mechanisms assume that radionuclides, when leaking from canisters, would be carried mainly by dripping water, which would flow into high-permeability fractures below the drifts. Another reason for using this type of releasing is that such handling of radionuclide release results in more conservative estimates (i.e., shorter transport times) for TSPA calculations. There may be other radionuclide leak mechanisms from drifts, such as releasing to matrix tuffs, that need to be considered. The argument supporting this release-to-matrix scenario assumes that rock blocks directly below drifts may be very "dry" (with much lower liquid saturation than surrounding rocks) because capillary effects along drift tunnel walls may divert or bypass significant amounts of percolating water from the area below drifts. Therefore, once dropping water, carrying radionuclides within drifts, falls on the rock, it will be immediately sucked into matrix rocks by the strong capillary forces of the dry matrix.

This modeling study of radionuclide release directly to the matrix, and its effects on repository performance is based on the UZ Flow Model (CRWMS M&O 2000 [122797]) for unsaturated flow fields. Specifically, the current model is built on the more likely flow scenarios, as discussed in Section 6.5.3, in which fractures within the vitric portion of the CHn units are excluded. The flow fields used in transport modeling are exp_m1 and exp_m2 (see Table 6.5-5), i.e., using the UZ 3-D TSPA grid and Conceptual Model #1 with modifications to fracture properties of the vitric zones and zeolites associated with perched water bodies (DTN:

LB0104AMRU0185.009). Radionuclides are handled as conservative (nonsorbing) or reactive (sorbing) tracers released from repository matrix blocks, with uniform initial concentrations, and transported by advection and diffusion processes, under ambient percolation, at the present-day infiltration rate. Transport is simulated using T2R3D V1.4 (LBNL 1999 [113942]). Studies are further documented in Bodvarsson (2001 [156334], YMP-LBNL-YSW-4, pp. 21–24).

6.5.4.2 Results and Analyses

The 3-D transport modeling results are in part summarized in Figure 6.5-30. For transport of a nonsorbing or conservative tracer, Figure 6.5-30 compares breakthrough curves for radionuclides at the water table, released from repository matrix blocks (M-Release) and fracture blocks (F-Release), using two flow fields and different molecular diffusion coefficients. Figure 6.5-30 shows that for low molecular diffusion ($D_m = 3.2 \times 10^{-11}$ m^2/s), significantly longer (one order of magnitude) transport times are obtained when radionuclides are released to (or from) matrix blocks rather than fractures. However, for higher values of diffusion coefficients (i.e., $D_m = 1.6 \times 10^{-10}$ m^2/s) increase in transport times by matrix release is relatively small, but travel times still increase by a factor of 2. This indicates that the main transport mechanism for radionuclides from the repository within the TSw unit is the advection by fracture flow. As matrix diffusion coefficients increase, more radionuclides diffuse from matrix into flowing water in fractures, resulting in more rapid downwards migration.

In addition, Figure 6.5-30 shows very small differences made by the two flow fields, exp_m1 and exp_m2, on release-to-matrix transport results. In either case, radionuclide transport times increase by the matrix release mechanism rather than fracture release. Additional modeling studies with sorbing tracer (^{237}Np) show little difference in UZ transport times between matrix and fracture radionuclide release, because the retardation or sorbing effect is a more dominant factor in this case.

- Flow/exp-m1, F-Release, $D_m = 3.2 \times 10^{-11}$ m^2/s
- Flow/exp-m2, F-Release, $D_m = 1.6 \times 10^{-10}$ m^2/s
- Flow/exp-m2, M-Release, $D_m = 3.2 \times 10^{-11}$ m^2/s
- Flow/exp-m2, M-Release, $D_m = 1.6 \times 10^{-10}$ m^2/s
- Flow/exp-m1, M-Release, $D_m = 3.2 \times 10^{-11}$, m^2/s
- Flow/exp-m1, M-Release, $D_m = 1.6 \times 10^{-10}$ m^2/s

Y-axis: **Fractional Breakthrough at Water Table**

X-axis: **Time since Releasing (years)**
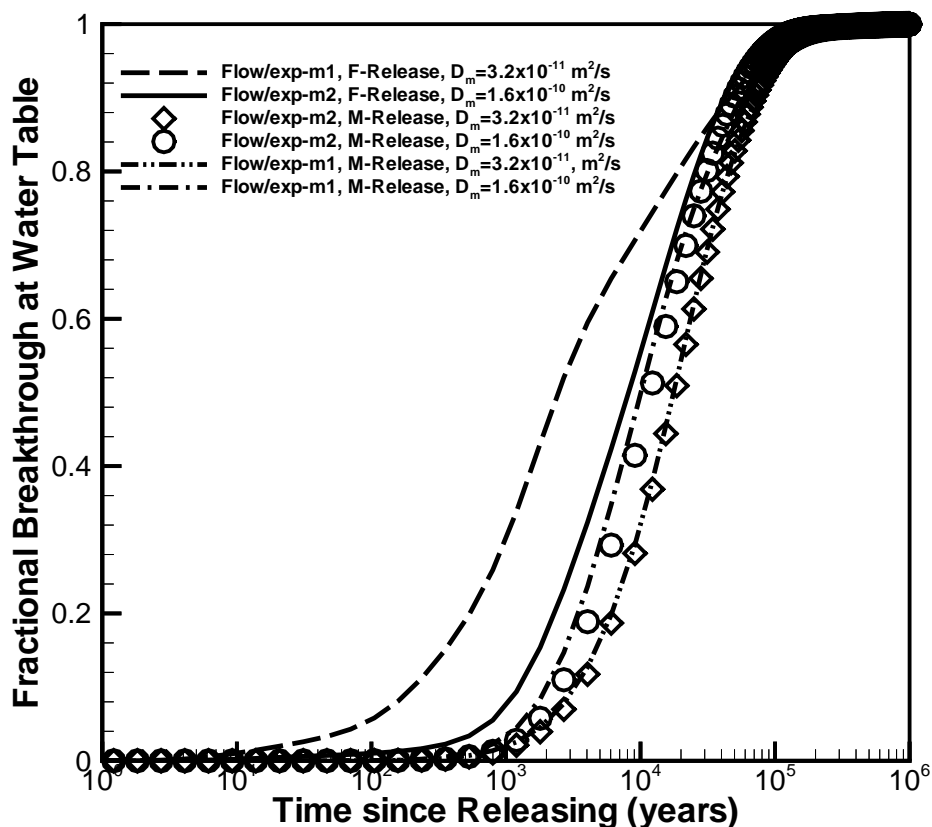
DTNs: LB0104AMRU0185.009, LB0104AMRU0185.010

Figure 6.5-30.   Comparisons Between Simulated Cumulative Breakthrough Curves of Conservative Tracer/Radionuclide Mass Arriving at the Water Table, Using Different CHn Vitric and Zeolitic Fracture Permeabilities with Perched Water Conceptual Model #1

6.5.4.3   Testing to Reduce Uncertainty

Whether radionuclides are released to matrix or to fracture rocks at repository drifts depends critically on the moisture condition of the tuffs immediately below the drifts. On the time scale of thousands of years, efforts to test or estimate long-term moisture conditions near drifts may prove to be difficult. However, observation could be feasible on a smaller time scale, such as 10 to 100 years, using existing tunnels at Yucca Mountain. This may provide certain valuable corroborative evidence regarding a "dry" condition existing below a horizontal tunnel or large cave. In addition, tracer tests may be conducted using the ESF or ECRB to investigate tracer distribution and partition between matrix and fractures in rocks below the tunnels.

7. SUMMARY AND CONCLUSIONS

7.1 CONCLUSIONS AND RECOMMENDATIONS FOR UNSATURATED ZONE FLOW PATTERNS AND ANALYSIS

The analyses and models presented here are in general supplemental to analyses and models reported in previous AMRs. The purpose of this supplemental work is to better characterize the nature and degree of conservatism that was incorporated into the previous work because of uncertainty in processes and properties and because of simplifications of processes and properties necessary for analysis and modeling. The supplemental work documented here has focused on several areas key to UZ flow and transport: synthesis of available geochemical data in order to allow better and more widespread use of this important data type, transport modeling methods intended to improve matrix diffusion characterization, improved characterization of several processes affecting seepage into waste emplacement drifts, and improved characterization and broadened uncertainty studies of flow and transport from the repository horizon to the water table. Except for the model results reported in Section 6.4.2, the investigations documented in this AMR are scoping studies to aid in determining whether work beyond the scope of the models and analyses used to support TSPA-SR (CRWMS M&O 2000 [153246]) is warranted and do not support TSPA as documented in either *FY01 Supplemental Science and Performance Analyses, Volume 2: Performance Analyses* (BSC 2001 [154659]) or *Total System Performance Assessment for the Site Recommendation* (CRWMS M&O 2000 [153246]). The model results reported in Section 6.4.2 are used for TSPA sensitivity studies as documented in *FY01 Supplemental Science and Performance Analyses, Volume 2: Performance Analyses* (BSC 2001 [154659], Section 3.2.2.3) Conclusions and recommendations specific to each study are reported below.

7.2 CONCLUSIONS AND RECOMMENDATIONS REGARDING SYNTHESIS OF GEOCHEMICAL INFORMATION

Section 6.2 presents a synthesis of available geochemical information from Yucca Mountain that support the conceptual models for the UZ Flow and Transport Model. The following conclusions can be drawn from these data:

1. Vertical trends of ion concentrations (chloride, sulfate, sodium) in the different hydrogeologic units suggest at least some component of lateral flow within the nonwelded units. The increase in pore-water $^{87}Sr/^{86}Sr$ in the PTn tuff suggests enhanced water-rock interaction. The shift in dominance from divalent to monovalent cations reflects the ion-exchange reactions with zeolites in the CHn unit. Busted Butte tests show that vitric CHn exhibits strong capillary forces and matrix-dominated flow and tracer transport. Chloride concentrations in pore water support low infiltration (avg. ~6 mm/yr) with small, deep percolation (0.6–3.3 mm/yr).

2. ^{14}C activities in PTn and CHn pore waters suggest that their apparent ages range from modern to 5,200 years. Perched water analysis has yielded dates ranging from 3,500–11,000 years (from ^{14}C data) and from 2,000–12,000 years (from $^{36}Cl/Cl$ data).

3. Bomb-pulse ^{36}Cl and ^{3}H indicate faults/fracture zones can serve as fast flow pathways. However, the bulk of water moves much more slowly through the matrix. Lack of bomb-pulse tracers in perched water suggests no more than a small component of fast-flow water intersects the perched zones.

4. Due to the constraints of the geochemical studies, available geochemical evidence neither directly supports nor disproves the significant contribution of matrix diffusion in the UZ. Tests are suggested to evaluate matrix diffusion conceptual models for the UZ Flow and Transport Model.

7.3 CONCLUSIONS AND RECOMMENDATIONS FOR TRANSPORT COMPUTATION METHODS

Previously used transport methods and codes are reviewed and scoping studies of two methods for transport simulation with improved matrix diffusion characterization are conducted. Specific conclusions are reported below.

7.3.1 Conclusions and Recommendations Regarding Different Transport Computation Methods

For transport in fractured porous media with water flow occurring in both continua, T2R3D V1.4 (LBNL 1999 [113942]) (with a dual continuum grid) or DCPT V1.0 (LBNL 1999 [132448]) software codes may be a conservative predictor of radionuclide breakthrough at the Yucca Mountain water table, especially at early times. By using a residence time/transfer function approach based on analytical solutions for a simpler system, the FEHM V2.0 particle tracking algorithm does not have the discretization problem associated with large matrix blocks in a dual continuum grid (CRWMS M&O 2000 [141418]). But it can be either a conservative or an optimistic predictor compared with T2R3D V1.4 (LBNL 1999 [113942]) or DCPT V1.0 (LBNL 1999 [132448]), depending on the particular case or portion of the breakthrough because of the uncertainties introduced in the implementing the fracture-matrix diffusion processes. In site-scale transport simulations (CRWMS M&O 2000 [134732], Section 6.2.5), FEHM V2.0 (CRWMS M&O 2000 [141418]) is found to be generally conservative relative to DCPT V1.0 (LBNL 1999 [132448]). However, the implementation of the fracture-matrix diffusion processes for problems with water flow in both continua is complicated. By using a new method for calculating fracture-matrix particle transfer probability, DCPT V2.0 (LBNL 2001 [154342]) has neither the apparent inaccuracies associated with larger matrix blocks in a dual-permeability grid that T2R3D V1.4 (LBNL 1999 [113942]) and DCPT V1.0 (LBNL 1999 [132448]) have, nor does it have the uncertainties of FEHM V2.0 (CRWMS M&O 2000 [141418]).

Of the codes evaluated, DCPT V2.0 (LBNL 2001 [154342]) appears to be the most suitable simulator for such a system, considering numerical accuracy, efficiency issues, and the current understanding of transport processes in fractured porous media. T2R3D V1.4 (LBNL 1999 [113942]) with a MINC grid can be an alternative, but with the associated cost of poorer numerical efficiency and more complicated validation requirements.

In order to fully evaluate which code best reproduces transport at Yucca Mountain, well-controlled experiments of transport in unsaturated, fractured porous rock will be necessary to

verify the numerical models used and to deepen the understanding of the fracture-matrix mass transfer process. No analytical solution has ever been developed in the literature for transport in the unsaturated fractured porous media with global water flow occurring in both continua; neither have any such experiments been performed. An example of a well-controlled experiment could be a lab experiment using tracer with a large-enough block (1 m^3) of the fractured rock. This experiment is important for building an accurate numerical model because many aspects of the fracture-matrix interaction process are still unknown. Many numerical experiments show that fracture-matrix mass transfer is a critical process that controls how fast nuclides migrate to the water table.

Development of the numerical models of flow and transport with higher spatial resolution is another necessary task to reduce the uncertainty of predictions. The current numerical models use rather coarse grids (vertically up to 60 m and laterally up to 200 m) because of limitations on computational resources. T2R3D and FEHM will suffer numerical mixing due to the coarser grids, while DCPT will suffer inaccurate interpolation of the pore velocity field. Furthermore, a coarse grid is expected to allow TOUGH2 to underestimate the capillary effects in the case where the critical layers are thin, which will lead to very different flow fields and transport pathways for nuclides. In such a complex and heterogeneous media as the UZ of Yucca Mountain, the effects on the travel time of the nuclides could be very large. Calculation of detailed flow fields for the UZ requires parallelization of the TOUGH2. Considerable efforts are also required to develop particle trackers that can simulate transport with large grids very efficiently.

7.3.2 Conclusions and Recommendations Regarding Matrix Block Discretization and Its Effects on UZ Flow and Transport Simulations

In Section 6.3.2, flow and transport simulations made using two-dimensional DKM and MINC grids are compared. The grids are a model of an east-west cross section in the northern, zeolitic portion of Yucca Mountain. The MINC simulation results show that under steady-state flow conditions all the matrix continua within a given gridblock have almost the identical water saturations and potentials, indicating that the matrix can be treated as a single continuum. In other words, the dual-permeability concept is valid for modeling steady-state flow processes in the unsaturated zone of Yucca Mountain.

Comparisons between simulation results indicate that the current dual-permeability approach may overestimate fracture fluxes in some units, because a too-large connection distance is used between the fracture and matrix gridblocks. This is consistent with the noted discrepancy between the previously simulated fracture fluxes in the vitric Calico Hill formation and those implied from the tracer test results at the Busted Butte site. It is recommended to use a reduced connection distance in generating DKM grids for future flow simulations. The determination of this reduced distance needs further investigation.

Simulation results demonstrate the significance effects of matrix diffusion and accurate representation of the concentration gradient near fracture-matrix interfaces on the overall radionuclide transport processes in the unsaturated zone of Yucca Mountain. Because the DKM underestimates matrix diffusion at early time, it is very likely that this model provides conservative estimates of the breakthrough time for radionuclide transport from the potential

repository to the water table. This issue can be resolved in future site-scale flow and transport simulations using one of the following three approaches.

- The most reliable approach is to directly use MINC for both flow and transport in the site-scale UZ model. This approach is computationally intensive.

- The second approach is to take advantage of the finding that the DKM is valid for modeling steady-state flow processes as long as a reduced connection distance is used. In this case, flow fields are simulated with the DKM and then mapped into a MINC grid. The transport is simulated using the MINC grid and the computationally efficient T2R3D V1.4 (LBNL 1999 [113942]) which only solves the solute transport equation.

- The third approach is to improve the current particle trackers such that they could handle sharp concentration gradients for a DKM grid and the corresponding flow fields. A detailed discussion of the current particle trackers and their capabilities is given in Section 6.3.1.

7.4 CONCLUSIONS AND RECOMMENDATIONS FOR PROCESSES AFFECTING SEEPAGE

Conclusions about how improved characterization of the key factors of drift degradation and percolation affect seepage into waste emplacement drifts are documented below.

7.4.1 Conclusions and Recommendations for Seepage Enhancement due to Drift Degradation

Conclusions about how two aspects of drift degradation, rock fall and rock bolts, affect seepage are reported below.

7.4.1.1 Conclusions and Recommendations Regarding Seepage Enhancement due to Rockfall

Four rockfall scenarios were selected, for which seepage calculations were conducted. Results in this section are based on seepage calibration model results and a review of available *in situ* field results appropriate to the Tptpmn lithostratigraphic unit and one set of data for the Tptpll unit. Seepage enhancement resulting from rockfall is estimated to be between 0 and 5 percent. As more data from these units (where the potential repository resides) are obtained in field measurements, parameter values, with their uncertainties and probability weightings, should be developed and then seepage predictions from tables in this section can be used to obtain the best estimates (with uncertainty ranges) for Yucca Mountain. These scoping calculations confirm that the approach used for seepage enhancement due to drift degradation in TSPA-SR (CRWMS M&O 2000 [153246]) is conservative.

In summary, this section identifies that rockfall scenarios could have an effect on seepage into the drift. Seepage enhancement due to rockfall is given in DTN: LB0104AMRU0185.011.

7.4.1.2 Conclusions and Recommendations Regarding the Effect of Rock Bolts on Seepage

The potential for seepage enhancement due to rock bolts is investigated using a two-dimensional, radial model of a spherical opening with a rock bolt at the crown. A large number of model parameter combinations are investigated by varying the percolation rate, the formation capillarity, and the capillarity and permeability of the grout material surrounding the rock bolt and by using several models representing varying degrees of connectivity between the rock-bolt hole and the surrounding fractured rock near the opening. The conclusion of this investigation of the potential for seepage enhancement caused by rock bolts is that there is no significant enhancement of seepage. These scoping calculations confirm that the approach used for seepage enhancement due to drift degradation in TSPA-SR (CRWMS M&O 2000 [153246]) is conservative.

7.4.2 Conclusions and Recommendations Regarding Focusing and Discrete Flow Paths in the TSw

A series of numerical studies have been conducted to evaluate flow focusing through fractures from the bottom of the PTn to the potential repository horizon. The studies were carried out using a 100 m wide and 150 m deep 2-D flow domain and covered the upper five different hydrogeologic units of the TSw at Yucca Mountain. Mean fracture parameters used in the simulations were those developed in the *Calibrated Properties Model* AMR (CRWMS M&O 2000 [144426]) as described in Section 6.4.2.2. The heterogeneous fracture permeability distributions were generated using a stochastic approach. The studies considered various percolation fluxes, correlation lengths, and uniform and nonuniform percolation-flux boundary conditions. The results obtained provide a quantitative analysis of flow focusing and discrete path formation. All simulation results indicate that the flow-focusing factor is about an order of magnitude smaller than the conservative value used for TSPA-SR (CRWMS M&O 2000 [153246]) calculations. The frequency distributions of normalized flux are insensitive to magnitudes and spatial distributions of infiltration fluxes on the upper boundary, and to spatial correlation structures of the permeability fields within the UZ domains. The results of this model are used to support sensitivity studies for TSPA-SR (BSC 2001 [154659], Section 3.2.2.3). Flow focusing distributions are given in DTN: LB0104AMRU0185.012.

7.4.3. Conclusions and Recommendations Regarding Percolation Redistribution and Lateral Flow in the PTn

Percolation flux affects both waste canister performance and solute travel times to the accessible environment. Percolation distribution strongly depends on the infiltration rates and their spatial and temporal distributions. The present-day mean infiltration in the Yucca Mountain flow and transport models was calibrated and the percolation distribution was analyzed using pore-water Cl concentration data. The surface infiltration area was divided into regions according to the availability and range of Cl data, the range of present-day mean infiltration data, and the hydrostructural and the hydrogeologic features. Infiltration rates in each region were calculated based on the pore-water Cl concentration data and the Cl infiltration flux. Model results of three-dimensional simulation using the calibrated infiltration map match the Cl data better compared with using uncalibrated infiltration map.

PTn lateral flow effects on percolation and Cl distribution were studied by 3-D simulation with increased horizontal permeability. The degree of the effect varies by location. As expected, a more uniform Cl distribution under PTn was observed in most places when lateral flow effects increased. Further calibration can be done by adjusting layer heterogeneity and anisotropic permeability in different regions based on the hydrostructural features, percolation fluxes, and the distribution of geochemical data.

This scoping study suggests that several approaches may be used to obtain UZ model results consistent with chloride data.

7.4.4 Conclusions and Recommendations Regarding the Effect of Episodic Percolation on Seepage

A two-dimensional, fracture-only model is used to conduct a scoping study to investigate the significance of episodic percolation at the repository level due to transient infiltration on the western slope of Yucca Mountain above the Solitario Canyon fault where the TSw outcrops. Transient infiltration events are simulated by applying all of the annual infiltration for the highest rate infiltration model over a one week period. The results of this model confirm the abstraction approach for TSPA-SR that does not include episodic percolation as a seepage enhancing factor (CRWMS M&O 2001 [154291], Section 6.4.4; BSC 2001 [154659], Section 3.2.2.4).

7.5 CONCLUSIONS AND RECOMMENDATIONS FOR PROCESSES AFFECTING UNSATURATED ZONE FLOW AND TRANSPORT BELOW THE REPOSITORY HORIZON

Conclusions reached using scoping studies for improved characterization of flow and transport between the repository and the water table are presented below. None of the results of studies documented in Section 6.5 are used for TSPA.

7.5.1 Conclusions and Recommendations Regarding Fracture Flow in the Vitric Calico Hills Formation

This section presents the incorporation of newly available data on the vitric CHn into the UZ Flow and Transport Model. The data, from the Busted Butte test site, suggest higher matrix permeability and lower matrix capillarity than the previously used data indicate. Further, tests at Busted Butte suggest that unsaturated flow and transport in the vitric CHn is completely matrix dominated. A new conceptual model in which fractures are not present in the vitric CHn is used, and new model parameters for these layers are estimated based prior information about the layer properties updated with the Busted Butte data. These new model parameters are given in DTN: LB0103CHVUPROP.001. Mountain-scale, three-dimensional simulations using this updated model show lower percolation fluxes at the water table directly under the vitric portion of the CHn and longer initial-breakthrough times for contaminants from the repository horizon at the water table. Direct validation of this model of the vitric CHn (with no fractures) is not possible because there are no relevant data against which to compare model predictions. However, the use of calibration, review of the estimated parameters for reasonableness, and technical review of the calibration approach through open literature as well as consistency with the Busted Butte test results make the model valid for its intended use of presenting an alternative model for flow and

transport through the vitric CHn. At this time, further development of alternative models is not warranted. Rather, more data on flow and transport through the layers between the bottom of the TSw and the water table is needed in order to discriminate between alternative models and allow development of a single robust model.

7.5.2   Conclusions and Recommendations Regarding Fault Characteristics

The role of major faults in the vicinity of the potential repository area in flow and transport processes within the UZ is uncertain given the absence of information about fault hydrological properties below the Topopah Spring Tuff. Sensitivity of modeled flow and transport behavior to changes in certain key hydrological parameters assigned to major faults below the potential repository horizon has therefore been evaluated. Results of this study indicate that changes in fracture permeability within the fault zones (increased and decreased by two orders of magnitude) and van Genuchten parameter α for both fractures and matrix within the fault zones (increased and decreased by one order of magnitude) have little impact on tracer transport from the potential repository horizon to the water table. Of the total cumulative tracer fluxes through the water table, about 15% go through the Drill Hole Wash fault, followed by Sundance and Ghost Dance faults, which combined contribute about 5%. The total tracer fluxes through faults are about 20% and the case with higher capillary pressure gives about 3% higher tracer fluxes.

It is therefore concluded that, with the current infiltration rate and conceptualization of fault zones and perched water, flow and transport between the potential repository horizon and the water table is not sensitive to these fault-zone parameters. The analysis conducted here used only one infiltration scenario with flow-through perched-water model. To explore all the uncertainties in the CHn/CFu flow and transport behavior, further studies need to be performed considering the combined factors of fractured or unfractured vitric CHn, permeable or impermeable faults, and flow-through or lateral-flow perched-water model. What may be more important is the percolation flux occurring within major fault zones, which is affected by infiltration rates and potential flow focusing within faults.

7.5.3   Conclusions and Recommendations Regarding Perched Water Models

Several perched water conceptual models have been examined and compared for their impact on the potential repository performance. Results from the 3-D UZ flow model indicate that, compared to the dominant processes of percolation fluxes or sorbing effects on rocks, which strongly affect flow and transport, perched water conceptual models have smaller effects on tracer or radionuclide transport from the potential repository to the water table. Perched water models were found to have a large impact on cumulative mass breakthrough curves of a tracer at the water only during the early period for a nonsorbing tracer (<30% breakthrough) with Conceptual Model #1. For late transport times (>30% breakthrough) of a non-sorbing tracer as well as the entire transport period for a sorbing tracer, different perched water conceptual models have only relatively small overall effects.

A more likely scenario for perched water occurrence has been discussed. This model matches the observed perched water and chloride data and at the same time allows significant vertical flow through perched water and low permeability zeolitic zones. In addition, matrix diffusion is found to have large impact on non-sorbing tracer transport and should be included in developing the

most reliable model scenario in estimating the groundwater travel or radionuclide transport times.

7.5.4 Conclusions and Recommendations Regarding Consideration of Direct Radionuclide Release into Matrix Rock

Modeling studies on radionuclide release into matrix rocks rather than fractures below repository drifts indicate that this type of release may have significant impact on the potential repository performance. In general, release-to-matrix mechanism or transport started from repository matrix blocks will increase radionuclide transport times in the UZ. The smaller the molecular diffusion coefficients are, the longer travel times will be for radionuclides released into matrix rocks under the currently predicted ambient percolation.

8. INPUTS AND REFERENCES

The following is a list of the references cited in this document. Column 1 represents the unique six digit numerical identifier, which is placed in the text following the reference callout (e.g., BSC 2001 [155051]). The purpose of these numbers is to assist the reader in locating a specific reference. Within the reference list, multiple sources by the same author (e.g., BSC 2001) are sorted alphabetically by title.

8.1   CITED DOCUMENTS

155853   Ahlers, R. 2000. Unsaturated Zone Modeling & Synthesis.   Scientific Notebook YMP-LBNL-GSB-1.1.2. ACC: MOL.20000726.0157.

154430   Archie, G.E. 1942. "The Electrical Resistivity Log as an Aid in Determining Some Reservoir Characteristics." *Petroleum Development and Technology, Transactions of American Institute of Mining and Metallurgical Engineers, Volume 146,* 54-62. New York, New York: American Institute of Mining and Metallurgical Engineers. TIC: 249687.

101379   Bear, J. 1988. *Dynamics of Fluids in Porous Media.* New York, New York: Dover Publications. TIC: 217568.

105170   Birkholzer, J.; Li, G.; Tsang, C-F.; and Tsang, Y. 1999. "Modeling Studies and Analysis of Seepage into Drifts at Yucca Mountain." *Journal of Contaminant Hydrology, 38*, (1-3), 349-384. New York, New York: Elsevier. TIC: 244160.

156334   Bodvarsson, G.S. 2001. "Scientific Notebooks Referenced in AMR U0185, Unsaturated Zone Flow Patterns and Analysis, DI: MDL-NBS-HS-000012 REV00." Interoffice correspondence from G.S. Bodvarsson (BSC) to File, October 12, 2001, with attachments. URN-0952

154874   BSC (Bechtel SAIC Company) 2001. *Analysis of Geochemical Data for the Unsaturated Zone.* ANL-NBS-HS-000017 REV 00 ICN 01. Las Vegas, Nevada: Bechtel SAIC Company. ACC: MOL.20010405.0013.

155950   BSC (Bechtel SAIC Company) 2001. *FY 01 Supplemental Science and Performance Analyses, Volume 1: Scientific Bases and Analyses.* TDR-MGR-MD-000007 REV 00 ICN 01. Las Vegas, Nevada: Bechtel SAIC Company. ACC: MOL.20010801.0404.

154659   BSC (Bechtel SAIC Company) 2001. *FY01 Supplemental Science and Performance Analyses, Volume 2: Performance Analyses.* TDR-MGR-PA-000001 REV 00. Las Vegas, Nevada: Bechtel SAIC Company. ACC: MOL.20010724.0110.

154622   BSC (Bechtel SAIC Company) 2001. *Geologic Framework Model Analysis Model Report.* MDL-NBS-GS-000002 REV 00 ICN 02. Las Vegas, Nevada: Bechtel SAIC Company. ACC: MOL.20010313.0505.

155187　　BSC (Bechtel SAIC Company) 2001. *Ground Control for Emplacement Drifts for SR*. ANL-EBS-GE-000002 REV 00 ICN 01. Las Vegas, Nevada: Bechtel SAIC Company. ACC: MOL.20010627.0028.

155667　　BSC (Bechtel SAIC Company) 2001. *Longevity of Emplacement Drift Ground Support Materials*. ANL-EBS-GE-000003 REV 01 ICN 01. Las Vegas, Nevada: Bechtel SAIC Company. ACC: MOL.20010613.0246.

155051　　BSC (Bechtel SAIC Company) 2001. *Technical Work Plan for Unsaturated Zone (UZ) Flow and Transport Process Model Report*. TWP-NBS-HS-000001 REV 01. Las Vegas, Nevada: Bechtel SAIC Company. ACC: MOL.20010404.0007.

101582　　Conca, J.L. and Wright, J. 1990. "Diffusion Coefficients in Gravel Under Unsaturated Conditions." *Water Resources Research, 26*, (5), 1055-1066. Washington, D.C.: American Geophysical Union. TIC: 237421.

104878　　CRWMS M&O (Civilian Radioactive Waste Management System Management and Operating Contractor) 1998. *Evaluation of Flow and Transport Models of Yucca Mountain, Based on Chlorine-36 and Chloride Studies for FY98*. BA0000000-01717-5700-00007 REV 00. Las Vegas, Nevada: CRWMS M&O. ACC: MOL.19981208.0119.

141389　　CRWMS M&O 2000. *Analysis Comparing Advective-Dispersive Transport Solution to Particle Tracking*. ANL-NBS-HS-000001 REV 00. Las Vegas, Nevada: CRWMS M&O. ACC: MOL.19990721.0518.

134732　　CRWMS M&O 2000. *Analysis of Base-Case Particle Tracking Results of the Base-Case Flow Fields (ID: U0160)*. ANL-NBS-HS-000024 REV 00. Las Vegas, Nevada: CRWMS M&O. ACC: MOL.20000207.0690.

145771　　CRWMS M&O 2000. *Analysis of Hydrologic Properties Data*. ANL-NBS-HS-000002 REV 00. Las Vegas, Nevada: CRWMS M&O. ACC: MOL.19990721.0519.

154123　　CRWMS M&O 2000. *Busted Butte Sample Lithology*. Input Transmittal 00337.T. Las Vegas, Nevada: CRWMS M&O. ACC: MOL.20000911.0285.

144426　　CRWMS M&O 2000. *Calibrated Properties Model*. MDL-NBS-HS-000003 REV 00. Las Vegas, Nevada: CRWMS M&O. ACC: MOL.19990721.0520.

141187　　CRWMS M&O 2000. *Conceptual and Numerical Models for UZ Flow and Transport*. MDL-NBS-HS-000005 REV 00. Las Vegas, Nevada: CRWMS M&O. ACC: MOL.19990721.0526.

114277　　CRWMS M&O 2000. *Development of Numerical Grids for UZ Flow and Transport Modeling*. ANL-NBS-HS-000015 REV 00. Las Vegas, Nevada: CRWMS M&O. ACC: MOL.19990721.0517.

151635   CRWMS M&O 2000. *Drift Degradation Analysis*. ANL-EBS-MD-000027 REV 01. Las Vegas, Nevada: CRWMS M&O. ACC: MOL.20001206.0006.

141400   CRWMS M&O 2000. *In Situ Field Testing of Processes*. ANL-NBS-HS-000005 REV 00. Las Vegas, Nevada: CRWMS M&O. ACC: MOL.20000504.0304.

141418   CRWMS M&O 2000. *Particle Tracking Model and Abstraction of Transport Processes*. ANL-NBS-HS-000026 REV 00. Las Vegas, Nevada: CRWMS M&O. ACC: MOL.20000502.0237.

144331   CRWMS M&O 2000. *Radionuclide Transport Models Under Ambient Conditions*. MDL-NBS-HS-000008 REV 00. Las Vegas, Nevada: CRWMS M&O. ACC: MOL.19990721.0529.

153314   CRWMS M&O 2000. *Seepage Model for PA Including Drift Collapse*. MDL-NBS-HS-000002 REV 01. Las Vegas, Nevada: CRWMS M&O. ACC: MOL.20010221.0147.

153246   CRWMS M&O 2000. *Total System Performance Assessment for the Site Recommendation*. TDR-WIS-PA-000001 REV 00 ICN 01. Las Vegas, Nevada: CRWMS M&O. ACC: MOL.20001220.0045.

151940   CRWMS M&O 2000. *Unsaturated Zone Flow and Transport Model Process Model Report*. TDR-NBS-HS-000002 REV 00 ICN 02. Las Vegas, Nevada: CRWMS M&O. ACC: MOL.20000831.0280.

122797   CRWMS M&O 2000. *UZ Flow Models and Submodels*. MDL-NBS-HS-000006 REV 00. Las Vegas, Nevada: CRWMS M&O. ACC: MOL.19990721.0527.

154291   CRWMS M&O 2001. *Abstraction of Drift Seepage*. ANL-NBS-MD-000005 REV 01. Las Vegas, Nevada: CRWMS M&O. ACC: MOL.20010309.0019.

153045   CRWMS M&O 2001. *Seepage Calibration Model and Seepage Testing Data*. MDL-NBS-HS-000004 REV 01. Las Vegas, Nevada: CRWMS M&O. ACC: MOL.20010122.0093.

154024   CRWMS M&O 2001. *Unsaturated Zone and Saturated Zone Transport Properties (U0100)*. ANL-NBS-HS-000019 REV 00 ICN 1. Las Vegas, Nevada: CRWMS M&O. ACC: MOL.20010201.0026.

102757   Day, W.C.; Potter, C.J.; Sweetkind, D.S.; and Dickerson, R.P. 1996. "Detailed Bedrock Geologic Map of the Central Block Area, Yucca Mountain - Implications for Structural Development of the Potential High-Level Radioactive Waste Repository Area in Nye County, Nevada." *Abstracts with Programs - Geological Society of America, 28*, (7), A-248. Boulder, Colorado: Geological Society of America. TIC: 234569.

100439   de Marsily, G. 1986. *Quantitative Hydrogeology: Groundwater Hydrology for Engineers*. San Diego, California: Academic Press. TIC: 208450.

100567   Deutsch, C.V. and Journel, A.G. 1992. *GSLIB Geostatistical Software Library and User's Guide*. New York, New York: Oxford University Press. TIC: 224174.

149540   DOE (U.S. Department of Energy) 2000. *Quality Assurance Requirements and Description*. DOE/RW-0333P, Rev. 10. Washington, D.C.: U.S. Department of Energy, Office of Civilian Radioactive Waste Management. ACC: MOL.20000427.0422.

100569   Domenico, P.A. and Schwartz, F.W. 1990. *Physical and Chemical Hydrogeology*. New York, New York: John Wiley & Sons. TIC: 234782.

135997   Doughty, C. 1999. "Investigation of Conceptual and Numerical Approaches for Evaluating Moisture, Gas, Chemical, and Heat Transport in Fractured Unsaturated Rock." *Journal of Contaminant Hydrology, 38*, (1-3), 69-106. New York, New York: Elsevier. TIC: 244160.

105655   Dyer, J.R. 1999. "Revised Interim Guidance Pending Issuance of New U.S. Nuclear Regulatory Commission (NRC) Regulations (Revision 01, July 22, 1999), for Yucca Mountain, Nevada." Letter from J.R. Dyer (DOE/YMSCO) to D.R. Wilkins (CRWMS M&O), September 3, 1999, OL&RC:SB-1714, with enclosure, "Interim Guidance Pending Issuance of New NRC Regulations for Yucca Mountain (Revision 01)." ACC: MOL.19990910.0079.

144839   Fabryka-Martin, J.; Wolfsberg, A.V.; Dixon, P.R.; Levy, S.; Musgrave, J.; and Turin, H.J. 1996. *Summary Report of Chlorine-36 Studies: Sampling, Analysis and Simulation of Chlorine-36 in the Exploratory Studies Facility*. Milestone 3783M. Los Alamos, New Mexico: Los Alamos National Laboratory. ACC: MOL.19970103.0047.

100144   Fabryka-Martin, J.T.; Flint, A.L.; Sweetkind, D.S.; Wolfsberg, A.V.; Levy, S.S.; Roemer, G.J.C.; Roach, J.L.; Wolfsberg, L.E.; and Duff, M.C. 1997. *Evaluation of Flow and Transport Models of Yucca Mountain, Based on Chlorine-36 Studies for FY97*. LA-CST-TIP-97-010. Los Alamos, New Mexico: Los Alamos National Laboratory. ACC: MOL.19980204.0916.

100145   Fabryka-Martin, J.T.; Wolfsberg, A.V.; Dixon, P.R.; Levy, S.S.; Musgrave, J.A.; and Turin, H.J. 1997. *Summary Report of Chlorine-36 Studies: Sampling, Analysis, and Simulation of Chlorine-36 in the Exploratory Studies Facility*. LA-13352-MS. Los Alamos, New Mexico: Los Alamos National Laboratory. ACC: MOL.19980812.0254.

156010   Faybishenko, B.; Doughty, C.; Steiger, M.; Long, J.C.S.; Wood, T.R.; Jacobsen, J.S.; Lore, J.; and Zawislanksi, P.T. 2000. "Conceptual Model of the Geometry and Physics of Water Flow in a Fractured Basalt Vadose Zone." *Water Resources*

Research, 36, (12), 3499-3520. [Washington, D.C.]: American Geophysical Union. TIC: 250750.

156009   Faybishenko, B.; Witherspoon, P.A.; Doughty, C.; Geller, J.T.; Wood, T.R.; and Podgorney, R.K. 2001. "Multi-Scale Investigations of Liquid Flow in a Fractured Basalt Vadose Zone." *Flow and Transport Through Unsaturated Fractured Rock.* 2nd Edition. Geophysical Monograph No. 42. Pages 161-182. [Washington, D.C.]: American Geophysical Union. TIC: 250749.

104043   Finsterle, S. 1997. *ITOUGH2 Command Reference, Version 3.1.* LBNL-40041. Berkeley, California: Lawrence Berkeley National Laboratory. ACC: MOL.19981008.0015.

151875   Finsterle, S. 2000. "Using the Continuum Approach to Model Unsaturated Flow in Fractured Rock." *Water Resources Research, 36*, (8), 2055-2066. [Washington, D.C.]: American Geophysical Union. TIC: 248769.

100147   Flint, A.L.; Hevesi, J.A.; and Flint, L.E. 1996. *Conceptual and Numerical Model of Infiltration for the Yucca Mountain Area, Nevada*. Milestone 3GUI623M. Denver, Colorado: U.S. Geological Survey. ACC: MOL.19970409.0087.

100033   Flint, L.E. 1998. *Characterization of Hydrogeologic Units Using Matrix Properties, Yucca Mountain, Nevada*. Water-Resources Investigations Report 97-4243. Denver, Colorado: U.S. Geological Survey. ACC: MOL.19980429.0512.

107377   Flint, L.E.; Hudson, D.B.; and Flint, A.L. 1999. "Unsaturated Hydraulic Parameters Determined from Direct and Indirect Methods." *Proceedings of the International Workshop on Characterization and Measurement of the Hydraulic Properties of Unsaturated Porous Media, Part 1, Riverside, California, October 22-24, 1997.* van Genuchten, M.Th.; Leij, F.J.; and Wu, L., eds. Pages 293-302. Riverside, California: University of California. TIC: 247322.

101173   Freeze, R.A. and Cherry, J.A. 1979. *Groundwater*. Englewood Cliffs, New Jersey: Prentice-Hall. TIC: 217571.

141512   Grathwohl, P. 2000. *Diffusion in Natural Porous Media: Contaminant Transport, Sorption/Desorption and Dissolution Kinetics*. Boston, Massachusetts: Kluwer Academic Publishers. TIC: 247983.

155955   Hinds, J. 2001. Unsaturated Zone Modeling & Synthesis. Scientific Notebook YMP-LBNL-YSW-JH-2. ACC: MOL.20010725.0216.

141521   Ho, C.K. 1997. "Evaporation of Pendant Water Droplets in Fractures." *Water Resources Research, 33*, (12), 2665-2671. Washington, D.C.: American Geophysical Union. TIC: 246969.

155876   Houseworth, J.; Moridis, G.; and Bodvarsson, G.S. 2001. "The Effects of the Drift Shadow on Radionuclide Transport." "*Back to the Future - Managing the Back End*

of the Nuclear Fuel Cycle to Create a More Secure Energy Future", Proceedings of the 9th International High-Level Radioactive Waste Management Conference (IHLRWM), Las Vegas, Nevada, April 29-May 3, 2001. La Grange Park, Illinois: American Nuclear Society. TIC: 247873.

122837   Hu, Q. and Brusseau, M.L. 1994. "The Effect of Solute Size on Diffusive-Dispersive Transport in Porous Media." *Journal of Hydrology, 158*, 305-317. Amsterdam, The Netherlands: Elsevier. TIC: 246801.

122846   Hu, Q. and Brusseau, M.L. 1995. "The Effect of Solute Size on Transport in Structured Porous Media." *Water Resources Research, 31*, (7), 1637-1646. Washington, D.C.: American Geophysical Union. TIC: 246800.

141523   Jackson, C.P.; Hoch, A.R.; and Todman, S. 2000. "Self-Consistency of a Heterogeneous Continuum Porous Medium Representation of a Fractured Medium." *Water Resources Research, 36*, (1), 189-202. Washington, D.C.: American Geophysical Union. TIC: 247466.

154293   Knight, J.H.; Philip, J.R.; and Waechter, R.T. 1989. "The Seepage Exclusion Problem for Spherical Cavities." *Water Resources Research, 25*, (1), 29-37. [Washington, D.C.]: American Geophysical Union. TIC: 240851.

117091   Lasaga, A.C. 1998. *Kinetic Theory in the Earth Sciences*. Princeton, New Jersey: Princeton University Press. TIC: 246279.

100588   Leverett, M.C. 1941. "Capillary Behavior in Porous Solids." *AIME Transactions, Petroleum Development and Technology, Tulsa Meeting, October 1940. 142*, 152-169. New York, New York: American Institute of Mining and Metallurgical Engineers. TIC: 240680.

153480   Li, G. 2000. Drift Scale Modeling. Scientific Notebook YMP-LBNL-CFT-GL-1. ACC: MOL.20000929.0042.

155675   Liu, H.H. 1999. Unsaturated Zone Modeling and Synthesis. Scientific Notebook YMP-LBNL-GSB-LHH-2. ACC: MOL.20010802.0134.

105729   Liu, H.H.; Doughty, C.; and Bodvarsson, G.S. 1998. "An Active Fracture Model for Unsaturated Flow and Transport in Fractured Rocks." *Water Resources Research, 34*, (10), 2633-2646. Washington, D.C.: American Geophysical Union. TIC: 243012.

153458   Looney, B.B. and Falta, R.W., eds. 2000. *Vadose Zone Science and Technology Solutions*. Volume II. Pages 591, 685-690. Columbus, Ohio: Battelle Press. TIC: 249256.

100590   Luckner, L.; van Genuchten, M.T.; and Nielsen, D.R. 1989. "A Consistent Set of Parametric Models for the Two-Phase Flow of Immiscible Fluids in the Subsurface."

Water Resources Research, 25, (10), 2187-2193. Washington, D.C.: American Geophysical Union. TIC: 224845.

139143   Millington, R.J. and Quirk, J.M. 1961. "Permeability of Porous Solids." *Transactions of the Faraday Society, 57*, (7), 1200-1207. Toronto, Canada: Royal Society of Chemistry. TIC: 246707.

133392   Mills, R. 1973. "Self-Diffusion in Normal and Heavy Water in the Range 1-45°." *The Journal of Physical Chemistry, 77*, (5), 685-688. Washington, D.C.: American Chemical Society. TIC: 246404.

100161   Montazer, P. and Wilson, W.E. 1984. *Conceptual Hydrologic Model of Flow in the Unsaturated Zone, Yucca Mountain, Nevada*. Water-Resources Investigations Report 84-4345. Lakewood, Colorado: U.S. Geological Survey. ACC: NNA.19890327.0051.

123099   Neretnieks, I. 1993. "Solute Transport in Fractured Rock - Applications to Radionuclide Waste Repositories." Chapter 2 of *Flow and Contaminant Transport in Fractured Rock*. Bear, J.; Tsang, C.F.; and de Marsily, G., eds.. 39-127. San Diego, California: Academic Press. TIC: 235461.

140371   NRC (U.S. Nuclear Regulatory Commission) 1999. *Issue Resolution Status Report Key Technical Issue: Unsaturated and Saturated Flow Under Isothermal Conditions*. Rev. 2. Washington, D.C.: U.S. Nuclear Regulatory Commission. ACC: MOL.19990810.0641.

153313   NRC (U.S. Nuclear Regulatory Commission) 2000. *Issue Resolution Status Report Key Technical Issue: Radionuclide Transport*. Rev. 2. Washington, D.C.: U.S. Nuclear Regulatory Commission. ACC: MOL.20010205.0058.

155700   Olesen, T.; Moldrup, P.; Henriksen, K.; and Petersen, L.W. 1996. "Modeling Diffusion and Reaction in Soils: IV. New Models for Predicting Ion Diffusivity." *Soil Science, 161*, (10), 633-645. [Baltimore, Maryland: Williams & Wilkins]. TIC: 250477.

144773   Or, D. and Ghezzehei, T.A. 2000. "Dripping into Subterranean Cavities from Unsaturated Fractures under Evaporative Conditions." *Water Resources Research, 36*, (2), 381-393. Washington, D.C.: American Geophysical Union. TIC: 246982.

105736   Paleologos, E.K.; Neuman, S.P.; and Tartakovsky, D. 1996. "Effective Hydraulic Conductivity of Bounded, Strongly Heterogeneous Porous Media." *Water Resources Research, 32*, (5), 1333-1341. Washington, D.C.: American Geophysical Union. TIC: 245760.

155954   Pan, L. 2001. Unsaturated Zone Modeling and Synthesis. Scientific Notebook YMP-LBNL-GSB-LP-3. ACC: MOL.20010921.0061.

155875   Pan, L. and Bodvarsson, G.S. 2001. *Modeling Transport in Fractured Porous Media with the Random-Walk Particle Method: The Transient Activity Range and the Particle-Transfer Probability*. LBNL-84042. Berkeley, California: Lawrence Berkeley National Laboratory.   Submit to RPC URN-0950

105743   Philip, J.R.; Knight, J.H.; and Waechter, R.T. 1989. "Unsaturated Seepage and Subterranean Holes: Conspectus, and Exclusion Problem for Circular Cylindrical Cavities." *Water Resources Research*, 25, (1), 16-28. Washington, D.C.: American Geophysical Union. TIC: 239117.

100605   Pruess, K. 1983. *GMINC - A Mesh Generator for Flow Simulations in Fractured Reservoirs*. LBL-15227. Berkeley, California: Lawrence Berkeley Laboratory. ACC: NNA.19910307.0134.

101707   Pruess, K. and Narasimhan, T.N. 1985. "A Practical Method for Modeling Fluid and Heat Flow in Fractured Porous Media." *Society of Petroleum Engineers Journal, 25*, (1), 14-26. Dallas, Texas: Society of Petroleum Engineers. TIC: 221917.

117112   Pruess, K.; Faybishenko, B.; and Bodvarsson, G.S. 1999. "Alternative Concepts and Approaches for Modeling Flow and Transport in Thick Unsaturated Zones of Fractured Rocks." *Journal of Contaminant Hydrology, 38*, (1-3), 281-322. New York, New York: Elsevier. TIC: 244160.

100819   Pruess, K.; Wang, J.S.Y.; and Tsang, Y.W. 1990. "On Thermohydrologic Conditions Near High-Level Nuclear Wastes Emplaced in Partially Saturated Fractured Tuff, 2. Effective Continuum Approximation." *Water Resources Research, 26*, (6), 1249-1261. [Washington, D.C.]: American Geophysical Union. TIC: 224854.

100642   Rautman, C.A. and Engstrom, D.A. 1996. *Geology of the USW SD-12 Drill Hole Yucca Mountain, Nevada*. SAND96-1368. Albuquerque, New Mexico: Sandia National Laboratories. ACC: MOL.19970613.0101.

101008   Rautman, C.A. and Engstrom, D.A. 1996. *Geology of the USW SD-7 Drill Hole Yucca Mountain, Nevada*. SAND96-1474. Albuquerque, New Mexico: Sandia National Laboratories. ACC: MOL.19971218.0442.

104252   Richards, L.A. 1931. "Capillary Conduction of Liquids Through Porous Mediums." *Physics, 1*, 318-333. [New York, New York: American Physical Society]. TIC: 225383.

139174   Ritcey, A.C. and Wu, Y.S. 1999. "Evaluation of the Effect of Future Climate Change on the Distribution and Movement of Moisture in the Unsaturated Zone at Yucca Mountain, NV." *Journal of Contaminant Hydrology, 38*, (1-3), 257-279. New York, New York: Elsevier. TIC: 244160.

102097   Rousseau, J.P.; Kwicklis, E.M.; and Gillies, D.C., eds. 1999. *Hydrogeology of the Unsaturated Zone, North Ramp Area of the Exploratory Studies Facility, Yucca*

Mountain, Nevada. Water-Resources Investigations Report 98-4050. Denver, Colorado: U.S. Geological Survey. ACC: MOL.19990419.0335.

154646   Rowell, D.L.; Martin, M.W.; and Nye, P.H. 1967. "The Measurement and Mechanism of Ion Diffusion in Soils. III. The Effect of Moisture Content and Soil-Solution Concentration on the Self-Diffusion of Ions in Soils." *The Journal of Soil Science, 18,* (2), 204-222. Oxford, England: Clarendon Press. TIC: 249762.

117127   Sonnenthal, E.L. and Bodvarsson, G.S. 1999. "Constraints on the Hydrology of the Unsaturated Zone at Yucca Mountain, NV from Three-Dimensional Models of Chloride and Strontium Geochemistry." *Journal of Contaminant Hydrology, 38,* (1-3), 107-156. New York, New York: Elsevier. TIC: 244160.

105043   Sudicky, E.A. and Frind, E.O. 1982. "Contaminant Transport in Fractured Porous Media: Analytical Solutions for a System of Parallel Fractures." *Water Resources Research, 18,* (6), 1634-1642. Washington, D.C.: American Geophysical Union. TIC: 217475.

106585   Thordarson, W. 1965. *Perched Ground Water in Zeolitized-Bedded Tuff, Rainier Mesa and Vicinity, Nevada Test Site, Nevada.* TEI-862. Washington, D.C.: U.S. Geological Survey. ACC: NN1.19881021.0066.

154674   USGS (U.S. Geological Survey) 2001. *Simulation of Net Infiltration for Modern and Potential Future Climates.* ANL-NBS-HS-000032 REV 00 ICN 01. Denver,Colorado: U.S. Geological Survey. ACC: MOL.20010405.0002.

100610   van Genuchten, M.T. 1980. "A Closed-Form Equation for Predicting the Hydraulic Conductivity of Unsaturated Soils." *Soil Science Society of America Journal, 44,* (5), 892-898. Madison, Wisconsin: Soil Science Society of America. TIC: 217327.

110043   Wang, J.S.Y. 1992. "Variations of Hydrological Parameters of Tuff and Soil." *High Level Radioactive Waste Management, Proceedings of the Third Annual International Conference, Las Vegas, Nevada, April 12-16, 1992. 1,* 727-731. La Grange Park, Illinois: American Nuclear Society. TIC: 204231.

104366   Wang, J.S.Y. and Elsworth, D. 1999. "Permeability Changes Induced by Excavation in Fractured Tuff." *Rock Mechanics for Industry, Proceedings of the 37th U.S. Rock Mechanics Symposium, Vail, Colorado, USA, 6-9 June 1999.* Amadei, B.; Kranz, R.L.; Scott, G.A.; and Smeallie, P.H., eds. 2, 751-757. Brookfield, Vermont: A.A. Balkema. TIC: 245246.

100611   Warren, J.E. and Root, P.J. 1963. "The Behavior of Naturally Fractured Reservoirs." *Society of Petroleum Engineers Journal, 3,* (3), 245-255. Dallas, Texas: Society of Petroleum Engineers. TIC: 233671.

117161   Wu, Y-S.; Haukwa, C.; and Bodvarsson, G.S. 1999. "A Site-Scale Model for Fluid and Heat Flow in the Unsaturated Zone of Yucca Mountain, Nevada." *Journal of Contaminant Hydrology, 38*, (1-3), 185-215. New York, New York: Elsevier. TIC: 244160.

155676   Wu, Y.S. 2001. Unsaturated Zone Modeling and Synthesis. Scientific Notebook YMP-LBNL-YSW-2. ACC: MOL.20010801.0330.

117167   Wu, Y.S.; Ritcey, A.C.; and Bodvarsson, G.S. 1999. "A Modeling Study of Perched Water Phenomena in the Unsaturated Zone at Yucca Mountain." *Journal of Contaminant Hydrology, 38*, (1-3), 157-184. New York, New York: Elsevier. TIC: 244160.

100194   Yang, I.C.; Rattray, G.W.; and Yu, P. 1996. *Interpretation of Chemical and Isotopic Data from Boreholes in the Unsaturated Zone at Yucca Mountain, Nevada*. Water-Resources Investigations Report 96-4058. Denver, Colorado: U.S. Geological Survey. ACC: MOL.19980528.0216.

101441   Yang, I.C.; Yu, P.; Rattray, G.W.; Ferarese, J.S.; and Ryan, J.N. 1998. *Hydrochemical Investigations in Characterizing the Unsaturated Zone at Yucca Mountain, Nevada*. Water-Resources Investigations Report 98-4132. Denver, Colorado: U.S. Geological Survey. ACC: MOL.19981012.0790.

149733   YMP (Yucca Mountain Site Characterization Project) 2000. *Q-List*. YMP/90-55Q, Rev. 6. Las Vegas, Nevada: Yucca Mountain Site Characterization Office. ACC: MOL.20000510.0177.

155724   YMP (Yucca Mountain Site Characterization Project) 2001. *Moisture Studies in the ESF*. Field Work Package FWP-ESF-96-004, Rev. 6. Las Vegas, Nevada: Yucca Mountain Site Characterization Office. ACC: MOL.20010425.0002.

155956   Zellmer, K. 2001. UZ Modeling and Synthesis. Scientific Notebook YMP-LBNL-YSW-KEZ-1. ACC: MOL.20010924.0058.

Software Cited

152614   Dynamic Graphics 1998. *Software Code: EARTHVISION*. 5.1. Silicon Graphics Indigo R4000. 10174-5.1-00.

152880   Lawrence Berkeley National Laboratory 03/06/2000. *Software Routine: minrefine3df.f*. V1.0. SUN. 10472-1.0-00.

154342   Lawrence Berkeley National Laboratory 03/31/2001. *Software Code: DCPT*. V2.0. PC w/MS Windows. STN: 10078-2.0-00. URN-0847

146496   Lawrence Berkeley National Laboratory 1/14/2000. *Software Code: TOUGH2 V1.4*. V1.4. Sun Workstation and DEC/ALPHA. 10007-1.4-01.

152823 Lawrence Berkeley National Laboratory 10/17/2000. *Software Routine: AddBound*. V1.0. SUN w/Unix OS. STN: 10357-1.0-00.

152824 Lawrence Berkeley National Laboratory 10/17/2000. *Software Routine: MoveMesh*. V1.0. SUN w/Unix OS. STN: 10358-1.0-00.

152826 Lawrence Berkeley National Laboratory 10/17/2000. *Software Routine: Perm2Mesh*. V1.0. SUN w/Unix OS. STN: 10359-1.0-00.

134136 Lawrence Berkeley National Laboratory 1999. *Software Code: GSLIB V1.0 Module SISIM V1.203*. V1.0. Sun, PC. 10001-1.0MSISIMV1.203-00.

154340 Lawrence Berkeley National Laboratory 1999. *Software Code: GSLIB*. V2.0MSISIMV2.0. SUN. STN: 10098-2.0MSISIMV2.0-00.

134754 Lawrence Berkeley National Laboratory 1999. *Software Code: infil2grid V1.6*. V1.6. PC with Windows/95 or 98. Sun or DEC Workstation with Unix OS. 10077-1.6-00.

113942 Lawrence Berkeley National Laboratory 1999. *Software Code: T2R3D V1.4*. V1.4. SUN, DEC / ALPHA. 10006-1.4-00.

112757 Lawrence Berkeley National Laboratory 1999. *Software Code: ITOUGH2 V3.2_drift*. V3.2_drift. SUN. 10055-3.2_DRIFT-00.

154337 Lawrence Berkeley National Laboratory 1999. *Software Code: ITOUGH2*. V3.2. SUN OS. STN: 10054-3.2-00.

152828 Lawrence Berkeley National Laboratory 2000. *Software Routine: CutNiche*. V1.3. SUN w/Solaris OS. 10402-1.3-00.

154341 Lawrence Berkeley National Laboratory 2001. *Software Code: Wingridder*. V1.1. PC w/MS Windows 98. STN: 10024-1.1-00.

154321 Lawrence Berkeley National Laboratory 2001. *Software Routine: AssignRock*. V1.0. SUN w/Solaris OS. STN: 10465-1.0-00.

154347 Lawrence Berkeley National Laboratory 2001. *Software Routine: mddf.f*. V2.0. SUN w/Solaris OS. STN: 10456-2.0-00.

152871 Lawrence Berkeley National Laboratory 2001. *Software Routine: Meshbd.f*. V1.0. SUN. 10467-1.0-00.

154343 Lawrence Berkeley National Laboratory 2001. *Software Routine: MINCgridv1.f*. V1.0. DEC-Alpha w/Unix OS. STN: 10469-1.0-00.

152872 Lawrence Berkeley National Laboratory 2001. *Software Routine: mininipresf.f*. V1.0. SUN. 10470-1.0-00.

154349   Lawrence Berkeley National Laboratory 2001. *Software Routine: mk_generGL.f.* V1.0. SUN w/Solaris OS. STN: 10476-1.0-00.

154346   Lawrence Berkeley National Laboratory 2001. *Software Routine: parallelf.java.* V1.0. PC w/Windows. STN: 10457-1.0-00.

156137   Lawrence Berkeley National Laboratory 2001. *Software Routine: RoutineRick1.* V1.1. SUN w/Unix. STN: 10474-1.1-00.   URN-0951

154345   Lawrence Berkeley National Laboratory 2001. *Software Routine: vf_con.for.* V1.0. PC w/Windows. STN: 10466-1.0-00.

139918   Lawrence Berkeley National Laboratory 9/16/99. *Software Code: iTOUGH2.* V4.0. SUN, DEC. 10003-4.0-00.

154322   LBNL (Lawrence Berkeley National Laboratory) 03/31/2001. *Software Code: TOUGH2.* V1.5. SUN and DEC-Alpha w/Unix OS. STN: 10007-1.5-00. URN-0845

153471   LBNL (Lawrence Berkeley National Laboratory) 2000. *Software Routine: bot_sum.f.* V1.0. SUN AND DEC. 10349-1.0-00.

154785   LBNL (Lawrence Berkeley National Laboratory) 2001. *Software Code: WINGRIDDER.* V2.0. PC. STN: 10024-2.0-00.   URN-0850

154788   LBNL (Lawrence Berkeley National Laboratory) 2001. *Software Routine: CalBT.for.* V1.0. PC. STN: 10504-1.0-00.

132448   LBNL 1999. *Software Code: DCPT.* V1.0. PC. 10078-1.0-00.

8.2   CODES, STANDARDS, REGULATIONS, AND PROCEDURES

AP-2.21Q, Rev. 1, BSCN 1. *Quality Determinations and Planning for Scientific, Engineering, and Regulatory Compliance Activities.* Washington, D.C.: U.S. Department of Energy, Office of Civilian Radioactive Waste Management. ACC: MOL.20010212.0018.

AP-3.10Q, Rev. 2, ICN 4, ECN 1. *Analyses and Models.* Washington, D.C.: U.S. Department of Energy, Office of Civilian Radioactive Waste Management. ACC: MOL.20010827.0114.

AP-SI.1Q, Rev. 3, ICN 1, ECN 1. *Software Management.* Washington, D.C.: U.S. Department of Energy, Office of Civilian Radioactive Waste Management. ACC: MOL.20010705.0239.

AP-SV.1Q, Rev. 0, ICN 2. *Control of the Electronic Management of Information.* Washington, D.C.: U.S. Department of Energy, Office of Civilian Radioactive Waste Management. ACC: MOL.20000831.0065.

QAP-2-3, Rev. 10, BSCN 2. *Classification of Permanent Items*. Washington, D.C.: U.S. Department of Energy, Office of Civilian Radioactive Waste Management. ACC: MOL.20010212.0283.

YMP-LBNL-QIP-SV.0 Rev. 2, Mod. 0. *Management of YMP-LBNL Electronic Data*. Berkeley, California: Lawrence Berkeley National Laboratory. ACC: MOL.20001108.0155.

8.3   SOURCE DATA, LISTED BY DATA TRACKING NUMBER

147022   GS000399991221.002. Rainfall/Runoff/Run-on 1999 Simulations. Submittal date: 03/10/2000.

156375   GS010708312272.002. Chemical Data for Pore Water from Tuff Cores of USW NRG-6, USW NRG-7/7A, USW UZ-14, USW UZ-N55 and UE-25 UZ#16. Submittal date: 09/05/2001.   URN-0954

145617   GS950608312272.001. Chemical Data for Pore Water from Tuff Cores of USW NRG-6, NRG7/7a, UZ-14 and UZ-N55, and UE-25 UZ#16. Submittal date: 05/30/1995.

107230   GS960308312312.005. Water-Level, Discharge Rate and Related Data from the Pump Tests Conducted at Well USW UZ-14, August 17 through August 30, 1993. Submittal date: 03/15/1996.

119786   GS970208312312.003. Water-Level and Related Data from Pump Tests Conducted at Well USW G-2, 4/8/96 - 12/17/96. Submittal date: 02/05/1997.

109746   GS980508312313.001. Water-Level and Related Data Collected in Support of Perched-Water Testing in Borehole USW WT-24, September 10, 1997 through February 3, 1998. Submittal date: 05/07/1998.

106752   GS980708312242.010. Physical Properties of Borehole Core Samples, and Water Potential Measurements Using the Filter Paper Technique, for Borehole Samples from USW WT-24. Submittal date: 07/27/1998.

106748   GS980808312242.014. Physical Properties of Borehole Core Samples and Water Potential Measurements Using the Filter Paper Technique for Borehole Samples from USW SD-6. Submittal date: 08/11/1998.

146134   GS990208312272.001. Analysis for Chemical Composition of Pore Water from Borehole USW UZ-14 and UE-25 UZ#16 and Groundwater from UE-25 UZ#16. Submittal date: 02/23/1999.

107185 GS990308312242.007. Laboratory and Centrifuge Measurements of Physical and Hydraulic Properties of Core Samples from Busted Butte Boreholes UZTT-BB-INJ-1, UZTT-BB-INJ-3, UZTT-BB-INJ-4, UZTT-BB-INJ-6, UZTT-BB-COL-5 and UZTT-BB-COL-8. Submittal date: 03/22/1999.

109822 GS990708312242.008. Physical and Hydraulic Properties of Core Samples from Busted Butte Boreholes. Submittal date: 07/01/1999.

148602 LA000000000034.001. Diffusion of Sorbing and Non-Sorbing Radionuclides. Submittal date: 01/22/1993.

156281 LA0002JF12213U.002. Chemistry Data for Porewater Extracted from ESF, Cross Drift and Busted Butte Drill Core. Submittal date: 02/15/2000.

145598 LA9909JF831222.004. Chloride, Bromide, and Sulfate Analyses of Busted Butte and Cross Drift Tunnel Porewaters in FY99. Submittal date: 09/29/1999.

153141 LB00090012213U.001. Air K Testing in Borehole SYBT-ERCB-LA#2 at CS 17+26 in Cross Drift. Submittal date: 11/03/2000.

153393 LB0010SCMREV01.002. Developed Data from Seepage Calibration Modeling AMR U0080. Submittal date: 11/29/2000.

153574 LB0011SMDCREV1.001. Seepage Model for PA Including Drift Collapse: 1. Model Input/Output Files AMR U0075 (MDL-NBS-HS-000002 REV01). Submittal date: 12/07/2000.

153570 LB0011SMDCREV1.002. Seepage Model for PA Including Drift Collapse: 2. Tables of Seepage Percentages AMR U0075 (MDL-NBS-HS-000002 REV01). Submittal date: 12/07/2000.

154586 LB0012AIRKTEST.001. Niche 5 Air K Testing 3/23/00-4/3/00. Submittal date: 12/21/2000.

146878 LB002181233124.001. Air Permeability and Pneumatic Pressure Data Collected Between October 27, 1999 through November 7, 1999 from Niche 5 (ECRB Niche 1620) of the ESF. Submittal date: 02/18/2000.

156336 LB0110MESHPROP.001. UZ Hydrostratigraphic Mesh with Faults and Zeolitic Alteration Zones. Submittal date: 10/08/2001. URN-0953

106787 LB990501233129.001. Fracture Properties for the UZ Model Grids and Uncalibrated Fracture and Matrix Properties for the UZ Model Layers for AMR U0090, "Analysis of Hydrologic Properties Data". Submittal date: 08/25/1999.

106785 LB990701233129.001. 3-D UZ Model Grids for Calculation of Flow Fields for PA for AMR U0000, "Development of Numerical Grids for UZ Flow and Transport Modeling." Submittal date: 09/24/1999.

125604   LB990701233129.002. 3-D Model Calibration Grid for Calculation of Flow Fields Using #3 Perched Water Conceptual Model (Non-Perched Water Model) for AMR U0050, "UZ Flow Models and Submodels." Submittal date: 03/11/2000.

122757   LB990801233129.003. TSPA Grid Flow Simulations for AMR U0050, "UZ Flow Models and Submodels" (Flow Field #3). Submittal date: 11/29/1999.

117129   LB990801233129.004. TSPA Grid Flow Simulations for AMR U0050, "UZ Flow Models and Submodels" (Flow Field #4). Submittal date: 11/29/1999.

144659   LB990801233129.019. TSPA Grid Flow Simulations for AMR U0050, "UZ Flow Models and Submodels." Flow Field #19: Present Day Mean Infiltration Map for Non-Perched Water Conceptual Model. Submittal date: 03/11/2000.

156331   LB990801233129.022. TSPA Grid Flow Simulations for AMR U0050, "UZ Flow Models and Submodels." Flow Field #22: Present Day Mean Infiltration for Non-Perched Water Conceptual Model. Submittal date: 03/11/2000

147115   LB9908T1233129.001. Transport Simulations for the Low, Mean, and Upper Infiltration Scenarios of the Present-Day, Monsoon, and Glacial Transition Climates for AMR U0050, "UZ Flow Models and Submodels". Submittal date: 03/11/2000.

123273   LB990901233124.004. Air Permeability Cross-Hole Connectivity in Alcove 6, Alcove 4, and Niche 4 of the ESF for AMR U0015, "In Situ Testing of Field Processes." Submittal date: 11/01/1999.

125868   LB991091233129.001. One-Dimensional, Mountain-Scale Calibration for AMR U0035, "Calibrated Properties Model." Submittal date: 10/22/1999.

126111   LB991091233129.004. Calibrated Fault Properties for the UZ Flow and Transport Model for AMR U0035, "Calibrated Properties Model." Submittal date: 10/22/1999.

147328   LB991121233129.001. Calibrated parameters for the present-day, mean infiltration scenario, used for simulations with perched water conceptual model #1 (flow through) for the mean infiltration scenarios of the present-day, Monsoon and Glacial transition climates. Submittal date: 03/11/2000.

147334   LB991121233129.002. Calibrated Parameters for the Present-Day, Mean Infiltration Scenario, Used for Simulations with Perched Water Conceptual Model #2 for the Mean Infiltration Scenarios of the Present-Day, Monsoon and Glacial Transition Climates. Submittal date: 03/11/2000.

147119   LB991131233129.003. Analytical and Simulation Results of Chloride and Chlorine-36 Analysis. AMR U0050, "UZ Flow Models and Submodels." Submittal date: 03/11/2000.

104055   LB997141233129.001. Calibrated Basecase Infiltration 1-D Parameter Set for the UZ Flow and Transport Model, FY99. Submittal date: 07/21/1999.

153777   MO0012MWDGFM02.002. Geologic Framework Model (GFM2000). Submittal
          date: 12/18/2000.

155989   MO0109HYMXPROP.001. Matrix Hydrologic Properties Data. Submittal date:
          09/17/2001.

156306   MO0109RDDAAMRR.003. Results from Drift Degradation Analysis. Submittal
          date: 09/24/2001.   Submit to RPC URN-0949

103769   MO9901MWDGFM31.000. Geologic Framework Model. Submittal date:
          01/06/1999.

8.4   OUTPUT DATA, LISTED BY DATA TRACKING NUMBER

LB0103CHVUPROP.001. Updated Site-Scale UZ Properties for the Calico Hills Vitric Units
[Model Layers ch1v and ch(2-5)v]: 1. Updated Drift-Scale Properties. Submittal date: Upon
completion of this AMR.

LB0103CHVUPROP.002. Updated Site-Scale UZ Properties For The Calico Hills Vitric Units
[Model Layers ch1v and ch(2-5)v]: 2. Inversion Modeling Input/Output Files. Submittal date:
Upon completion of this AMR.

LB0104AMRU0185.001. Section 6.3.1 Different Transport Computation Methods - Supporting
Files. Submittal date: Upon completion of this AMR.

LB0104AMRU0185.002. Section 6.3.2 Matrix Block Discretization and its Effects on UZ Flow
and Transport Simulations - Supporting Files. Submittal date: Upon completion of this AMR.

LB0104AMRU0185.003. Section 6.4.1.1 Drift Degradation: Rockfall - Supporting Files.
Submittal date: Upon completion of this AMR.

LB0104AMRU0185.004. Section 6.4.1.2 Drift Degradation: Rockbolts - Supporting Files.
Submittal date: Upon completion of this AMR.

LB0104AMRU0185.005. Section 6.4.2 Focusing and Discrete Flow Paths in the TSw -
Supporting Files. Submittal date: Upon completion of this AMR.

LB0104AMRU0185.006. Section 6.4.3 Percolation Redistribution and Lateral Flow in the PTN
- Supporting Files. Submittal date: Upon completion of this AMR.

LB0104AMRU0185.007. Section 6.4.4 The Effect of Episodic Percolation on Seepage -
Supporting Files. Submittal date: Upon completion of this AMR.

LB0104AMRU0185.008. Section 6.5.2 Modeling of the CHn and CFu: Fault Characteristics –
Supporting Files. Submittal date: Upon completion of this AMR.

LB0104AMRU0185.009. Section 6.5.3 Modeling of the CHn and CFu: Perched Water Models -
Supporting Files. Submittal date: Upon completion of this AMR.

LB0104AMRU0185.010. Section 6.5.4 Consideration of Radionuclide Release into Matrix Rock – Supporting Files. Submittal date: Upon completion of this AMR.

LB0104AMRU0185.011. Section 6.4.1.1 Drift Degradation: Rockfall - Data Summary. Submittal date: Upon completion of this AMR.

LB0104AMRU0185.012. Section 6.4.2 Focusing and Discrete Flow Paths in the TSw - Data Summary. Submittal date: Upon completion of this AMR.

LB0104AMRU0185.013. Section 6.5.1.3 Site-Scale Modeling Results - Supporting Files. Submittal date: Upon completion of this AMR.

LB0104AMRU0185.014.   Section 6.3.1 Different Transport Computation Methods - Data Summary. Submittal date: Upon completion of this AMR.